AD 273 332

U. S. ARMY
TRANSPORTATION RESEARCH COMMAND
FORT EUSTIS, VIRGINIA

TCREC TECHNICAL REPORT 61-103

$3.00

COMPARISON OF THEORETICAL AND EXPERIMENTAL MODEL HELICOPTER ROTOR PERFORMANCE IN FORWARD FLIGHT

Task 9R38-13-014-02

Contract DA 44-177-TC-548

July 1961

$05.00

prepared by :

UNITED AIRCRAFT CORPORATION
SIKORSKY AIRCRAFT DIVISION
Stratford, Connecticut

DISCLAIMER NOTICE

When Government drawings, specifications, or other data are used for any purpose other than in connection with a definitely related Government procurement operation, the United States Government thereby incurs no responsibility nor any obligation whatsoever; and the fact that the Government may have formulated, furnished, or in any way supplied the said drawings, specifications, or other data is not to be regarded by implication or otherwise as in any manner licensing the holder or any other person or corporation, or conveying any rights or permission, to manufacture, use, or sell any patented invention that may in any way be related hereto.

* * *

ASTIA AVAILABILITY NOTICE

Qualified requestors may obtain copies of this report from

Armed Services Technical Information Agency
Arlington Hall Station
Arlington 12, Virginia

* * *

This report has been released to the Office of Technical Services, U. S. Department of Commerce, Washington 25, D. C., for sale to the general public.

* * *

The information contained herein will not be used for advertising purposes.

* * *

The findings and recommendations contained in this report are those of the contractor and do not necessarily reflect the views of the Chief of Transportation or the Department of the Army.

DISCLAIMER NOTICE

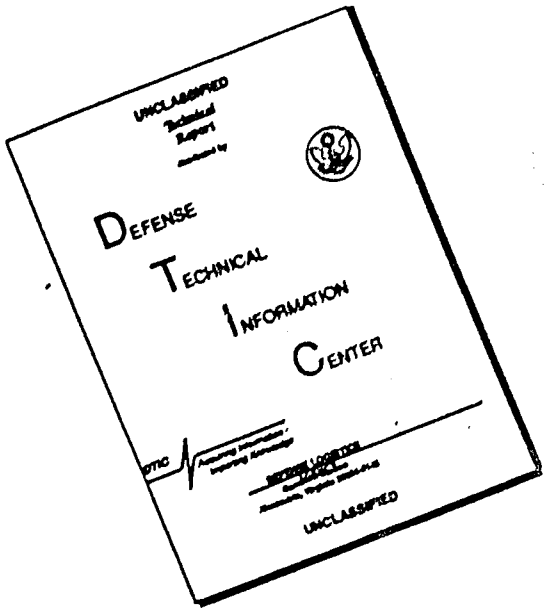

THIS DOCUMENT IS BEST QUALITY AVAILABLE. THE COPY FURNISHED TO DTIC CONTAINED A SIGNIFICANT NUMBER OF PAGES WHICH DO NOT REPRODUCE LEGIBLY.

Project 9R38-13-014-02
Contract DA 44-177-TC-548

July, 1961

COMPARISON OF THEORETICAL AND EXPERIMENTAL MODEL HELICOPTER ROTOR PERFORMANCE IN FORWARD FLIGHT

SER-50129

Prepared by:

UNITED AIRCRAFT CORPORATION
SIKORSKY AIRCRAFT DIVISION
Stratford, Connecticut

for

U. S. Army Transportation Research Command
Fort Eustis, Virginia

Prepared by:

John P. Rabbott, Jr.
Assistant Supervisor
Aircraft Advanced Research Section

UNITED AIRCRAFT CORPORATION
SIKORSKY AIRCRAFT DIVISION

HEADQUARTERS
U. S. ARMY TRANSPORTATION RESEARCH COMMAND
Fort Eustis, Virginia

FOREWORD

Under the terms of Contract DA 44-177-TC-548, Sikorsky Aircraft Division of the United Aircraft Corporation has conducted a study to determine the validity of various methods of calculating helicopter-rotor-blade performance in forward flight. This study is in conjunction with the efforts of the U. S. Army to improve the performance of rotary-wing aircraft.

The conclusions presented in this report are concurred in by the U. S. Army Transportation Research Command, Fort Eustis, Virginia, the cognizant agency for Contract DA 44-177-TC-548.

FOR THE COMMANDER:

APPROVED BY:

William R. Aiken, Jr.
WILLIAM R. AIKEN, JR.
USATRECOM Project Engineer

Raphael F. Garofalo
RAPHAEL F. GAROFALO
CWO-4 USA
Asst Adjutant

TABLE OF CONTENTS

ILLUSTRATIONS

APPENDIX II

SYMBOLS

a_o	coning angle, degrees
a_1	longitudinal flapping angle with respect to control axis, degrees
A_{1_S}	lateral cyclic pitch, degrees
b	number of blades
b_1	lateral flapping angle with respect to control axis, degrees
B_{1_S}	longitudinal cyclic pitch, degrees
c	blade chord, feet
c_1	rotor blade first mode edgewise bending
c_2	rotor blade second mode edgewise bending
C_d	airfoil section drag coefficient
C_l	airfoil section lift coefficient
C_D/σ	rotor drag coefficient-solidity ratio, $D/\pi R^2 \rho (\Omega R)^2 \sigma$
C_L/σ	rotor lift coefficient-solidity ratio, $L/\pi R^2 \rho (\Omega R)^2 \sigma$
C_T	rotor thrust coefficient, $T/\pi R^2 \rho (\Omega R)^2$
C_Q/σ	rotor torque coefficient-solidity ratio, $Q/\pi R^2 \rho (\Omega R)^2 R \sigma$
D	parasite drag, pounds
f	equivalent parasite area, square feet, D/q
f_1	rotor blade first mode flatwise bending
f_2	rotor blade second mode flatwise bending
FM	rotor figure of merit in hovering, $0.707 C_T^{3/2}/C_Q$
HP	rotor shaft horsepower

L	rotor lift, pounds
M	Mach number
$M_{(x)(\psi)}$	Mach number at radius station x, and azimuth position, ψ
q	free stream dynamic pressure, pounds per square foot
Q	rotor shaft torque, pound feet
r	radius to local blade station
R	rotor radius, feet
T	rotor thrust, pounds
v	rotor induced velocity, feet per second
V	forward speed, feet per second or knots, as appropriate
x	non-dimensional radius ratio, r/R
α	rotor angle of attack, degrees, angle between control axis and perpendicular to flight path
β_{1_S}	first harmonic flapping angle with respect to shaft axis, degrees
δ	mean blade section profile drag coefficient
$\theta_{.75R}$	collective pitch angle at 75 percent rotor radius
λ	inflow ratio, $V \sin\alpha - \nu / \Omega R$
μ	advance ratio, $V/ \Omega R$
ρ	mass density of air, slugs per cubic foot
σ	rotor solidity, $bc/\pi R$
ψ	azimuth angle, degrees, measured from downward position, in direction of rotation
Ω	rotor angular velocity, radians per second

I SUMMARY

An analytical and experimental program was conducted to determine the degree of correlation between theoretical and experimental model rotor performance over a range of forward speeds of 100 to 161 knots and tip speeds of 580 to 850 feet per second. The theory utilized synthesized airfoil data derived from hovering tests, and included both stall and compressibility effects. The model blades were dynamically scaled from the Sikorsky S-56 main rotor blades.

Theory and experiment correlate well below the theoretically predicted stall boundary, but above stall the theory is unduly conservative in estimating rotor power required.

The effects of compressibility on rotor power loading can be accurately predicted. A rotor with an NACA 0012 airfoil section incurs severe penalties in profile power when the advancing tip Mach number exceeds 0.85 to 0.90.

Significant amounts of model rotor blade dynamic twisting (up to 5 degrees change in pitch at the 3/4 radius station) occur both in hovering and in forward flight. Such twisting must be taken into account to properly synthesize airfoil data from hovering tests. The inclusion of dynamic twist in forward flight calculations significantly improves the correlation of theory and experiment at a given collective pitch and helps somewhat to reduce the overly conservative prediction of rotor power required at a given lift and propulsive force.

The investigation was jointly sponsored by the United States Army Transportation Research Command and Sikorsky Aircraft.

II CONCLUSIONS

A comparison of the results of an experimental and theoretical investigation of the performance of a dynamically scaled model helicopter rotor in hovering and forward flight leads to the following principal conclusions.

1. Theoretical forward flight calculations based on synthesized airfoil data which include stall and compressibility effects accurately predict the rotor power required below the theoretically determined stall limit. Above stall, theory becomes increasingly conservative as rotor lift or propulsive force is increased.

2. The calculated effects of compressibility on rotor power required agree with experimental results. For rotors with an NACA 0012 airfoil section serious compressibility losses are incurred when the advancing tip Mach number exceeds 0.85 to 0.90.

3. Model rotor blades which are representative of present day construction in regards to stiffness undergo substantial changes in pitch under rotation due to dynamic twisting effects. Inclusion of such twist is mandatory to synthesize reliable airfoil data from hovering tests. The inclusion of dynamic twist in forward flight results in substantial improvements in the correlation of theoretical and experimental rotor performance at a given collective pitch. Even when rotor performance is cross plotted to eliminate collective pitch as a variable, the inclusion of dynamic twist in the calculation procedure changes the theoretical performance such as to bring it into closer agreement with experiment, particularly at high rotor loading conditions.

4. An approximate inclusion of the effects of radial flow on rotor profile torque appears to improve the correlation of theory and experiment at advance ratios on the order of 0.5.

5. The experimental rotor control requirements (collective pitch, longitudinal cyclic pitch, and lateral cyclic pitch) are generally one to two degrees greater than the predicted values.

III RECOMMENDATIONS

Additional theoretical research, supported by experimental verification, is required in the following two areas to improve the correlation of theoretical and experimental rotor performance.

1. Determine which factors are not presently accounted for by theory that result in an overly conservative prediction of rotor blade stall. The investigation should include consideration of:

   a. The centrifugal field and radial pressure gradient effects on the boundary layer. Such effects may be less significant full scale than at model scale due to the relatively thinner boundary layer and therefore full scale experimentation is required.

   b. Unsteady airfoil effects.

   c. Variable induced velocity distribution.

2. Perform an analysis more rigorous than those to date to determine the quantitative effects of radial flow on rotor profile torque and rotor drag.

IV INTRODUCTION

Classical rotor aerodynamic theories, such as References 1 and 2, appear to be inadequate for design of modern high performance helicopters due to the neglect of the effects of the rotor blade stall and of the effects of compressibility on performance, stability, and control. To minimize such limitations, more exact equations describing the operation of the rotor were derived, such as Reference 3, which eliminated the customary small angle assumptions and provided for the inclusion of non-linear airfoil section characteristics. Solution of such equations is accomplished through the use of numerical integration techniques involving high speed computing machines.

The purpose of the present investigation was to determine the degree of correlation between experimental rotor performance obtained from wind tunnel tests of a dynamically scaled model rotor with the theoretical performance predicted by the numerical approach described above. Dynamic similarity between model and full scale rotor blades is required to include the effects of realistic aeroelastic deformations on rotor performance and to obtain useful blade stresses. Because of the uncertainty of the validity of applying airfoil section characteristics derived from two-dimensional wind tunnel data to a rotor which experiences three-dimensional flow, the airfoil characteristics were synthesized from hovering tests of the rotor which was used in the wind tunnel program.

The investigation was jointly sponsored by the United States Army Transportation Research Command and Sikorsky Aircraft under Contract DA 44-177-TC-548.

V DESCRIPTION OF MODEL AND FACILITIES

Rotor Blades

The rotor blades are 9 feet in diameter, 2.69 inch chord with an NACA 0012 airfoil section and are dynamically scaled from the Sikorsky S-56 (H-37, HR2S) main rotor blades at a design tip speed of 696 feet per second. A five bladed rotor head was used for the program which results in a rotor solidity of 0.079. Figure 1 shows the component parts of a model blade and also a fully assembled blade. The S-56 rotor blade is composed of a hollow extruded aluminum spar to which trailing edge pockets, fabricated of aluminum ribs and skin, are bonded. The model spar is built up of formed 7075 aluminum sheet bonded together. The trailing edge pockets are composed of balsa wood ribs covered with Mylar coated paper. Five normal bending, five chordwise, and four torsional strain gages are located on the spar of one of the five blades at positions shown in the accompanying table.

% Radius/Type	Flatwise Bending	Chordwise Bending	Torsion
17.4			x
21.0	x	x	
33.4	x	x	
36.3			x
47.2	x	x	
63.9	x	x	
69.0			x
80.5	x	x	
91.0			x

Due to periodic instrumentation difficulties, not all of the strain gages were functioning throughout the program. Figure 2 compares the frequency characteristics of model and full scale rotor blades.

Static Test Apparatus

Hovering tests were conducted on the Sikorsky 1000 horsepower Tail Rotor Precession Test Stand, shown in figure 3. The rotor disc is in a vertical plane. The upper gear box and horizontal drive shaft are supported in flexures to permit axial movement of the assembly, which is restrained by a Baldwin load cell to measure rotor thrust.

Rotor torque is normally measured below the gear box but for the present test a special dual capacity strain gage torque spool was incorporated into the horizontal drive shaft behind the rotor head to eliminate any torque tares in the drive system. The two torque measurements agreed within 3% - the difference chargeable to the gear box losses. Clifton rotary transformers were located on the flapping and lag hinge axes to measure blade motions which were recorded on a Consolidated Recording Oscillograph. Rotor thrust and torque were recorded on chart drive, damped precision potentiometers. If there was any wind present, the test stand was precessed about a vertical axis to keep the rotor disc pointed edgewise into the wind and the method of Reference 4 was used to account for the effect of ambient wind on induced rotor torque. Normally tests were conducted at less than 5 knot wind conditions and at Mach numbers below 0.5, at zero wind. (The effects of ambient wind on rotor performance will be discussed subsequently.) The estimated system accuracies are:

thrust		±5 pounds
torque	low range	± .6 pound feet
	high range	±1.8 pound feet
blade motion		±1/4 degree
RPM		±5

Wind Tunnel

Forward flight tests were conducted in the United Aircraft Corporation large subsonic wind tunnel. This is a closed return tunnel powered by a 9000 horsepower motor and has a maximum tunnel speed of approximately 175 knots. The test section is octagonal in cross section, 18 feet across the flats. Remote controlled air exchangers are employed to maintain constant stagnation temperature during operation. Figure 4 is an artist drawing which shows the general arrangement of the tunnel.

Helicopter Rotor Test Rig

The helicopter rotor test rig is equipped with a six component strain gage balance and is powered by a variable frequency electric motor rated at 375 horsepower at 6000 RPM. Figure 5a shows an overall view of the rig mounted in the wind tunnel and figure 5b shows the details of the hub and swash plate area. The five bladed hub (identical to that used for the static tests) is equipped with coincident flapping and lagging hinges located at

0.056 radius. Lagging motion is restrained by friction dampers. Clifton rotary transformers are used to sense flapping and lagging motion. A conventional swash plate is driven by three precision electric actuators whose position is sensed by slide wire potentiometers integral with the actuators. Collective and cyclic pitch are remotely set in from a servo system in the wind tunnel control room and the yaw table of the wind tunnel provides variation in shaft angle of attack. An instrumentation plate is mounted in the rotor head and contains dummy half bridges to complement the active strain gages on the rotor blade.

The drive motor is supported by frictionless hydrostatic oil bearings. The motor case is restrained from rotation by a strain gage torque beam to measure rotor power. Axial displacement of the motor-shaft system is limited by a strain gage thrust beam. A four component strain gage balance supports the rotor head and shaft and measures longitudinal force, lateral force, hub rolling moment, and hub pitching moment. Electrical signals are transmitted from the rotating to the stationary system through a 100 channel slip ring assembly.

Dynamic data from the rotor test rig are recorded on a 20 channel EPSCO data acquisition system. Each channel is scanned from 20 to 36 times per revolution, depending on rotor speed, for 10 revolutions. The information is received from the rig in analog form, digitized, and recorded on magnetic tape. At the completion of each run, the data are transmitted to an IBM 7090 data processing unit and reduced. The EPSCO unit has a visual display of all 20 channels of information in bargraph form, a two-channel oscilloscope, and a six-channel direct writing oscillograph, all of which may be used for monitoring purposes during the course of testing.

Two data reduction programs are available. The primary program reduces the six component performance data to dimensional and coefficient form in the wind axis system including a tunnel wall correction to rotor angle of attack similar to that of Reference 5. Normally the correction is less than 1 degree. Tare forces and moments on the rotor hub (obtained from measurements with blades off) are subtracted from the measured data so that the reduced performance corresponds to the rotor blades alone. Blade motion and blade stress data are reduced to average and peak to peak values.

A second data reduction program is available which will perform an harmonic analysis of any or all of the 20 channels of information. Due to the expensive nature of such a program, it is normally used only for detailed analysis of specific data areas.

VI PRESENTATION AND DISCUSSION OF RESULTS

A. Hovering Phase

The airfoil section characteristics were synthesized from the experimental hovering data by a method similar to that of Reference 6. The theoretical hovering performance prediction method is based on strip analysis wherein the rotor blade induced velocity is derived from a balance of blade element-momentum forces and a tip loss factor of 0.97 is assumed to account for the shed vorticity at the blade tip. No small angle assumptions are employed. Such a method is commonly used and results in good correlation with overall hovering performance. However, figure 9 of Reference 7 shows that the calculated spanwise loading distribution obtained by such a technique, using two-dimensional data, does not completely check experimental results either due to the assumption of two-dimensional flow or due to the assumed independence of adjacent blade elements. Such limitations are also inherent in the present synthesized airfoil data.

In the process of synthesization, unreasonably low lift curve slopes were generated at the higher Mach numbers and/or high blade angles. Analysis of the torsional moments on the rotor blade showed that significant amounts of dynamic twist were present at certain conditions. The torsional moment distribution versus radius was combined with the experimentally determined torsional stiffness distribution to calculate the actual blade pitch, and twist distribution, for each operating condition. Considerable effort is involved in such calculations but it is required for a proper interpretation of the airfoil data. Figure 6 presents the calculated values of dynamic pitch change at the 3/4 radius station versus the nominal, or nonrotating collective pitch for the range of tip Mach numbers - note that up to 5 degrees change in collective pitch is shown.

As a checkon the calculated values of rotor blade dynamic twist some photographs of the blade tip were taken. Due to the very high noise levels generated by the model rotor at high tip Mach numbers, night time testing is not possible and the photography had to be done during daylight hours. Highly reflective "Scotchlite" strips were mounted on the tip of one blade and on targets at the blade cuff to increase the intensity of the reflected light but the combination of the bright background, small chord, and high tip speed made the task of obtaining clear photos extremely difficult. Eight separate photos of the blade tip angle were obtained for the condition of a nominal collective pitch angle $\theta_{.75R} = 13$ degrees and a tip Mach number

of 0.7. The calculated dynamic twist at the blade tip, as obtained from the torsion measurements was 1.5 degrees. The average of the photographic measurements checked the calculated value within 0.5 degrees. Figure 7 is a sample photograph of the blade tip. For future work on small scale high speed rotors, the torsional stress measurement technique is superior to the photographic technique, and at any scale the former method has the very significant advantage that the complete blade twist distribution is obtained rather than only the value of twist at the blade tip.

Figure 8 presents the variation of experimental thrust coefficient versus torque coefficient for tip Mach numbers of .3, .4, .5, .6, .7, .8, .9, and .95, and contains data from two separate tests. The open symbols represent data obtained during the first test program in November when zero ambient wind conditions are difficult to obtain. The solid symbol represent similar data obtained during a May test program when zero wind conditions are readily attainable. At tip Mach numbers of 0.3 and 0.4, figure 8a, where maximum rotor thrust and therefore maximum section lift coefficients are attainable there is a significant difference in rotor performance between the two sets of data. A similar effect was noticed in Reference 8. Inasmuch as it can be reasoned, as in Reference 8, that the lower values of maximum thrust are due to ambient wind conditions, these data points were disregarded in fairing the curves and in synthesizing the airfoil data.

Figure 9 presents thrust coefficient versus corrected collective pitch for the range of tip Mach numbers of 0.3 to 0.95.

The effect of tip Mach number on rotor hovering figure of merit is shown in figure 10. The maximum figure of merit is constant up to a tip Mach number of 0.7 although some compressibility losses are evidenced above $C_T/\sigma = 0.09$ at 0.7 Mach number. Also included on figure 10 for comparison purposes is an experimental curve for figure of merit for a full scale H-37 rotor at a tip Mach number of 0.6. The model rotor has a substantially lower figure of merit throughout the operating range, attributable to the low Reynolds number of the model tests. From a comparison such as is made in figure 10 it would be expected that the airfoil section characteristics for the model would be appreciably different than for full scale rotors and also that the forward flight model rotor performance potentials would be significantly less than for a full scale rotor.

The synthesized airfoil section data are presented in figure 11 as lift coefficient and drag coefficient versus angle of attack at con-

stant Mach number and as drag coefficient versus Mach number at constant angle of attack. The end point of each curve of figures 11a-11c is the limit of the experimental data as determined by available lag angle (45 degrees) or power. The dashed lines represent the estimated section characteristics beyond the limit of the experimental data. The variation of lift curve slope with Mach number is consistant with the usual experimental results or theory such as the Prandtl-Glauert rule. The increase in maximum lift coefficient from a Mach number of 0.1 to 0.3 is attributed to Reynolds number effects. (For the model rotor the relation between Reynolds number and Mach number is $RN = 1.56 \times 10^6 \times M$ at NACA standard conditions.) Similarly the greater than normal curvature at low angles of attack is attributed to low Reynolds number separation. The rate of growth of drag coefficient with angle of attack at low angles is greater than normally anticipated but is appropriate for the low test Reynolds numbers and is consistent with the curvature of the lift data.

In and near the reversed flow region extremely large variation in angles are encountered, but at low Mach numbers. Therefore, figure 11d was prepared to cover the 0 to 180 degrees angle range, based on Reference 9, but adjusted for Reynolds numbers appropriate to the model tests.

As shown in figure 1 inboard of approximately 25 per cent radius the rotor blade is composed of a spar section only, equivalent to a 0012 airfoil section with the rear 60 per cent cut off. To be able to account for the contribution of the spar section to the rotor forces in forward flight, a low speed two-dimensional wind tunnel test was run on an actual rotor blade spar section. The results are shown in figure 12 and were used in all forward flight calculations. (The unusually high maximum lift coefficient is due to the fact that spar chord is used as a reference, and not the full airfoil chord. The percentage reduction in reference area is greater than the percentage reduction in section lift due to the removal of the rear part of the airfoil section.)

B. Forward Flight Phase

1. Experimental and Analytical Techniques - The wind tunnel testing procedure is to set a desired tip speed, shaft angle of attack, and tunnel speed. The minimum value of collective pitch at each shaft angle is the value required for approximately zero lift, and at each collective pitch angle, longitudinal and lateral cyclic pitch are adjusted to eliminate first harmonic flapping with respect to the rotor shaft. The maximum collective pitch is determined by

a limiting combined flatwise and edgewise vibratory blade stress at any radial station of ±10, 000 psi.

Inasmuch as the limitations to classical rotor theory, described in the introduction, are well known, the primary emphasis of the theoretical treatment will be placed on the numerical integration, non-linear approach to the calculation of rotor performance, such as is described in Reference 3. An IBM 7090 or Philco 2000 electronic data processing unit is used to solve the differential equations of blade flapping and to perform the necessary force and moment integrations. For given inflow ratio, λ , advance ratio, μ , collective pitch angle, $\theta_{.75R}$, and assumed starting values of flapping angle, flapping velocity, and flapping acceleration, the time history of flapping motion is calculated for finite increments of azimuth until a steady solution is determined. Equilibrium is defined as the condition where the flapping angle and flapping velocity repeat within 0. 001 radian for successive revolutions. The forces acting on the rotor blade are calculated at fifteen radial stations and a variable number of azimuth increments depending on the advance ratio. At advance ratios below 0. 4, increments in azimuth of 20 to 30 degrees are appropriate, but at greater advance ratios, reduction in the azimuth increments to 10 degrees is required. The use of too large an increment in azimuth position at moderate to high advance ratios can result in gross errors in performance. For single point calculations, the program has an option of iterating on pitch angle, $\theta_{.75R}$, and inflow ratio, λ , to provide a specified value of rotor lift and propulsive force. The primary simplifying assumptions in the generalized rotor theory are:

a. uniform inflow

b. rigid blade

c. no radial flow effects

d. no unsteady effects

The following forward flight conditions were investigated both theoretically and experimentally.

V, Knots	ΩR, feet per second		$M_{(1.0)(90)}$	Experimental Range of α_s, deg.	Experimental Range of $\theta_{.75R}$, deg.
100	650	0.26	0.73	-20 to 8 at 4	0 to 16 at 2
125	650	.32	.77	-20 to 8 at 4	-2 to 18 at 2
150	650	.39	.81	-20 to 4 at 4	-2 to 20 at 2
161	580	.47	.76	-16 to 4 at 4	0 to 15 at 1
161	700	.39	.87	-20 to 8 at 4	-2 to 16 at 2
161	750	.36	.91	-20 to 12 at 4	-4 to 16 at 2
161	800	.34	.96	-20 to -12 at 4	5 to 14 at 1
161	850	.32	1.0	-20 to 0 at 4	3 to 12 at 1

The first three operating conditions were chosen to investigate the effects of a variation in forward speed, at constant tip speed, similar to present day helicopter operation. The second group relates the effects of varying tip speed (tip Mach number) at a high constant forward speed. Inasmuch as the method of presentation of the theoretical and experimental rotor performance and blade motions is identical for all conditions, a sample of the basic data will be given and the more important results of both groups of data summarized in general form. The complete basic performance and blade motion data are presented in Appendix I.

2. Constant Tip Speed Operation - Figure 13 presents the theoretical variation of lift coefficient-solidity ratio, C_L/σ, drag coefficient-solidity ratio, C_D/σ, torque coefficient-solidity ratio, C_Q/σ, coning angle, a_o, longitudinal flapping angle, a_1, and lateral flapping angle, b_1, with rotor angle of attack, α, at various nominal collective pitch angles for the condition of 100 knots forward speed and 650 feet per second tip speed. Note that as the data are for a constant advance ratio (ie., a constant forward speed and tip speed) the tip speed ratio, $V\cos\alpha / \Omega R$, varies with rotor angle of attack. Therefore, the rotor lift curve slope, which is proportional to tip speed ratio, varies accordingly with rotor angle. The dashed lines in figure 13a noted as the stall limit, is the theoretically determined onset of rotor blade stall. Early stall criteria such as the blade section angle of attack at the retreating tip are not applicable when compressibility effects are present as there no longer is a discrete stall angle. Therefore, the rotor stall criteria of the present study is based on a limiting profile drag torque coefficient defined as follows:

$$C_{Q_d} = \frac{\int_o^R C_{d_o} \quad \rho/2 \ (\Omega R)^2 \ u_T^2 \ c \ r \ dr}{\pi R^2 \rho \ (\Omega R)^2 \ R}$$

The limiting section drag coefficient $C_{d_o} = 0.15$ and $u_T = 0.4$. C_{d_o} corresponds approximately to the drag coefficient at the section angle of attack just past maximum lift coefficient at most Mach numbers. When the limiting value of profile drag torque is exceeded at any azimuth on the retreating side of the rotor disc, the rotor is considered to be entering the stalled region. Figure 13c and similar plots at other conditions shows that the

theoretical stall limit generally corresponds to the point of inflection of the C_Q/σ vs. α curves. As will be pointed out later in the comparison of experimental and theoretical rotor performance, the calculated stall limit in general also approximates the point at which the theoretical calculations diverge from experiment after which point the theory becomes conservative.

Figure 14 presents the experimental basic rotor performance and blade motions vs. rotor angle of attack at constant collective pitch. As discussed in the previous section on experimental techniques, the model rotor is operated in the wind tunnel such that the first harmonic blade flapping with respect to the shaft is trimmed to zero. Therefore, the longitudinal and lateral flapping coefficients presented in figure 14e and f and other similar figures may also be interpreted as $a_1 = B_{1s}$ and $b_1 = - A_{1s}$.

The theoretical and experimental variation of lift with rotor angle of attack in figures 13 and 14 is generally similar but the theoretical maximum lift capability is less than experiment, as shown by the comparison in figure 14a at $\theta_{.75R} = 10$ degrees. The absolute rotor maximum lift is even greater than indicated in figure 14a because the upper limit of collective pitch is determined by vibratory stress limits, as discussed earlier. In figures 13b and 14b theory and experiment show a similar variation of drag with angle of attack, but for a given collective pitch angle, theory predicts a greater propulsive force as in figure 14b. The most striking difference between figures 13c and 14c which present C_Q/σ versus α, is that at a constant pitch, as rotor angle of attack is increased algebraically theory predicts a rapid increase in torque, corresponding to rotor blade stall, but no such evidence is given by experiment. However, it will be shown later that comparison of the individual theoretical and experimental model rotor forces at a given value of collective pitch is not significant due to dynamic twisting effects. Therefore, overall rotor performance is presented in figure 15 as C_Q/σ versus C_D/σ at selected values of C_L/σ, a method of presentation which eliminates blade pitch angle and rotor angle of attack as a variable. Theory and experiment agree well at low lift and the theory is generally conservative with an increasing divergence from experiment as rotor lift is increased.

Figure 16 compares theoretical and experimental blade motions versus C_D/σ at two values of C_L/σ, for the same forward speed of 100 knots and tip speed of 650 feet per second. Generally, the experimental values are greater than the calculated blade motions.

Because the longitudinal flapping, a_1 , is equivalent to the longitudinal cyclic pitch, B_{1S}, and the lateral flapping, b_1, is equivalent to the lateral cyclic pitch, A_{1S}, the predicted control motions are unconservative and more control displacement is required than predicted by theory-the reverse of the comparison of rotor performance. Surprisingly good agreement is shown for collective pitch, on the cross plot basis of figure 16d, when the effects of dynamic blade twist, to be discussed subsequently, are considered.

Similar rotor performance and blade motion data are presented in Appendix I as figures 29-32 for V = 125 knots, ΩR = 650 feet per second and in figures 33-36 for V = 150 knots, ΩR = 650 feet per second.

Because the discrepancies between calculated and measured rotor performance in the regime of theoretically predicted stall, and because of the significant effects of dynamic twist that were encountered in hovering, the effects of rotor blade dynamic twist in forward flight was investigated. The condition selected was a nominal collective pitch angle of 12 degrees at V = 150 knots and ΩR = 650 feet per second for a range of rotor angle of attack. As the available theory does not include torsional flexibility the changes in rotor blade pitch angle and twist distribution were calculated from the wind tunnel blade torsional stress measurements.

The computing program was modified so that blade pitch could be varied in any fashion with radius and azimuth, as an input item. The radial distribution of torsion moment as determined from blade torsion strain gages was plotted versus azimuth. At 10 degree increments in azimuth the torsion moment distribution was combined with the experimentally determined rotor blade torsional stiffness to calculate the incremental change in blade twist, and therefore, pitch angle. Approximately four man weeks of calculation were required to evaluate the dynamic twist change for a single nominal blade pitch angle. The resulting local pitch angles and twist distributions were incorporated in the analytical performance prediction program and the results are given in figure 17. In figure 17a the inclusion of dynamic twist in the standard theory results in a general shift in the lift curve and the two theoretical calculations bracket the experimental line. A similar comparison is made in figure 17b for drag coefficient-solidity ratio versus angle of attack. The effect of including dynamic twist is to bring the theory into substantially better

agreement with experiment at constant collective pitch particularly in the region of maximum propulsive force. A similar beneficial effect is shown in figure 17c which presents torque coefficient-solidity ratio versus rotor angle of attack. Not only does theory and experiment agree well below stall, but in the theoretically predicted stalled region substantial reductions in the discrepancy between calculated and measured torque are achieved. An overall comparison between the two calculated methods is made in figure 17d, as C_Q/σ versus C_{H_x}/σ at constant C_{L_1}/σ so that collective pitch and rotor angle of attack are eliminated as variables. The solid line is rigid blade theory while the square symbols represent the theory including dynamic twist effects. At low and moderate values of lift coefficient-solidity ratio, little or no effect is shown, but at high lift loadings the calculated rotor performance based on rigid blade theory becomes increasingly pessimistic. (The dashed lines of figure 17d connect points of equal nominal collective pitch for both theoretical calculations.)

Comparison of theory and experiment in figure 17d shows that even with the inclusion of dynamic twist there are still substantial differences between the overall analytical and experimental rotor performance at high values of lift coefficient-solidity ratio. The divergence between theory and experiment in stall can best be seen in figure 18 which compares the two on the basis of C_Q/σ versus C_{L_1}/σ at constant values of $1/\pi R^2$ for forward speeds of 100, 125, and 150 knots at a tip speed of 650 feet per second. A parasite area of one percent of the disc area is typical of a moderately clean helicopter and a parasite area of one-half percent of the disc area is typical of a modern high speed, high performance helicopter such as described in Reference 10. The theoretical onset of rotor blade stall is noted on figure 18 as a dotted line. Figure 18 shows that while the calculated rotor torque is essentially identical to the measured value at low values of rotor lift, there is a constant divergence between the two as rotor lift is increased. Fortunately, the calculated torque is conservative. The reason for the continuous divergence between theory and experiment in figure 18a, and to a lesser extent in figure 18b from the lowest values of C_{L_1}/σ, is not known. As can be seen from figure 25, to be presented subsequently, the calculated stall line is generally a good indication of the point at which the theoretical rotor torque begins to diverge from the experimental value. It has not been determined which factors are present in practice that are not accounted for by theory to postpone rotor stall well

past the theoretically predicted region. It is proposed that the centrifugal effects on the boundary layer air attached to the rotor blade and/or the spanwise pressure gradient due to aerodynamic loading may provide an automatic boundary layer control for the rotor. An attempt was made to partially account for such phenomena by synthesizing airfoil data from hovering tests rather than using two-dimensional wind tunnel data but both the centripetal acceleration and the radial aerodynamic pressure gradient are greater in forward flight than in hovering. Therefore, such effects merit further consideration. The calculated angle of attack distribution and therefore the rotor forces are in error to the extent that the actual induced velocity differs from the assumed uniform value, but there is no method available at present to determine the true induced velocity distribution. The effects of a variation in inflow would be greatest at the lowest advance ratio, figure 18a, and would decrease as advance ratio increased. Part of the discrepancy may also arise from the assumption of the applicability of steady state airfoil data, as an airfoil undergoing oscillation in angle of attack, such as a rotor blade section does, is known to attain significant increases in maximum lift coefficient. Inclusion of such effects is beyond the scope of the present report but merits further study. The unsteady effect cannot be the total answer, however, as Reference 11 shows that even in the case of a propeller in axial flight where no unsteady effects are present, a theory based on strip analysis and two-dimensional airfoil data predicts blade stalling considerably before stall actually occured on the propeller.

Figures 19 and 20 respectively, compare the calculated and measured power loading and control requirements versus forward speed for a given lift coefficient-solidity ratio and parasite area at a tip speed of 650 feet per second. Two conditions: C_L/σ = 0.04, $f/\pi R^2$ = 0.005 and C_L/σ = 0.06, $f/\pi R^2$ = 0.010, were chosen to represent, from figure 18, a condition typical of operation below and above the theoretical stall limit. Below stall, C_L/σ = 0.04, the theoretical power loading is slightly conservative but at C_L/σ = 0.06 the theory would predict considerably greater rotor horsepower required than is needed in practice. Examination of figure 20 however shows that theory is not conservative in predicting the collective pitch and the cyclic pitch required for zero first harmonic flapping with respect to the shaft. While the calculated variation of control displacement with forward speed matches experiment well, the actual magnitude differs in the order of one to two degrees. Note that in

contrast to the comparisons of rotor power loading the relative correlation of predicted and measured control requirements is generally the same when the rotor is below or above the calculated stall boundary. The differences between the calculated and measured control requirements may be partially explained by the experimental dynamic twisting of the model rotor blade in addition to the possible effects of flatwise bending.

3. Constant Forward Speed Operation - Basic rotor performance and blade motion data are presented in Appendix I in a form similar to the data discussed previously for the conditions of 161 knots forward speed and a range of tip speeds of 580, 700, 750, and 850 feet per second. In addition, a very limited amount of data are presented for 800 feet per second operation. In the section "Description of Equipment" it was noted that the model rotor blades are dynamically scaled from the Sikorsky H-37 rotor at a design tip speed of 696 feet per second. During testing at the high speed conditions of 161 knots forward speed and tip speeds of 800 and 850 feet per second numerous failures of the blade pockets were encountered due to greater than design aerodynamic and centrifugal loading. After obtaining a limited amount of data at 800 feet per second tip speed by periodic repair or replacement of damaged blades it was decided to discontinue testing at this condition to insure that a more complete map could be obtained at the desired maximum tip speed of 850 feet per second wherein the advancing tip Mach number equals 1.0. Although limited in scope the 800 feet per second data are presented to help demonstrate more explicitly the trends with Mach number that are demonstrated by the complete performance maps. (It is interesting to note that the most frequent type of pocket failure at the high advancing tip Mach number conditions was a spanwise fracture of the paper skin and balsa wood ribs of the pocket at approximately 50 to 60 percent chord - probably due to the severe repetitive loading of the once per revolution shock wave located in the region of the blade tip.) Inasmuch as the method of presentation of the present group of data is similar to that of previous conditions only the novel features and the summarized results will be discussed.

Figure 21 compares the theoretical and experimental variation of C_Q/σ with C_D/σ at constant C_L/σ for V = 161 knots, ΩR = 580 feet per second. Contrary to the results presented earlier, the calculated rotor torque is somewhat less than measured below the stall boundary. It was hypothesized that the contribution of the

radial component of local velocity at a blade section might be significant at an advance ratio as high as the present value, $\mu = 0.47$. Because such a phenomena is neglected in existing theory and considerable extension of the theory would be required to include radial velocity effects rigorously, a crude approximation was taken from Appendix II of Reference 12. Simple theory without a radial velocity component gives rotor profile torque as:

$$C_{Qo} = \frac{\sigma \delta}{8} \quad (1 + 3 \mu^2)$$

The approximate expression from Reference 12 with radial flow is

$$C_{Qo} = \frac{\sigma \delta}{8} \quad (1 + 4.65 \mu^2)$$

The difference between the two expressions was calculated and added to the rotor profile torque as determined from the generalized rotor performance theory and the results are shown in figure 21. The contribution to the total rotor torque is appreciable and results in an improved correlation between theory and experiment below the stall boundary. A review of the cross plotted performance data at the various operating conditions similar to figure 21 shows that in general when the rotor has attained a lift coefficient-solidity ratio of $C_L/\sigma = 0.06$, the calculated performance curve is displaced from the measured curve throughout the range of rotor drag due to the conservative prediction of rotor performance in stalled operation. Note however in contrast that the basic theory of figure 21d at $C_L/\sigma = 0.06$ matches experiment exactly below stall. Therefore, the inclusion of radial flow torque contribution makes the comparison in figure 21 more consistent with that of the other operating conditions previously discussed and subsequent conditions.

Due to the crude assumptions involved in the correction factor of Reference 12, the effects of radial velocity in rotor performance will not be persued further in the present study, but this brief consideration indicates that a more refined treatment should be considered for rotor performance calculations at advance ratios on the order of 0.5 or greater.

As noted in the section on hovering performance, the hovering figure of merit for the model rotor was appreciably lower than that corresponding to a full scale geometrically similar rotor attributable to the reduced Reynolds number of the model tests. A similar comparison of model and full scale rotor performance

in forward flight is presented on a theoretical basis in figure 22 for the condition of 161 knots toward speed and 700 feet per second tip speed. For a given lift and propulsive force, the full scale rotor torque is significantly less than that required by the model rotor. Because the induced and parasite power is identical for both calculations at a given condition, the difference in C_Q/σ is due entirely to the increased profile drag coefficients of the model rotor blade sections.

A comparison of the calculated and measured rotor performance and blade motions at an operating condition (V = 161 knots, ΩR = 850 feet per second) wherein the advancing tip Mach number equals 1.0 is made in figures 23 and 24. In figure 23 the experimental and theoretical rotor torque required at a given lift and drag compare very well and in case of significant differences the theory is again generally conservative. The differences between the calculated and measured rotor blade motions of figure 24 are of the same order as encountered with the previously discussed operating conditions but note that the calculated blade motions are now greater, rather than less than the experimental values - the reverse of previous experience. It cannot be determined whether the reversal of trend is due to experimental error, an inadequacy in the theory, or to possible effects of dynamic twisting, which are presumably large at this operating condition.

The comparison of analytical and experimental rotor performance at 161 knots forward speed is made in figure 25 as C_Q/σ vs C_L/σ at constant values of $f/\pi R^2$. Figures 25b, c, and d, at tip speed of 700, 750, and 850 feet per second respectively, demonstrate excellent correlation between theory and experiment below the calculated stall boundary and the usual divergence above stall. In figure 25, as in figure 21 previously, the standard generalized rotor performance method generally predicts less rotor torque below stall than measured. However, the approximate inclusion of radial velocity effects, described earlier and shown in figure 25a as a dotted line, improves the correlation.

The effects of compressibility on rotor performance in forward flight, as determined by the change in rotor power loading with advancing tip Mach number, are demonstrated in figure 26 both experimentally and theoretically. The noted condition is for a forward speed of 161 knots, a disc loading of 4 pounds per square foot and a parasite area of 0.5 percent of the disc area. The solid

line of figure 26 with symbols is experimental. The dotted curve is theoretical including Mach number effects. Good correlation between experiment and theory is obtained, except at a tip Mach number of 0.75 (μ = 0.47) where the theoretical curve is stalled.

Because the forward speed, lift, and parasite area are constant in figure 26, the increase in rotor power loading with advancing tip Mach number is entirely due to increased section profile drag. However, as the tip Mach number is raised by increasing the tip speed, some change in power loading would be expected, even in incompressible flow. Therefore, the dashed curve of figure 26, based on airfoil section characteristics at M=0.3, has been added to aid in the distinction between the profile power losses due to compressibility and those due to tip speed alone. Referred to an advancing tip Mach number of 0.85, the theoretical increase in incompressible rotor profile power loading with tip speed is noted on figure 26a as $\Delta(HP/L)_{\Omega R}$. If this increment is subtracted from the experimental increase in power loading between $M_{(1.0)(90)}$ = 0.85 and 1.0, the remainder is due to compressibility losses only, and is noted as $\Delta(HP/L)_M$. The same data are presented in figure 26b vs the cube of advancing tip Mach number, $M^3_{(1.0)(90)}$, as an aid in determining more precisely the Mach number for compressibility drag rise. The experimental data below a Mach number of about 0.85 and the unstalled theory without compressibility effects both vary linearly with the cube of advancing tip Mach number, as might be expected. The deviation of the experimental data from linearity at $M_{(1.0)(90)} = 1.0$ is attributed to compressibility losses and is labeled $\Delta(HP/L)_M$, as in figure 26a. The figure demonstrates that the advancing tip Mach number, at least for rotors with a NACA 0012 airfoil section, should not exceed approximately 0.87 to 0.90 in order to avoid serious compressibility losses.

For the same conditions as in figure 26, that is 161 knots forward speed, 4 pounds per square foot disc loading and a parasite area of 0.5 percent of the disc area, a comparison is made in figure 27 of the variation of rotor coning angle and control requirements with advance ratio. The advance ratio may also be converted to tip Mach number, as in figure 26, but the latter parameter is not felt to be as significant in the present comparison as the advance ratio. The calculated and measured coning angle and lateral cyclic pitch required correlate very well throughout the range. The longitudinal cyclic pitch and collective pitch generally vary one to two degrees between theory and ex-

periment as has been demonstrated previously. At the lowest advance ratio, $\mu = 0.32$ the experimental values are less than calculated, as described in the earlier discussion of figure 24. Without further investigation, the reasons for the discrepancy between calculated and measured blade motions at the lowest advance ratio (highest Mach number) cannot be ascertained but rotor blade dynamic twisting may be a significant factor.

REFERENCES

1. Bailey, F. J., Jr.: "A Simplified Theoretical Method of Determining the Characteristics of a Lifting Rotor in Forward Flight," NACA Report 716, 1941.

2. Gessow, Alfred and Almer D. Crim: "An Extension of Lifting Rotor Theory to Cover Operation at Large Angles of Attack at High Inflow Conditions," NACA TN 2665, 1952.

3. Gessow, Alfred and Almer D. Crim: "A Method for Studying the Transient Blade-Flapping Behavior of Lifting Rotors at Extreme Operating Conditions," NACA TN 3366, 1955.

4. Carpenter, Paul J.: "Effect of Wind Velocity on Performance of Helicopter Rotors as Investigated with the Langley Helicopter Apparatus," NACA TN 1698, 1948.

5. Heyson, Harry H.: "Jet-Boundary Corrections for Lifting Rotors Centered in Rectangular Wind Tunnels," NASA Technical Report R-71, 1960.

6. Powell, Robert D. and Paul J. Carpenter: "Lift and Profile Drag Characteristics of an NACA 0012 Airfoil Section as Derived from Measured Helicopter-Rotor Hovering Performance," NACA TN 4357, 1958.

7. Rabbott, John P., Jr.: "Static Thrust Measurements of the Aerodynamic Loading on a Helicopter Rotor Blade," NACA TN 3688, 1956.

8. Powell, Robert D., Jr., and Paul J. Carpenter: "Low Tip Mach Number Stall Characteristics and High Tip Mach Number Compressibility Effects on a Helicopter Rotor Having an NACA 0009 Tip Airfoil Section," NACA TN 4355, 1958.

9. Critzos, Chris C., Harry H. Heyson, and Robert W. Boswinkle, Jr.: "Aerodynamic Characteristics of NACA 0012 Airfoil Section at Angles of Attack from 0° to 180°," NACA TN 3361, 1955.

10. Fradenburgh, E. A.: "High Performance Single Rotor Helicopter Study," U. S. Army Transportation Research Command Technical Report 61-44, April, 1961.

11. Rogallo, Vernon L., and Paul F. Yoggy: "A Wind Tunnel Investigation of the Stall-Flutter Characteristics of a Supersonic Type Propeller at Positive and Negative Thrust," NASA Memo 3-9-59A, 1959.

12. Sikorsky, I. A.: "Correlation of Helicopter Performance Equations," Institute of the Aeronautical Sciences, Preprint No. 694, Paper Presented at the 25th Annual Meeting, January 28-31, 1957.

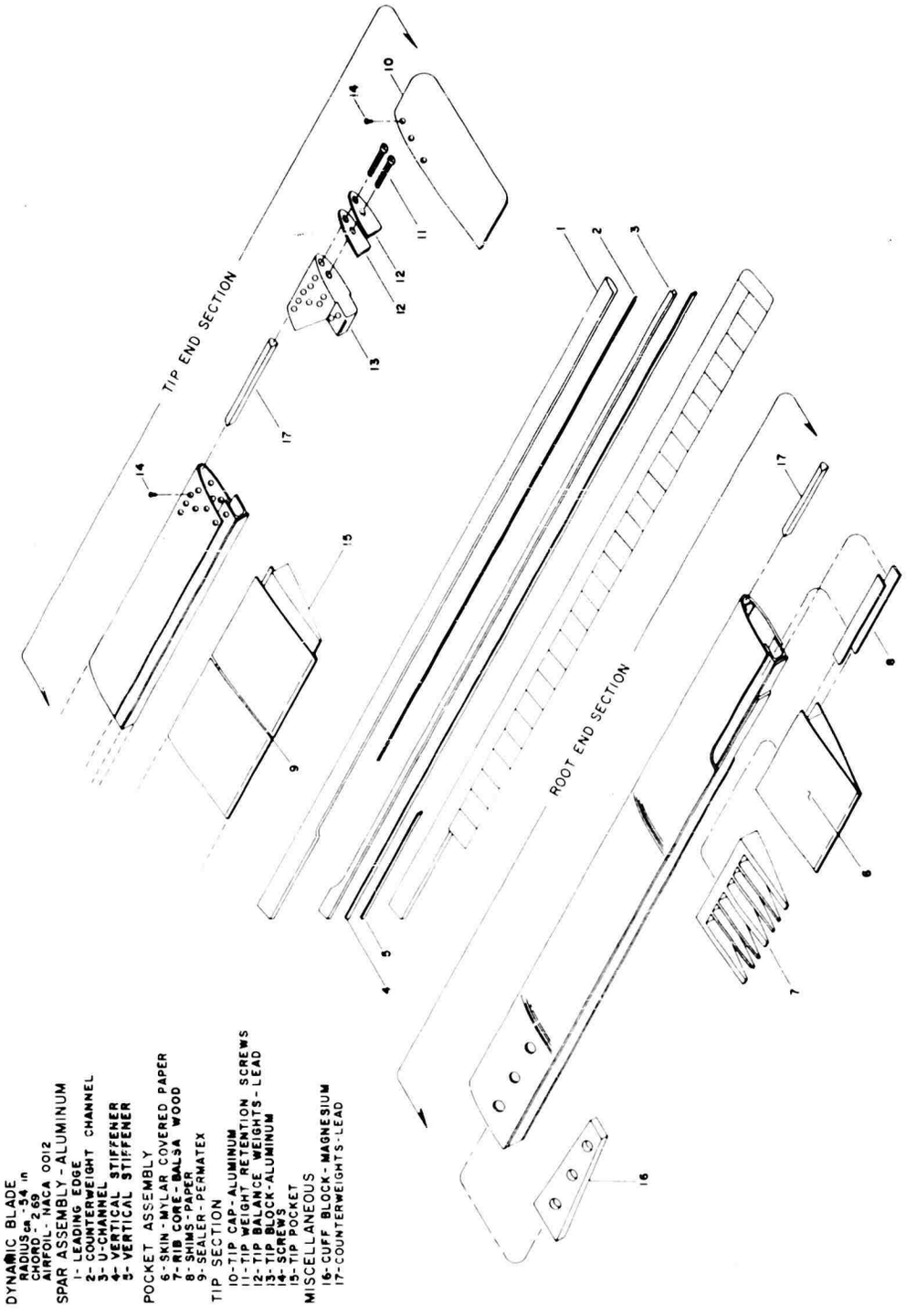

FIG. 1. DYNAMICALLY SCALED BLADE - EXPLODED VIEW

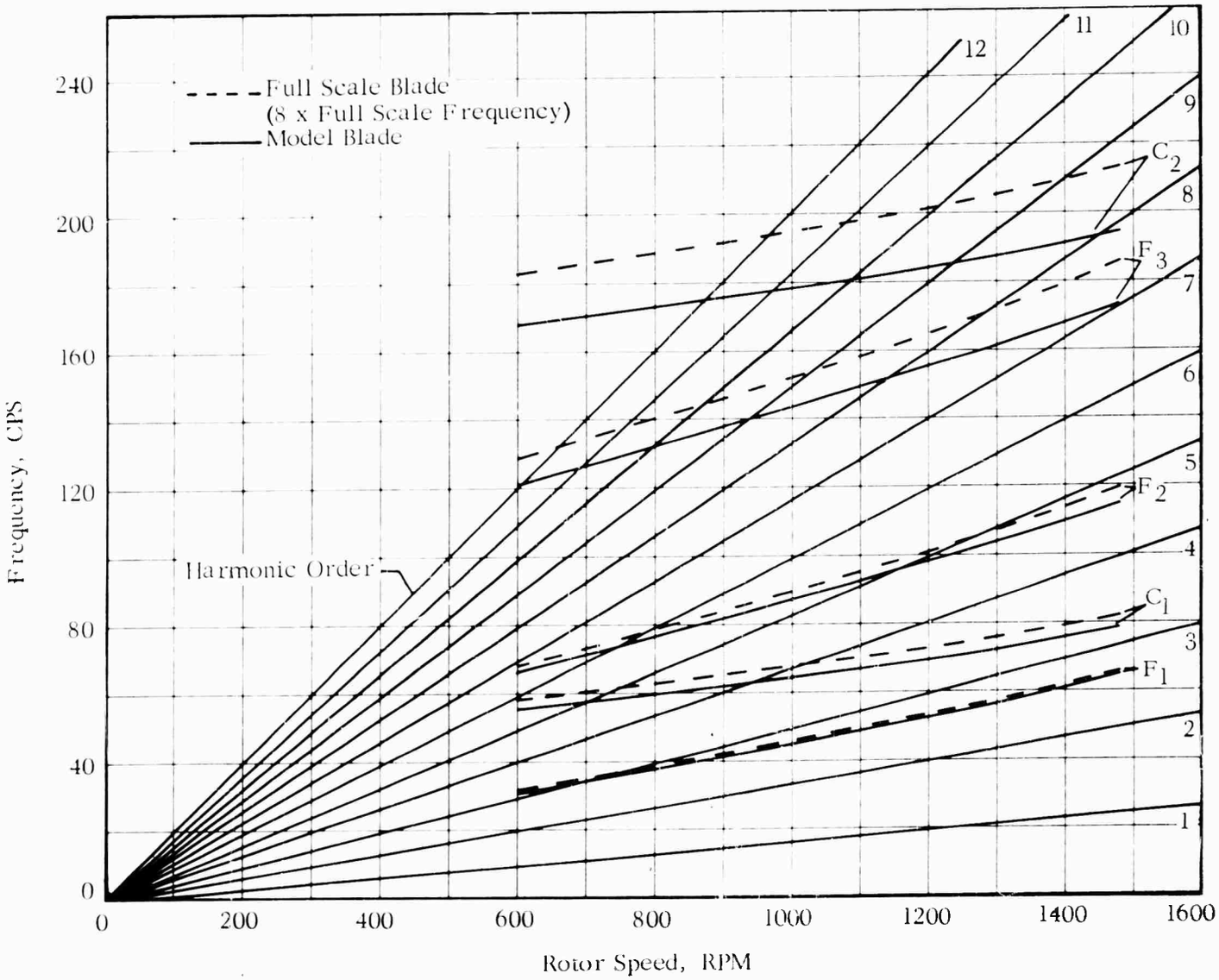

FIG. 2. COMPARISON OF MODEL AND FULL SCALE ROTOR BLADE NATURAL FREQUENCIES

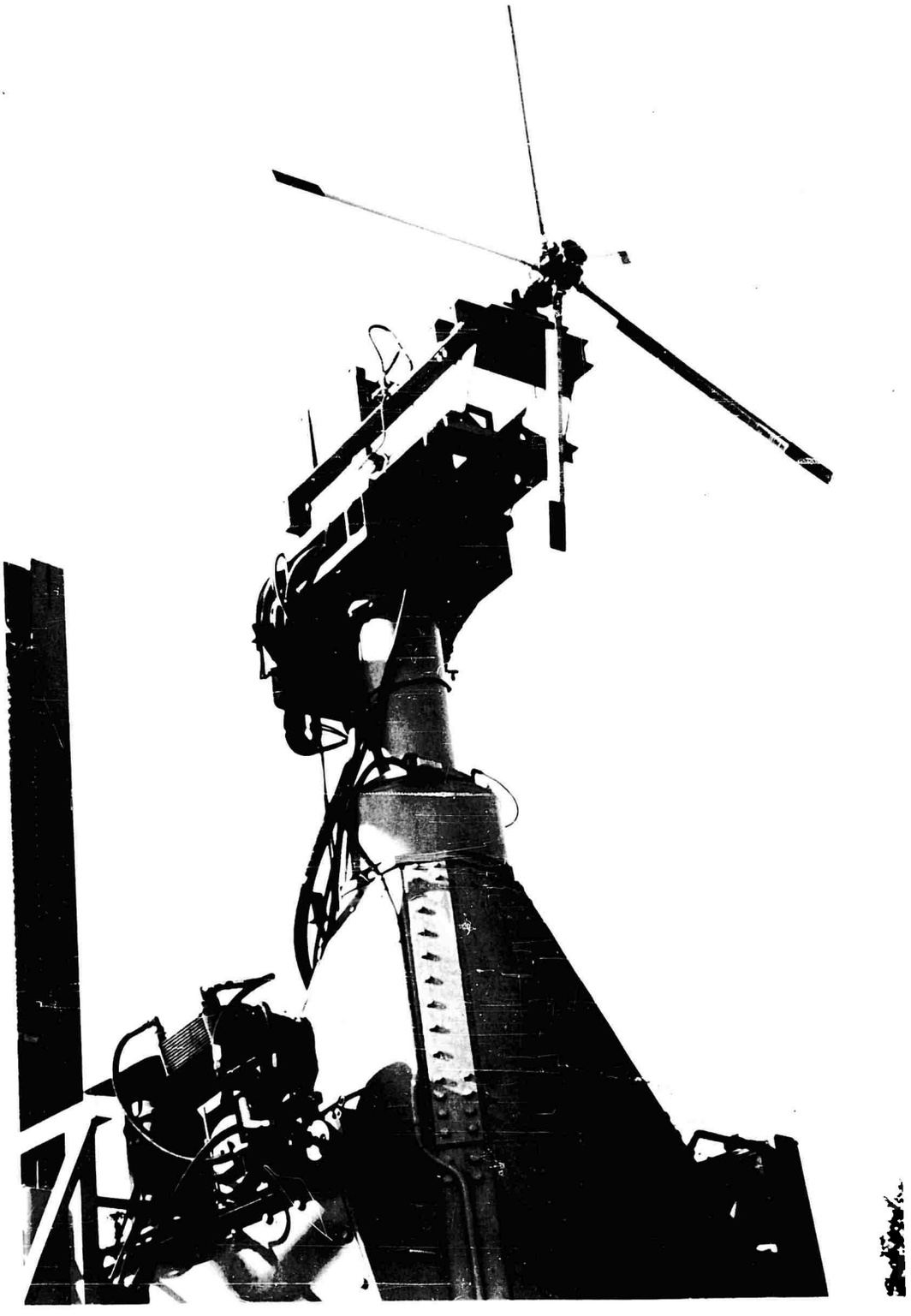

FIG. 5. SIKORSKY 1000 HORSEPOWER TAIL ROTOR PRECESSION STAND

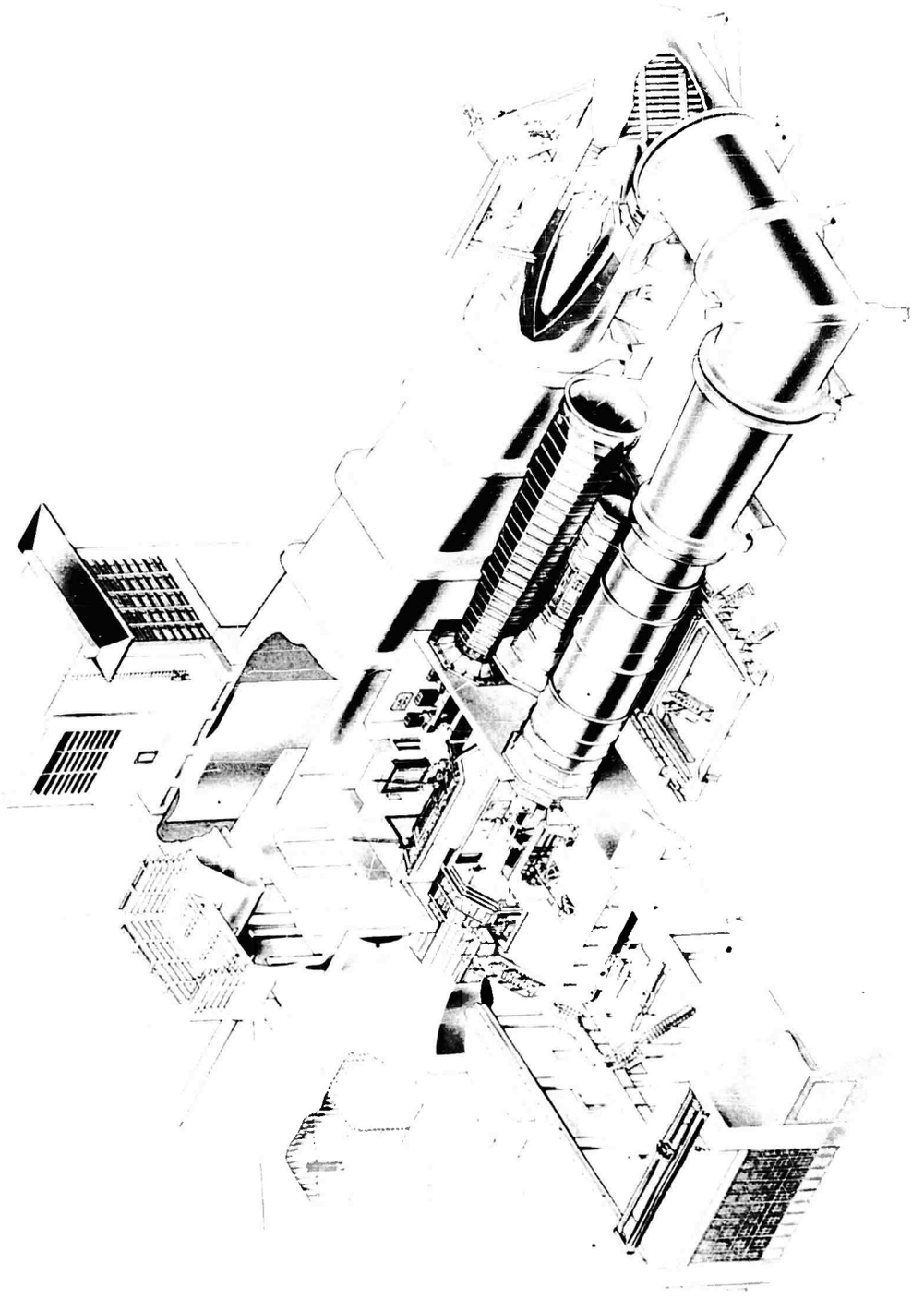

FIG. 4. UAC SUBSONIC WIND TUNNEL

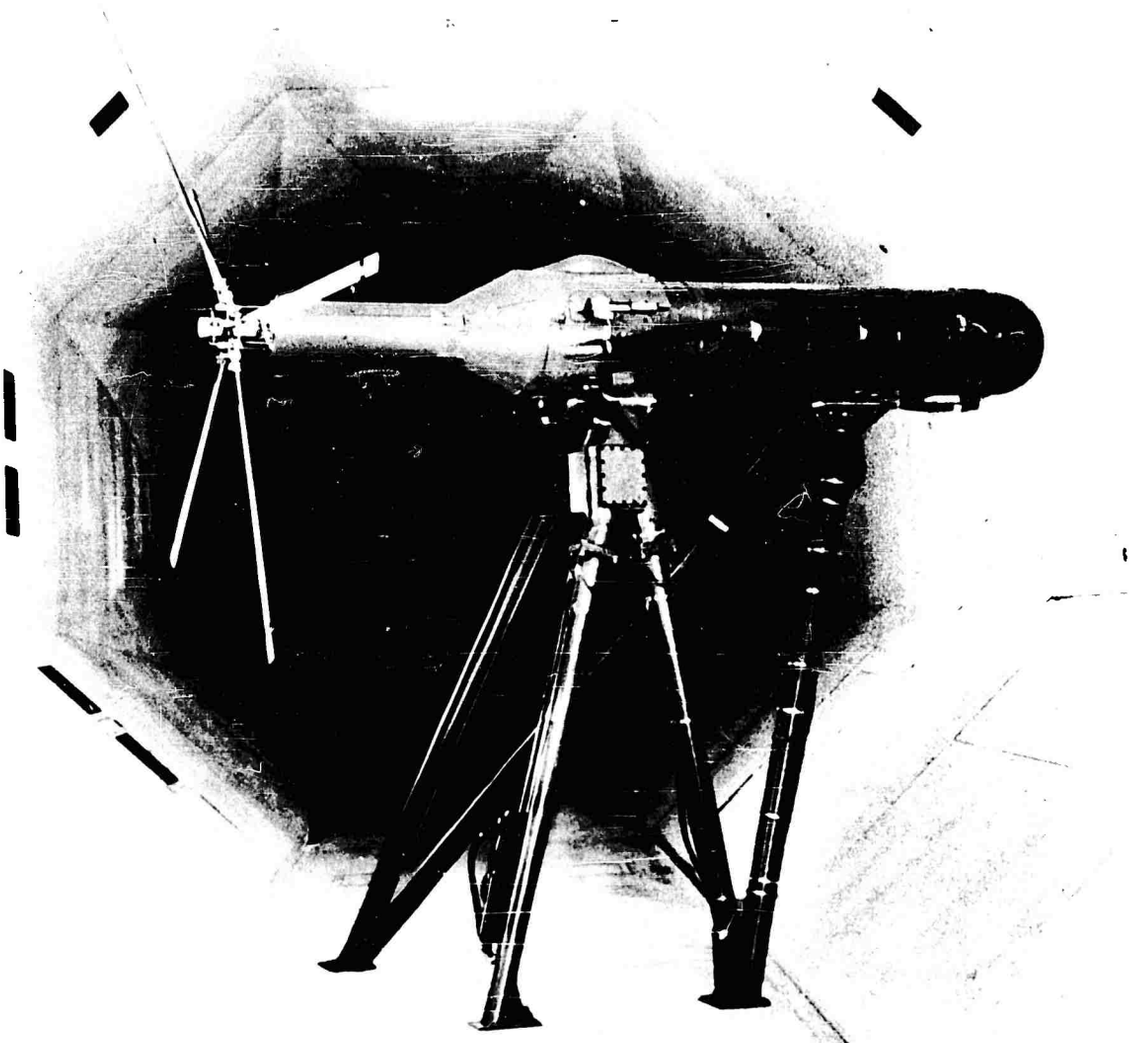

(a) General View of Model Installation in Wind Tunnel

FIG. 3. SHORT-SPAN HELICOPTER ROTOR TEST RIG

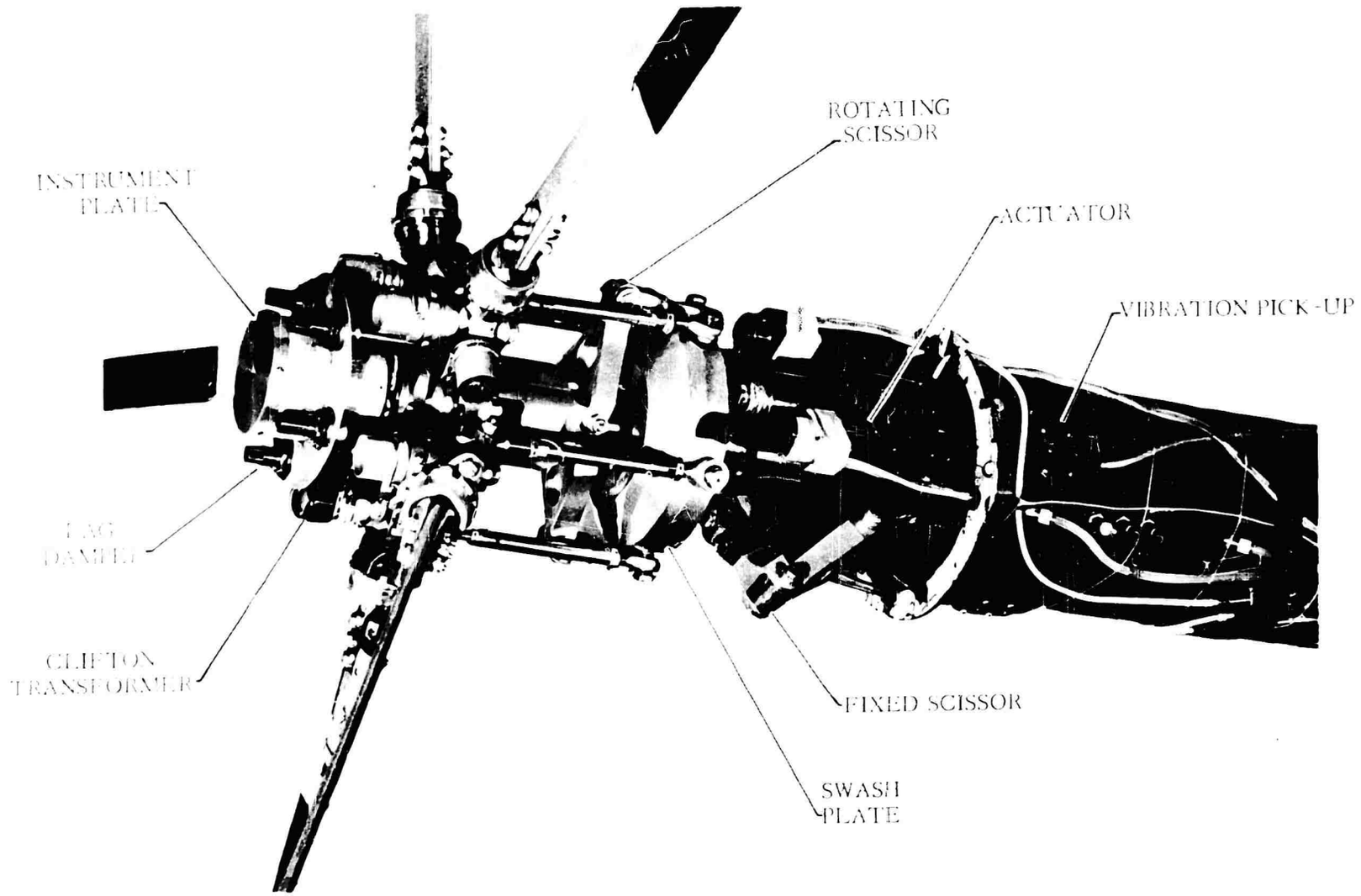

(b) Details of Hub and Swash Plate Area

FIGURE 5 CONCLUDED

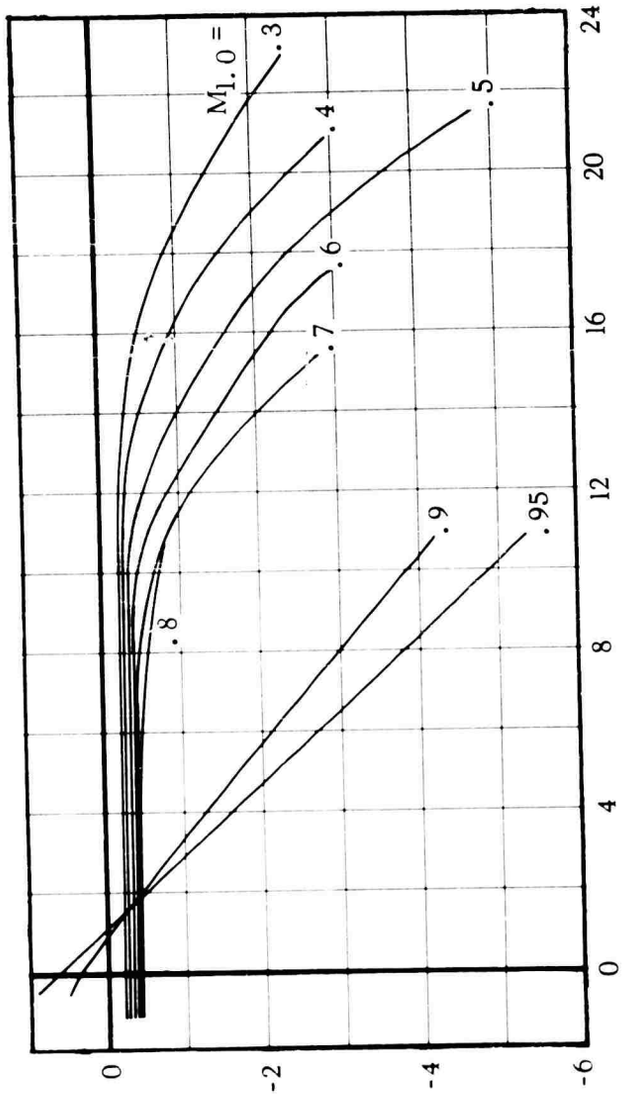

FIG. 6. EXPERIMENTAL DYNAMIC BLADE TWIST IN HOVERING

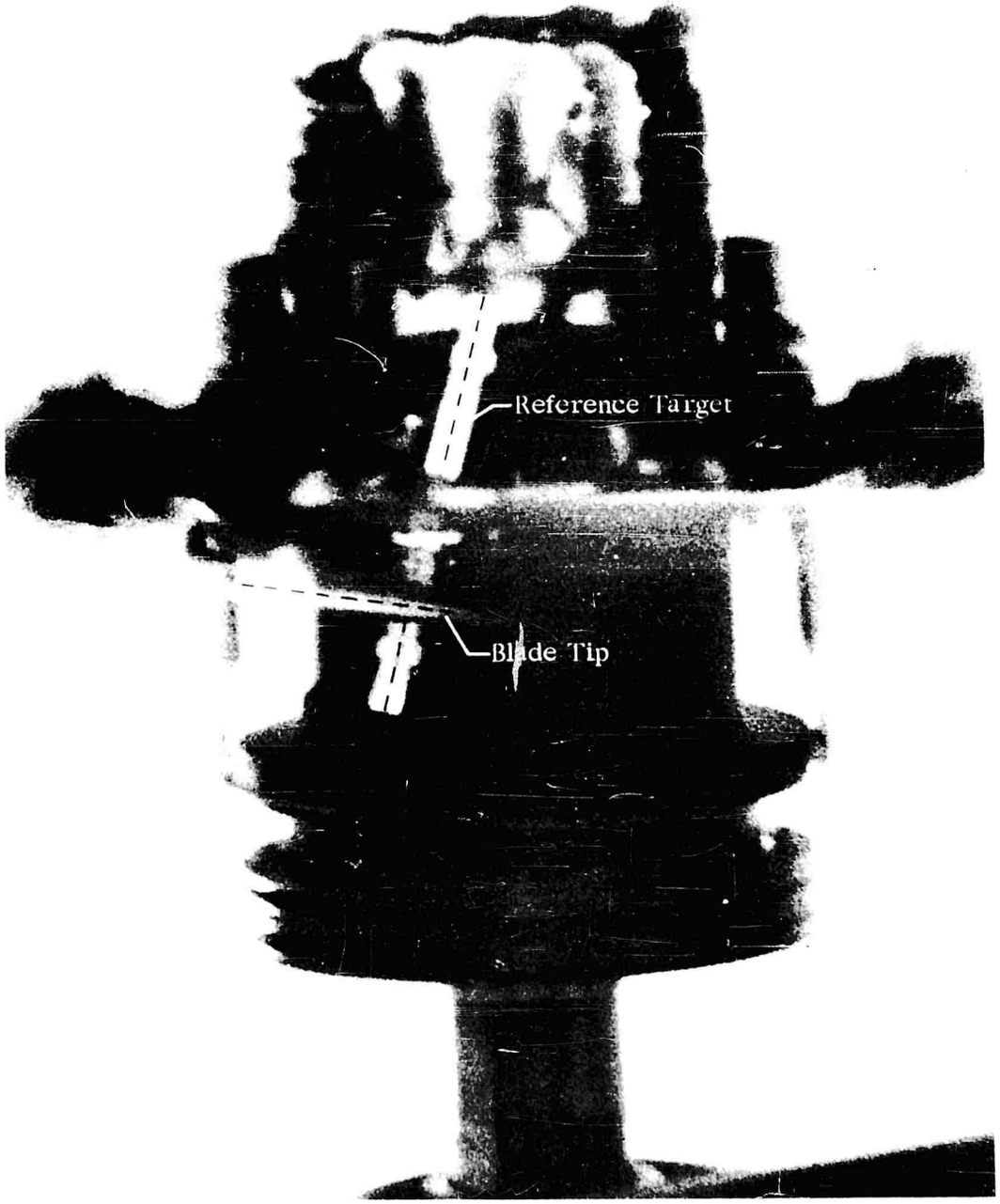

FIG. 7. EXAMPLE OF PHOTOGRAPHIC TECHNIQUE FOR MEASURING DYNAMIC TWIST IN HOVERING

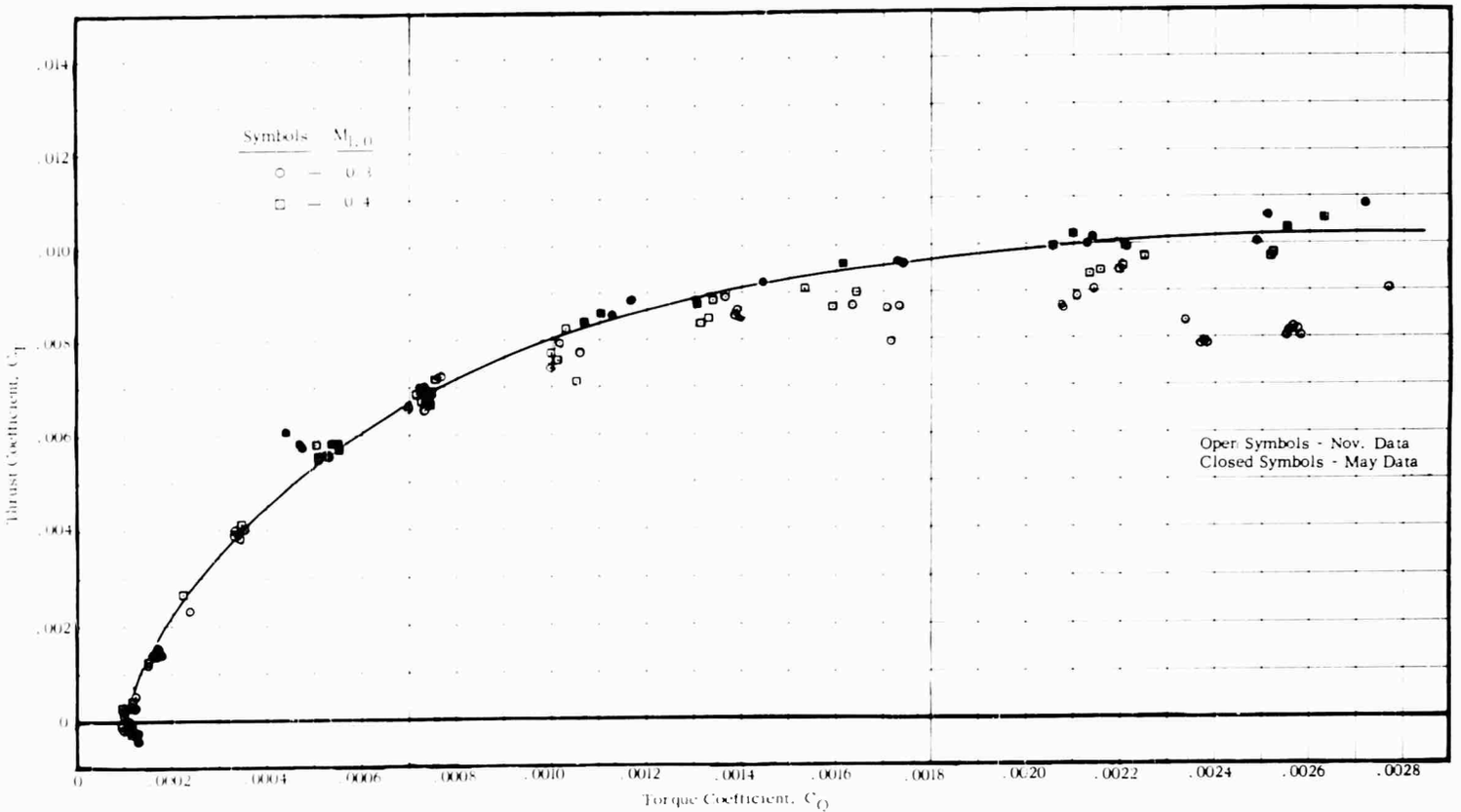

(a) Tip Mach Number = 0.3, 0.4

FIG. 8. EXPERIMENTAL ROTOR PERFORMANCE IN HOVERING

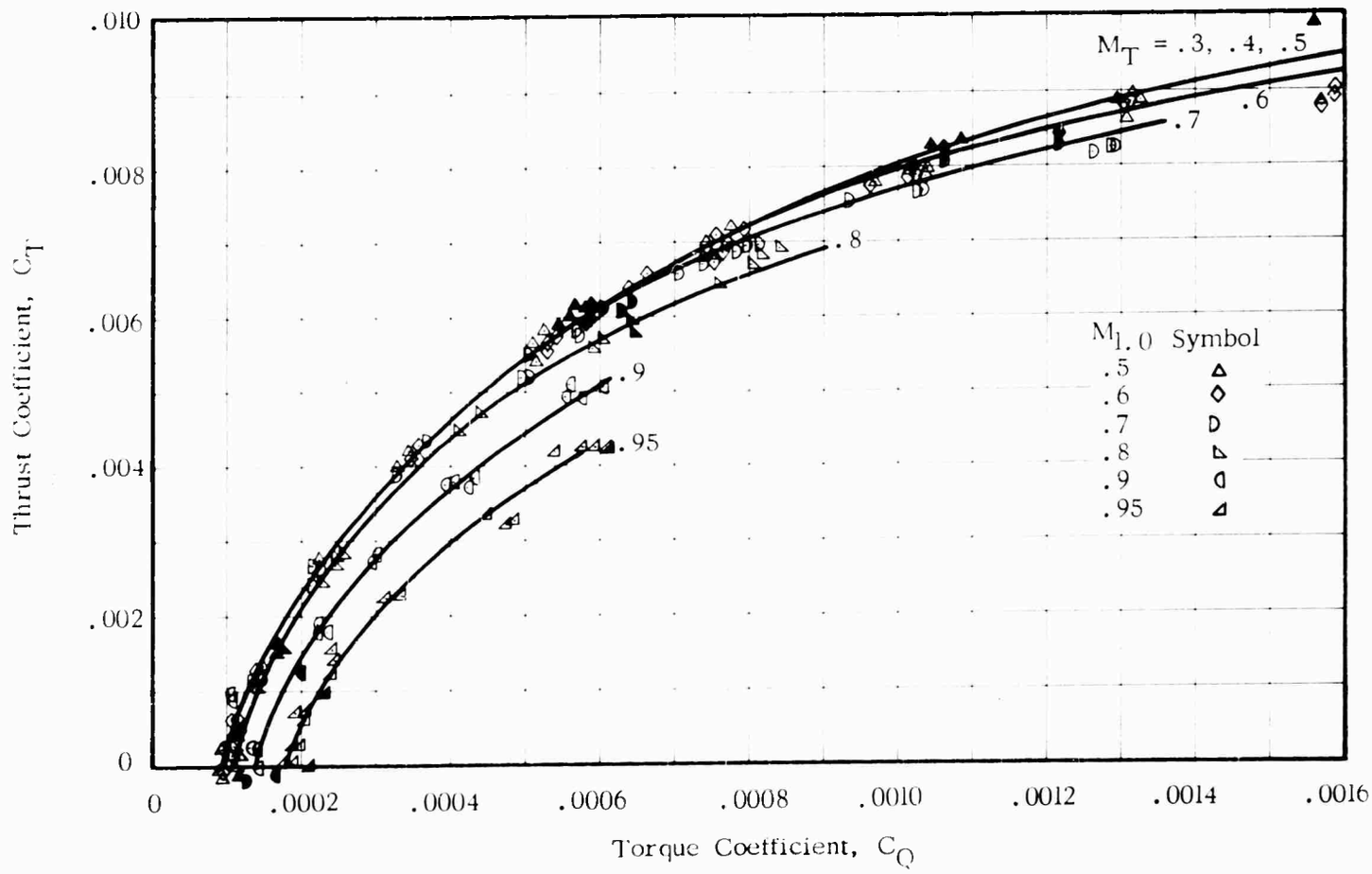

(b) Tip Mach Number = 0.3 - 0.95

Figure 8. -Concluded

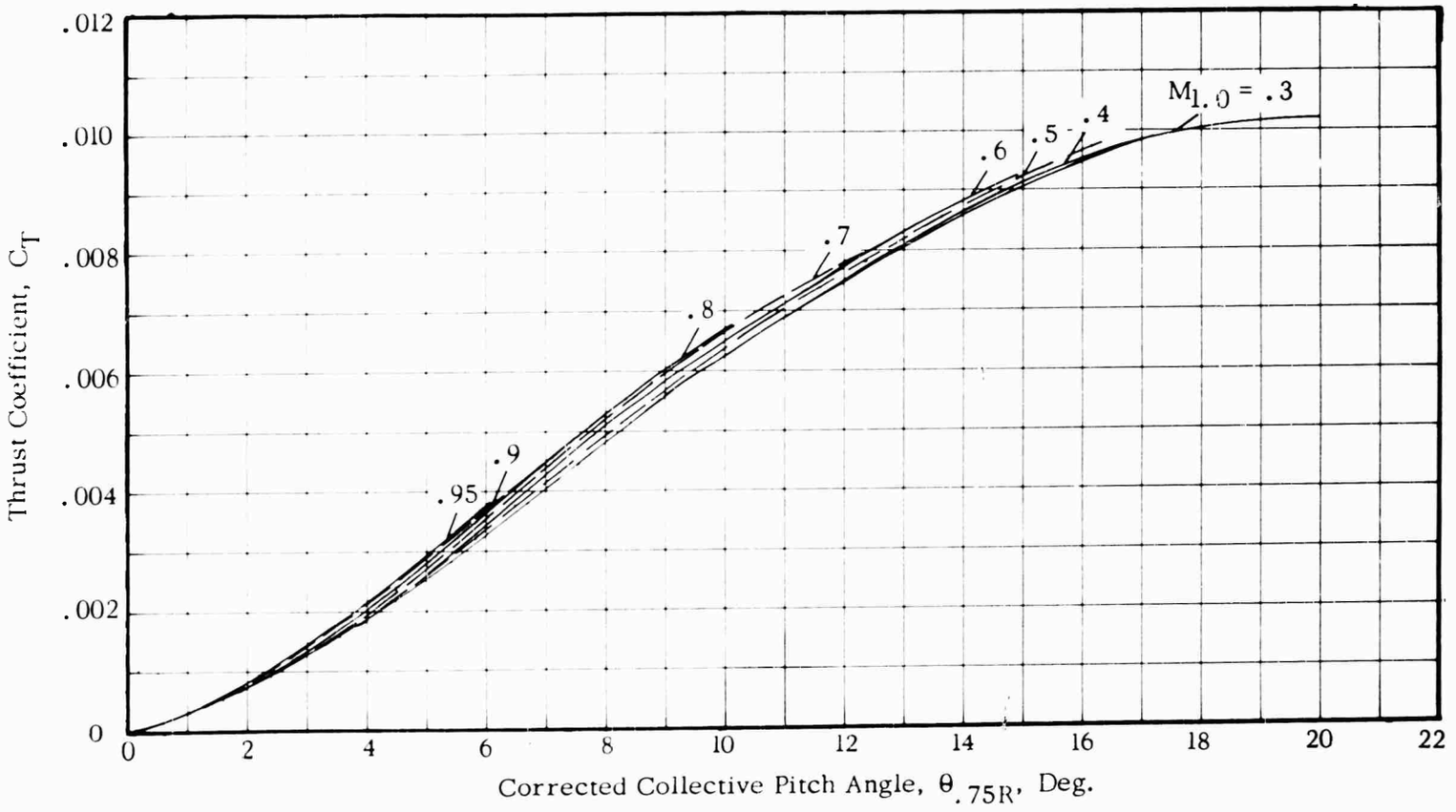

FIG. 9. THRUST COEFFICIENT VS CORRECTED COLLECTIVE PITCH

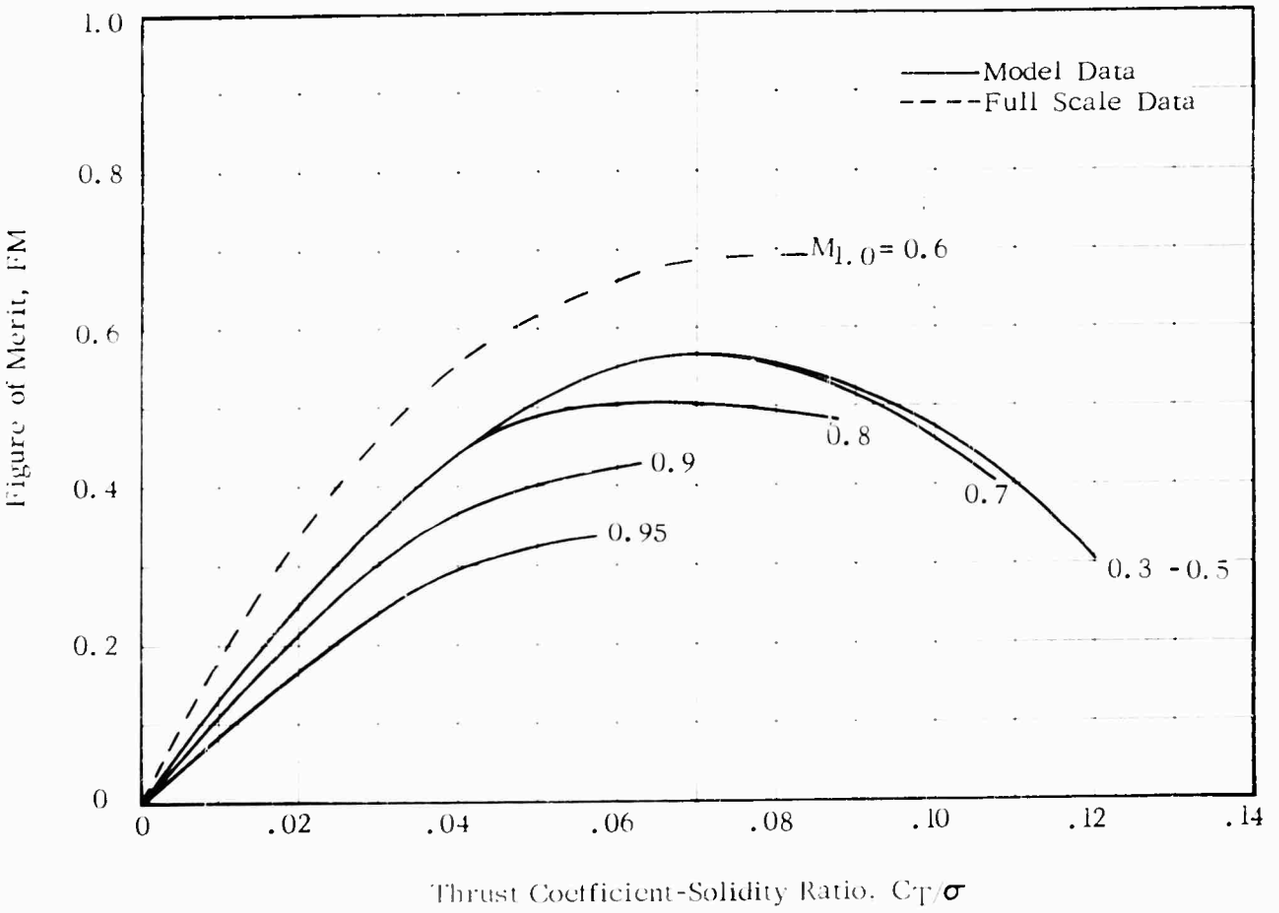

FIG. 10. EFFECT OF TIP MACH NUMBER ON ROTOR FIGURE OF MERIT

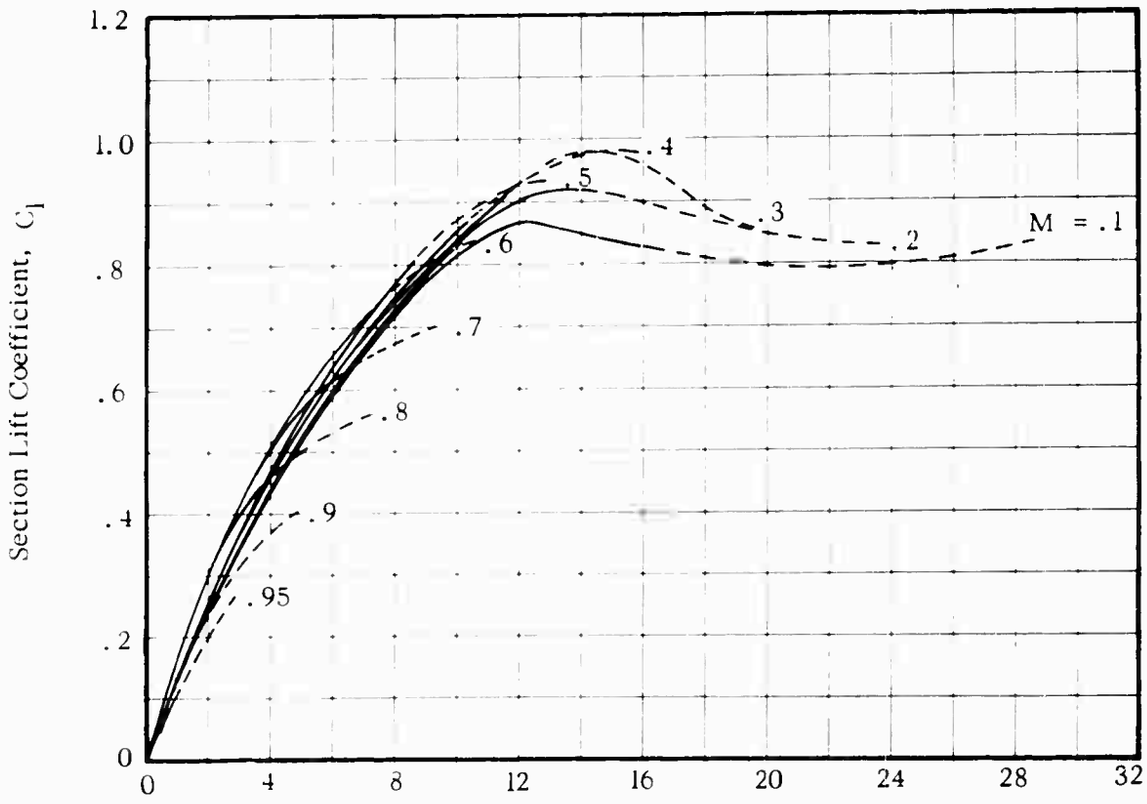

(a) C_l vs. α

FIG. 11. AIRFOIL SECTION CHARACTERISTICS

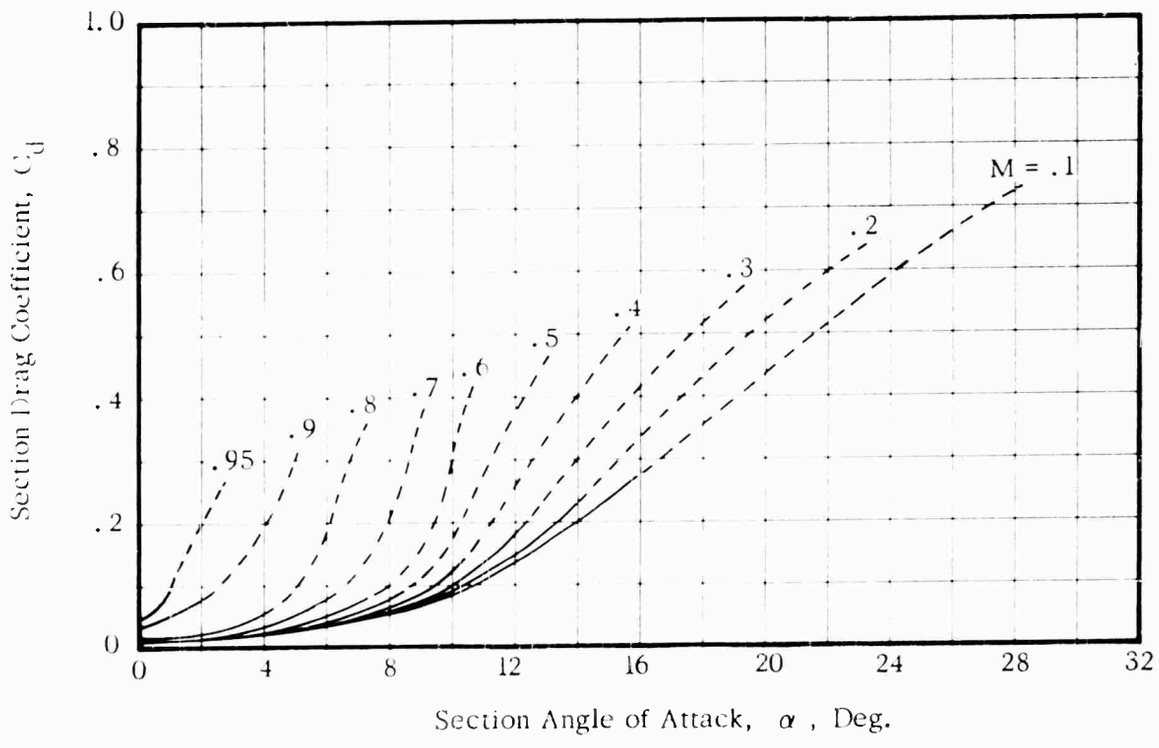

(b) C_d vs. α

Figure 11. - Continued

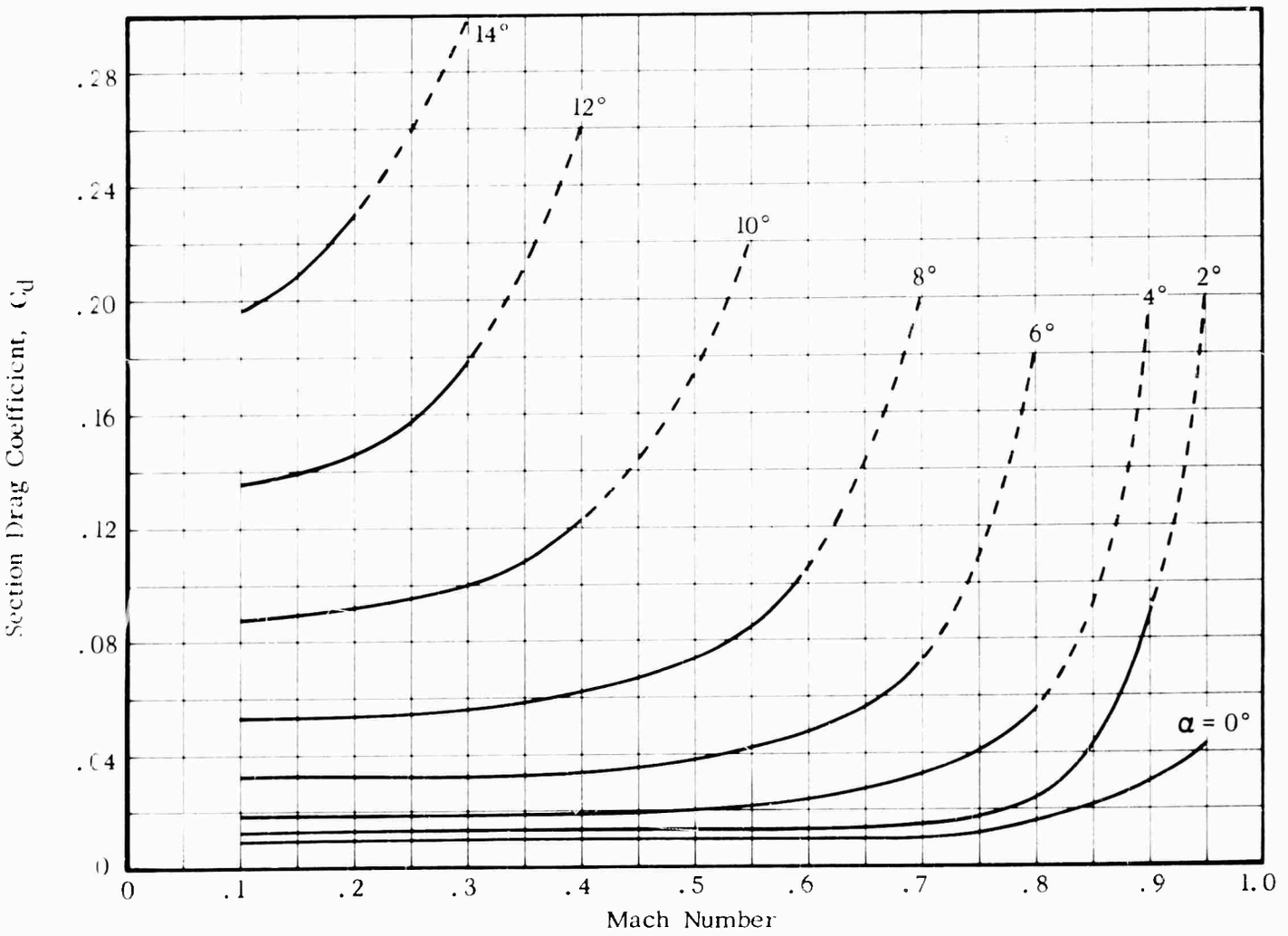

(c) C_d vs Mach Number

Figure 11. - Continued

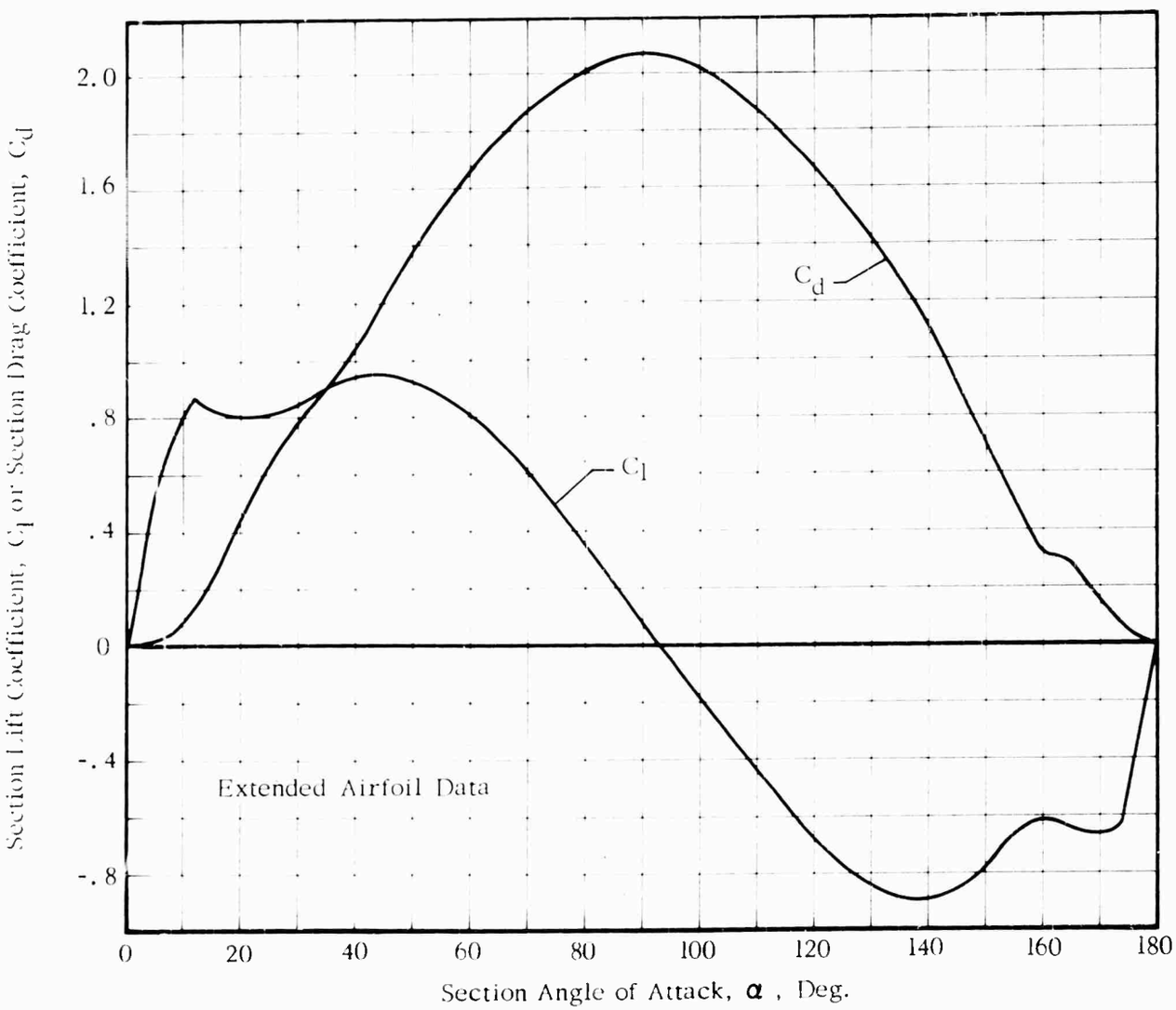

(d) C_l or C_d vs α, α = 0 - 180 Deg.

Figure 11. - Concluded

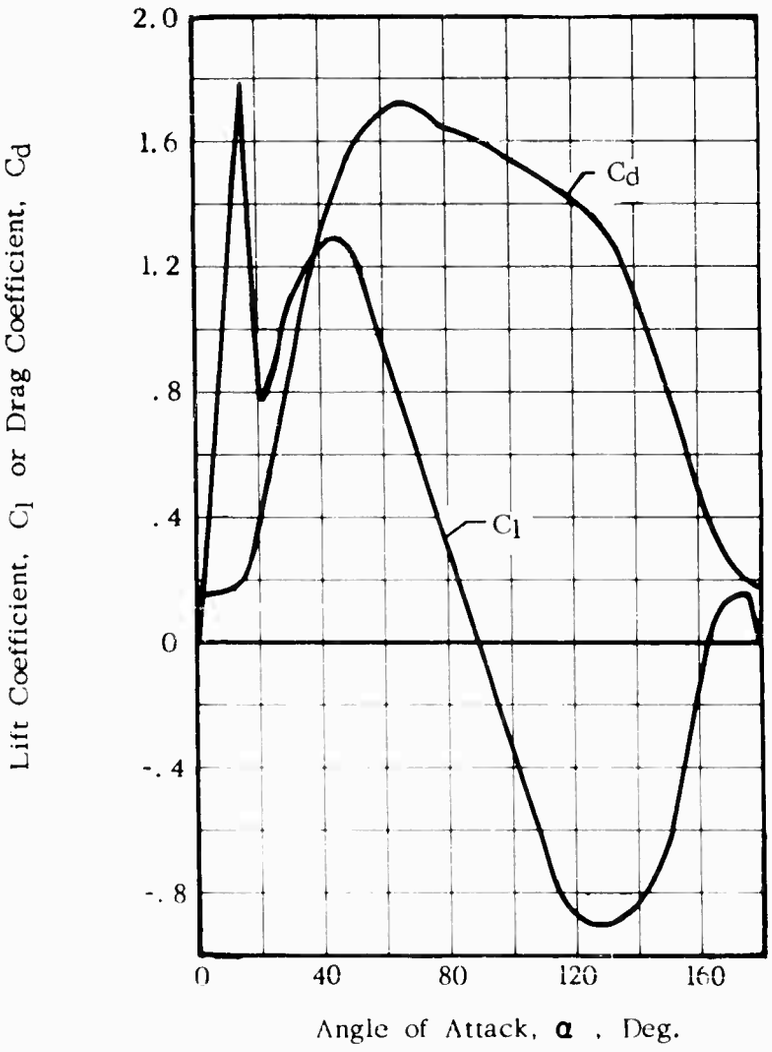

FIG. 12. SPAR SECTION LIFT AND DRAG COEFFICIENTS

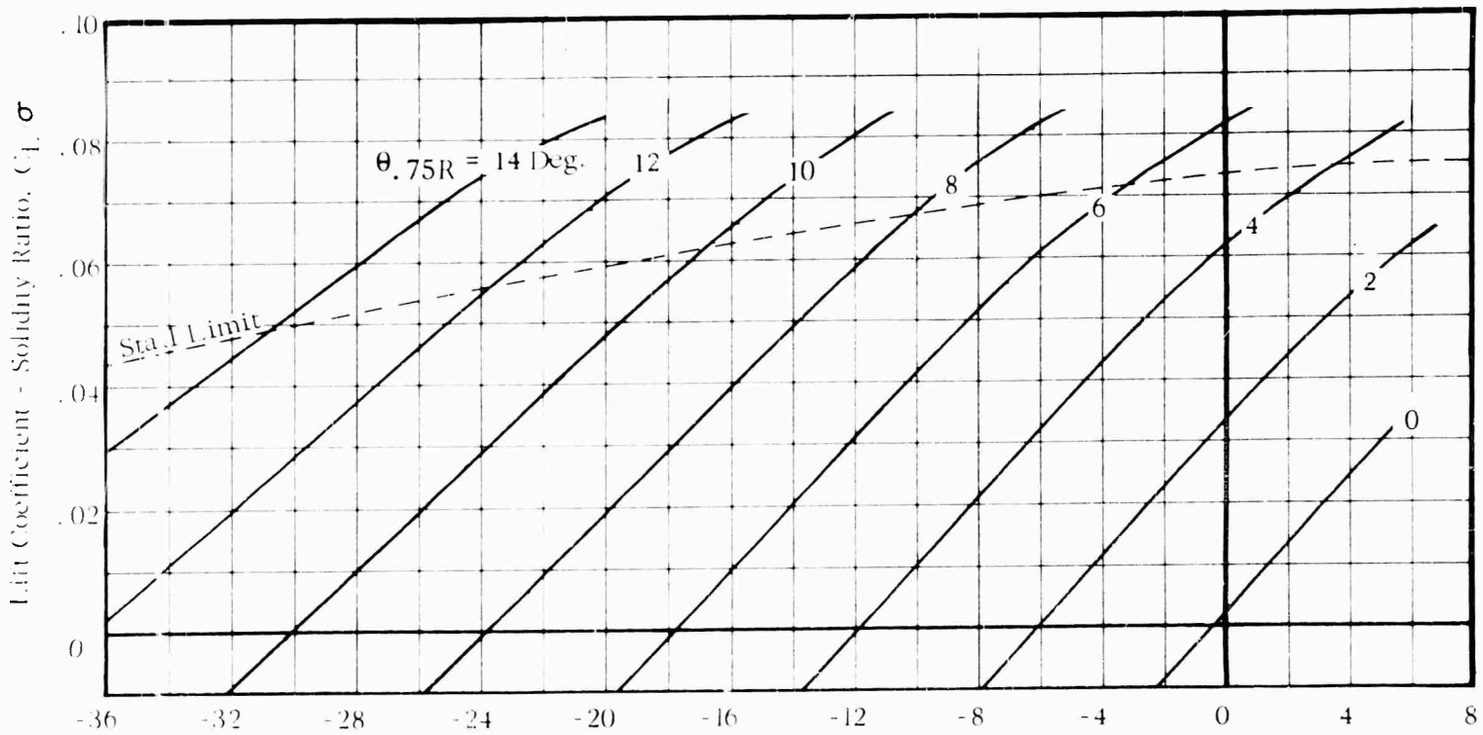

(a) C_L/σ vs α

FIG. 13. THEORETICAL ROTOR PERFORMANCE AND BLADE MOTIONS

V = 100 Kts. ΩR = 650 Ft/Sec. μ = 0.26

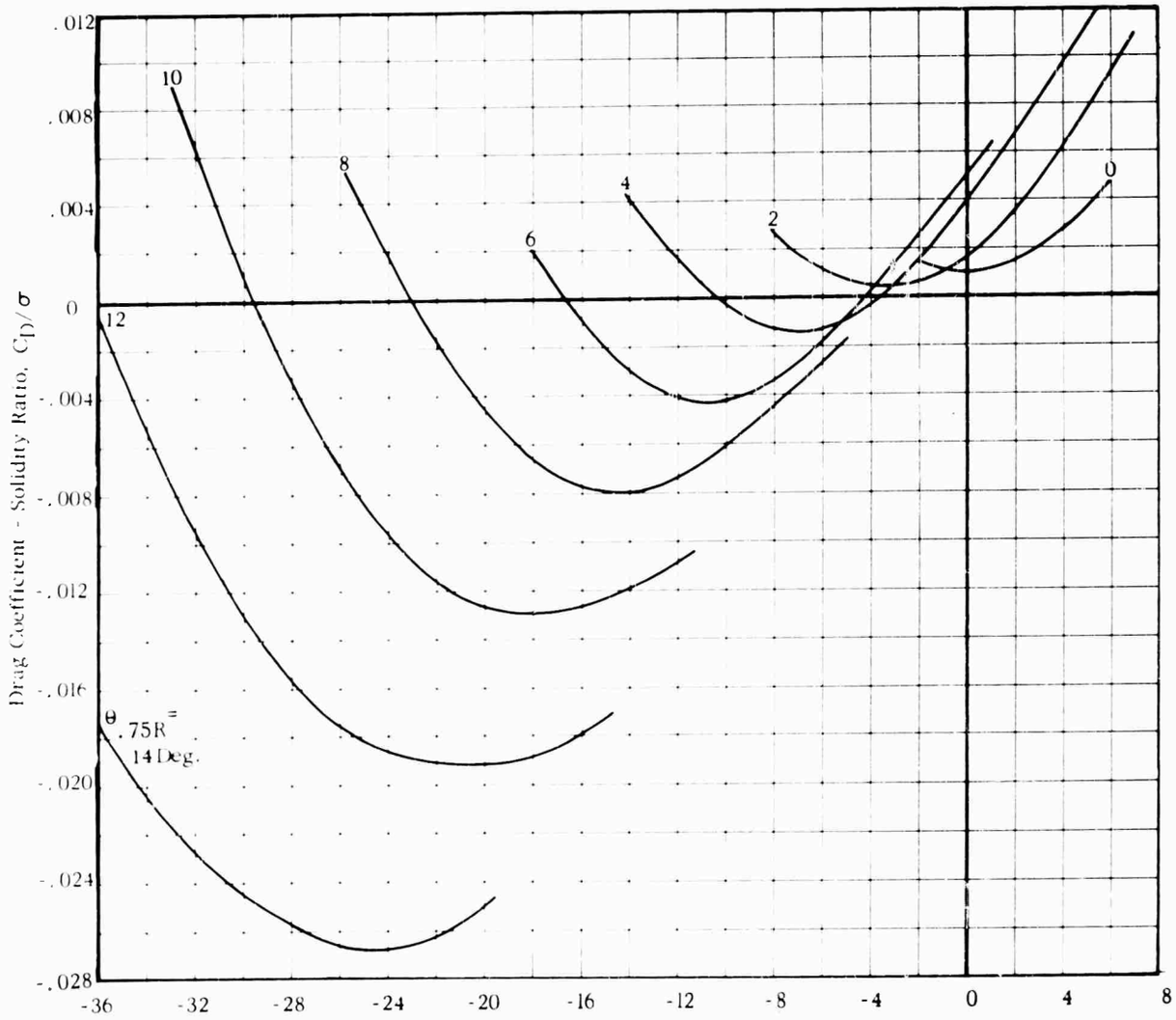

(b) C_D/σ vs α

Figure 13. -Continued

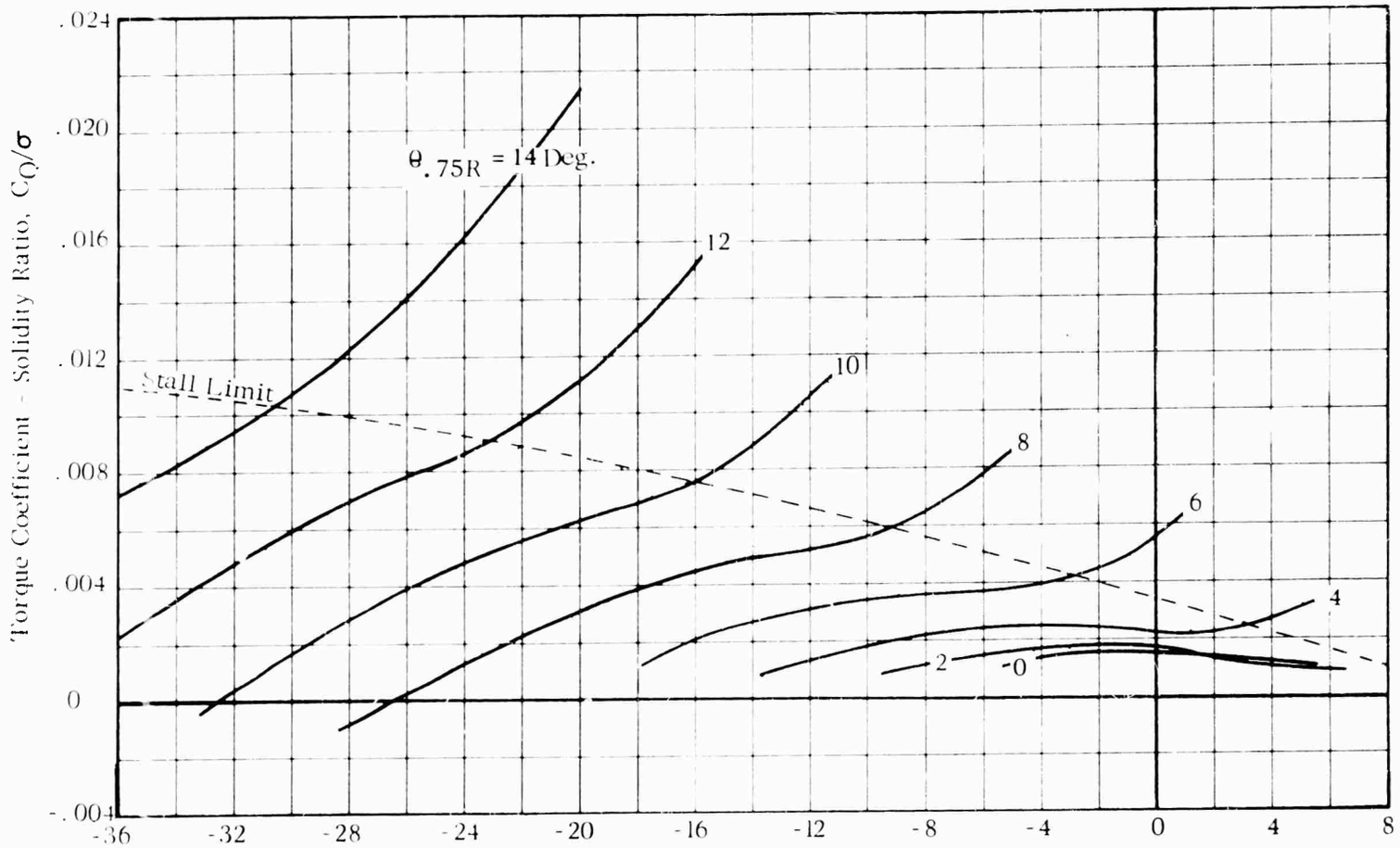

(c) C_Q/σ vs α

Figure 13. -Continued

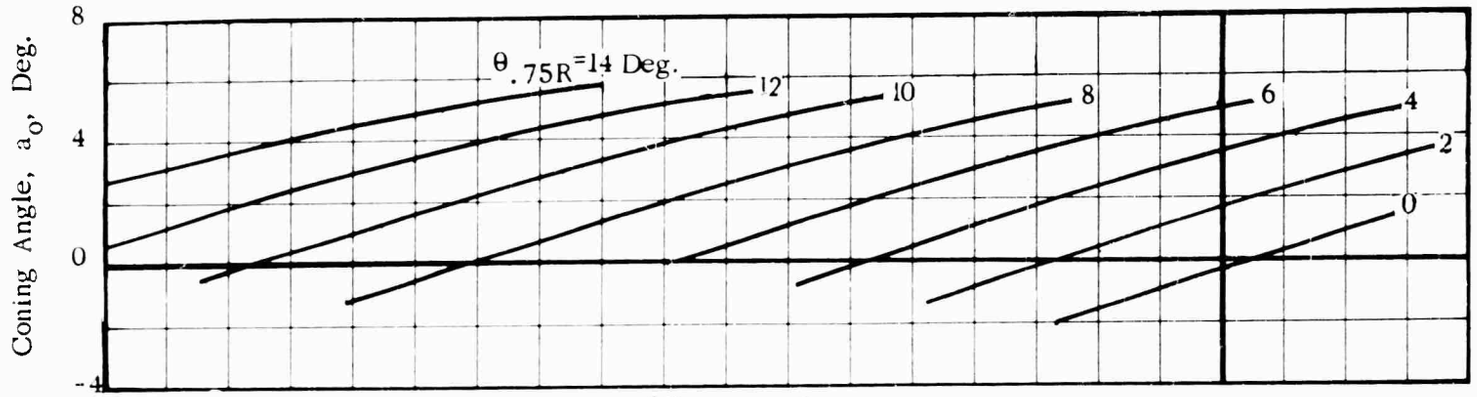

(d) a_o vs α

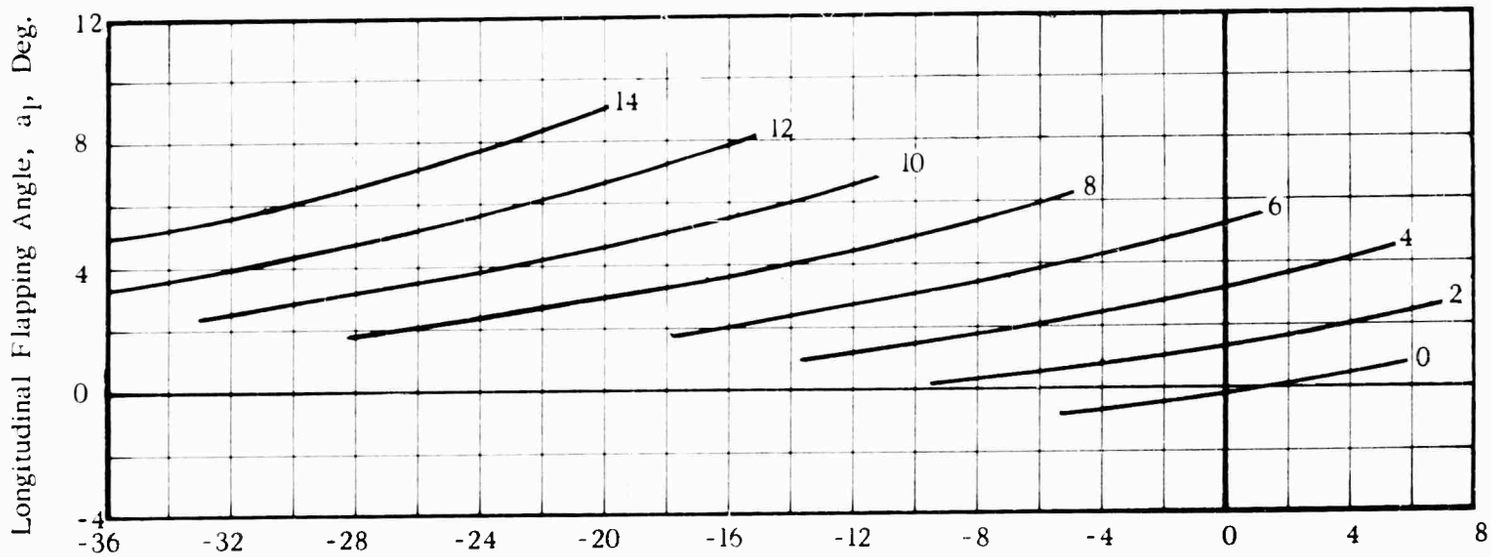

(e) a_1 vs α

Figure 13. -Continued

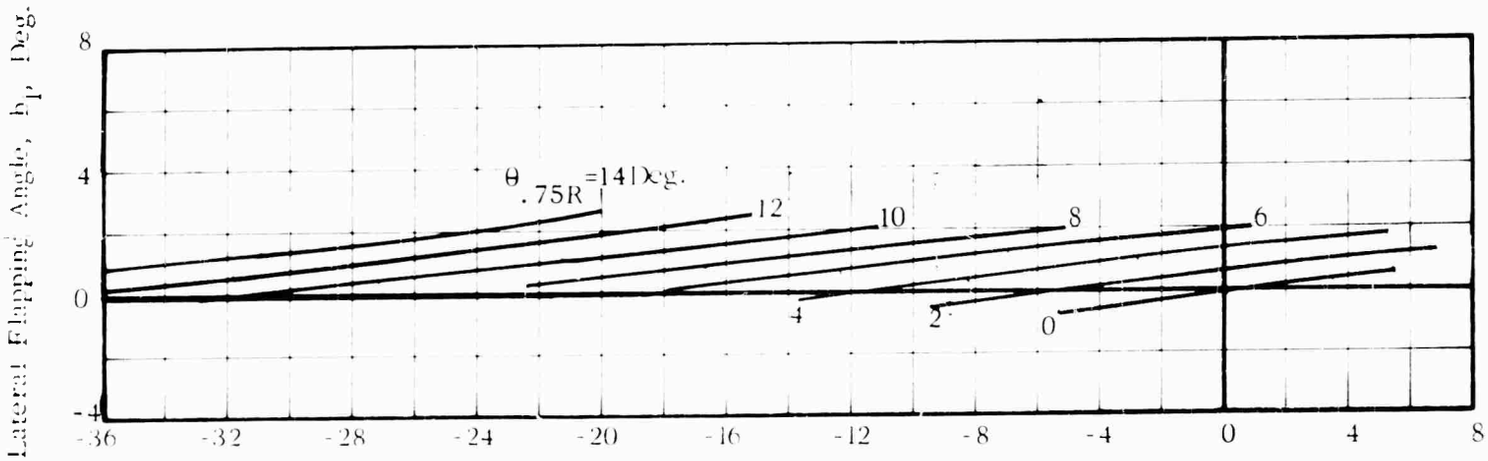

(f) b_1 vs α

Figure 13. -Concluded

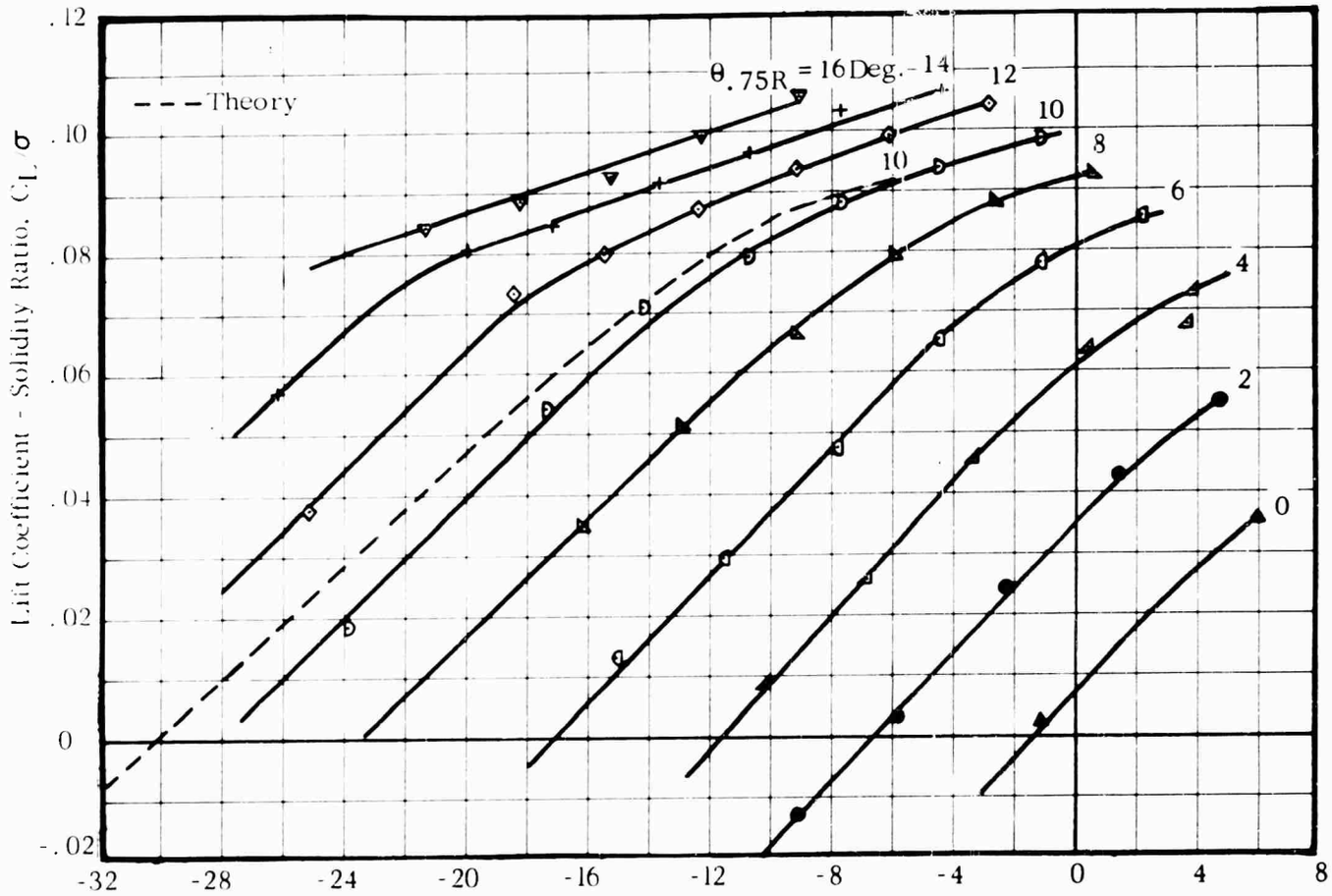

(a) C_L/σ vs α

FIG. 14. EXPERIMENTAL ROTOR PERFORMANCE AND BLADE MOTIONS

V = 100 Kts. ΩR = 650 Ft/Sec. μ = 0.26

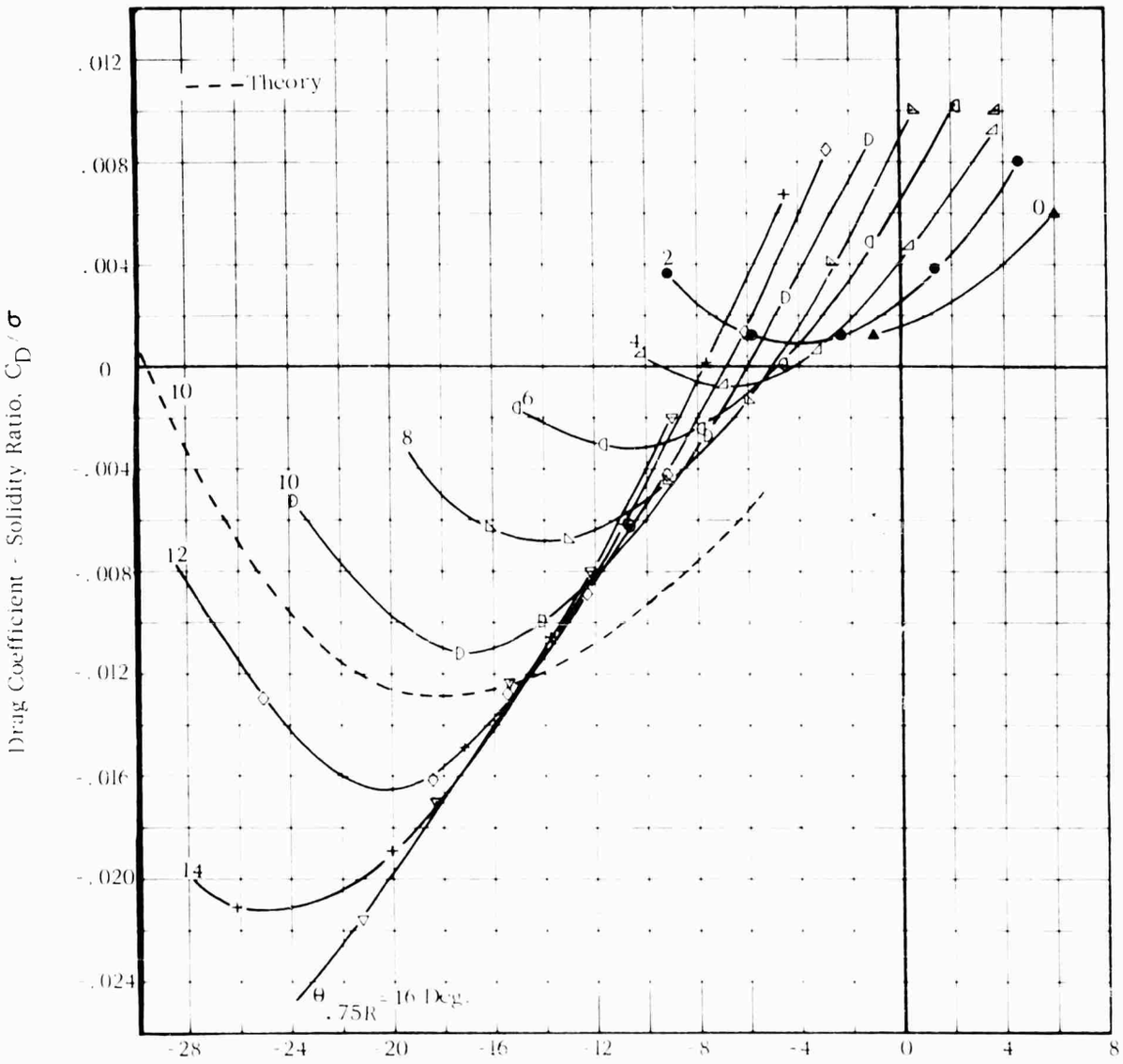

(b) C_D/σ vs α

Figure 14. -Continued

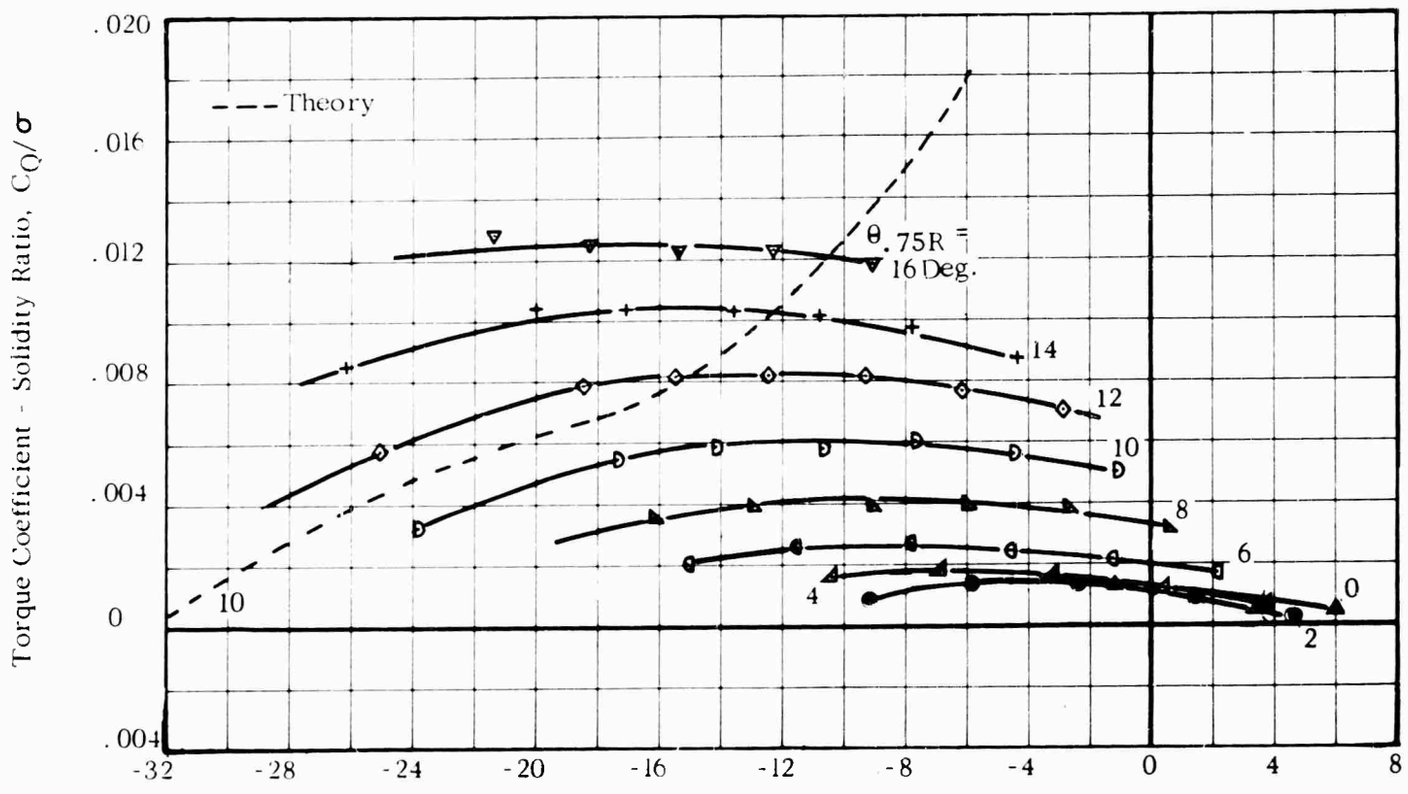

(c) C_Q/σ vs α

Figure 14. -Continued

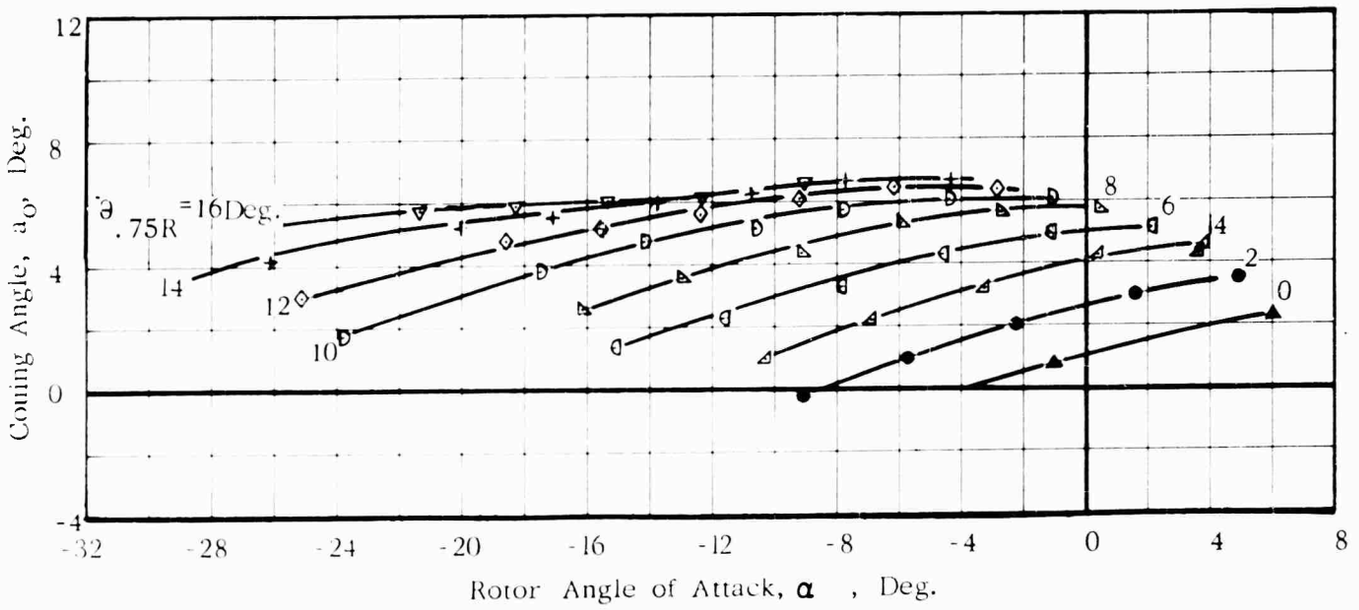

(d) a_o vs α

Figure 14. -Continued

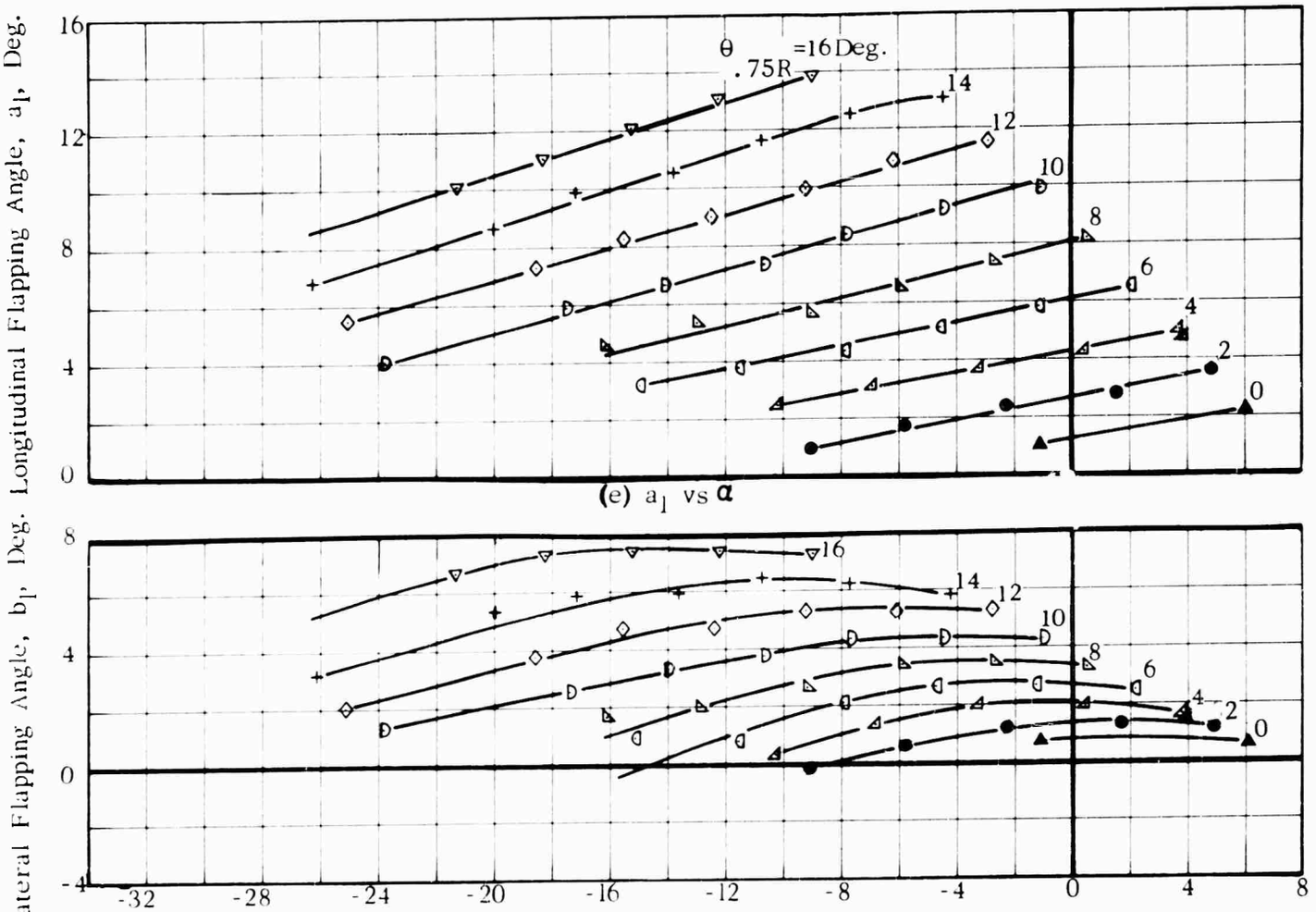

(e) a_1 vs α

(f) b_1 vs α

Figure 14. -Concluded

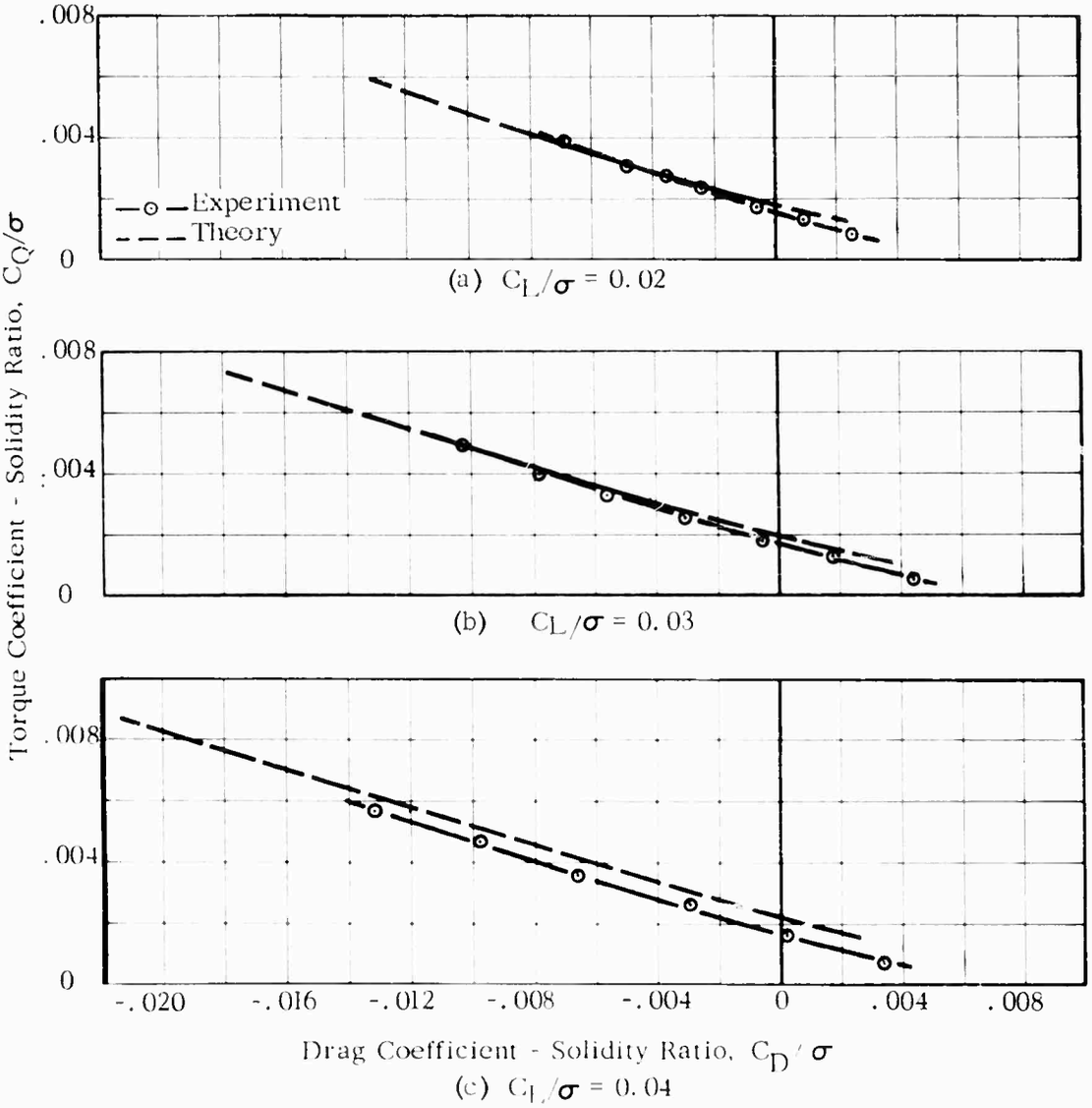

FIG. 15. COMPARISON OF THEORETICAL AND EXPERIMENTAL ROTOR POWER REQUIRED AT CONSTANT LIFT

V = 100 Kts. ΩR = 650 Ft/Sec. μ = 0.26

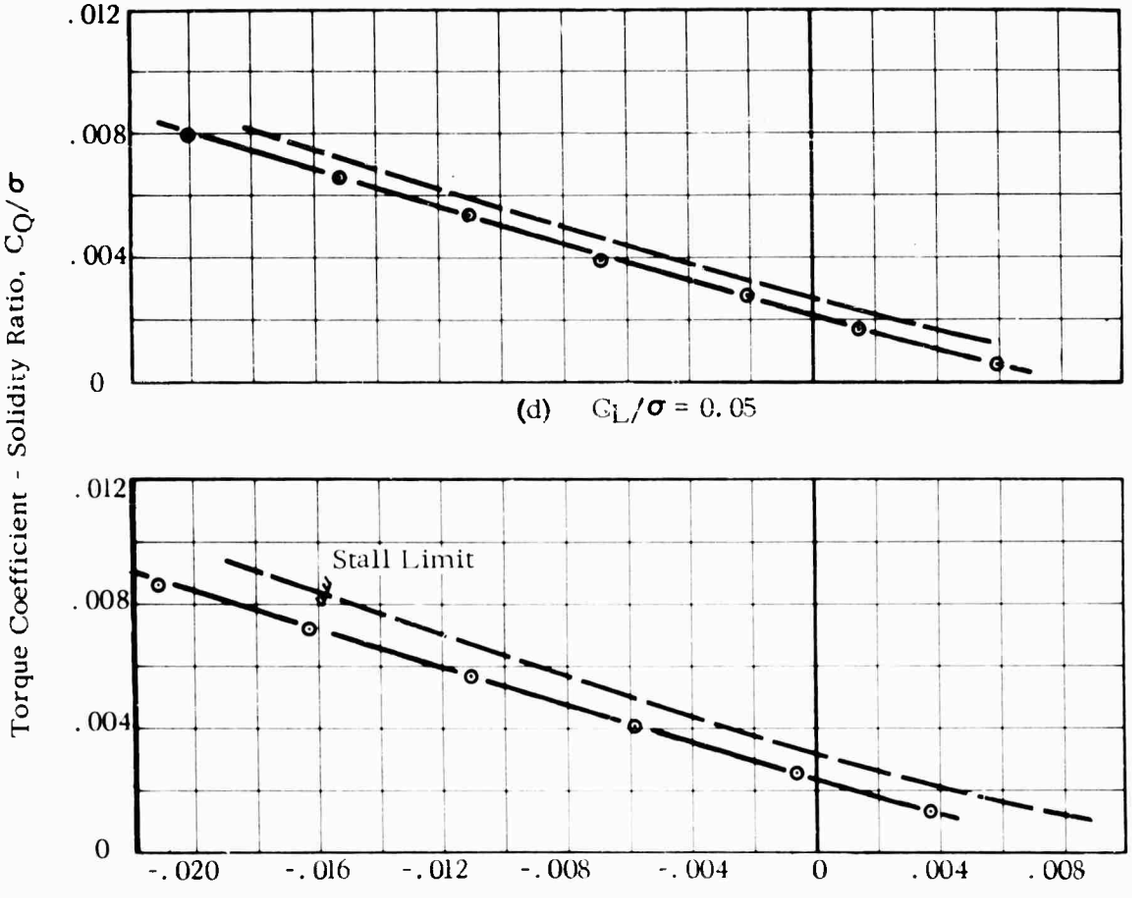

(d) $C_L/\sigma = 0.05$

(e) $C_L/\sigma = 0.06$

Figure 15. -Continued

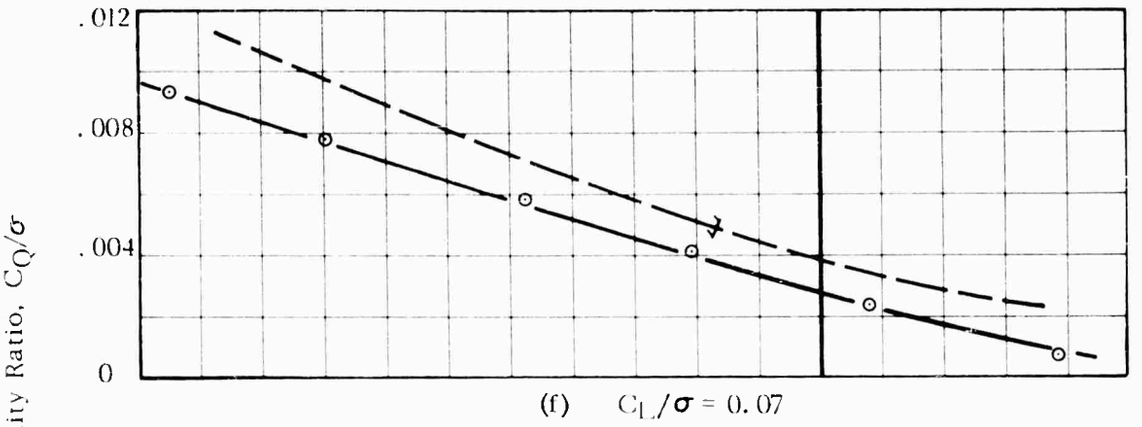

(f) $C_L/\sigma = 0.07$

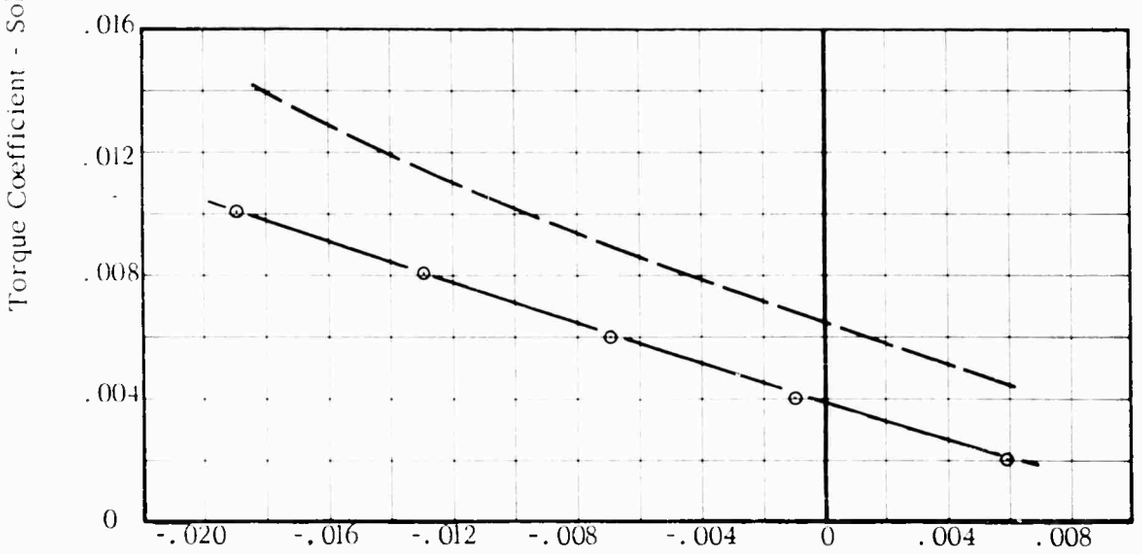

Torque Coefficient - Solidity Ratio, C_Q/σ

Drag Coefficient - Solidity Ratio, C_D/σ

(g) $C_L/\sigma = 0.08$

Figure 15. -Concluded

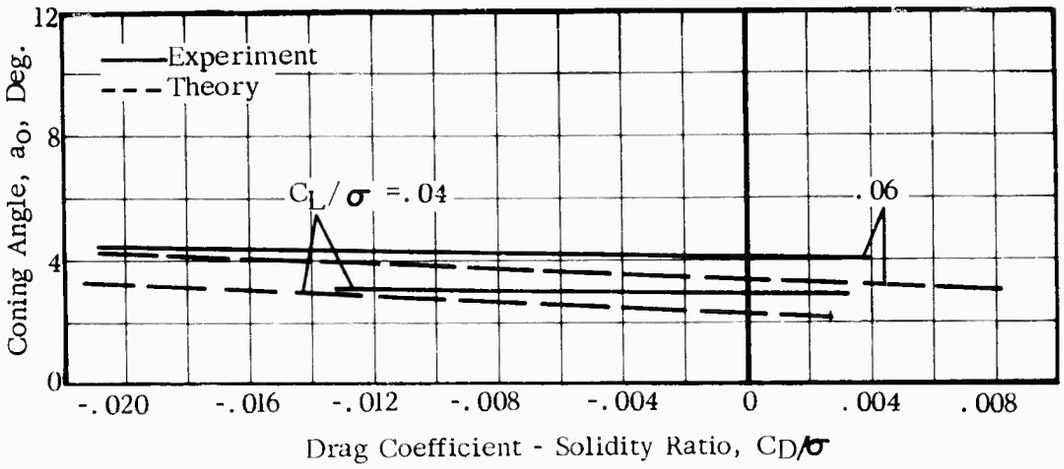

(a) Coning Angle, a_o, Deg.

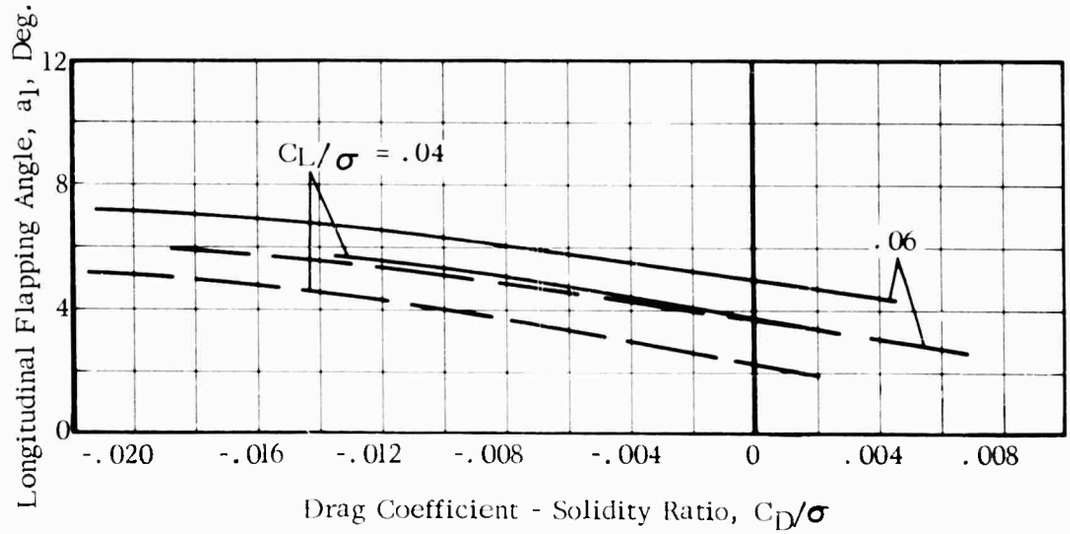

(b) Longitudinal Flapping Angle, a_1, Deg.

FIG.16. COMPARISON OF THEORETICAL AND EXPERIMENTAL BLADE MOTIONS

V = 100 Kts. ΩR = 650 Ft/Sec. μ = 0.26

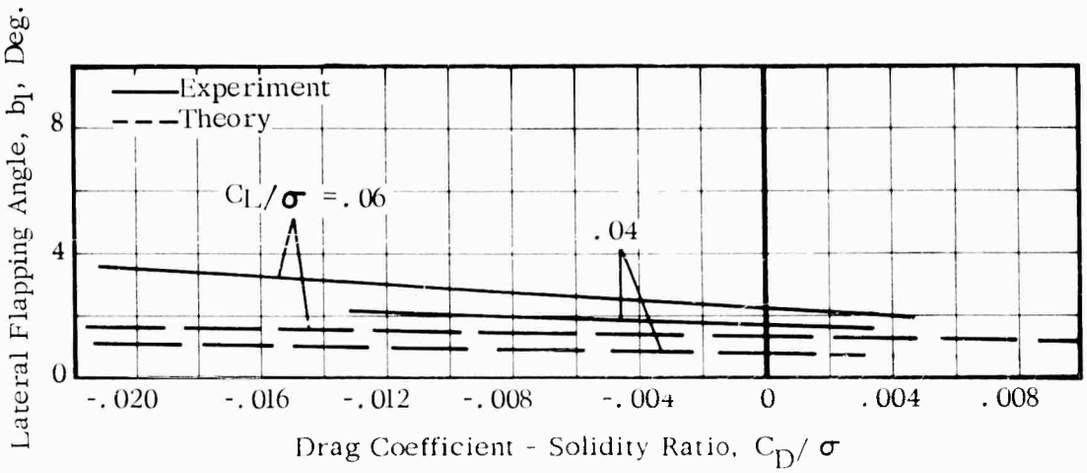

(c) Lateral Flapping Angle, b_1, Deg.

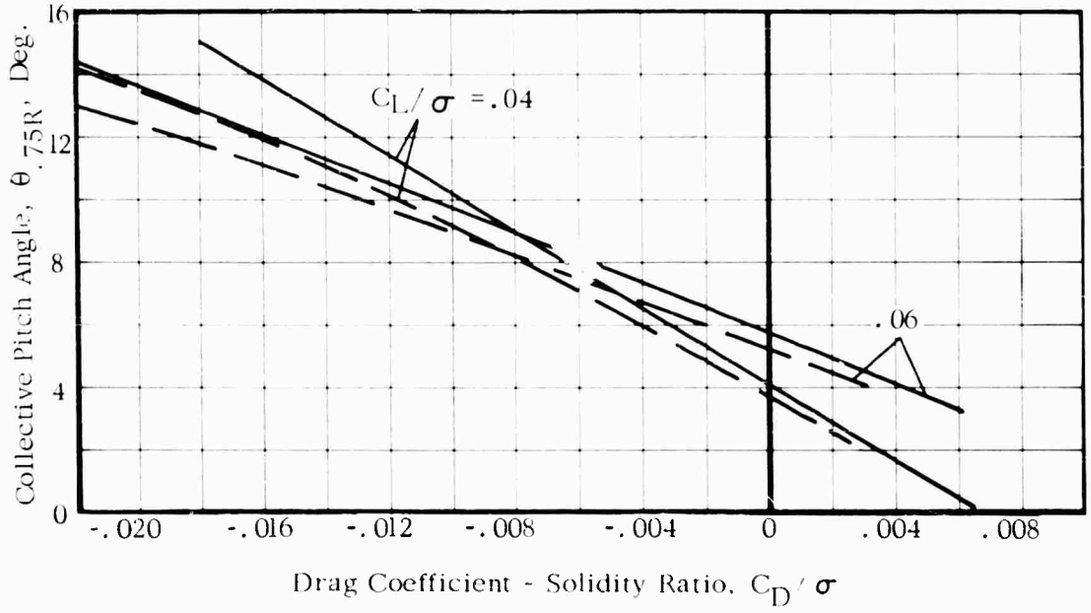

(d) Collective Pitch Angle, $\theta_{.75R}$, Deg.

Figure 16. -Concluded

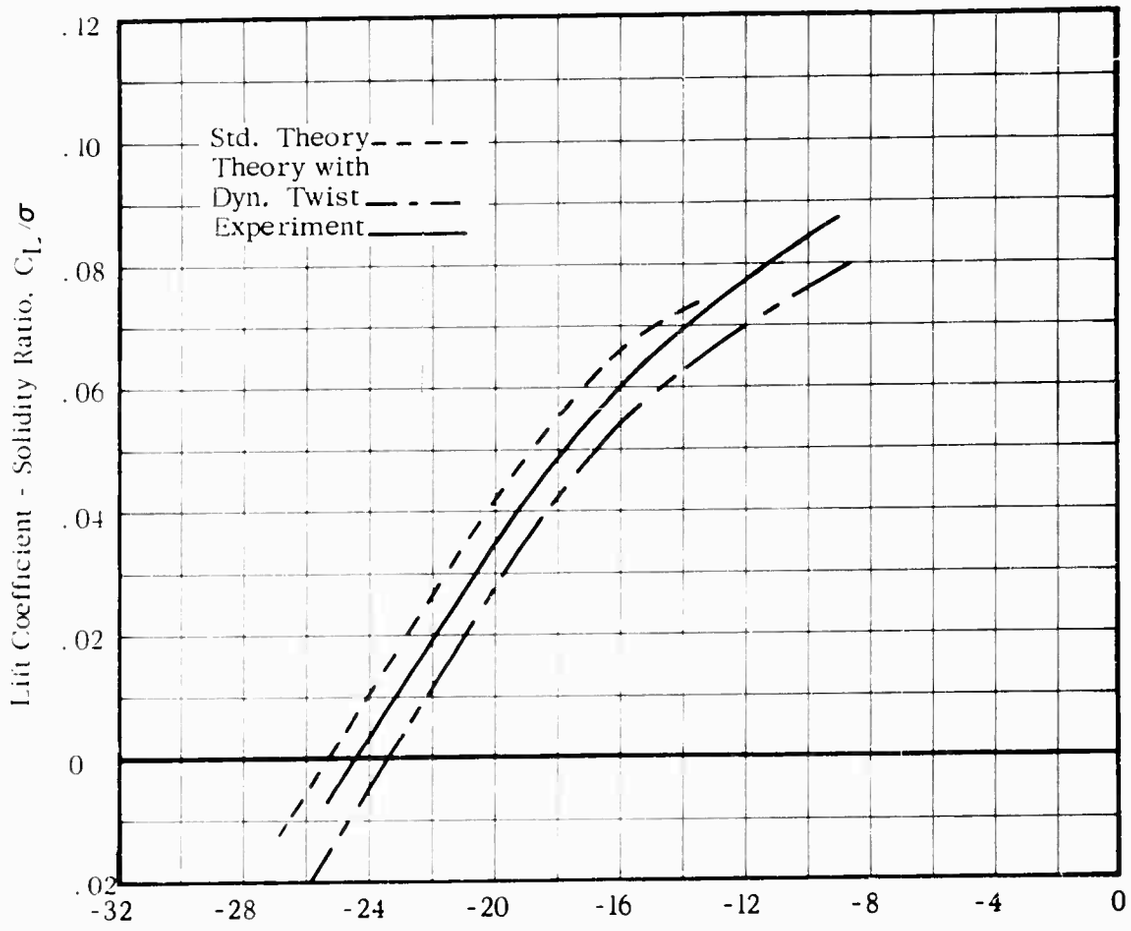

(a) C_L/σ vs α

FIG. 17. EFFECT OF DYNAMIC TWIST ON ROTOR PERFORMANCE IN FORWARD FLIGHT

V = 150 Kts. ΩR = 650 Ft/Sec. μ = 0.39 $\theta_{.75R} = 12°$

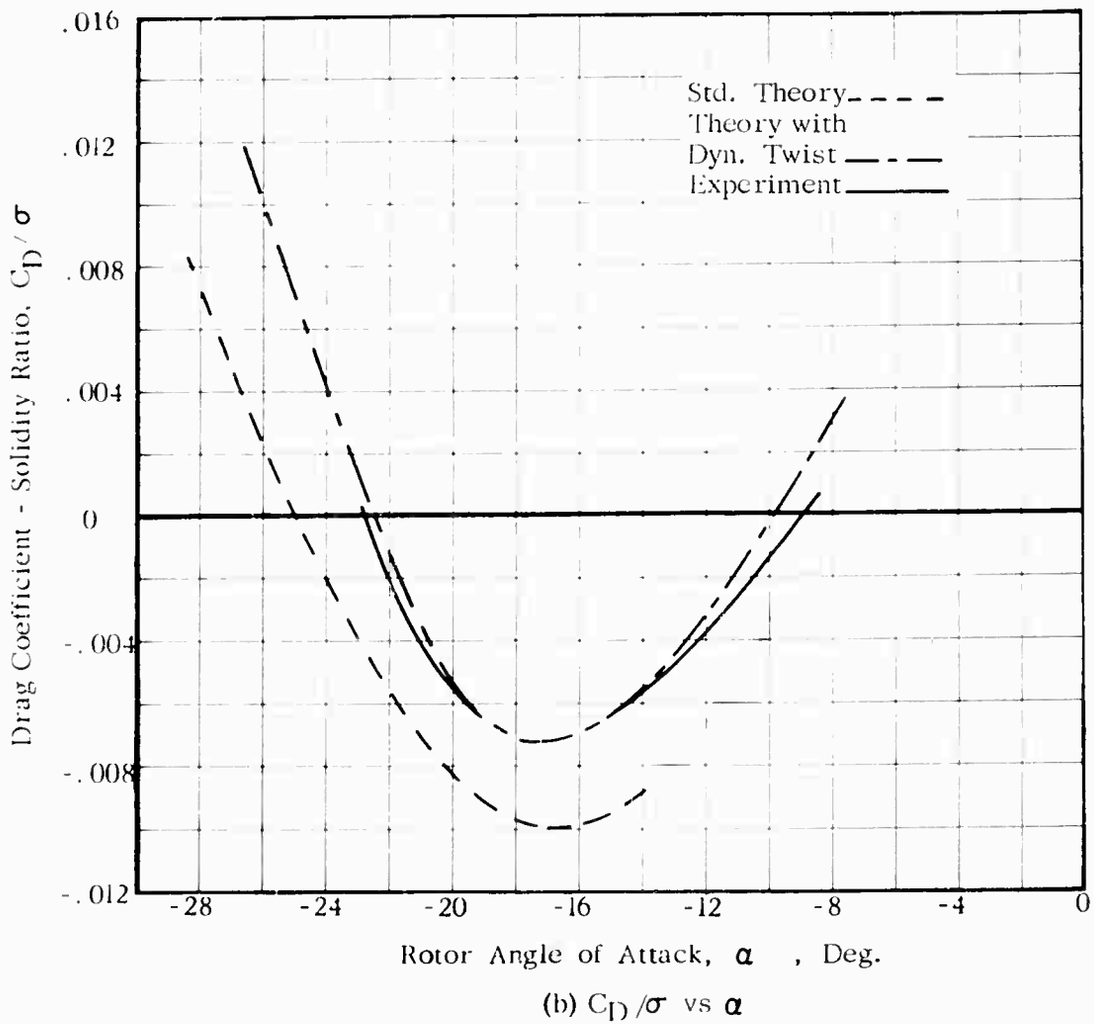

(b) C_D/σ vs α

Figure 17. -Continued

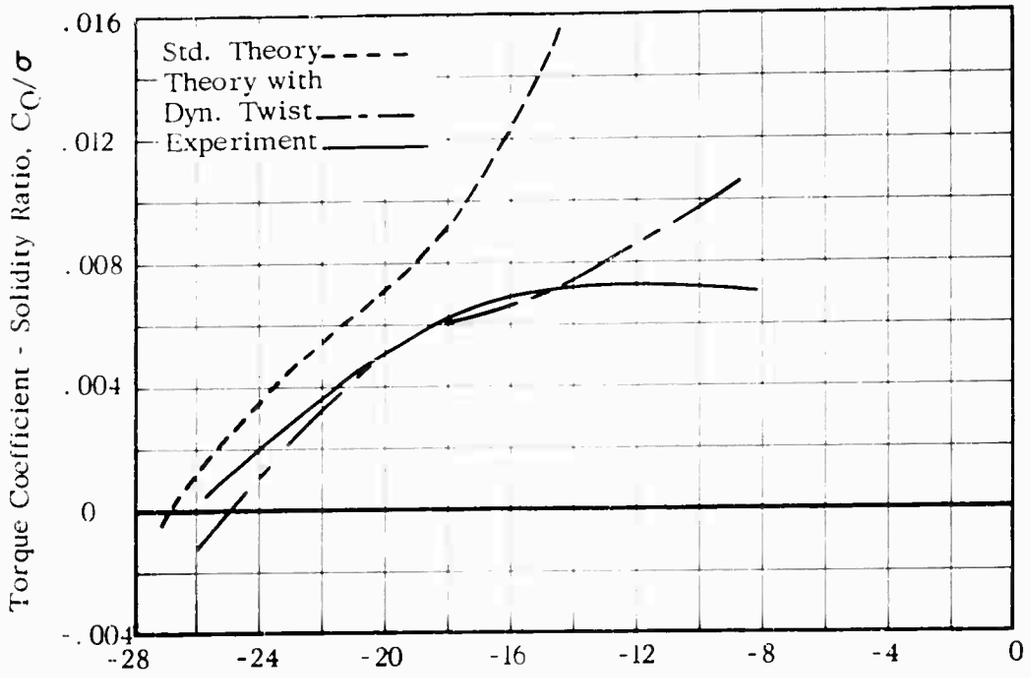

(c) C_Q/σ vs α

Figure 17. -Continued

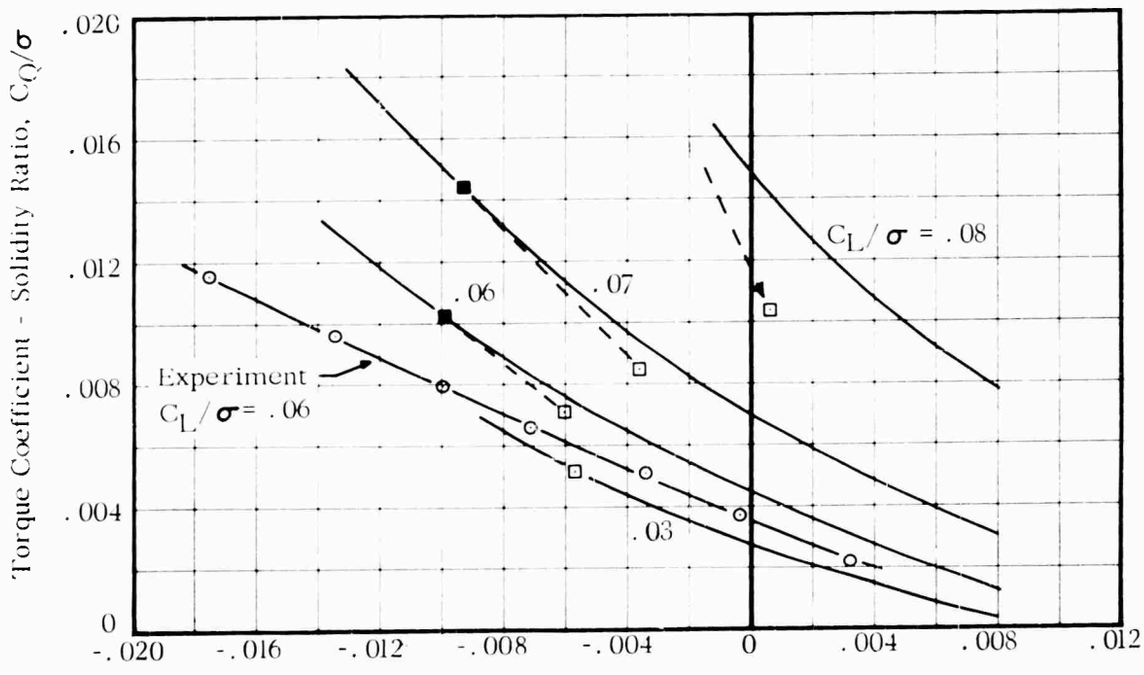

(d) C_Q/σ vs C_D/σ

Figure 17. -Concluded

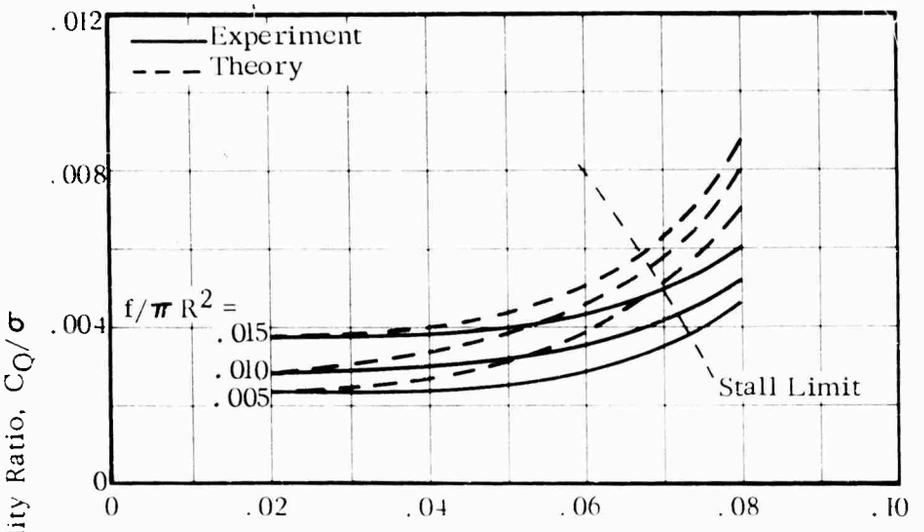

(a) V = 100 Kts., μ = .26

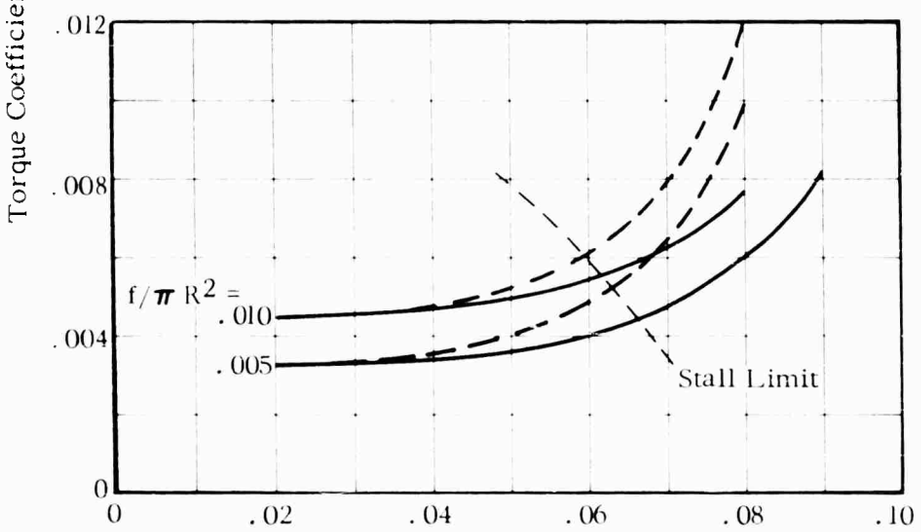

(b) V = 125 Kts., μ = .32

FIG. 18. COMPARISON OF THEORETICAL AND EXPERIMENTAL ROTOR POWER REQUIRED AT CONSTANT PARASITE DRAG, ΩR = 650 FT/SEC.

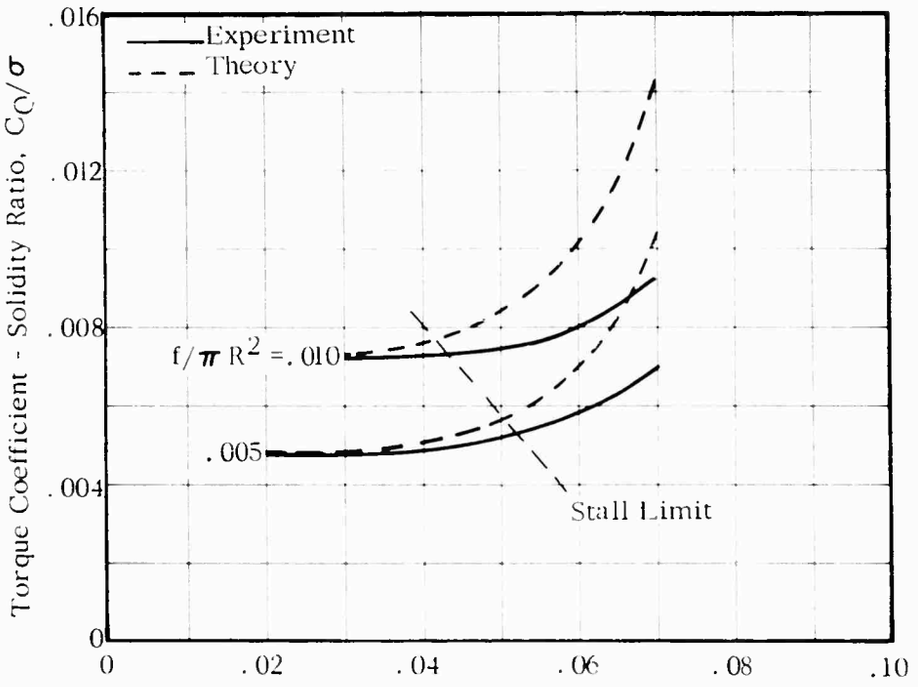

(c) V = 150 Kts., μ = .39

Figure 18. -Concluded

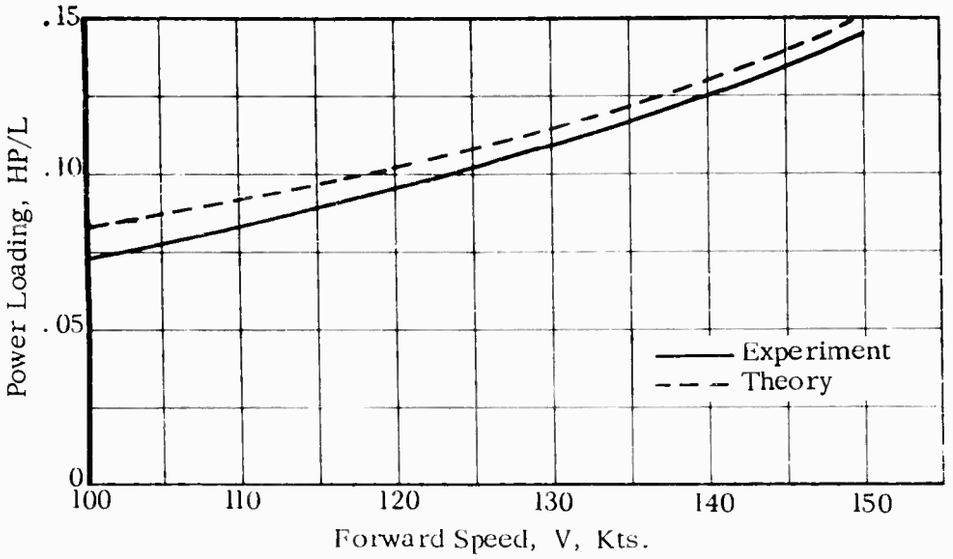

(a) $C_L/\sigma = 0.04$, $f/\pi R^2 = 0.005$

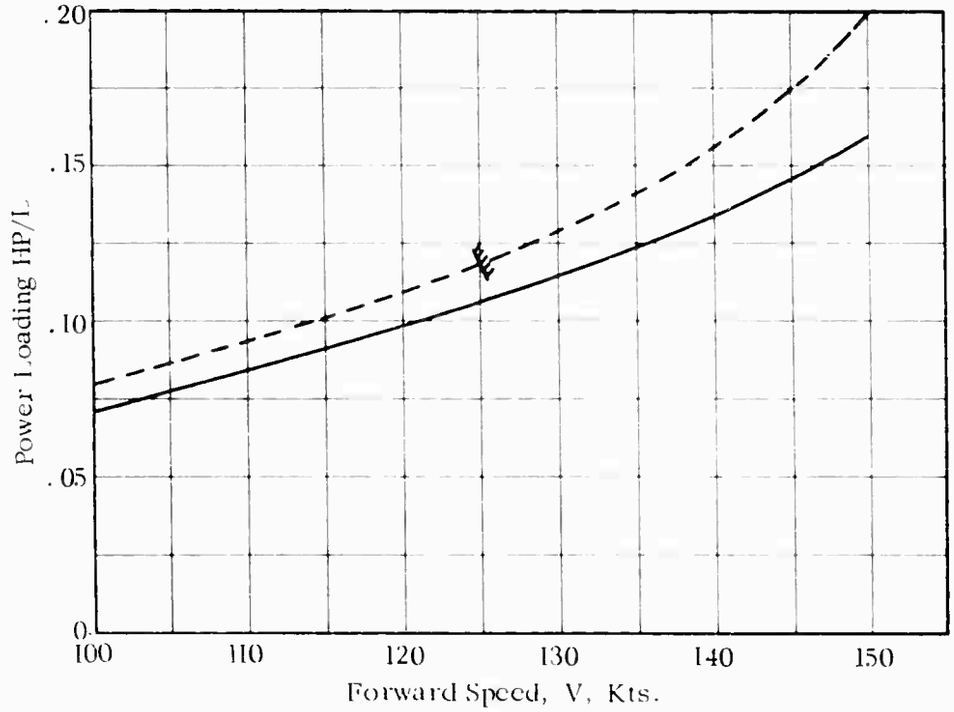

(b) $C_L/\sigma = 0.06$, $f/\pi R^2 = 0.010$

FIG. 19. COMPARISON OF THEORETICAL AND EXPERIMENTAL POWER LOADING VS. FORWARD SPEED, $\Omega R = 650$ FT/SEC

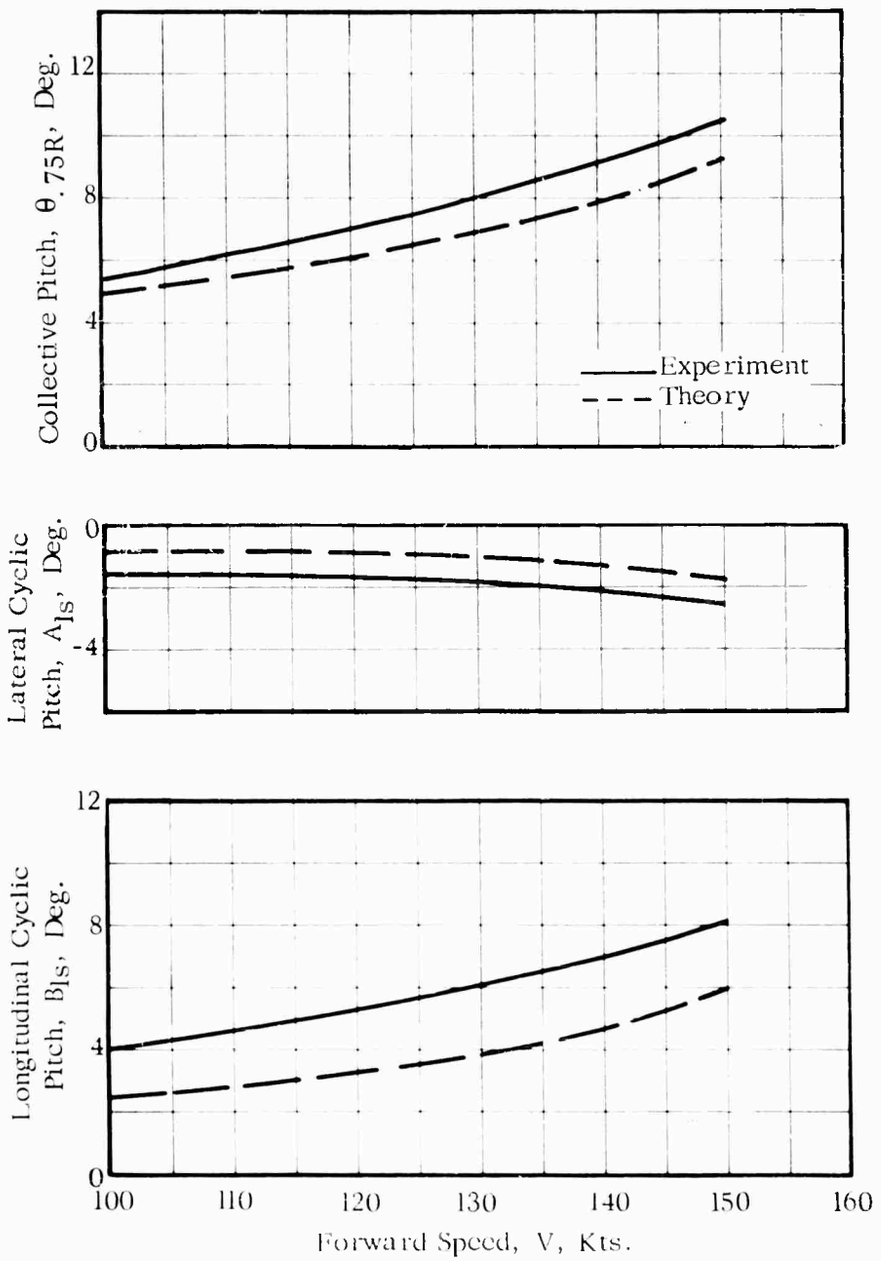

(a) $C_l/\sigma = 0.04$, $f/\pi R^2 = 0.005$

FIG. 20. COMPARISON OF THEORETICAL AND EXPERIMENTAL CONTROL REQUIREMENTS FOR $\beta_{1s} = 0$, $\Omega R = 650$ FT/SEC.

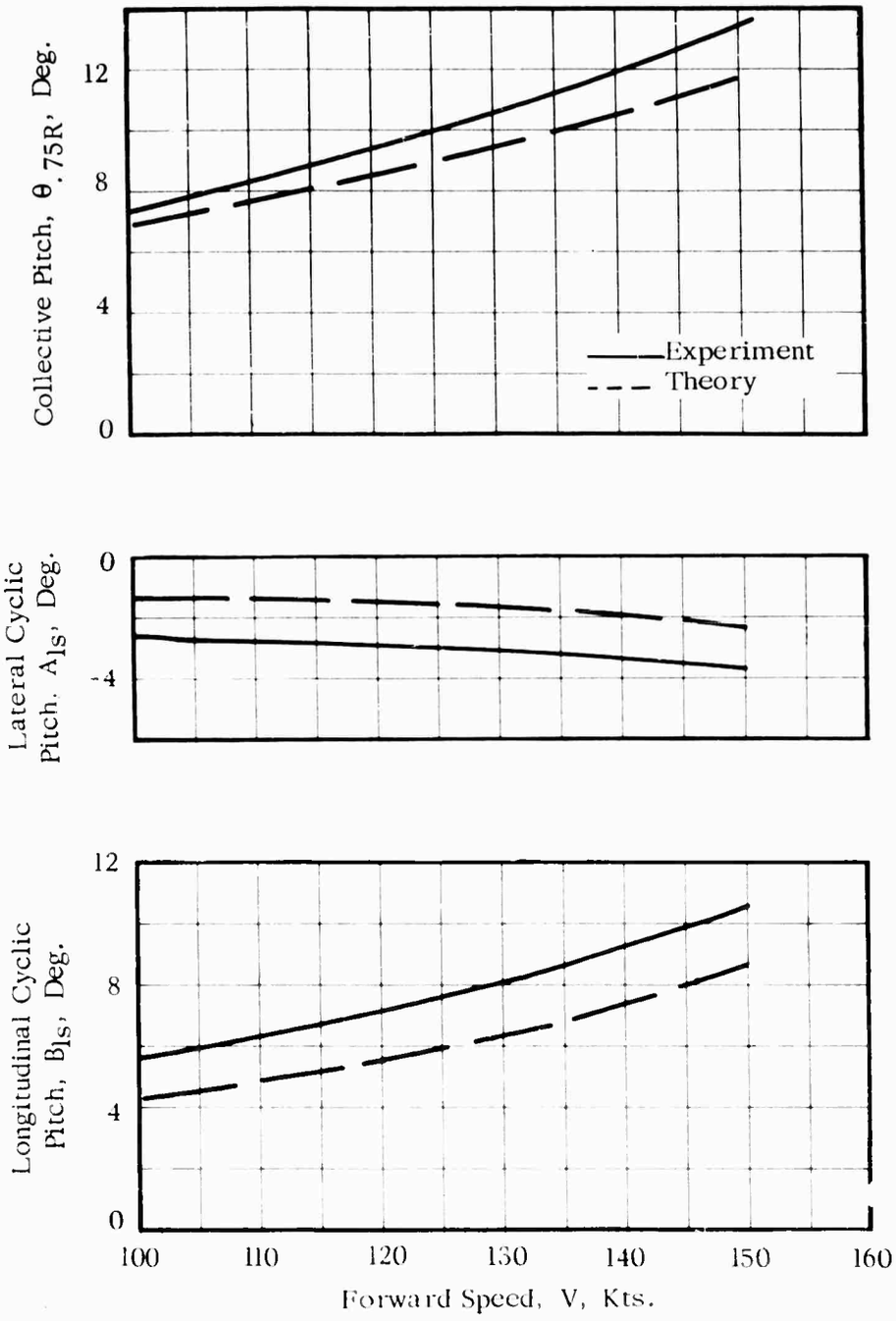

(b) $C_L/\sigma = 0.06$, $f/\pi R^2 = 0.010$

Figure 20. -Concluded

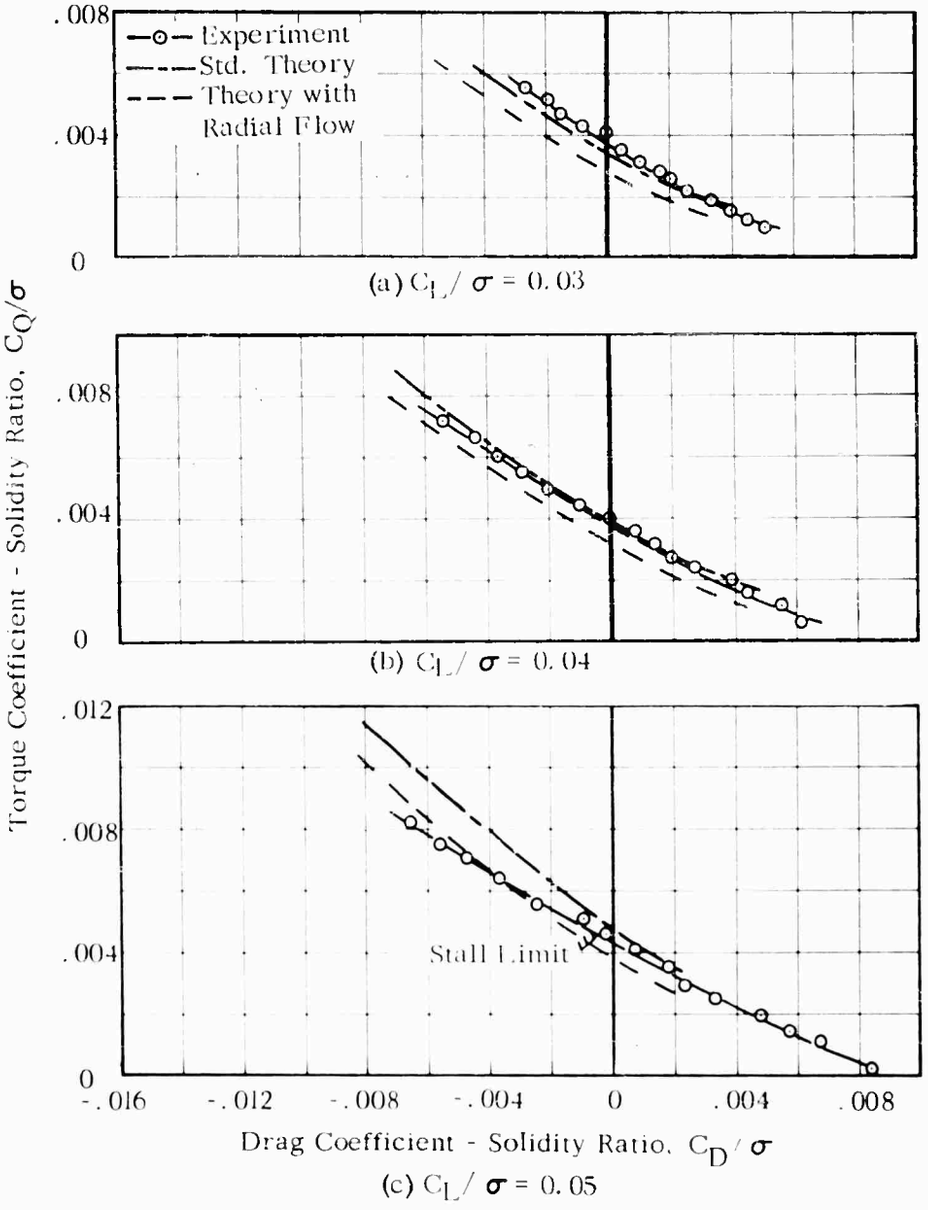

FIG. 21. EFFECT OF RADIAL FLOW CORRECTION ON ROTOR POWER REQUIRED AT CONSTANT LIFT

V = 161 Kts. ΩR = 580 ft/sec. μ = 0.47

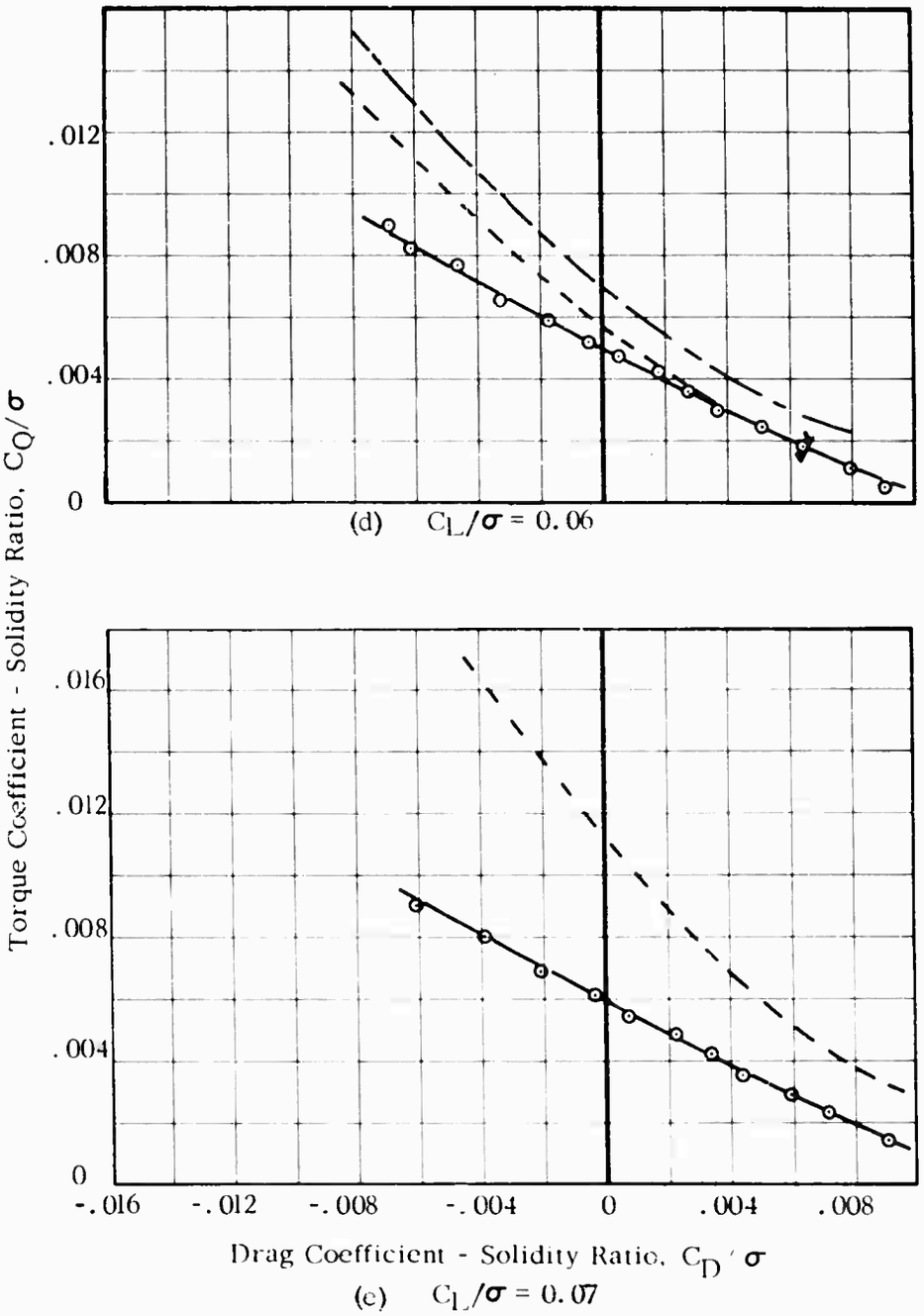

Figure 21. -Concluded

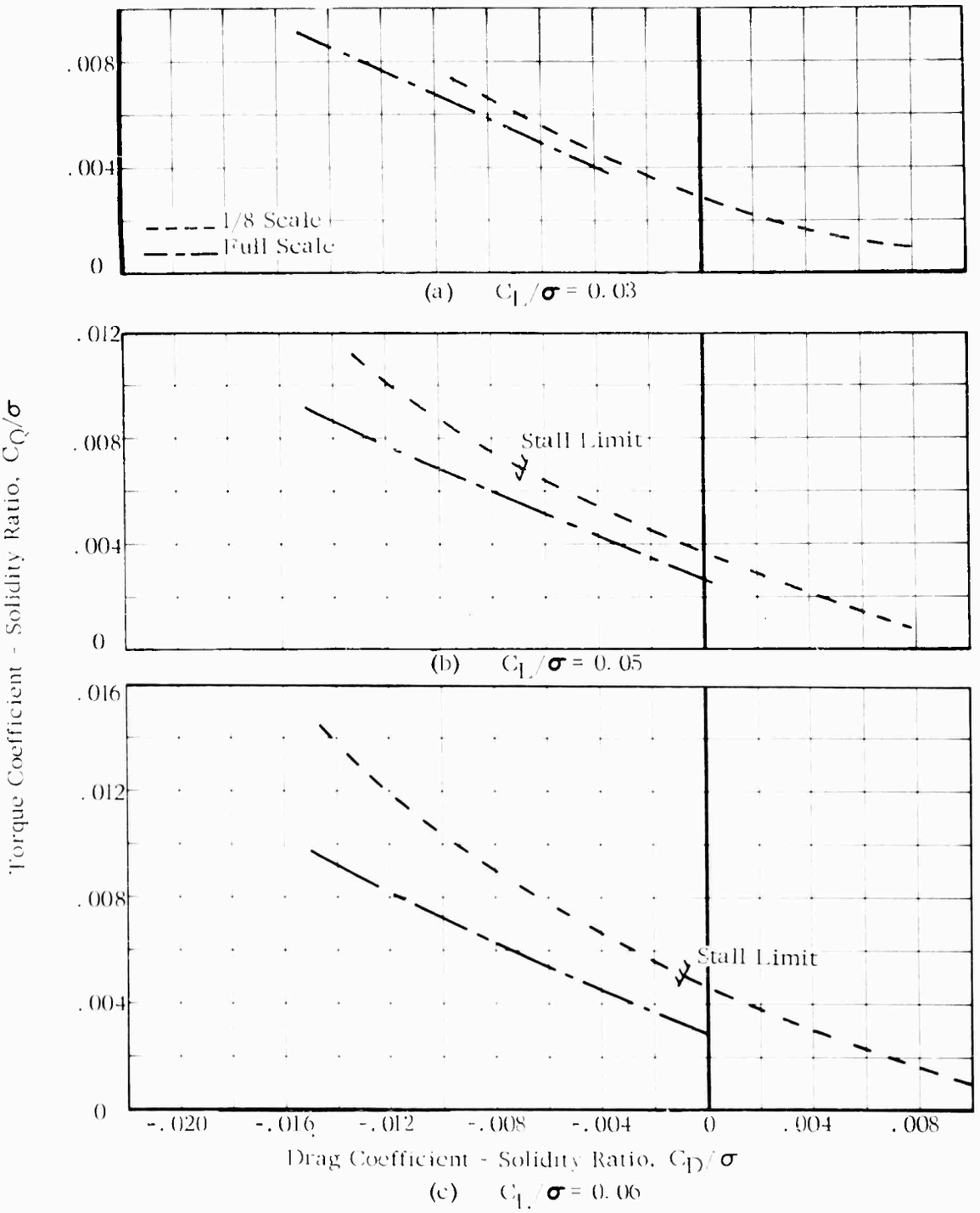

FIG. 22. COMPARISON OF FULL SCALE AND MODEL THEORETICAL ROTOR PERFORMANCE
V= 161 kts. ΩR= 700 ft/sec μ = 0.39

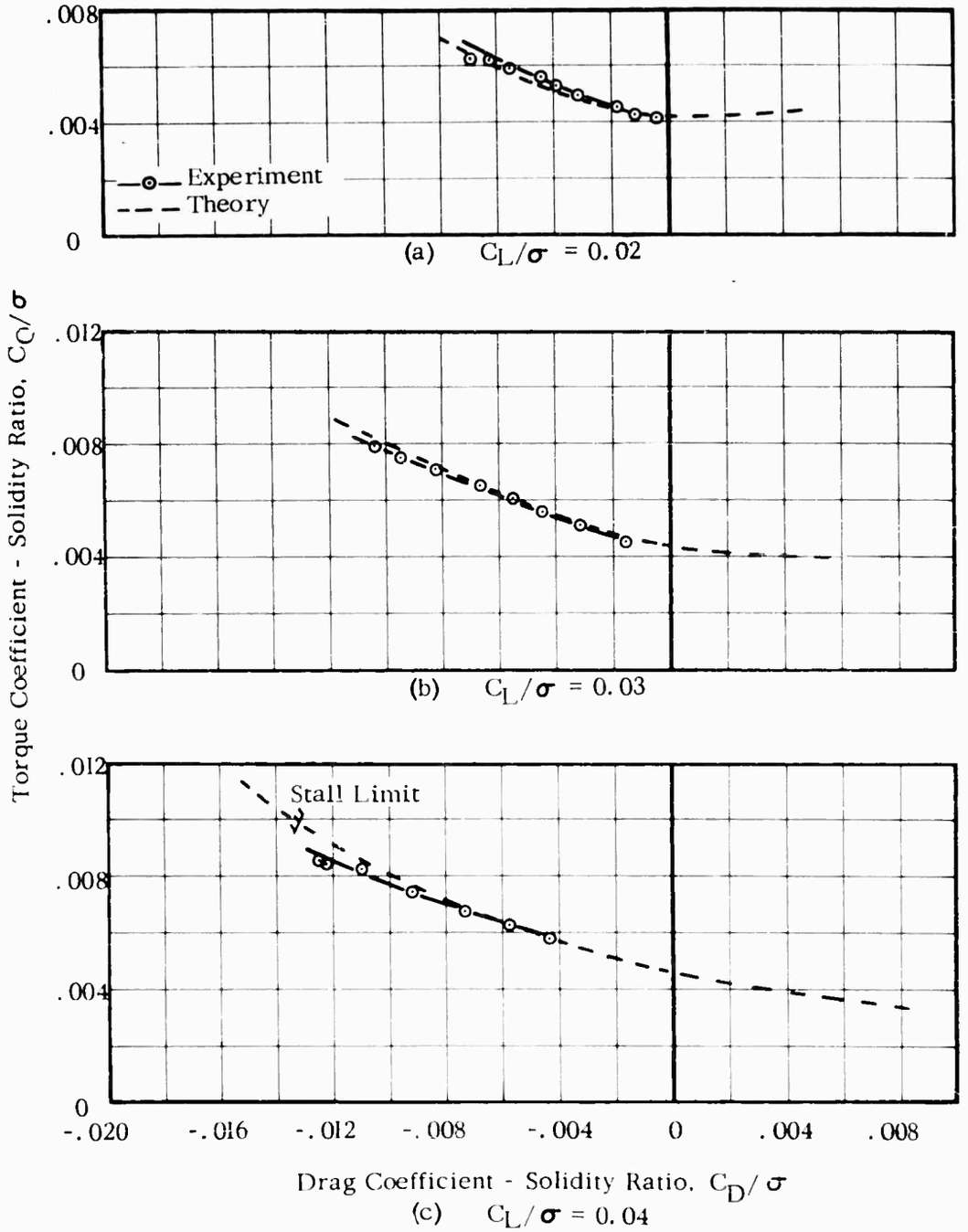

FIG. 23. COMPARISON OF THEORETICAL AND EXPERIMENTAL ROTOR POWER REQUIRED AT CONSTANT LIFT

V = 161 Kts. ΩR = 850 Ft/Sec. μ = 0.32

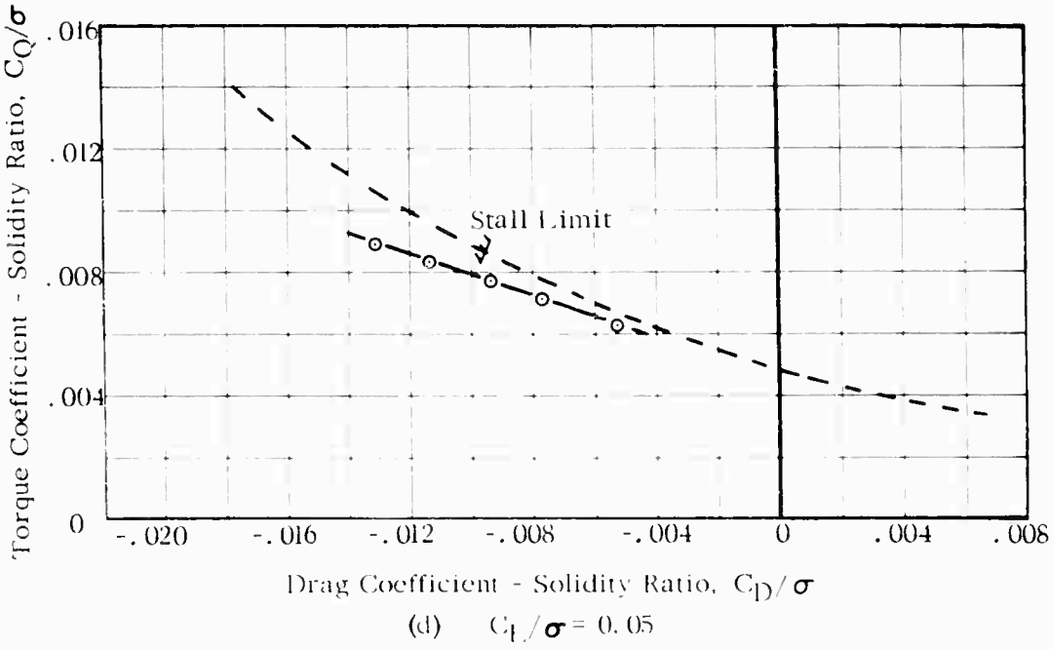

(d) $C_L/\sigma = 0.05$

Figure 23. -Concluded

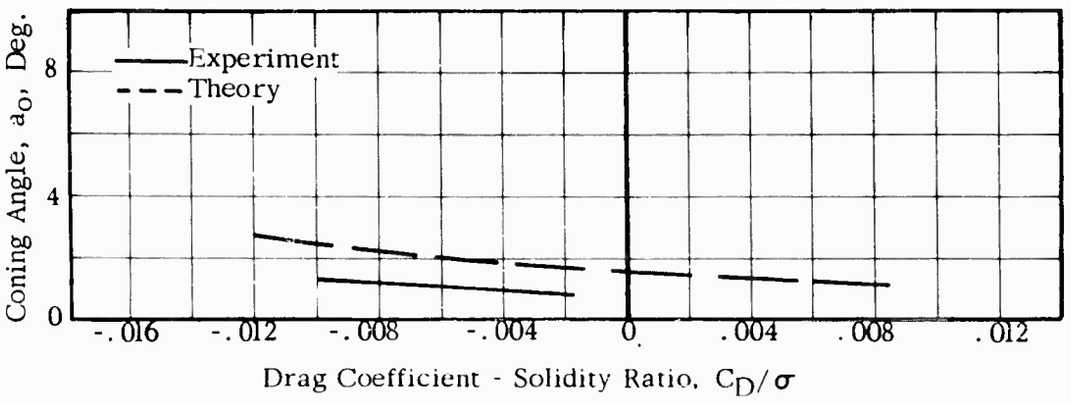

(a) Coning Angle, a_o, Deg.

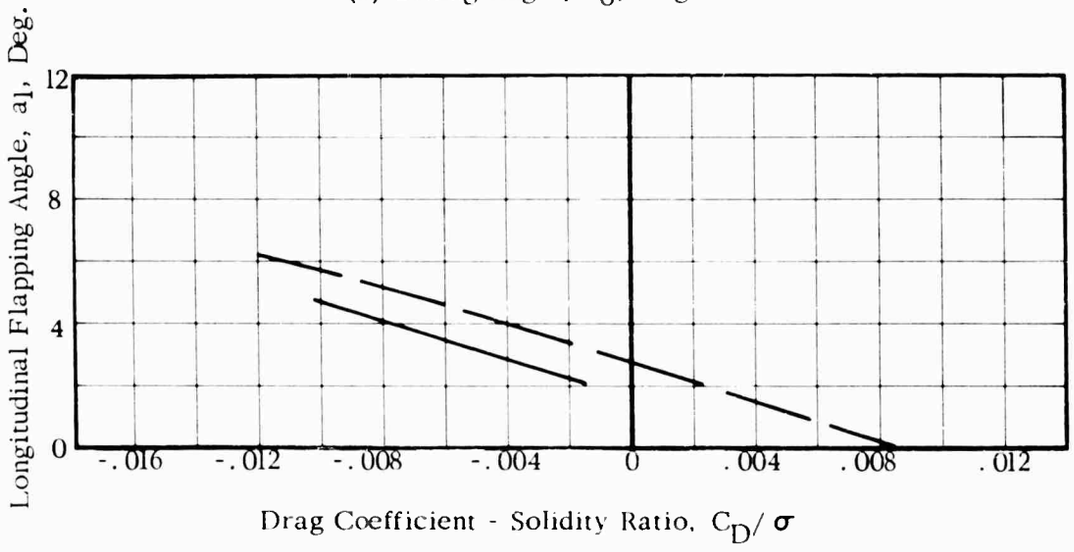

(b) Longitudinal Flapping Angle, a_1, Deg.

FIG.24. COMPARISON OF THEORETICAL AND EXPERIMENTAL BLADE MOTIONS

V = 161 Kts. ΩR = 850 Ft/Sec. $L/\pi R^2 = 4$

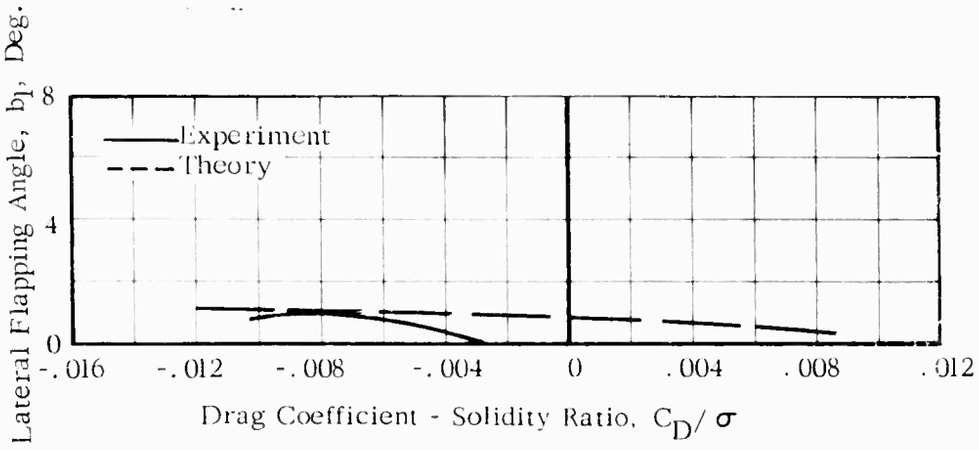

(c) Lateral Flapping Angle, b_1, Deg.

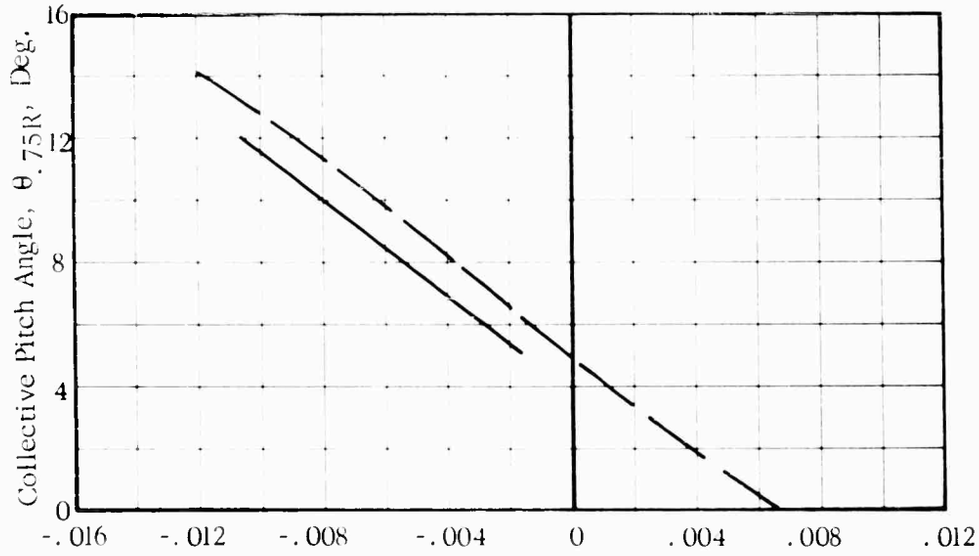

(d) Collective Pitch Angle, $\theta_{.75R}$, Deg.

Figure 24. -Concluded

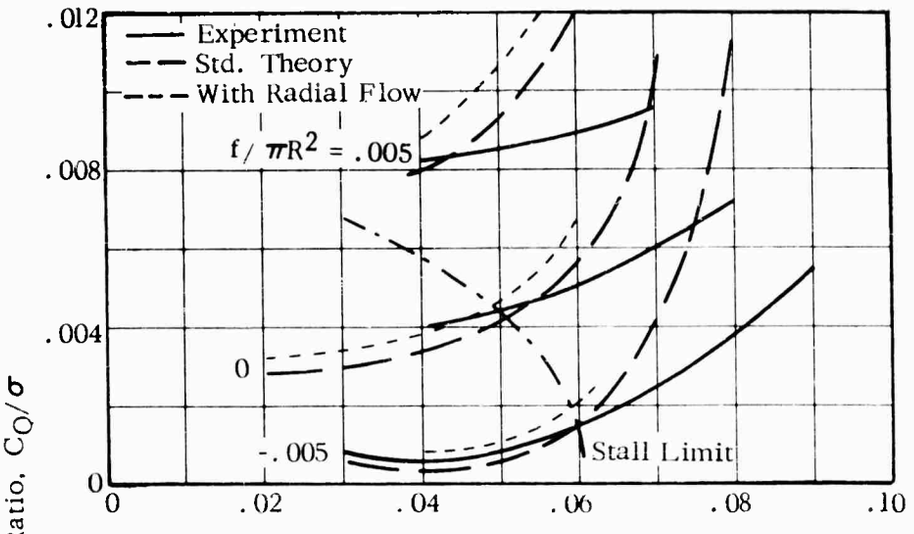

(a) ΩR = 580 Ft/Sec, μ = .47, $M_{(1.0)(90)}$ = .76

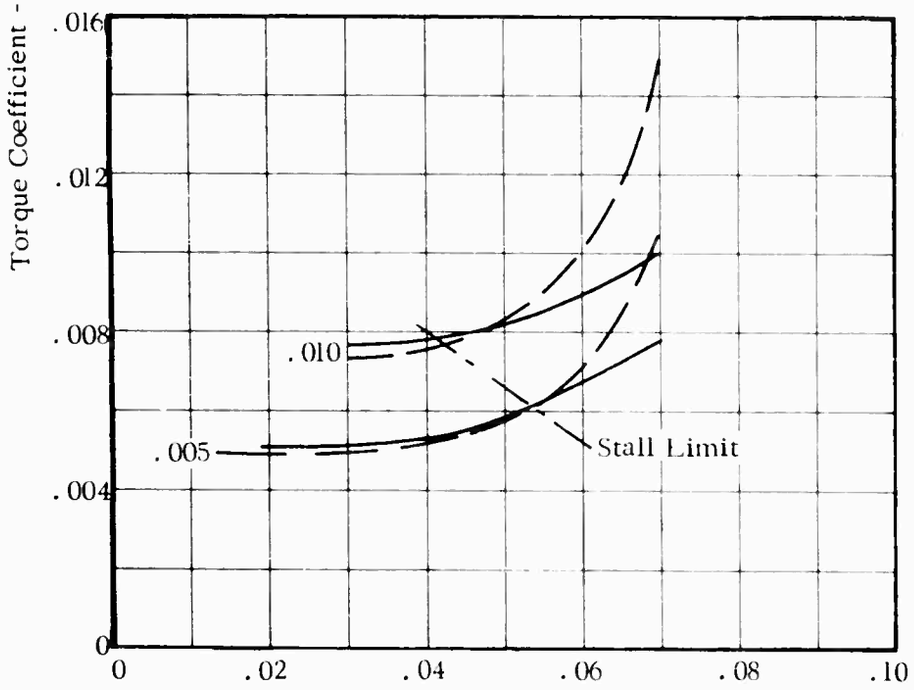

(b) ΩR = 700 Ft/Sec, μ = .39, $M_{(1.0)(90)}$ = .88

FIG. 25. COMPARISON OF THEORETICAL AND EXPERIMENTAL ROTOR POWER REQUIRED AT CONSTANT PARASITE DRAG, V = 161 KTS.

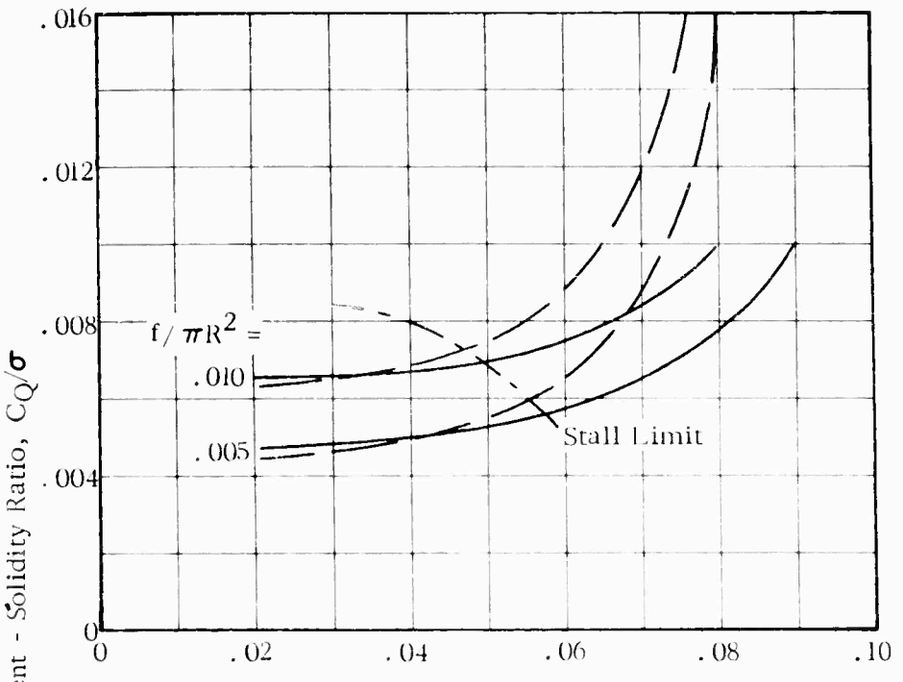

(c) ΩR = 750 Ft/Sec, μ = .36, $M_{(1.0)(90)}$ = .91

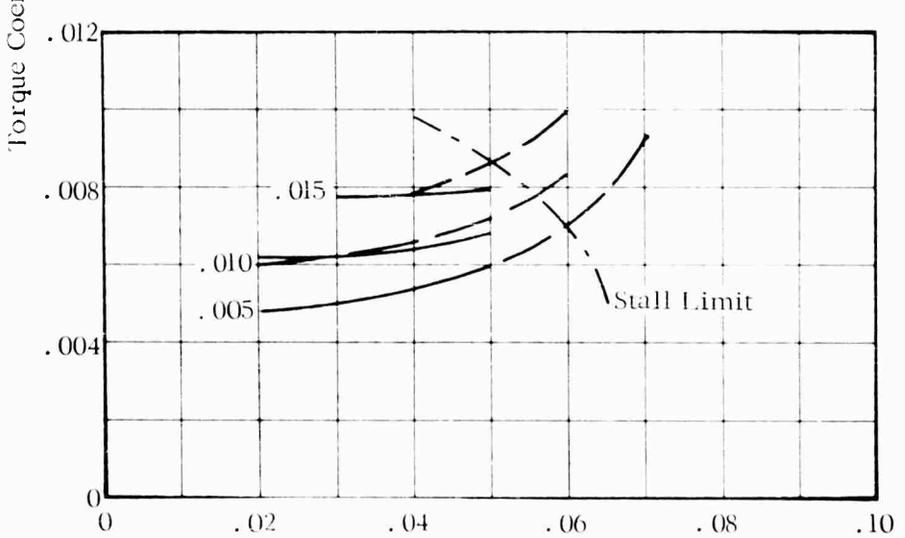

(d) ΩR = 850 Ft/Sec, μ = .32, $M_{(1.0)(90)}$ = 1.0

Figure 25. -Concluded

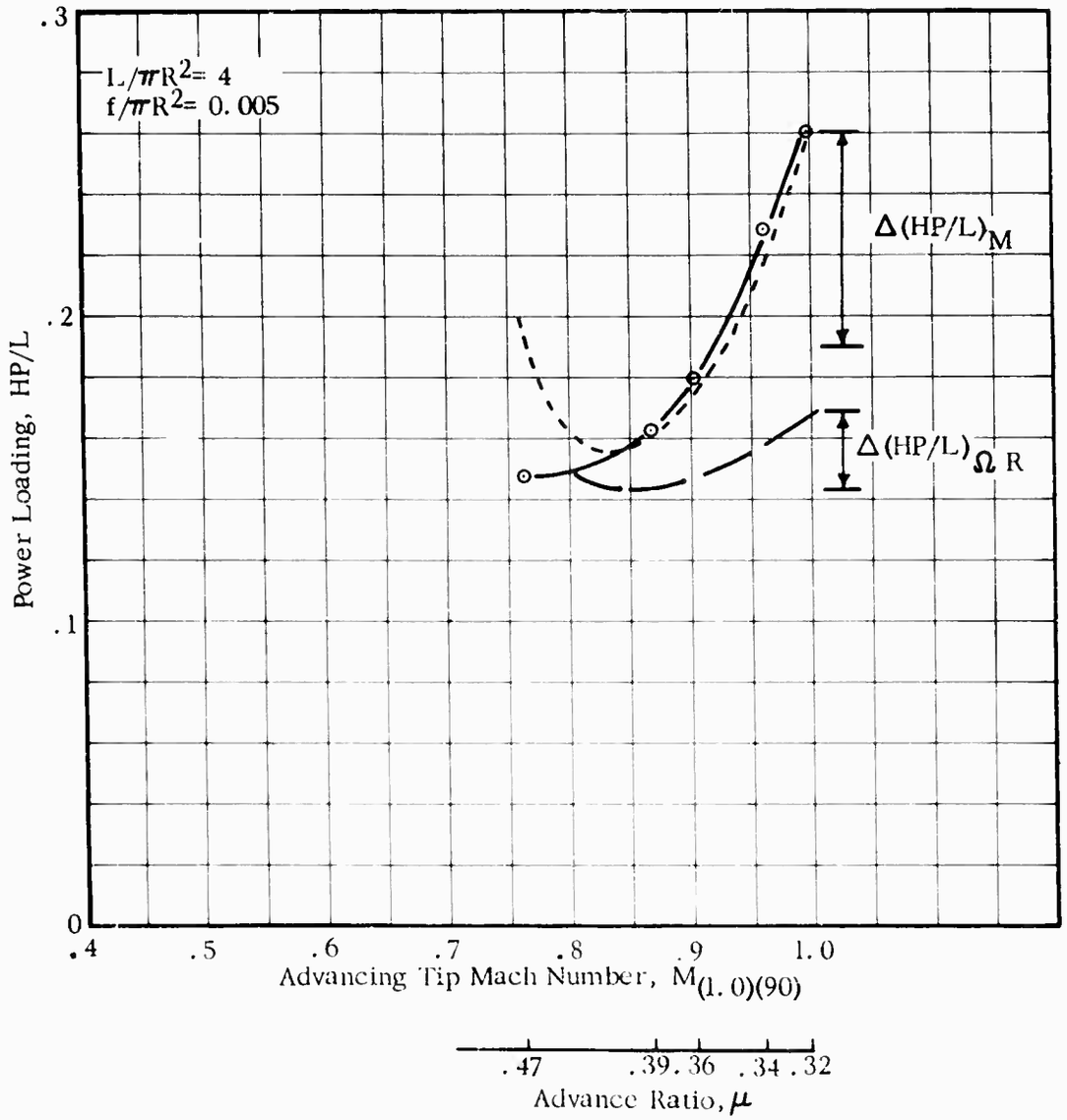

(a) Power Loading vs $M_{(1.0)(90)}$

FIG. 26. EFFECT OF ADVANCING TIP MACH NUMBER ON ROTOR POWER LOADING, V = 161 KTS.

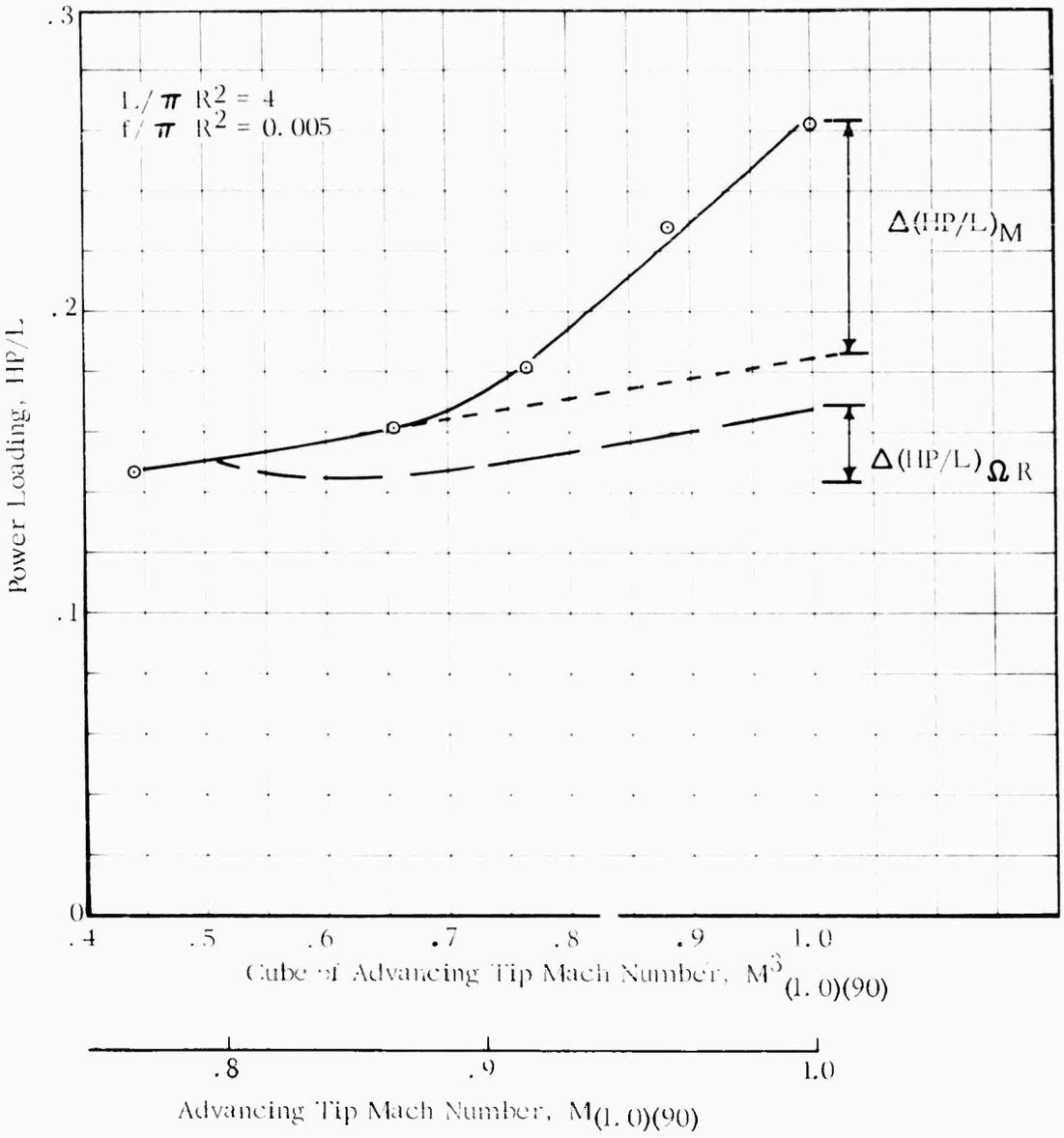

(b) Power Loading vs $M^3_{(1.0)(90)}$

Figure 26. -Concluded

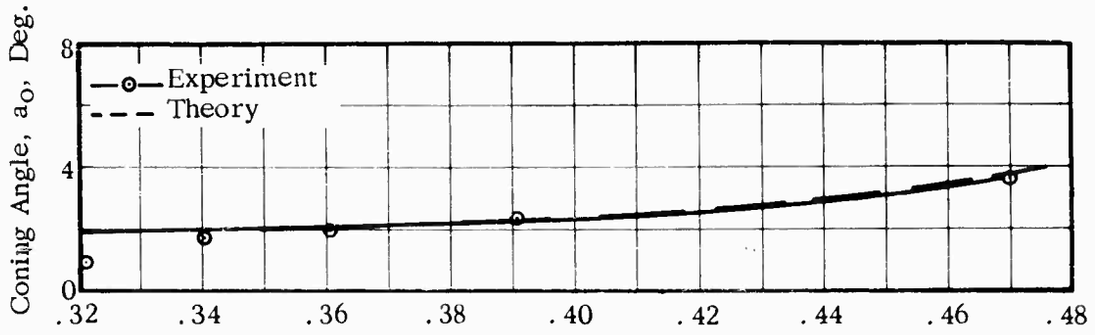

(a) a_o vs μ

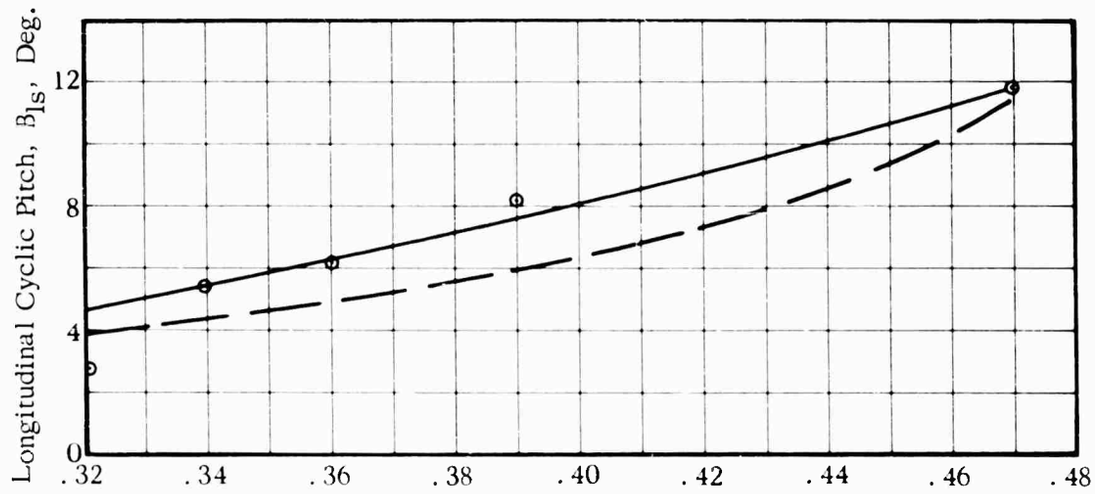

(b) B_{ls} vs μ

FIG. 27. COMPARISON OF THEORETICAL AND EXPERIMENTAL CONTROL REQUIREMENTS VS ADVANCE RATIO

$L/\pi R^2 = 4$ LB./FT.^{2} V= 161 Kts. $f/\pi R^2 = 0.005$

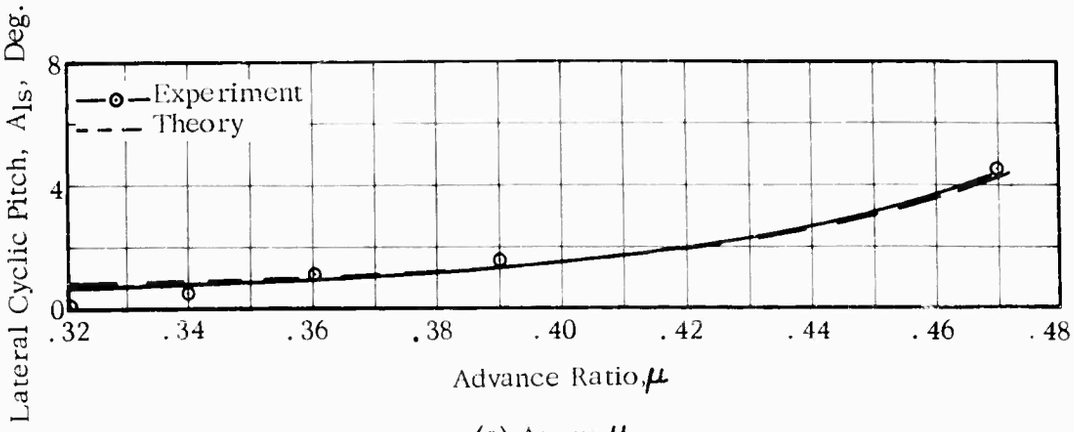

(c) A_{1s} vs μ

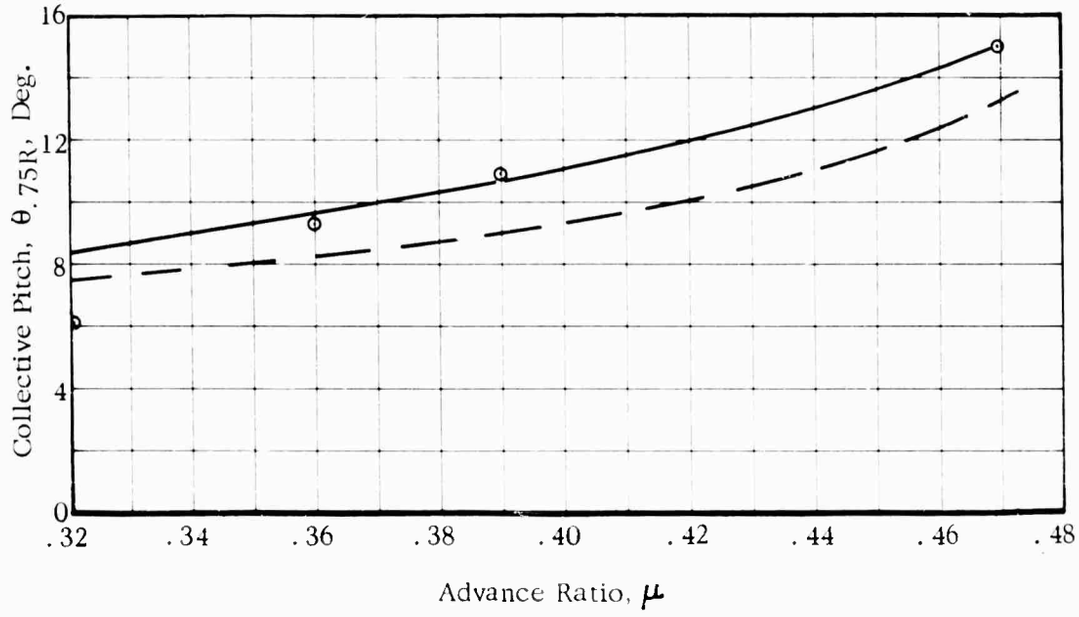

(d) $\theta_{.75R}$ vs μ

Figure 27. -Concluded

APPENDIX I

Basic rotor performance and blade motions, both theoretical and experimental, are presented in figures 28-50.

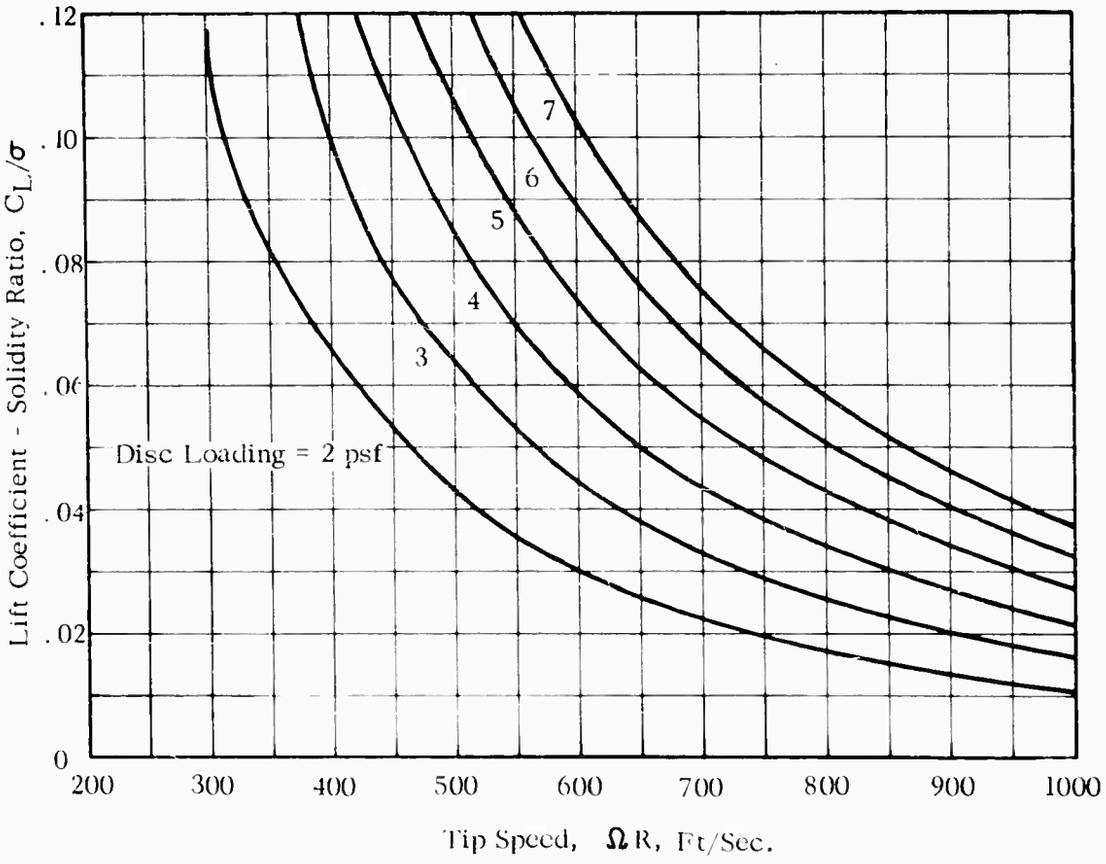

FIG. 28. RELATIONSHIP BETWEEN DISC LOADING, TIP SPEED, AND LIFT COEFFICIENT - SOLIDITY RATIO

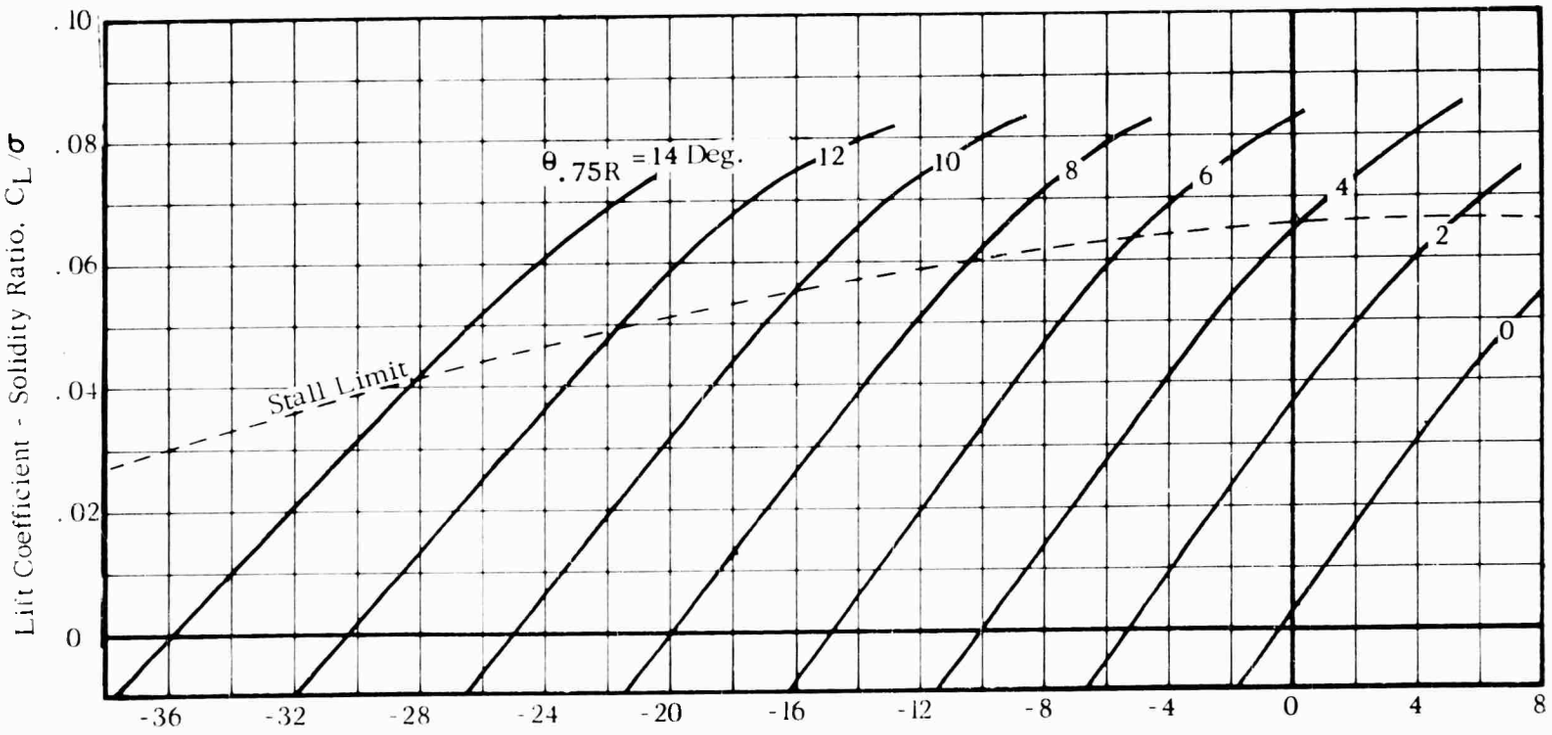

(a) C_L/σ vs α

FIG. 29. THEORETICAL ROTOR PERFORMANCE AND BLADE MOTIONS

V = 125 Kts. ΩR = 650 Ft/Sec. μ = 0.32

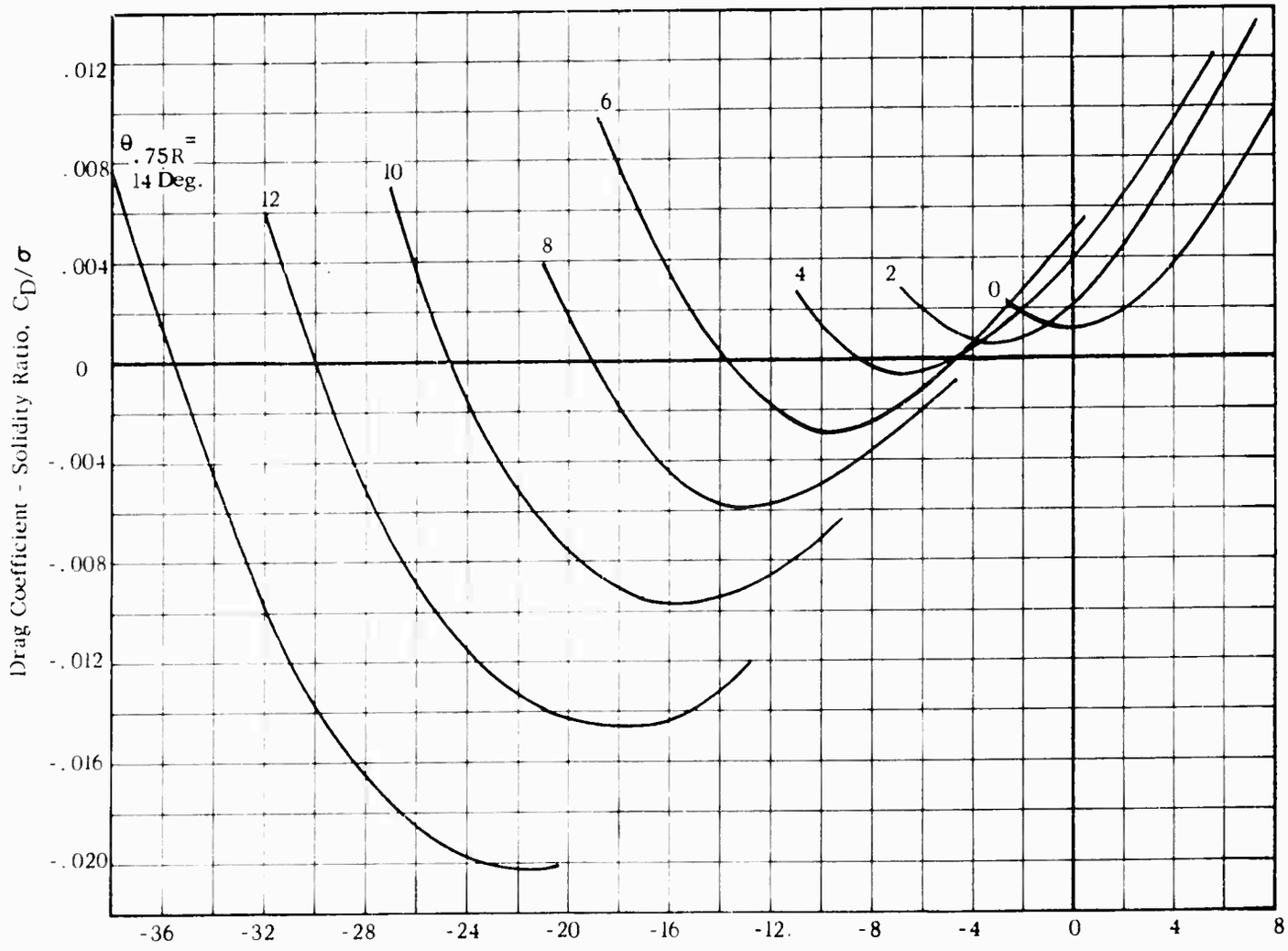

(b) C_D/σ vs α

Figure 29. -Continued

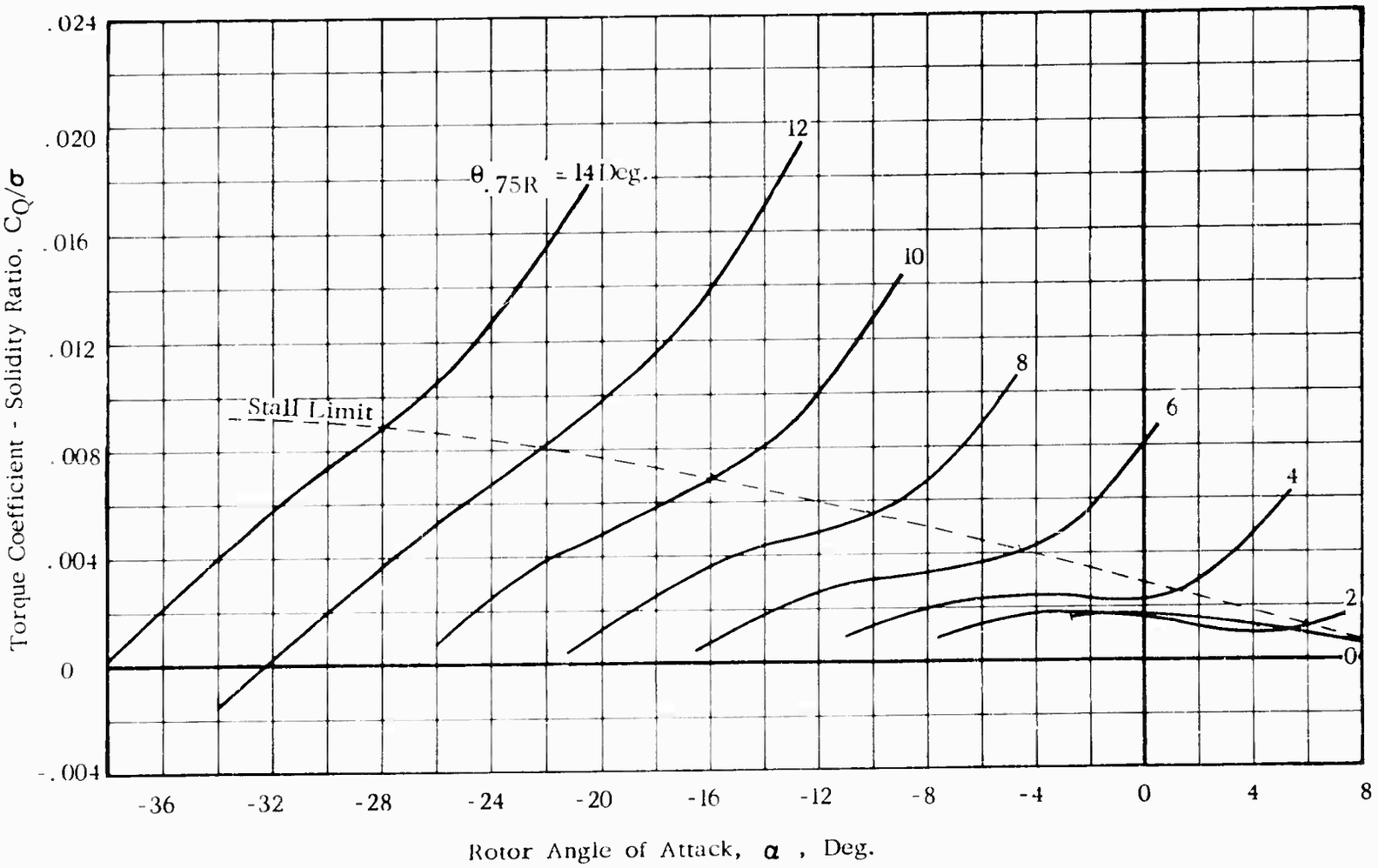

(c) C_Q/σ vs α

Figure 29. -Continued

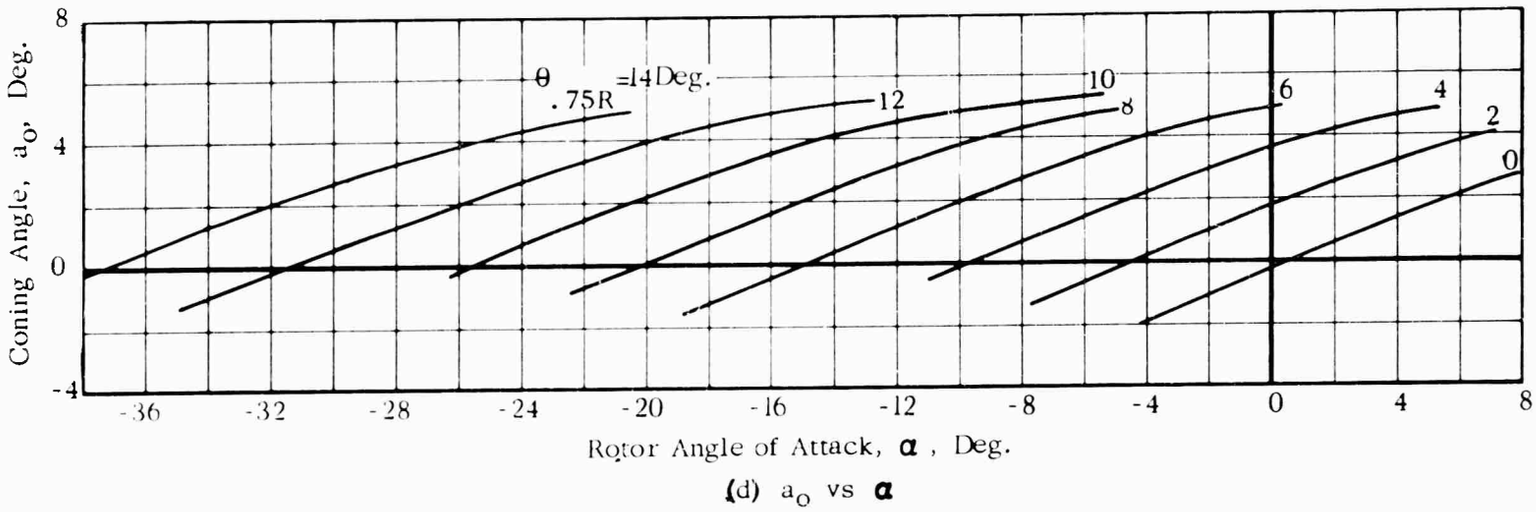

(d) a_o vs α

Figure 29. -Continued

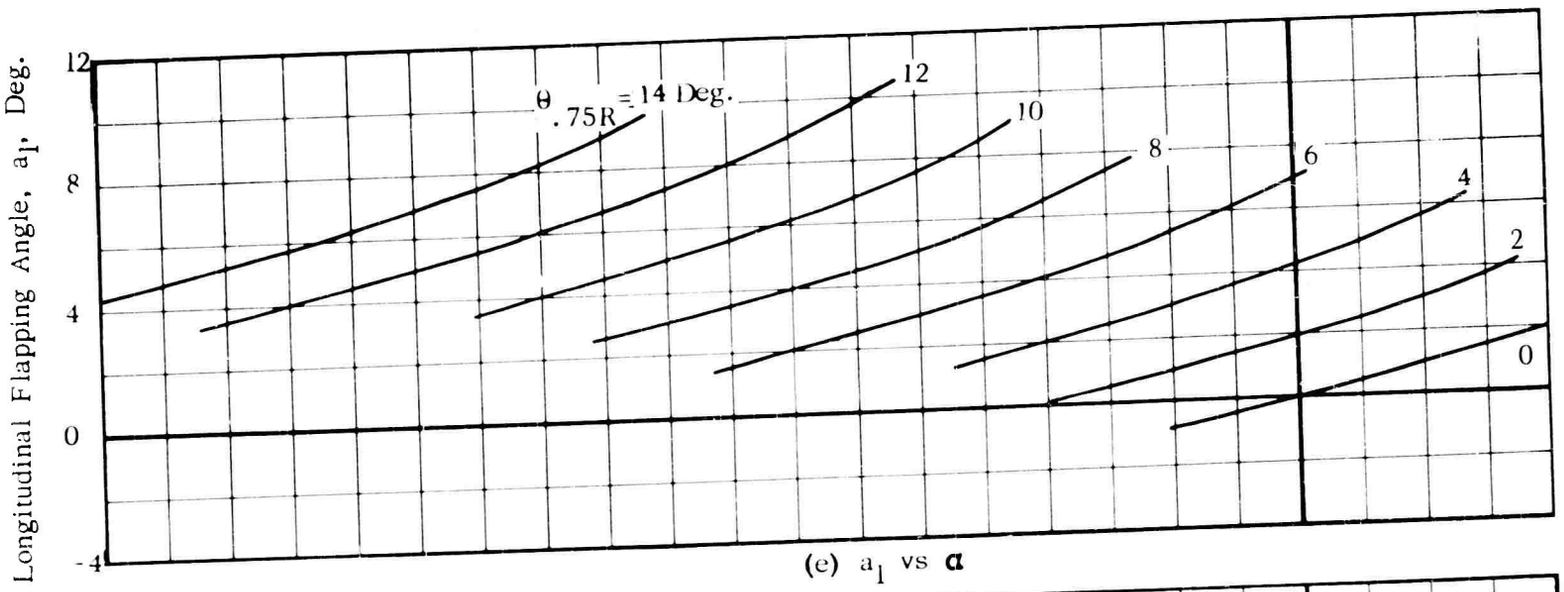

(e) a_1 vs α

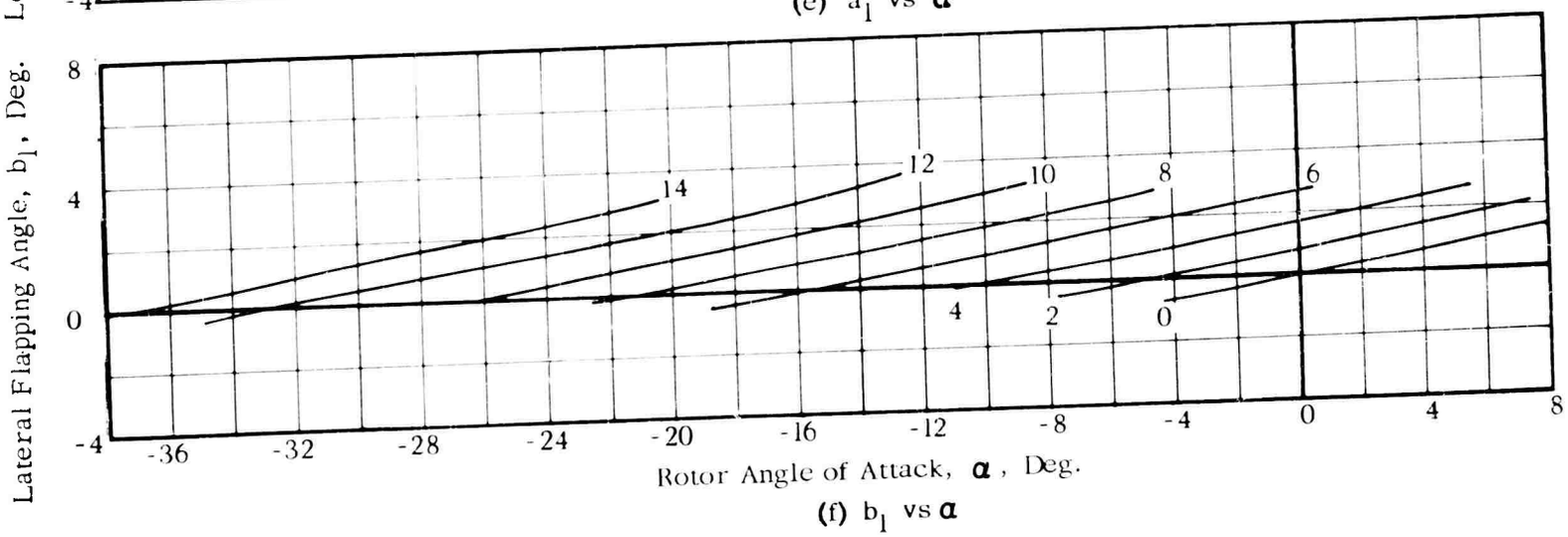

(f) b_1 vs α

Figure 29. -Concluded

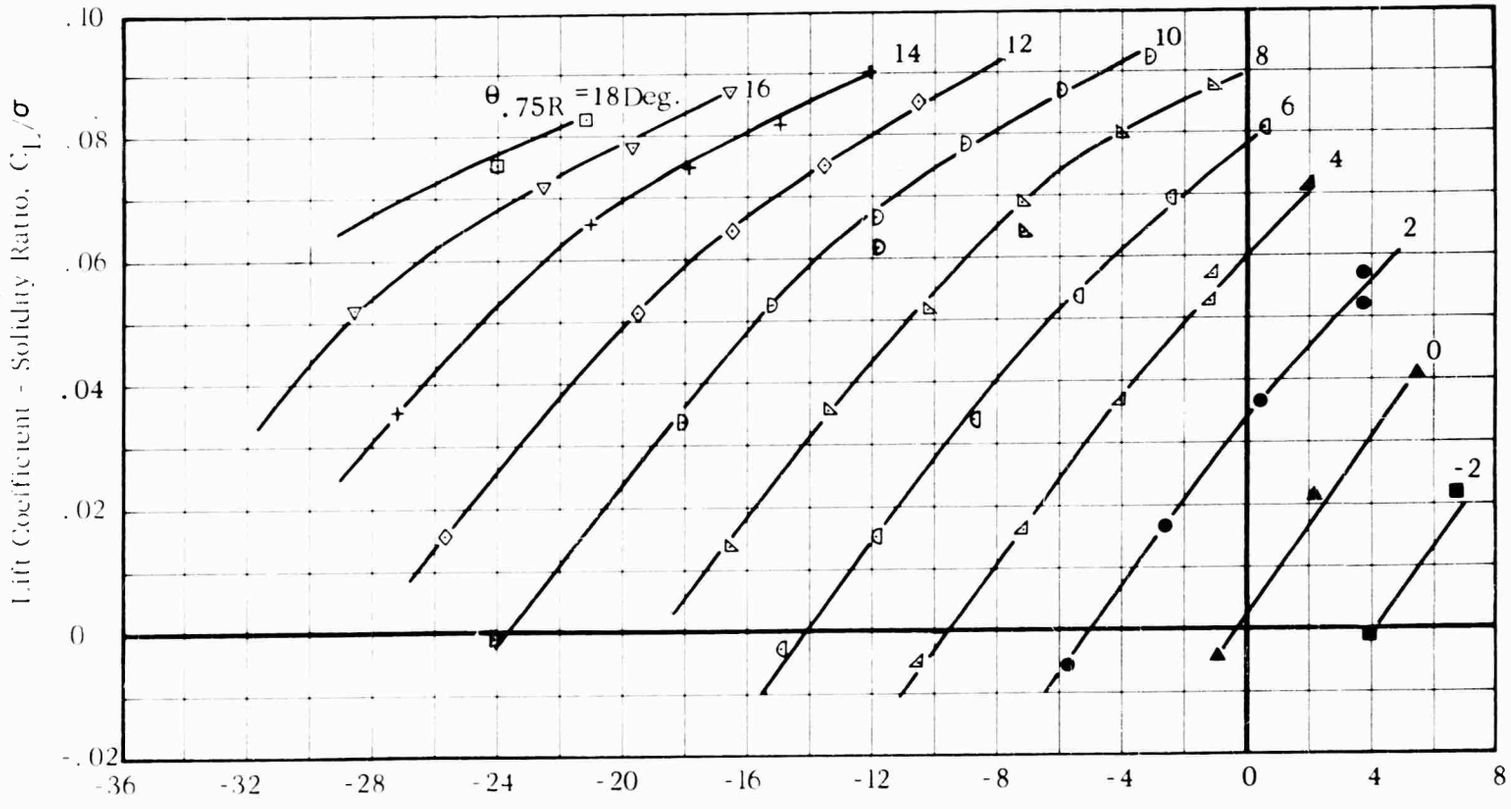

(a) C_L/σ vs α

FIG. 30. EXPERIMENTAL ROTOR PERFORMANCE AND BLADE MOTIONS

V = 125 Kts. ΩR = 650 Ft/Sec. μ = 0.32

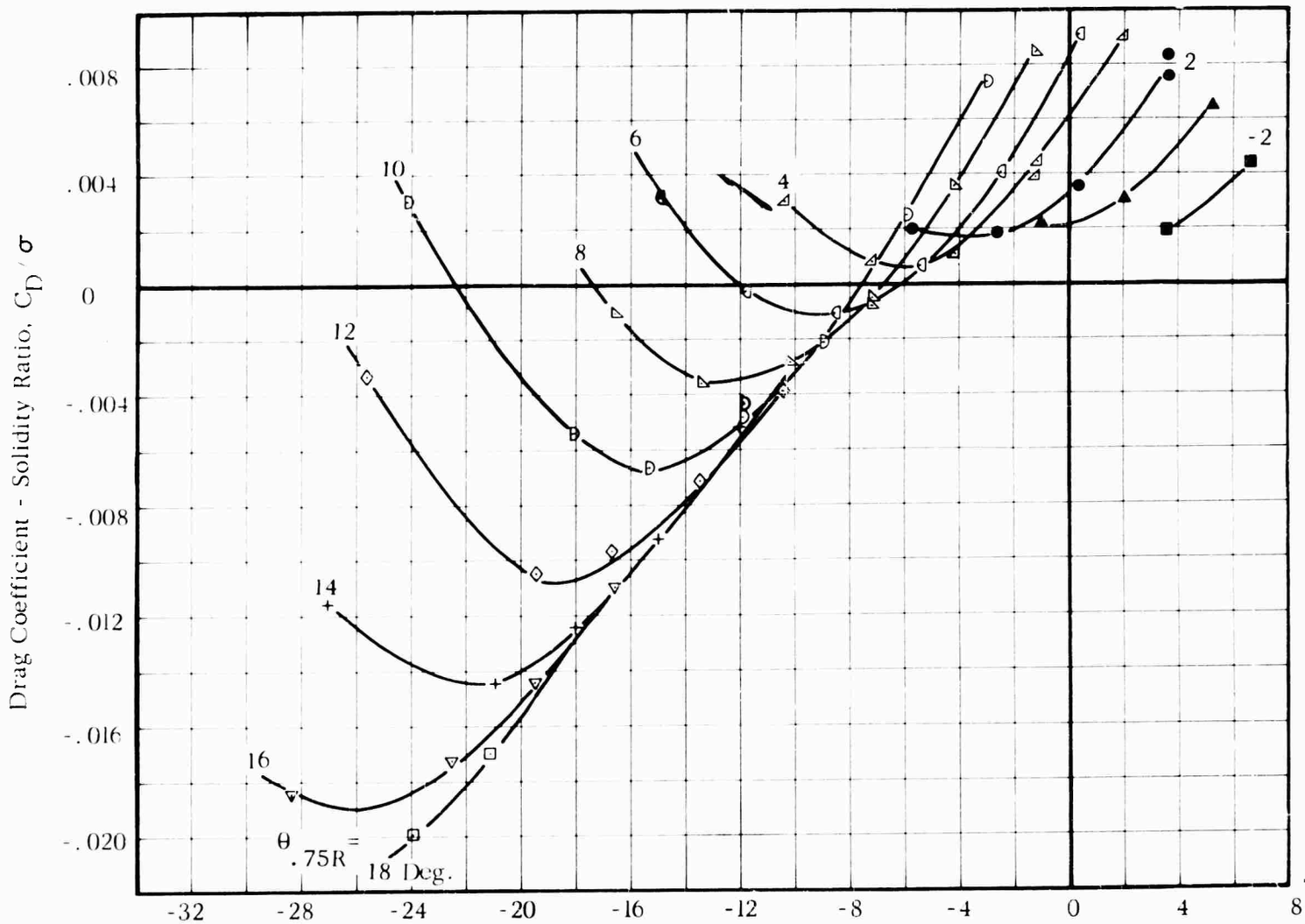

(b) C_D/σ vs α

Figure 30. -Continued

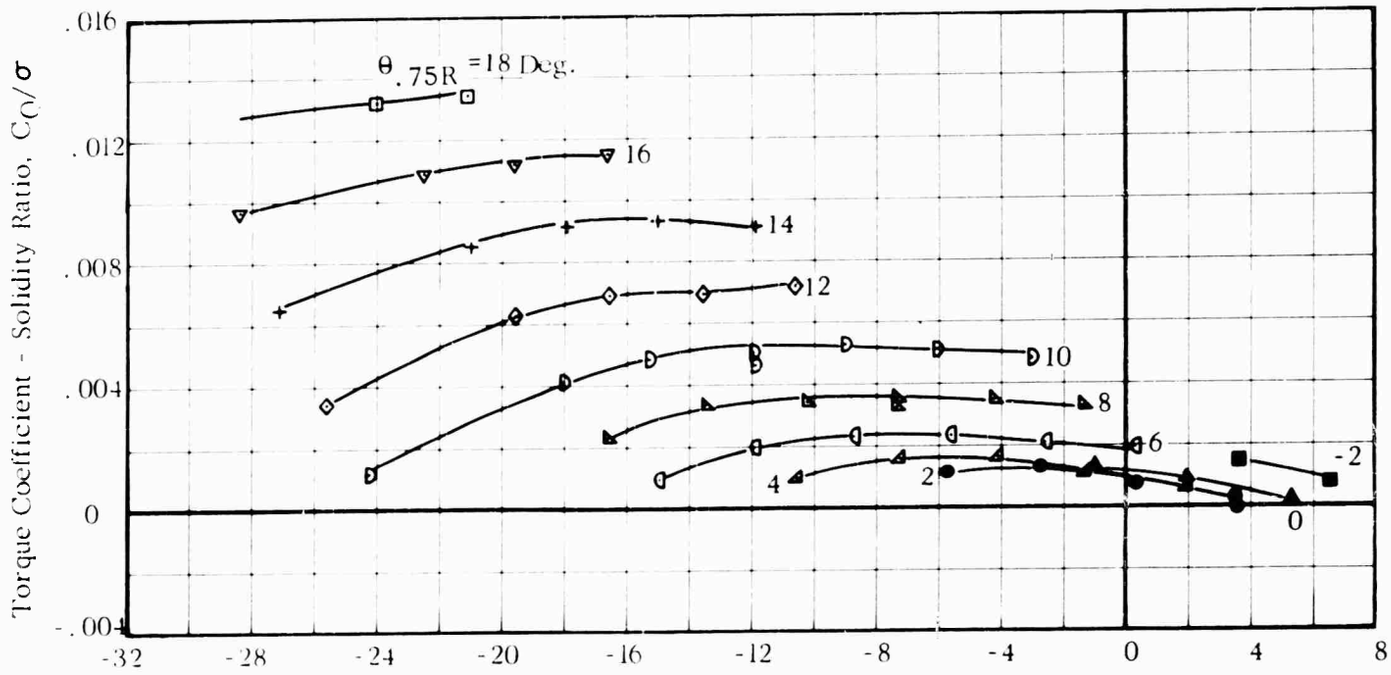

(c) C_Q/σ vs α

Figure 30. -Continued

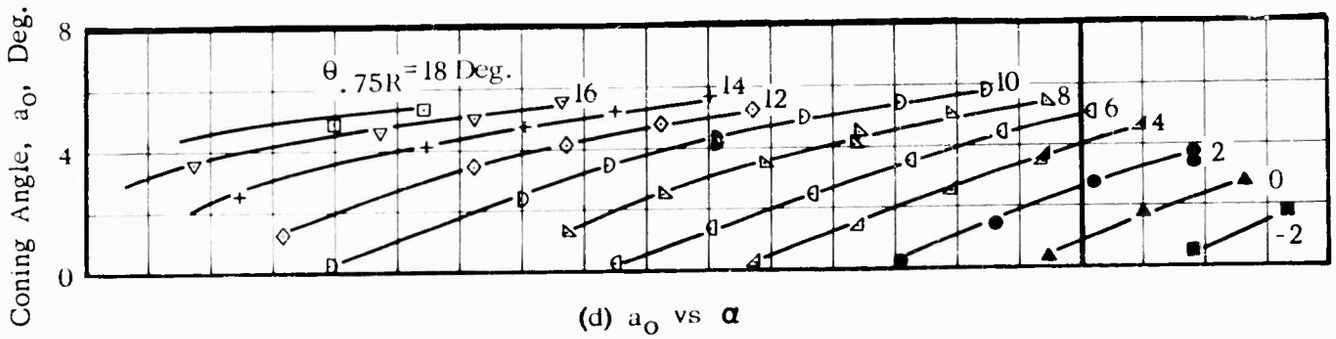

(d) a_o vs α

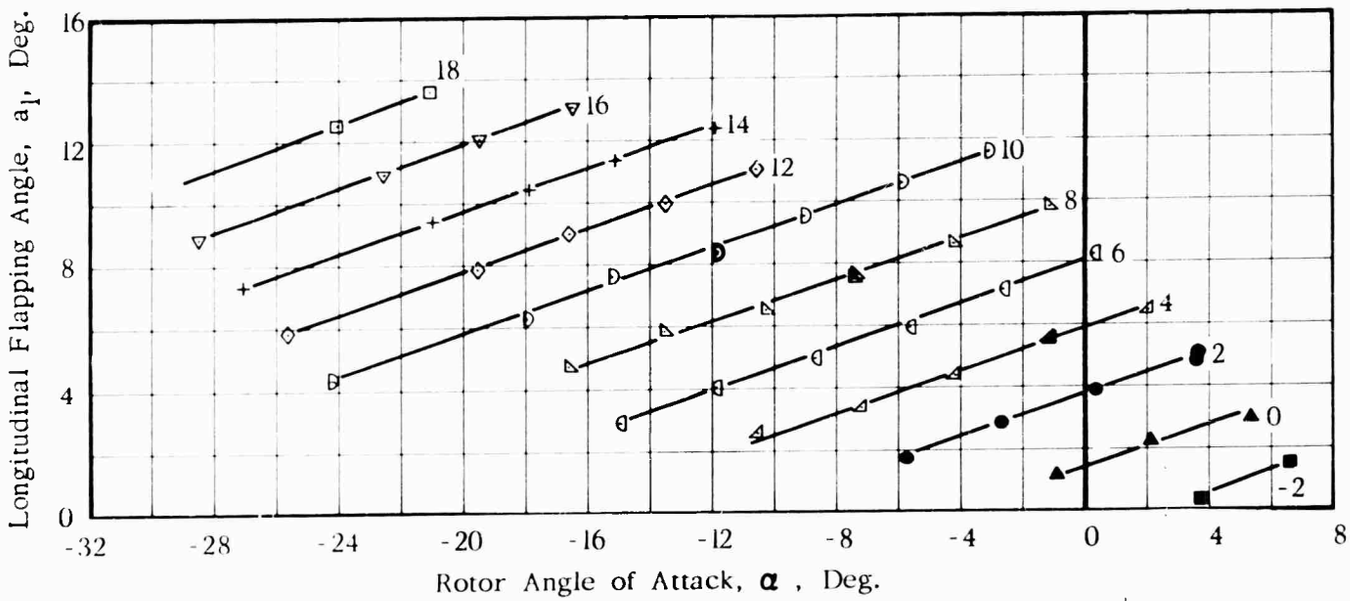

(e) a_1 vs α

Figure 30. -Continued

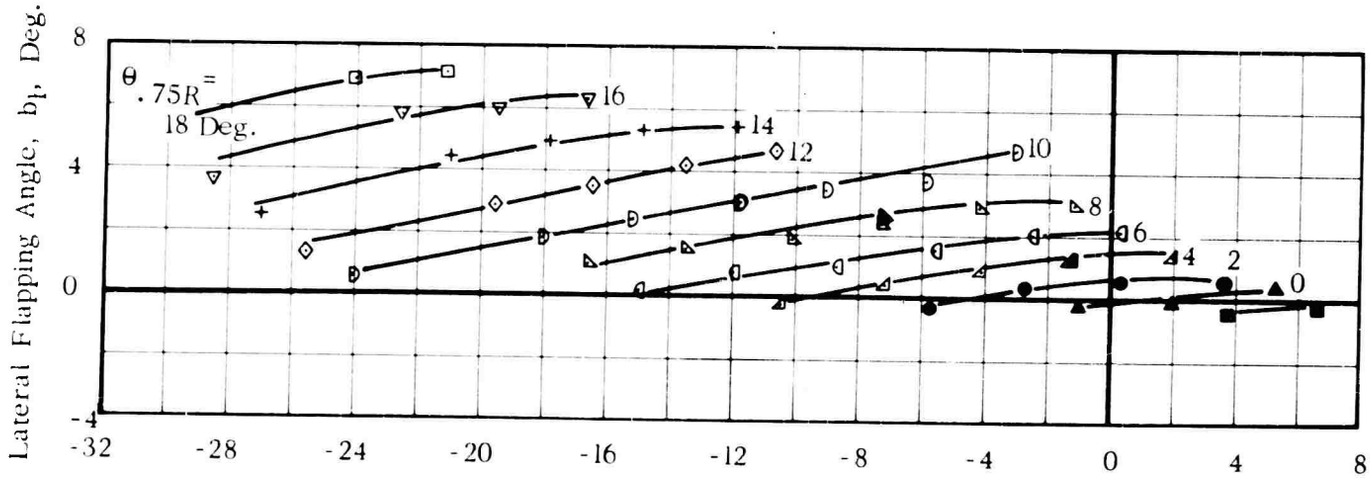

(f) b_1 vs α

Figure 30. -Concluded

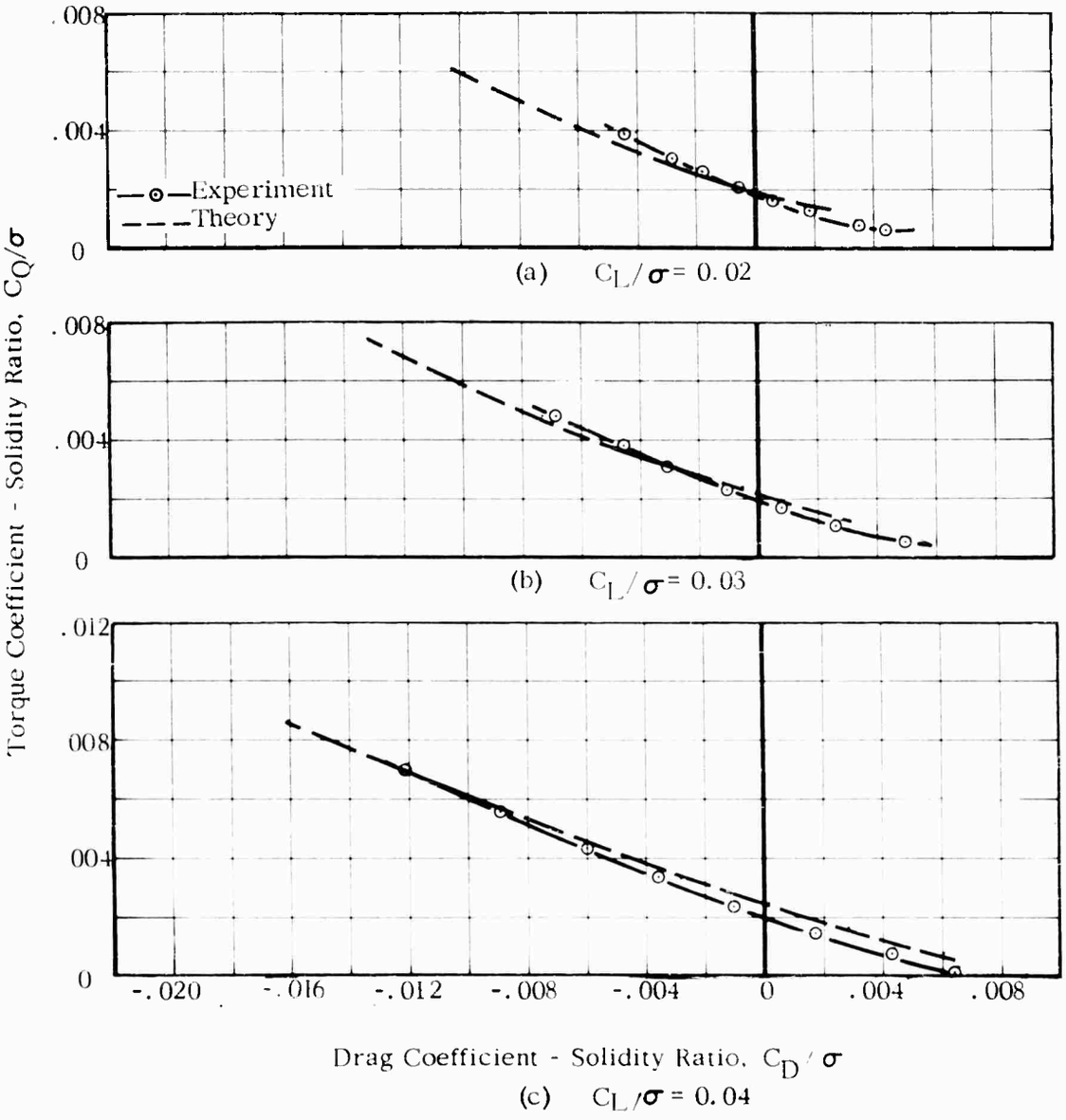

FIG. 31. COMPARISON OF THEORETICAL AND EXPERIMENTAL ROTOR POWER REQUIRED AT CONSTANT LIFT

V = 125 Kts. ΩR = 650 Ft/Sec. μ = 0.32

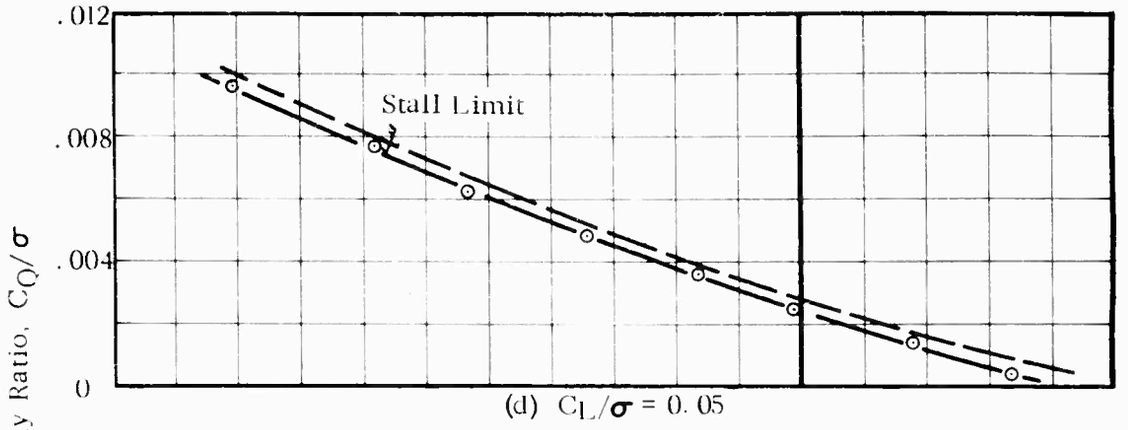

(d) $C_L/\sigma = 0.05$

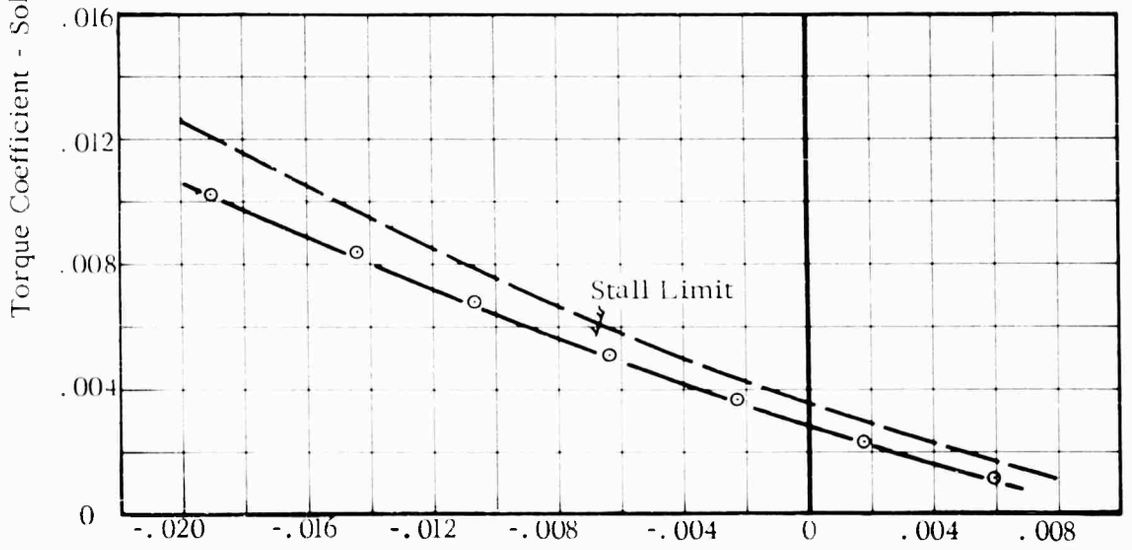

(c) $C_L/\sigma = 0.06$

Figure 31. -Continued

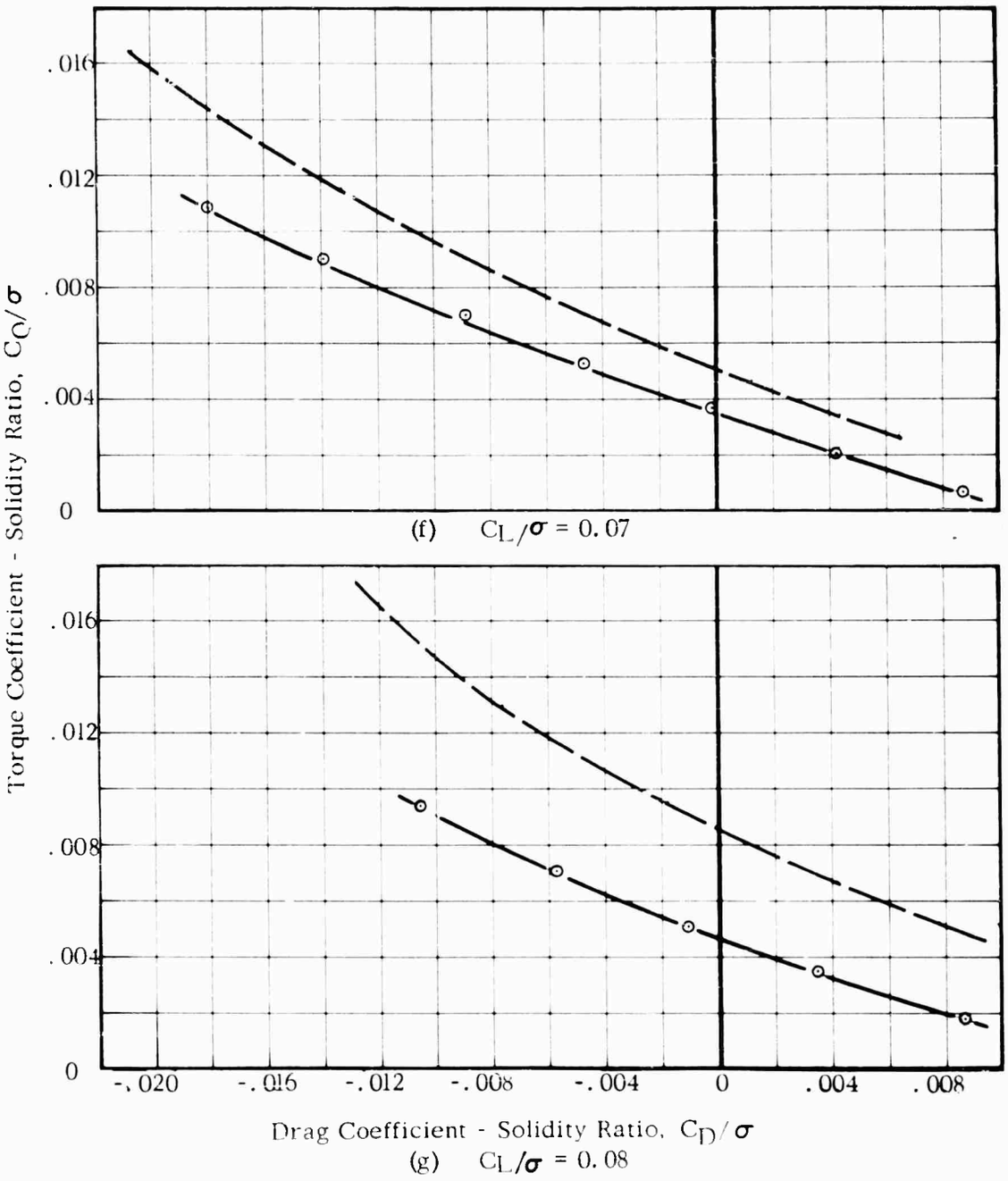

Figure 31. -Concluded

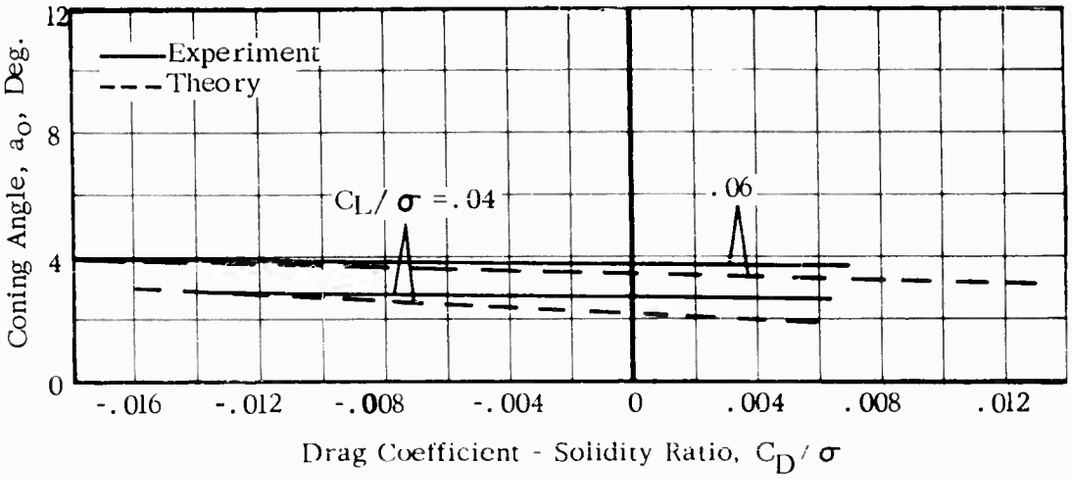

(a) Coning Angle, a_o, Deg.

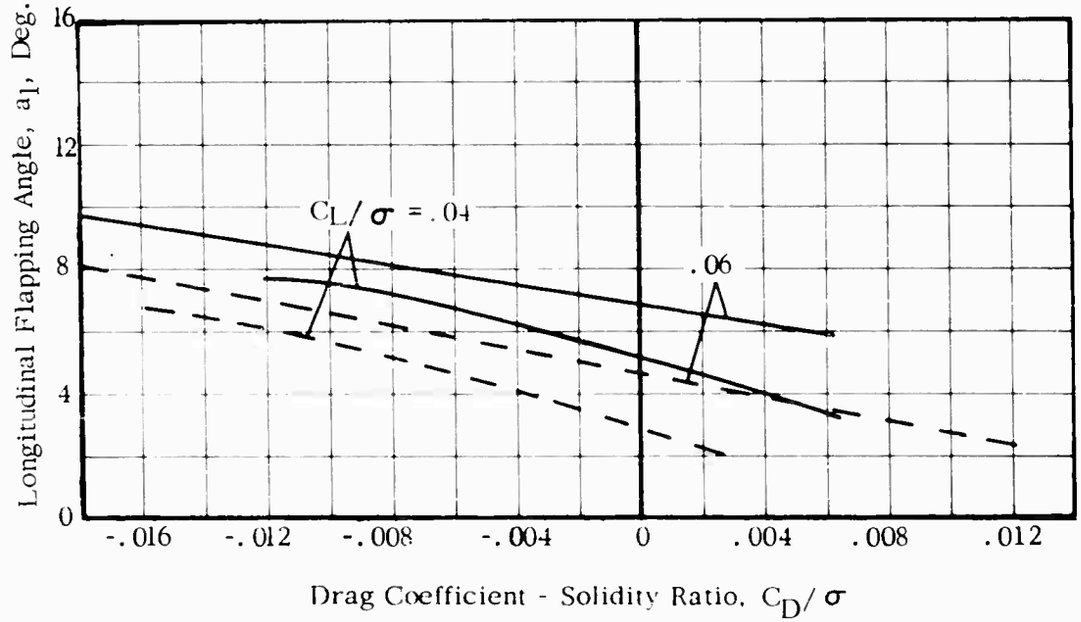

(b) Longitudinal Flapping Angle, a_1, Deg.

FIG.32. COMPARISON OF THEORETICAL AND EXPERIMENTAL BLADE MOTIONS

V = 125 Kts. ΩR = 650 Ft/Sec. μ = 0.32

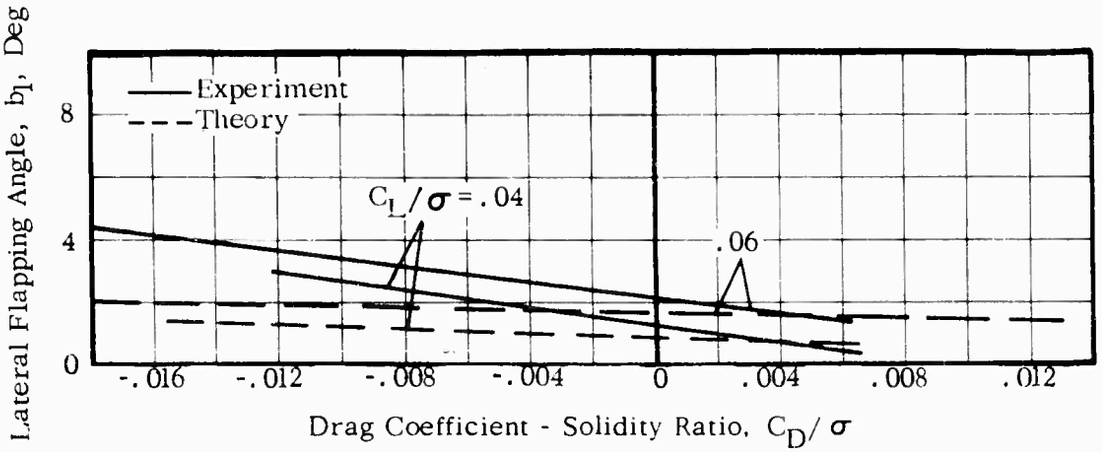

(c) Lateral Flapping Angle, b_1, Deg.

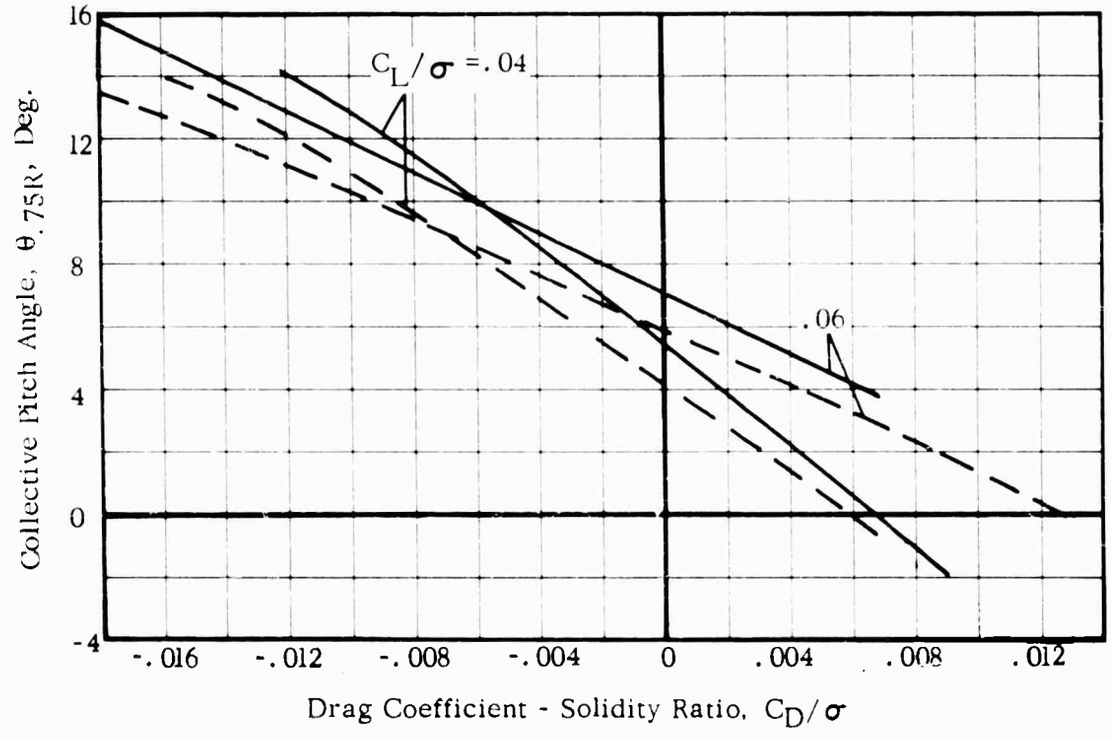

(d) Collective Pitch Angle, $\theta_{.75R}$, Deg.

Figure 32. -Concluded

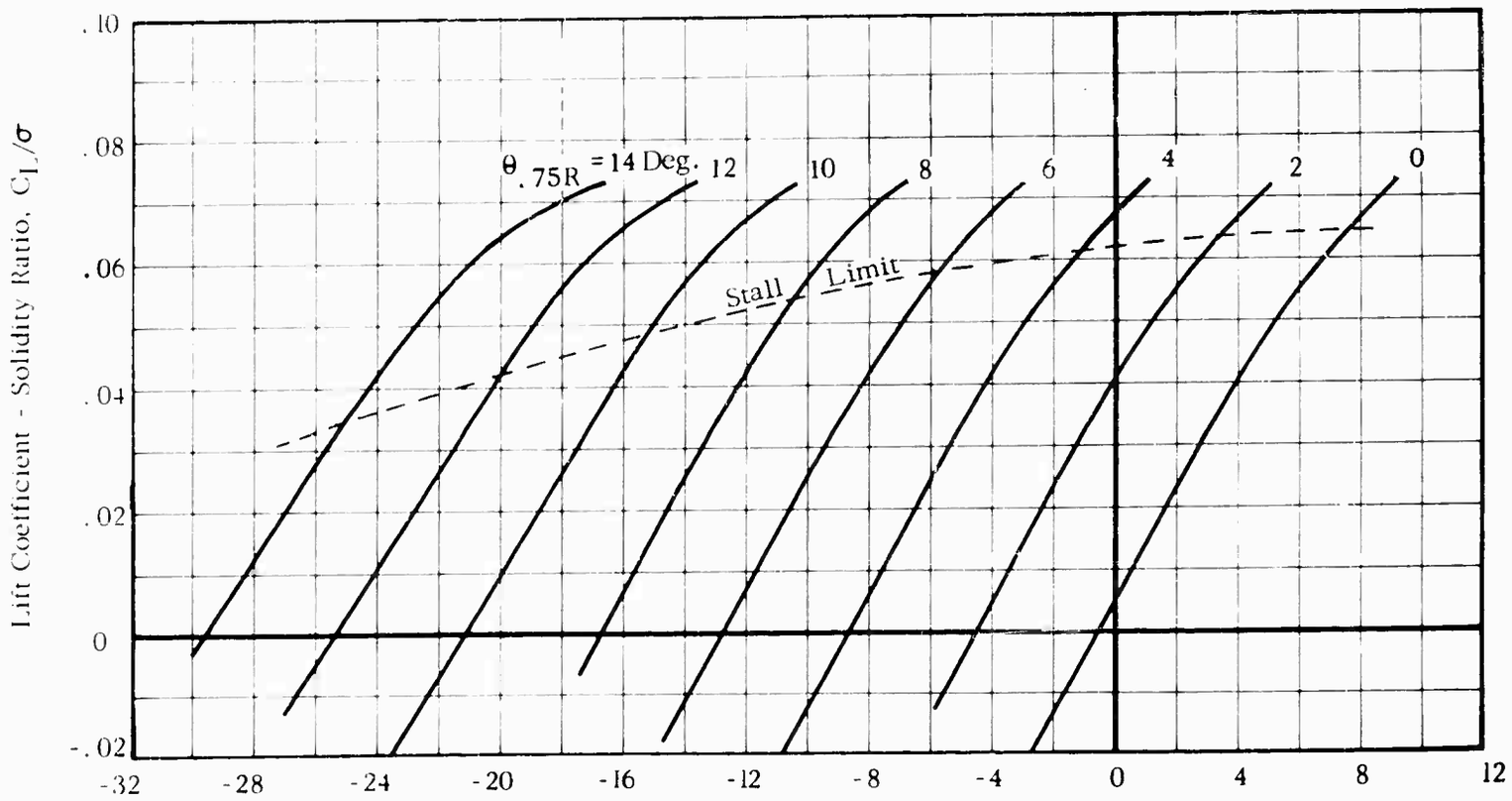

(a) C_L/σ vs α

FIG. 33. THEORETICAL ROTOR PERFORMANCE AND BLADE MOTIONS

V = 150 Kts. ΩR = 650 Ft/Sec. μ = 0.39

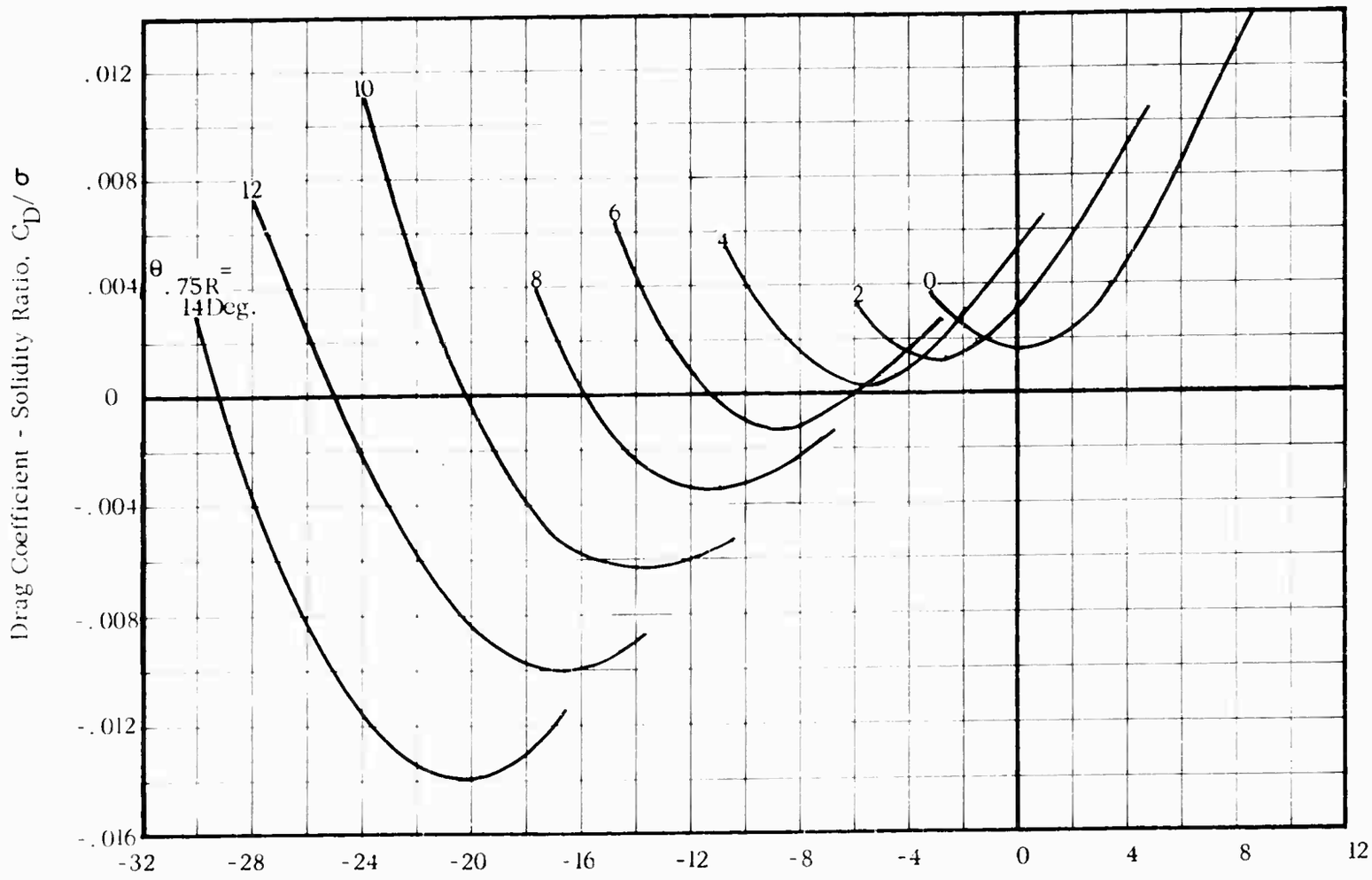

(b) C_D/σ vs α

Figure 33. -Continued

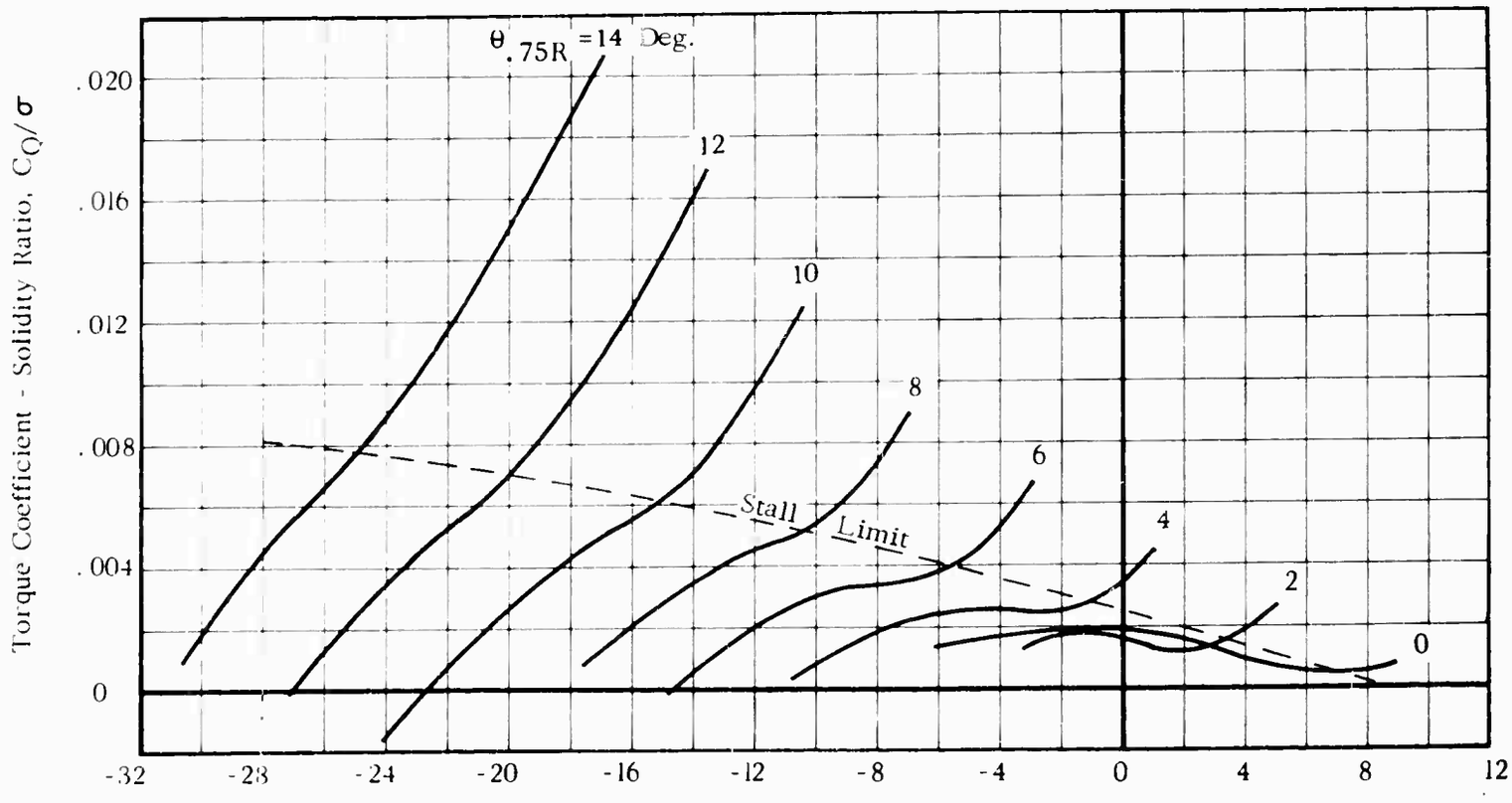

(c) C_Q/σ vs α

Figure 33. -Continued

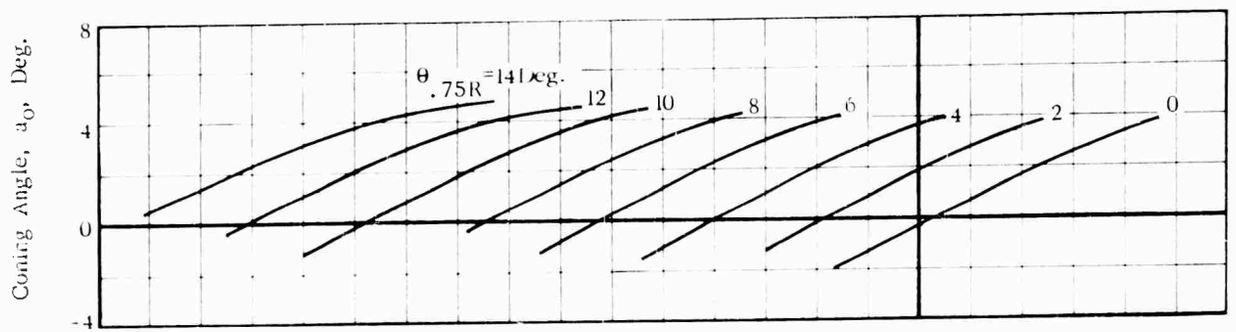

(d) a_0 vs α

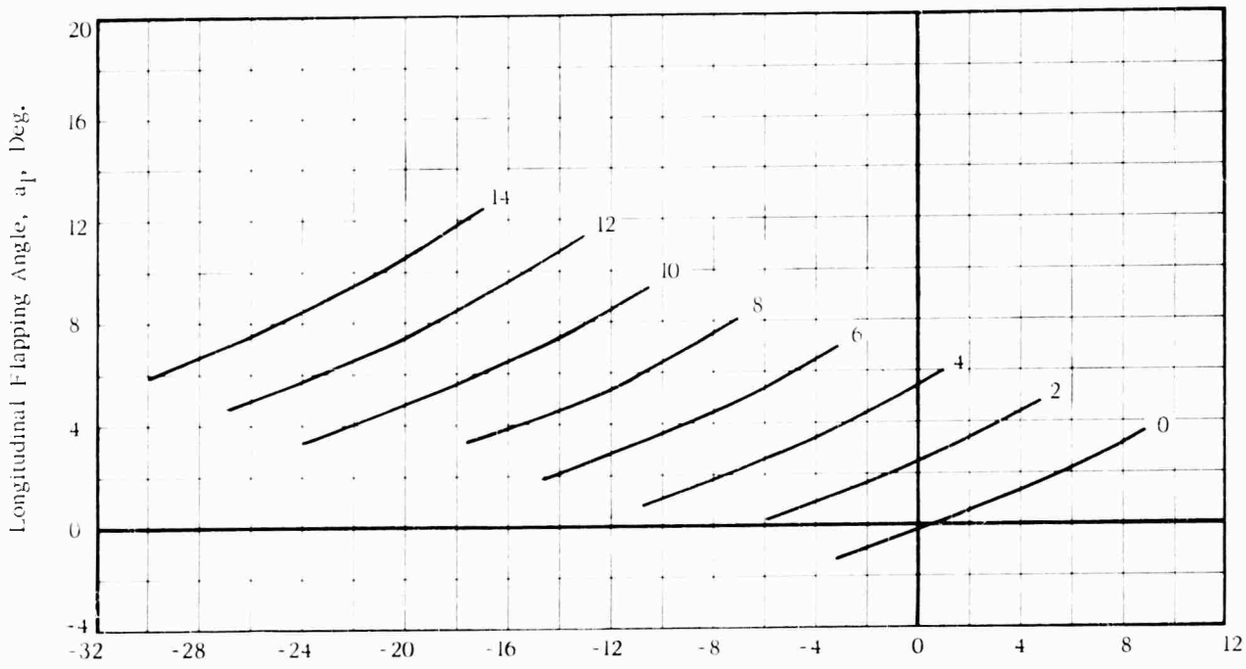

(e) a_1 vs α

Figure 33. Continued

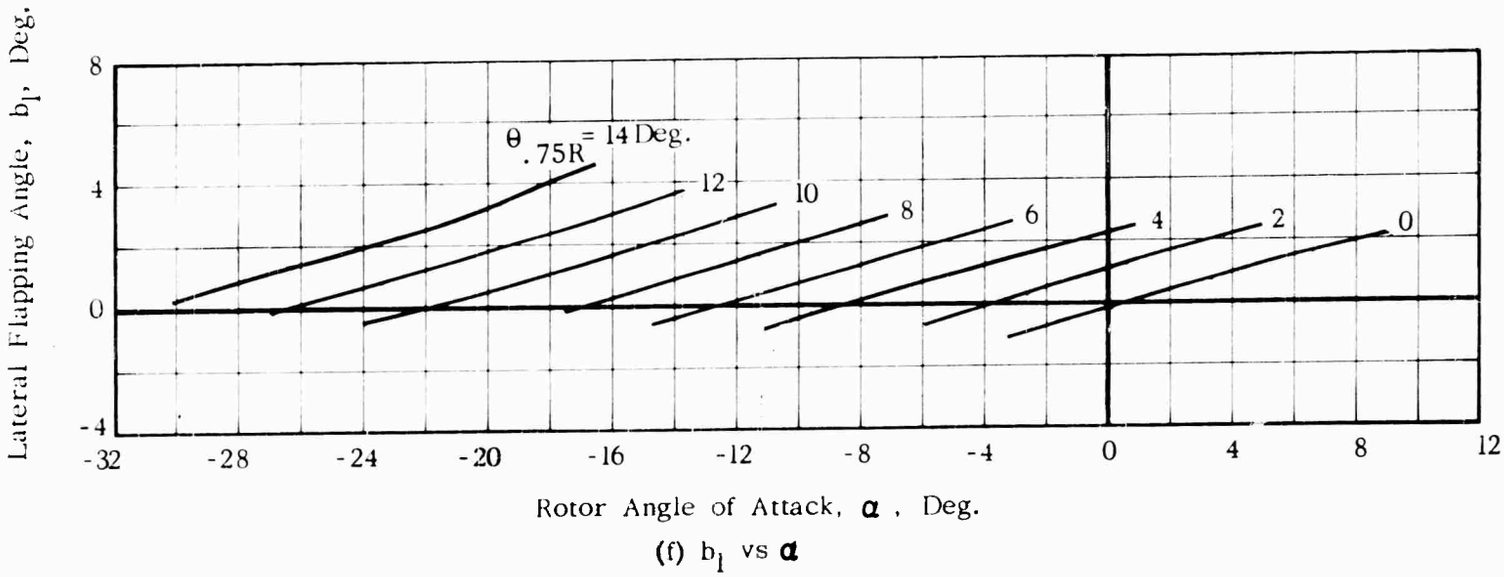

(f) b_1 vs α

Figure 33. -Concluded

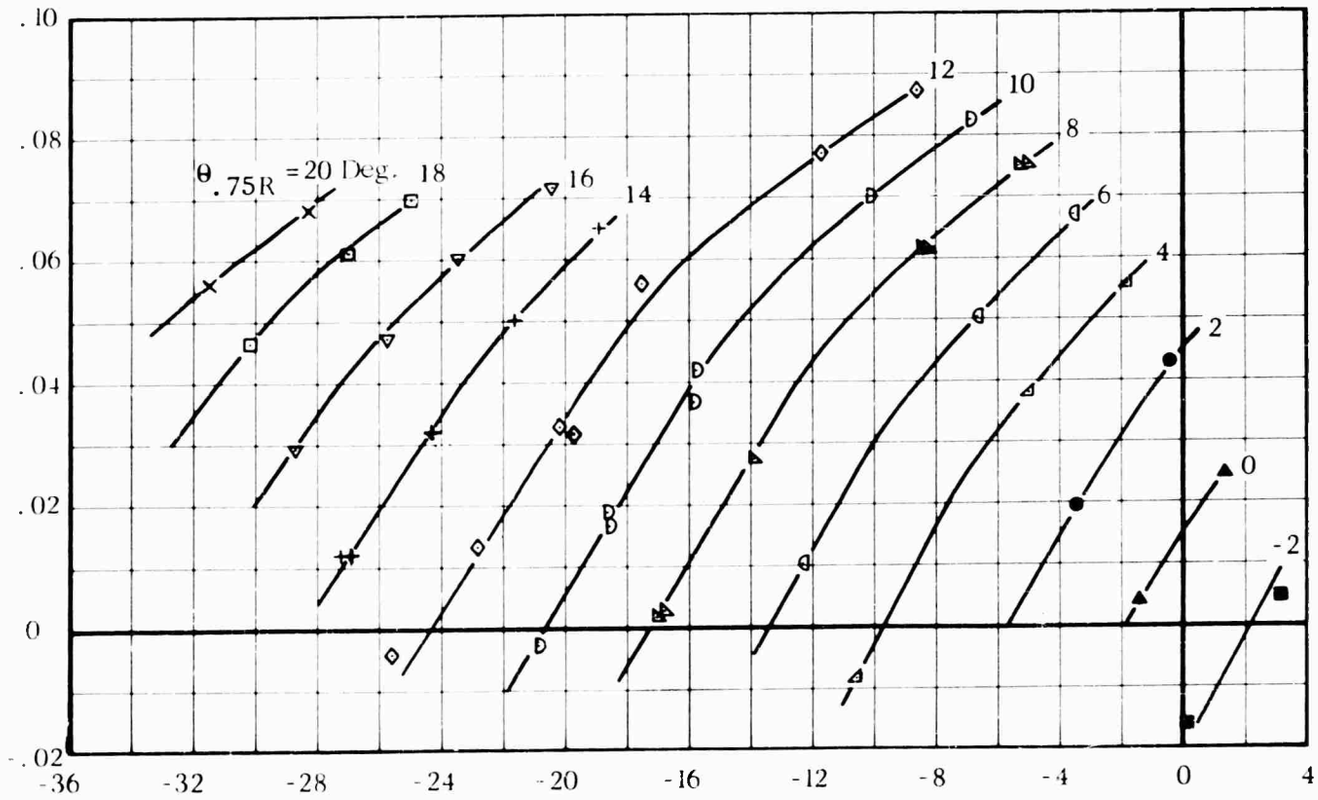

(a) C_L/σ vs α

FIG. 34. EXPERIMENTAL ROTOR PERFORMANCE AND BLADE MOTIONS

V = 150 Kts. ΩR = 650 Ft/Sec. μ = 0.39

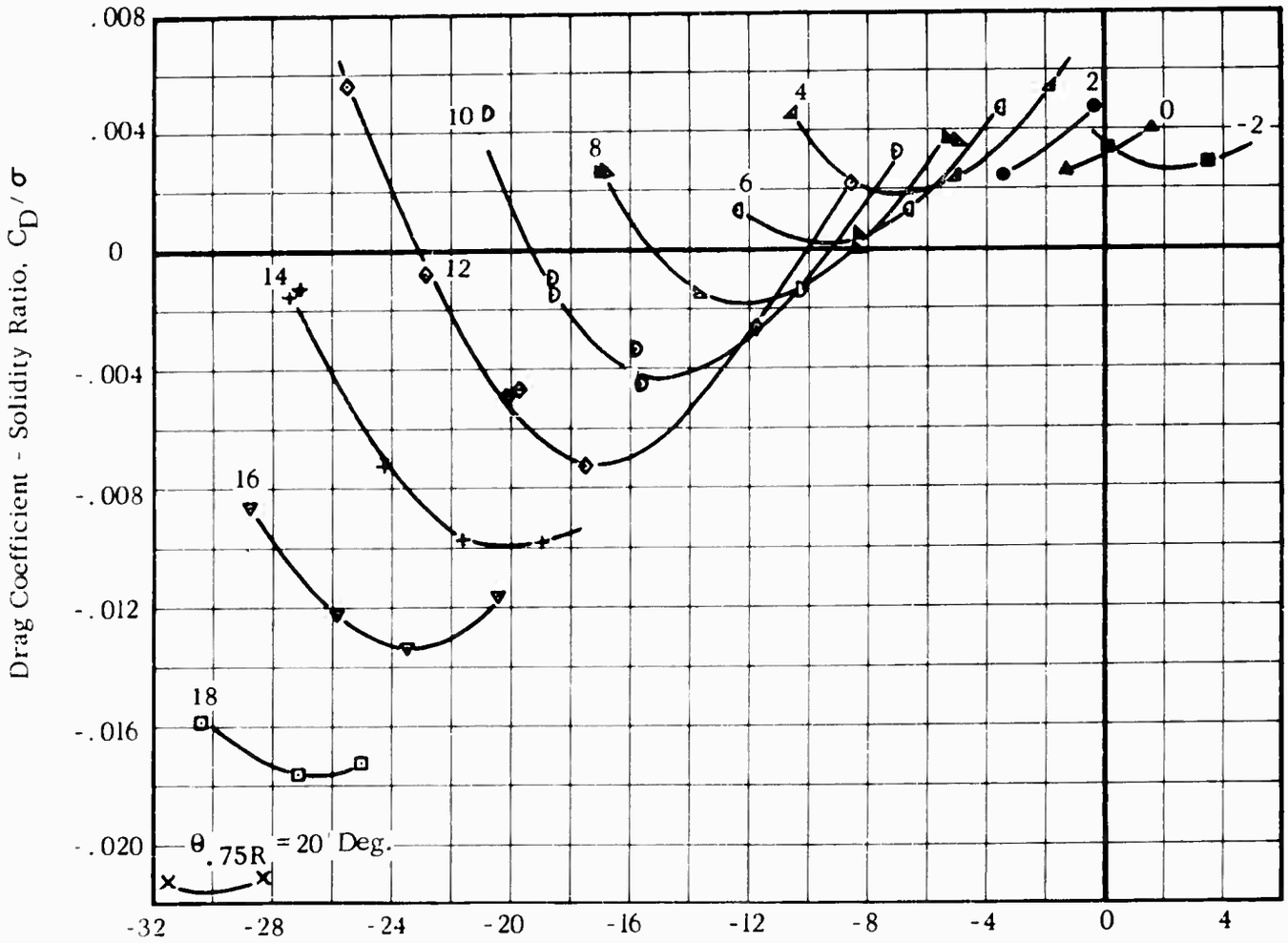

(b) C_D/σ vs α

Figure 34. -Continued

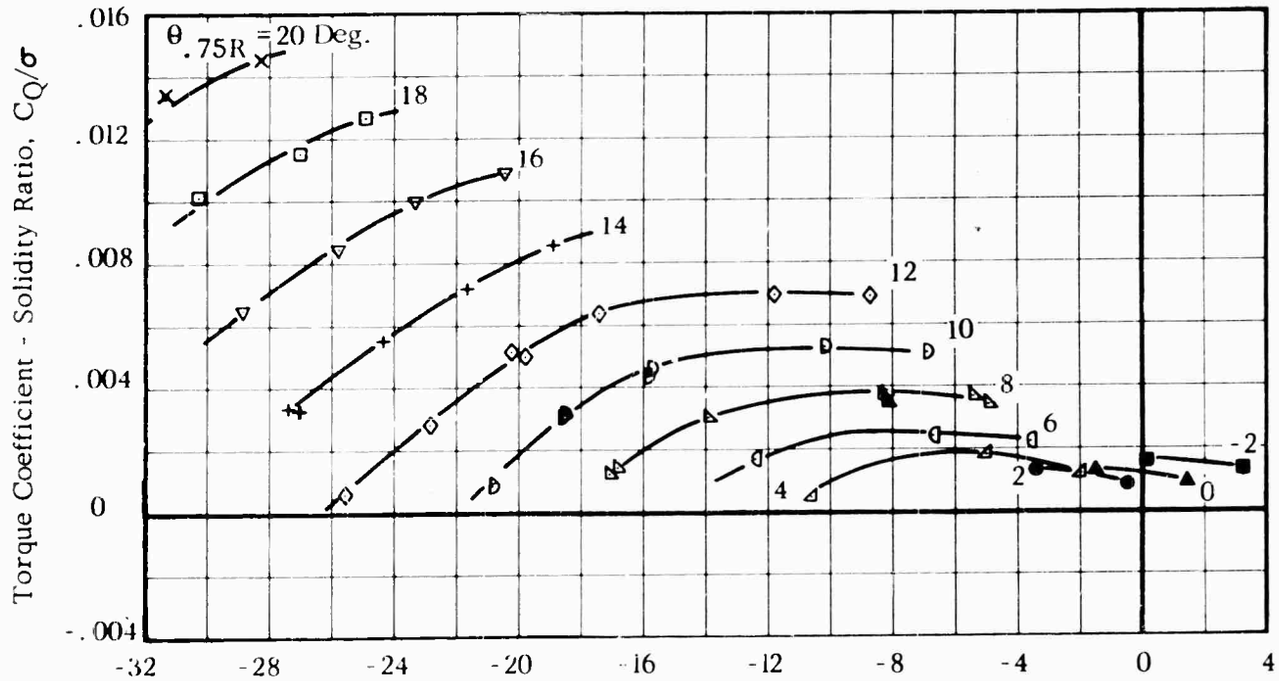

(c) C_Q/σ vs α

Figure 34. -Continued

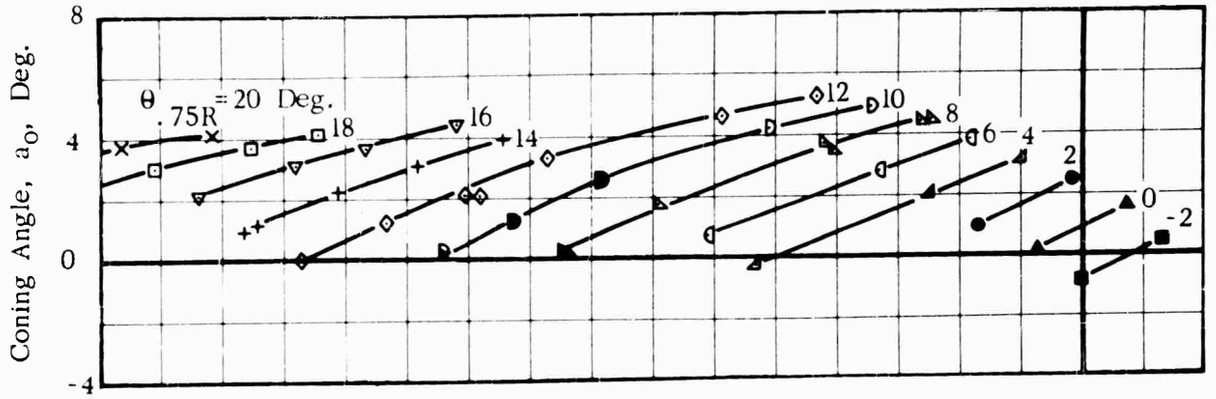

(d) a_o vs α

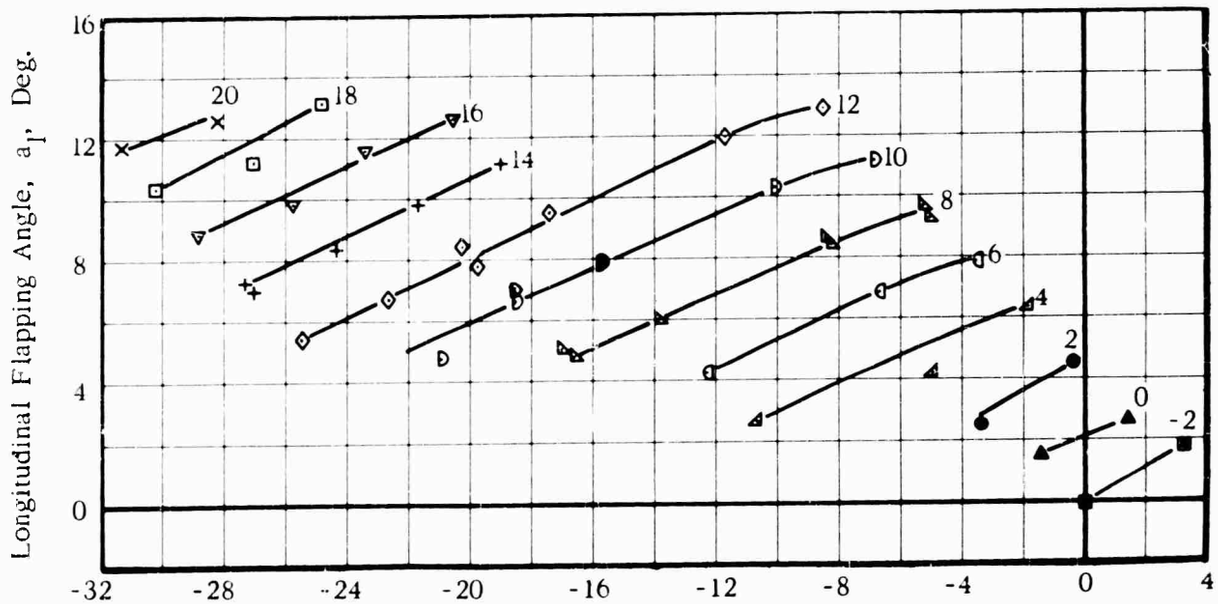

(e) a_1 vs α

Figure 34. Continued

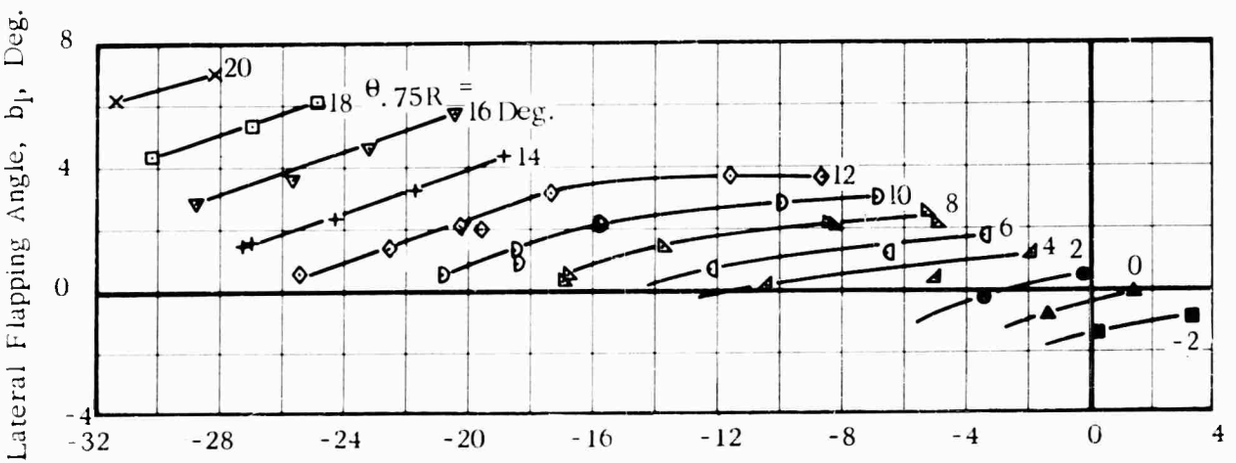

(f) b_1 vs α

Figure 34. -Concluded

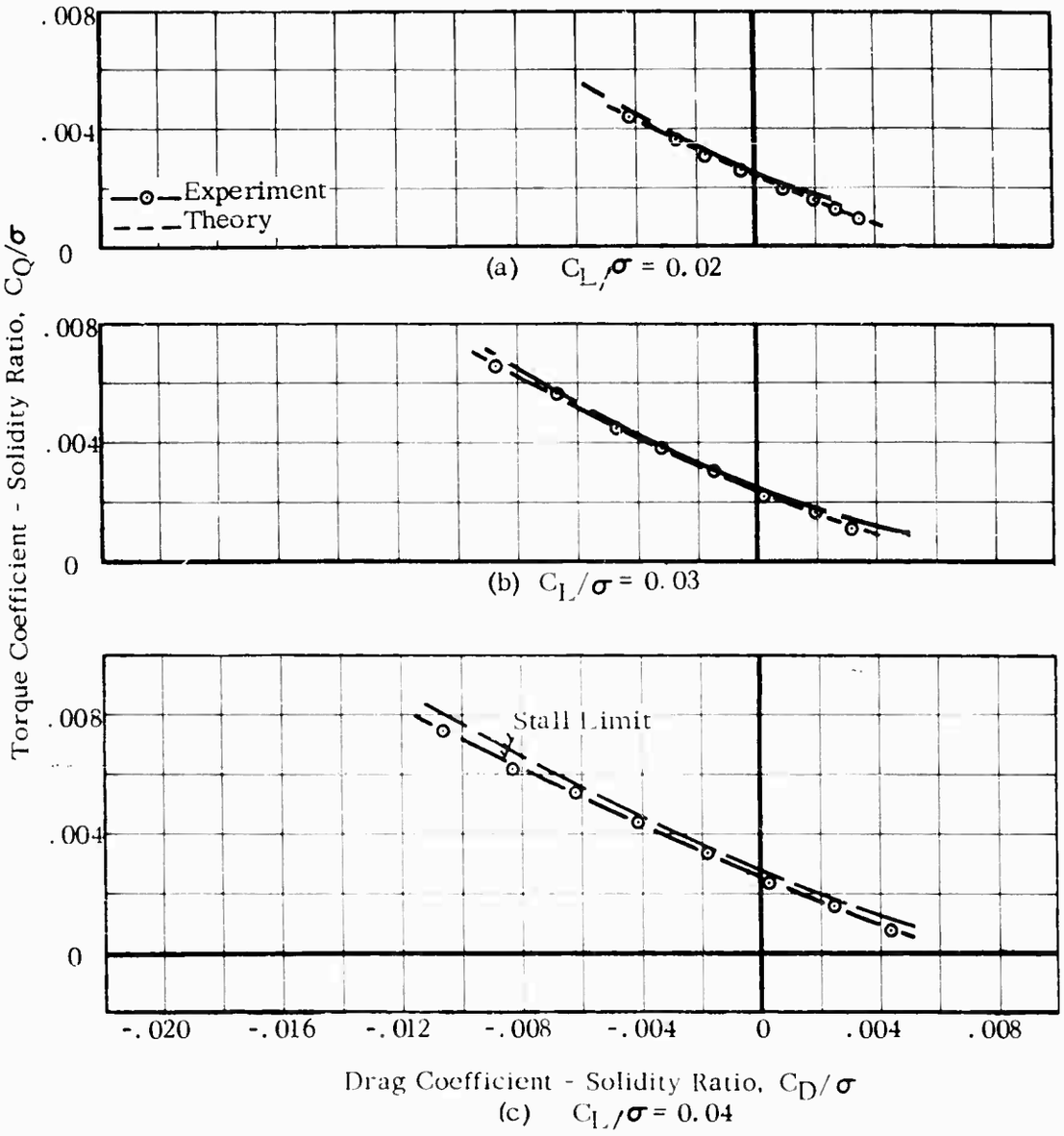

FIG. 35. COMPARISON OF THEORETICAL AND EXPERIMENTAL ROTOR POWER REQUIRED AT CONSTANT LIFT

V = 150 Kts. ΩR = 650 Ft/Sec. μ = 0.39

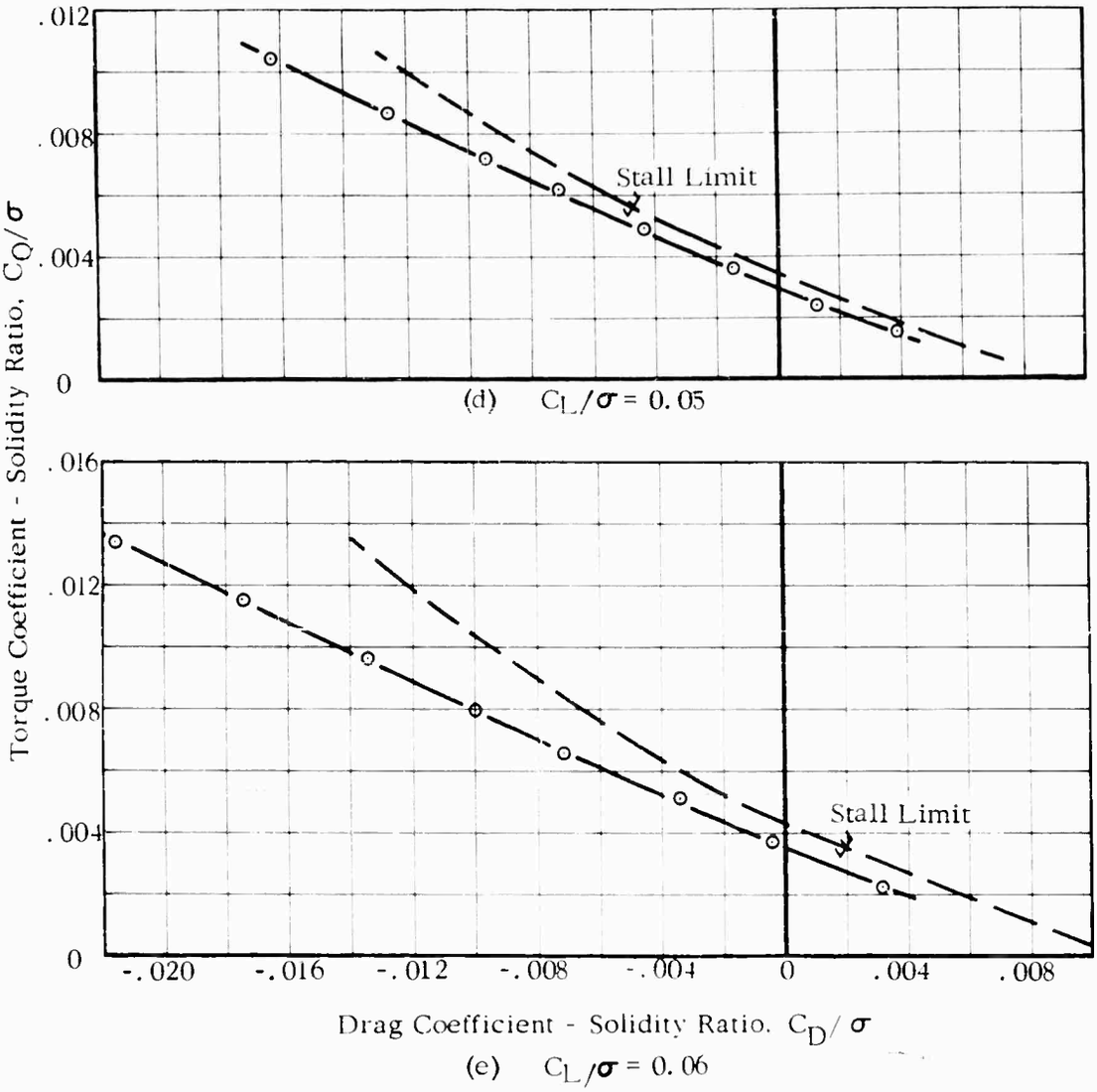

Figure 35. -Concluded

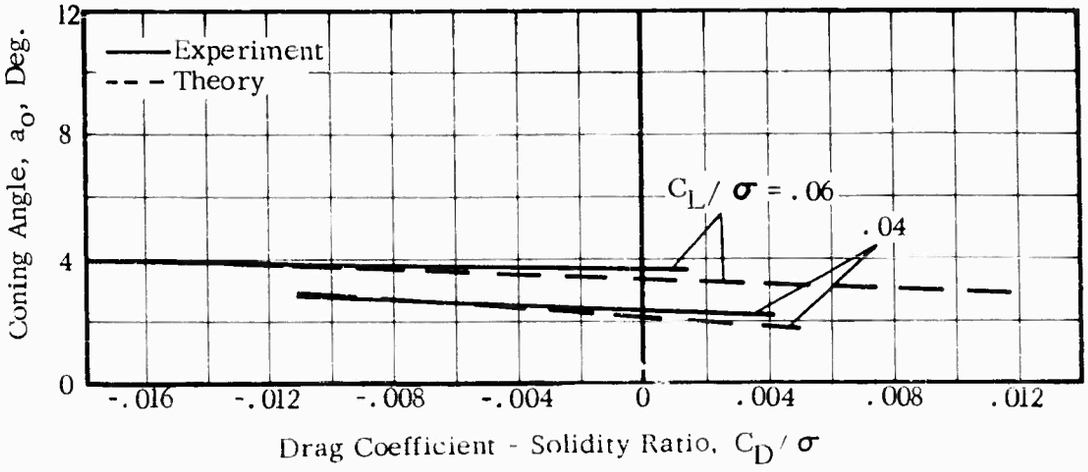

(a) Coning Angle, a_o, Deg.

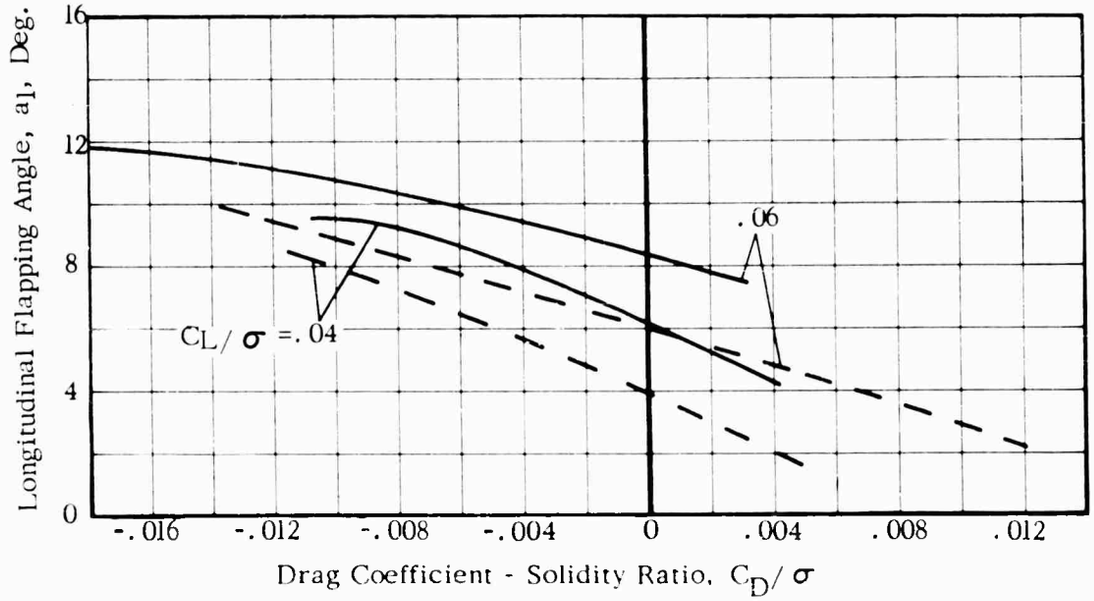

(b) Longitudinal Flapping Angle, a_1, Deg.

FIG.36.COMPARISON OF THEORETICAL AND EXPERIMENTAL BLADE MOTIONS

V = 150 Kts. ΩR = 650 Ft/Sec. μ = 0.39

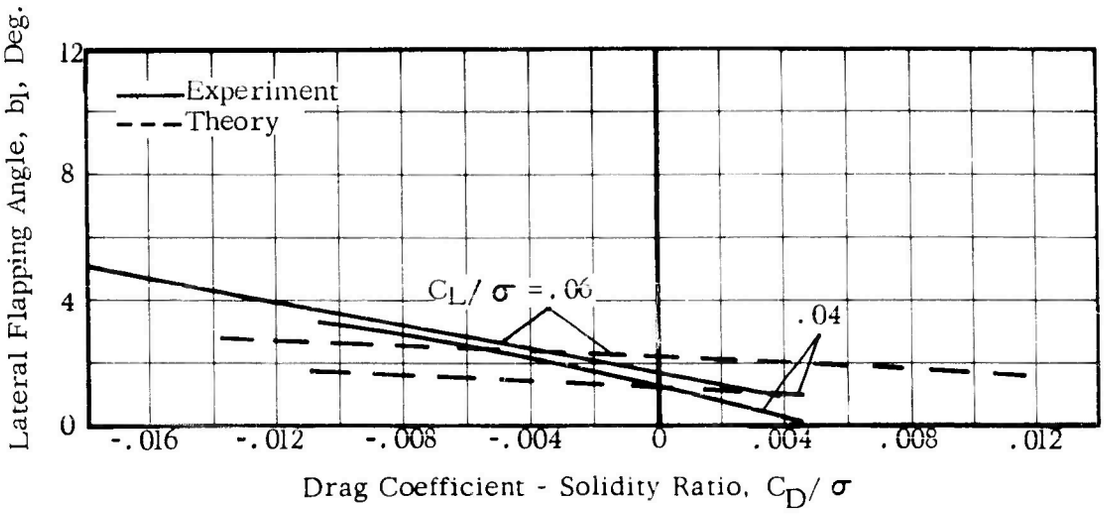

(c) Lateral Flapping Angle, b_1, Deg.

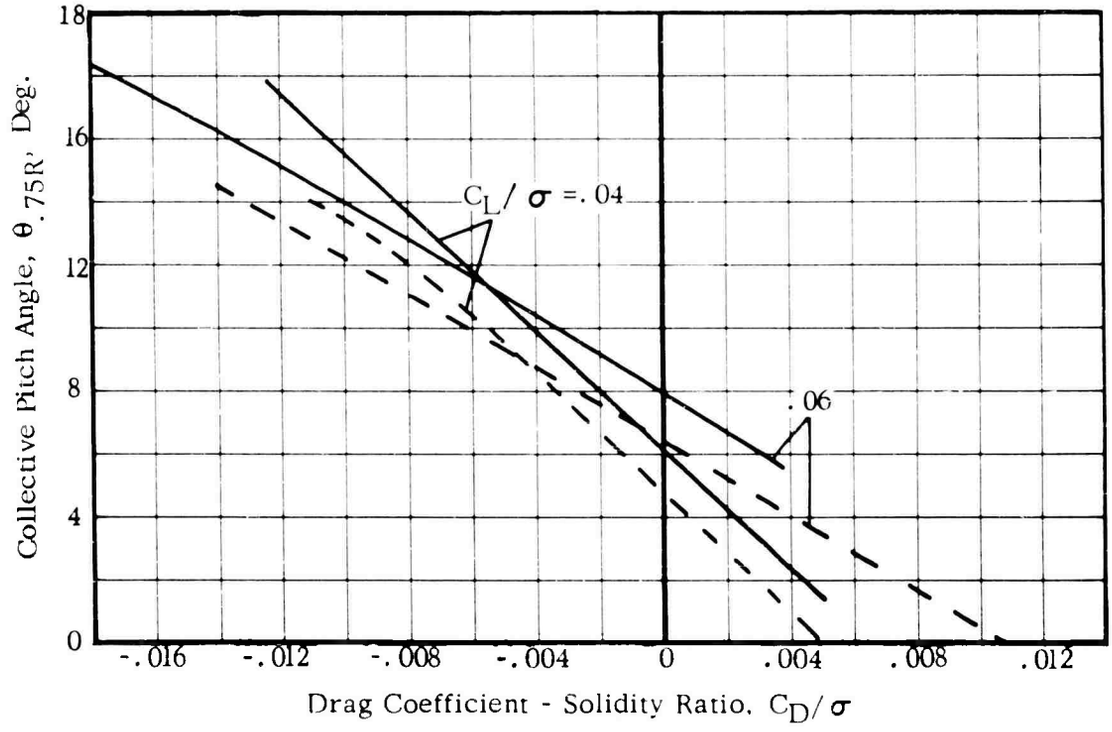

(d) Collective Pitch Angle, $\theta_{.75R}$, Deg.

Figure 36. -Concluded

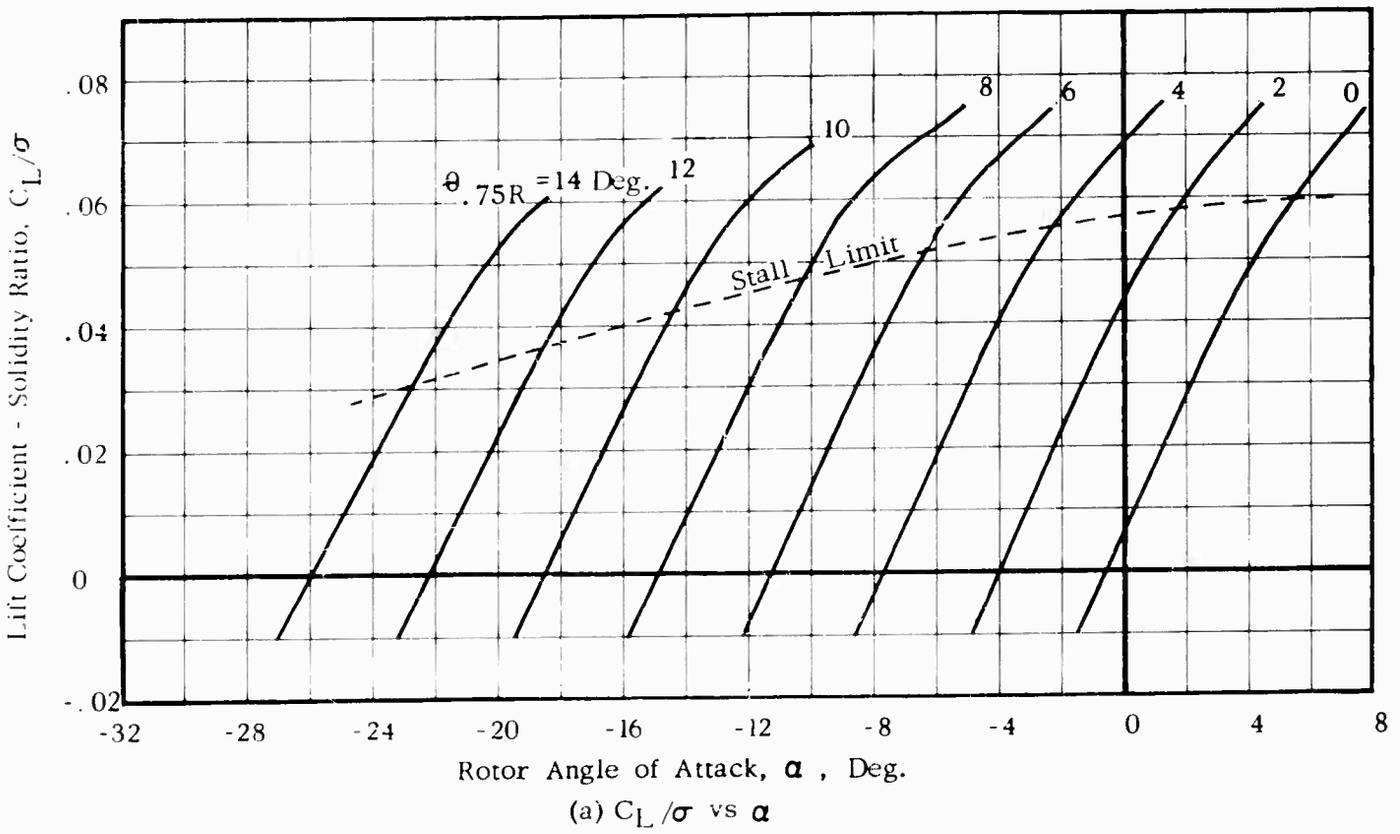

(a) C_L/σ vs α

FIG. 37. THEORETICAL ROTOR PERFORMANCE AND BLADE MOTIONS

V = 161 Kts. ΩR = 580 Ft/Sec. μ = 0.47

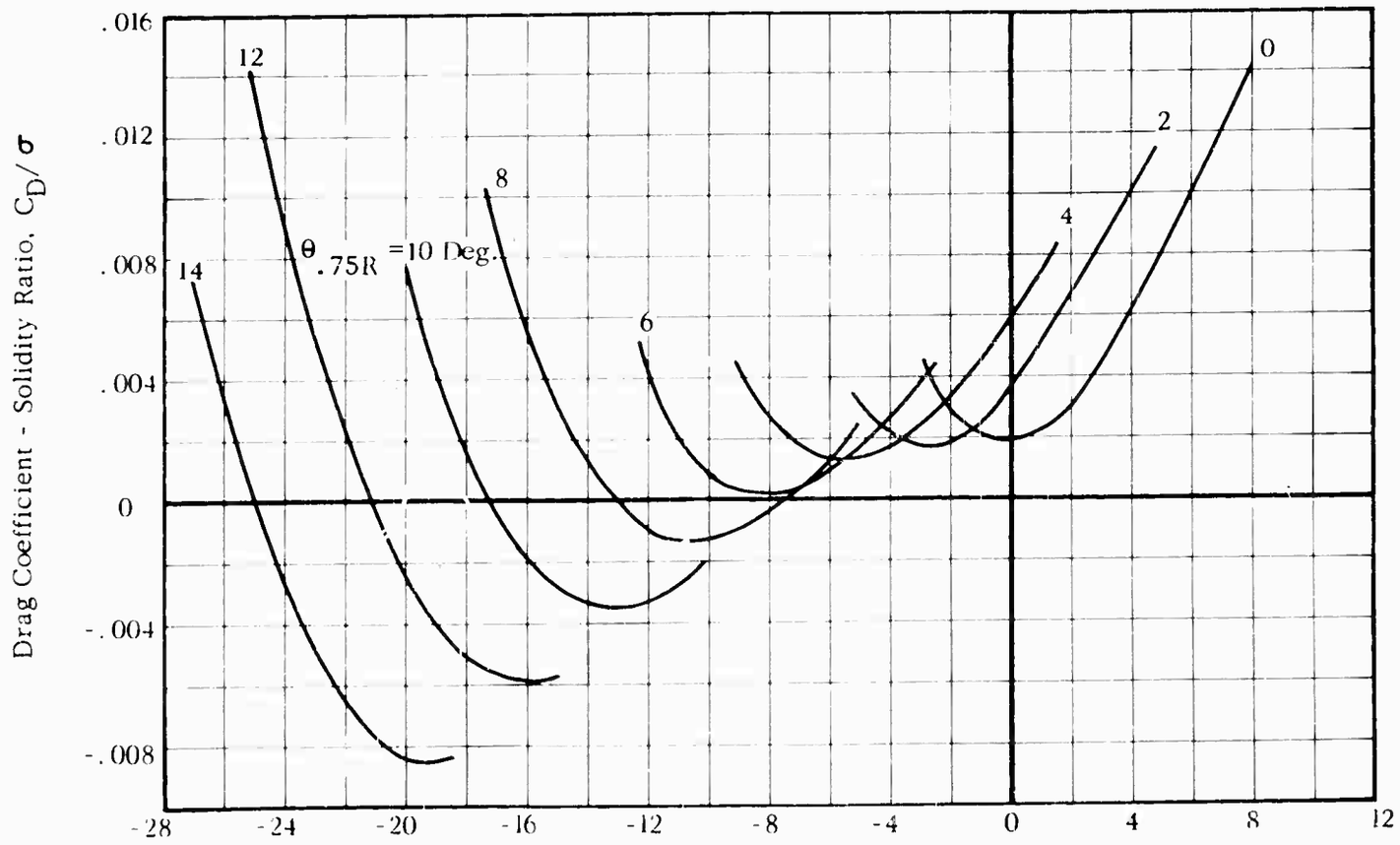

(b) C_D/σ vs α

Figure 37. -Continued

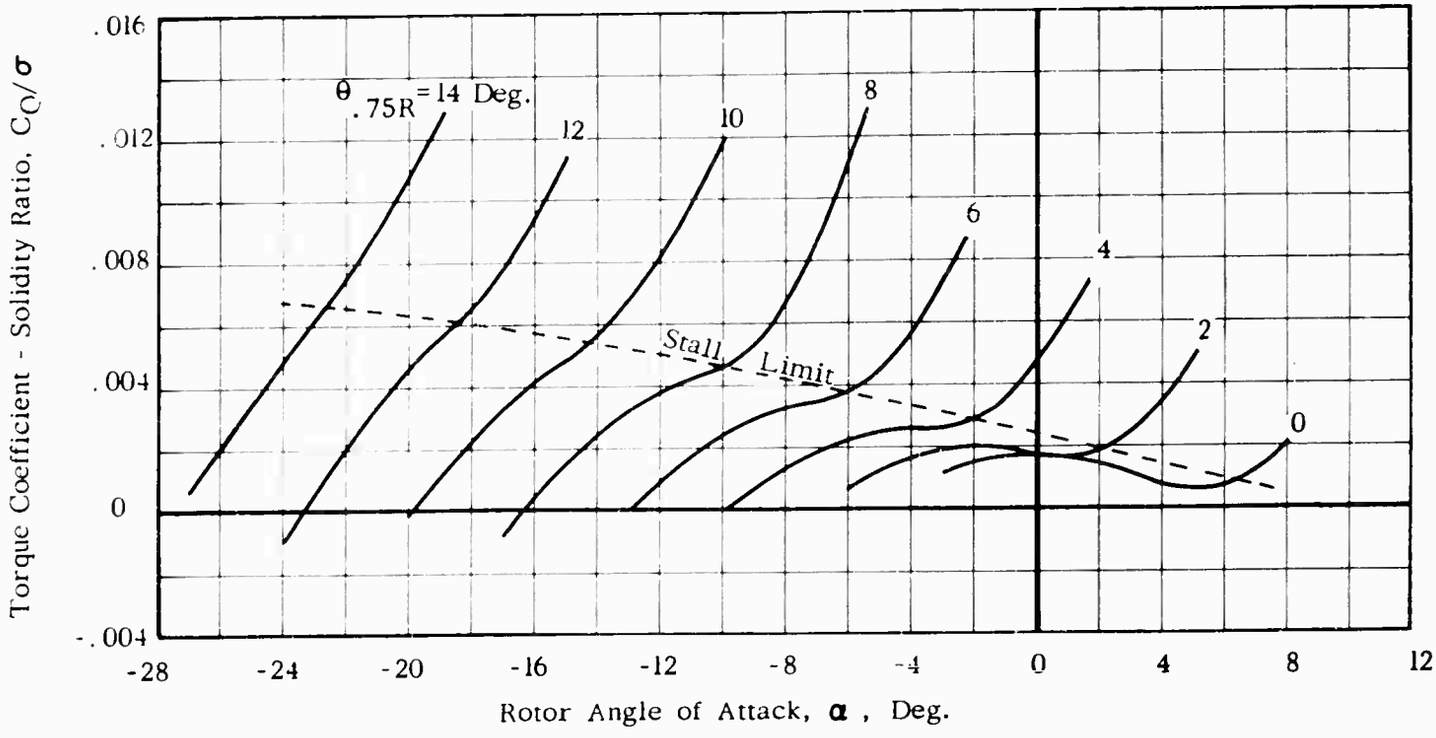

(c) C_Q/σ vs α

Figure 37. -Continued

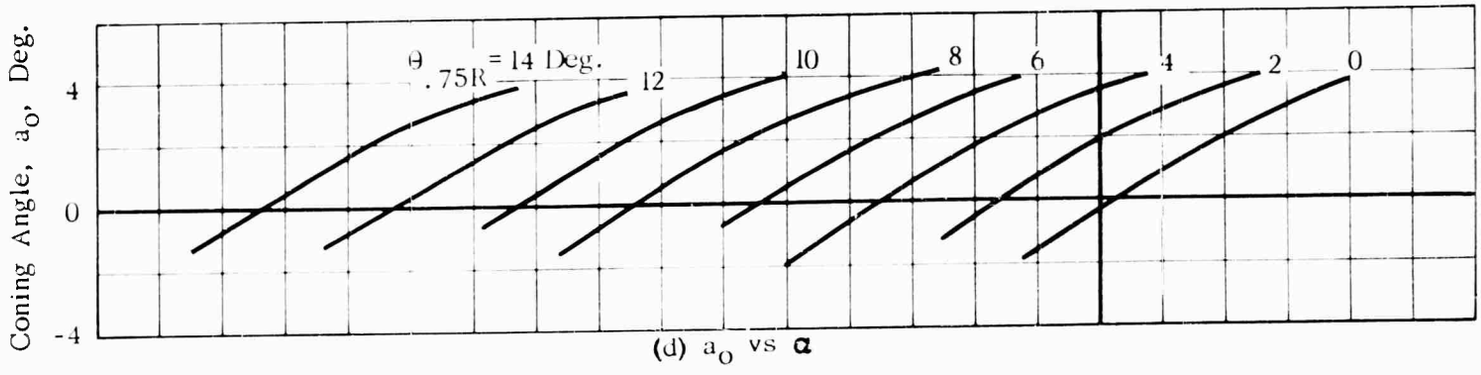

(d) a_o vs α

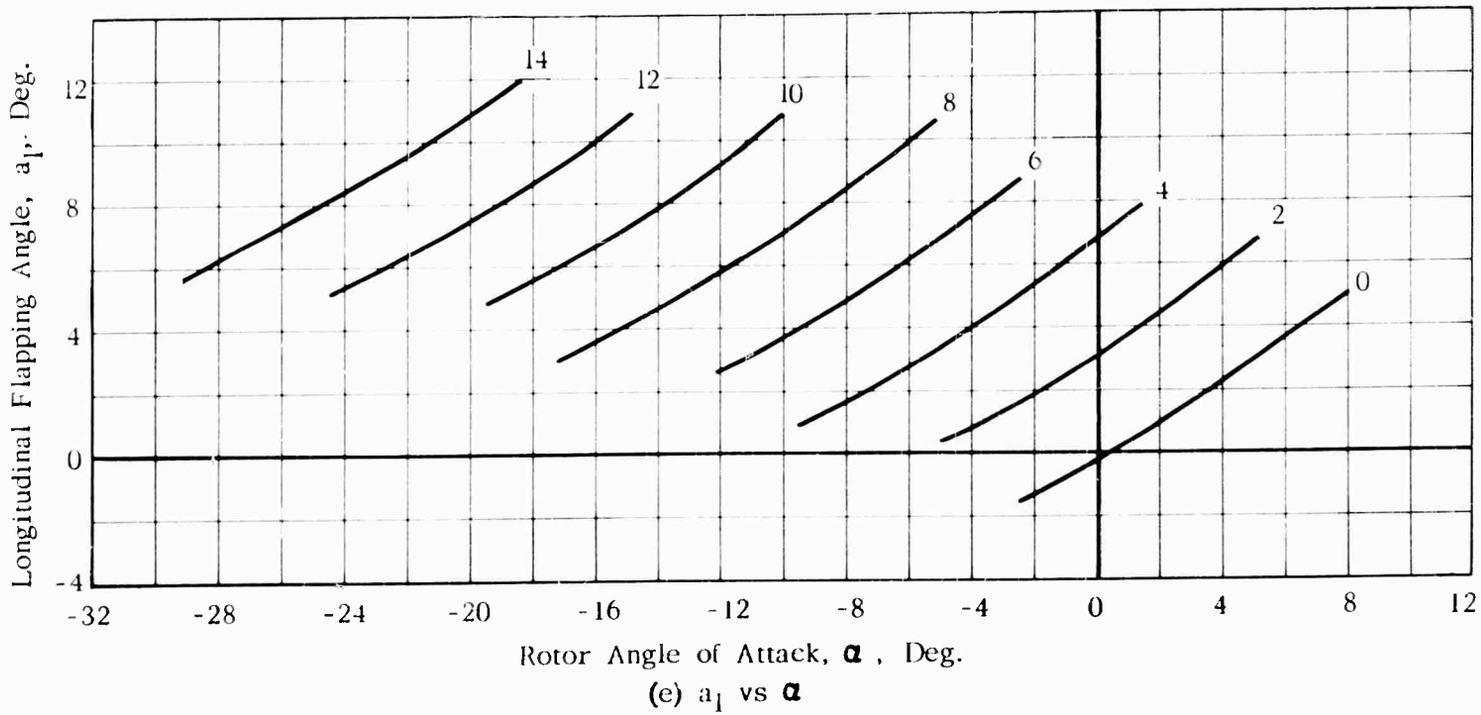

(e) a_1 vs α

Figure 37. Continued

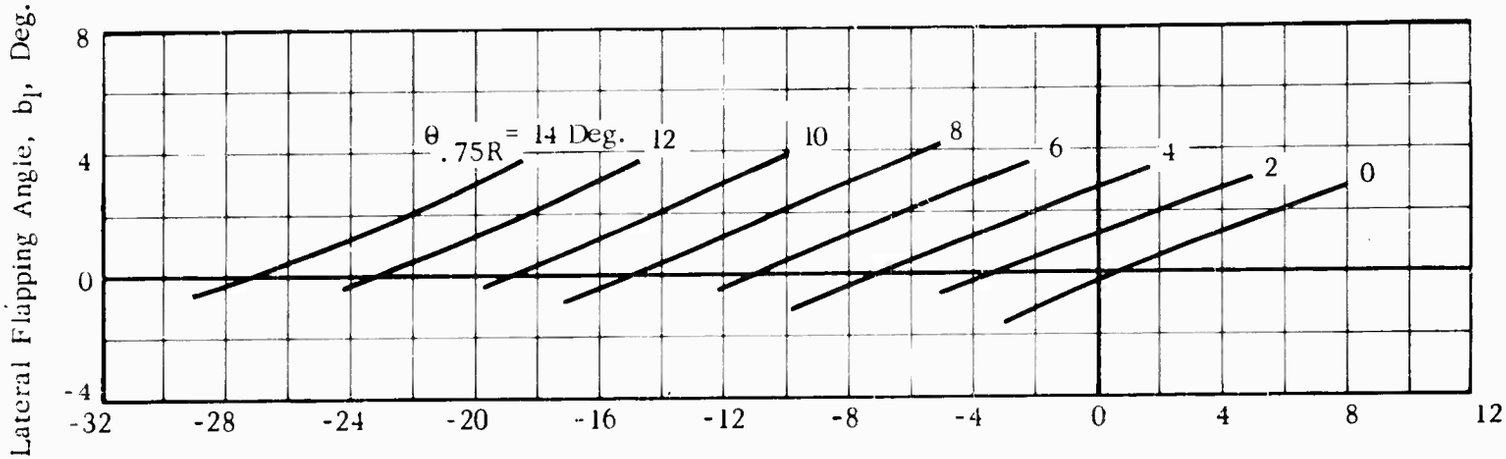

(f) b_1 vs α

Figure 37. -Concluded

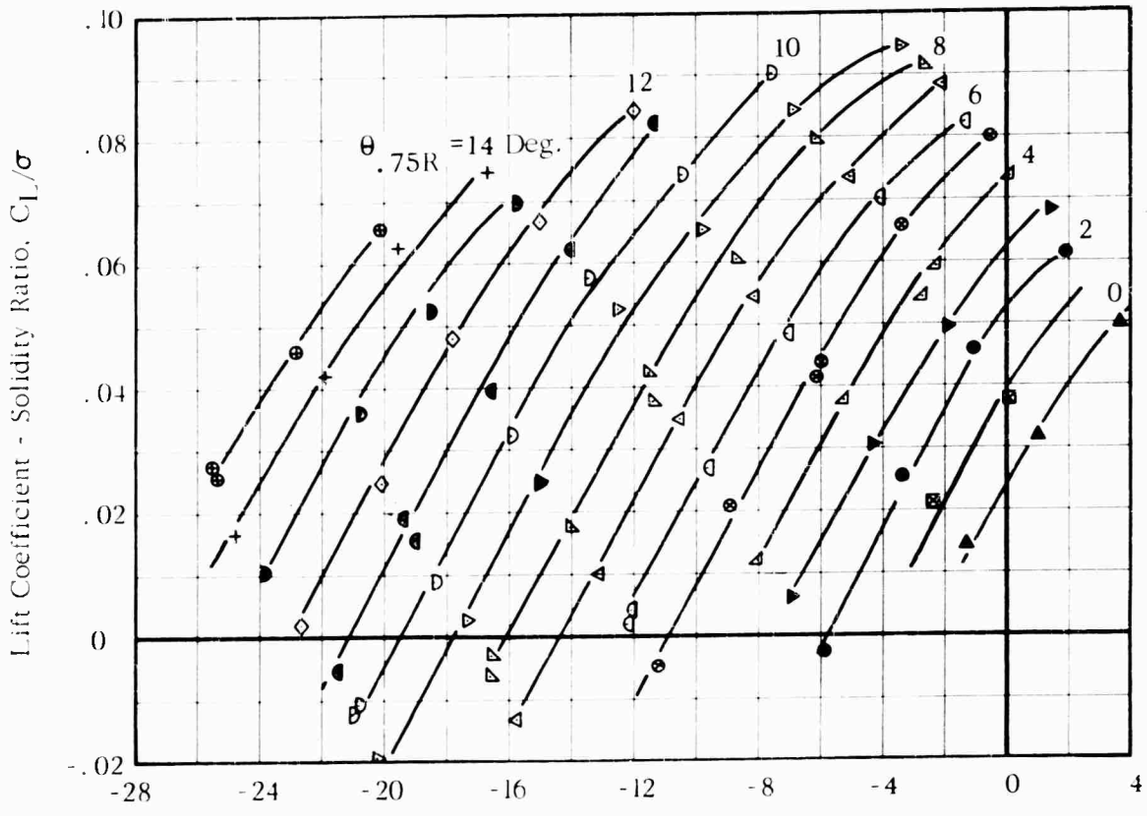

(a) C_L/σ vs α

FIG. 38. EXPERIMENTAL ROTOR PERFORMANCE AND BLADE MOTIONS

V = 161 Kts. ΩR = 580 Ft/Sec. μ = 0.47

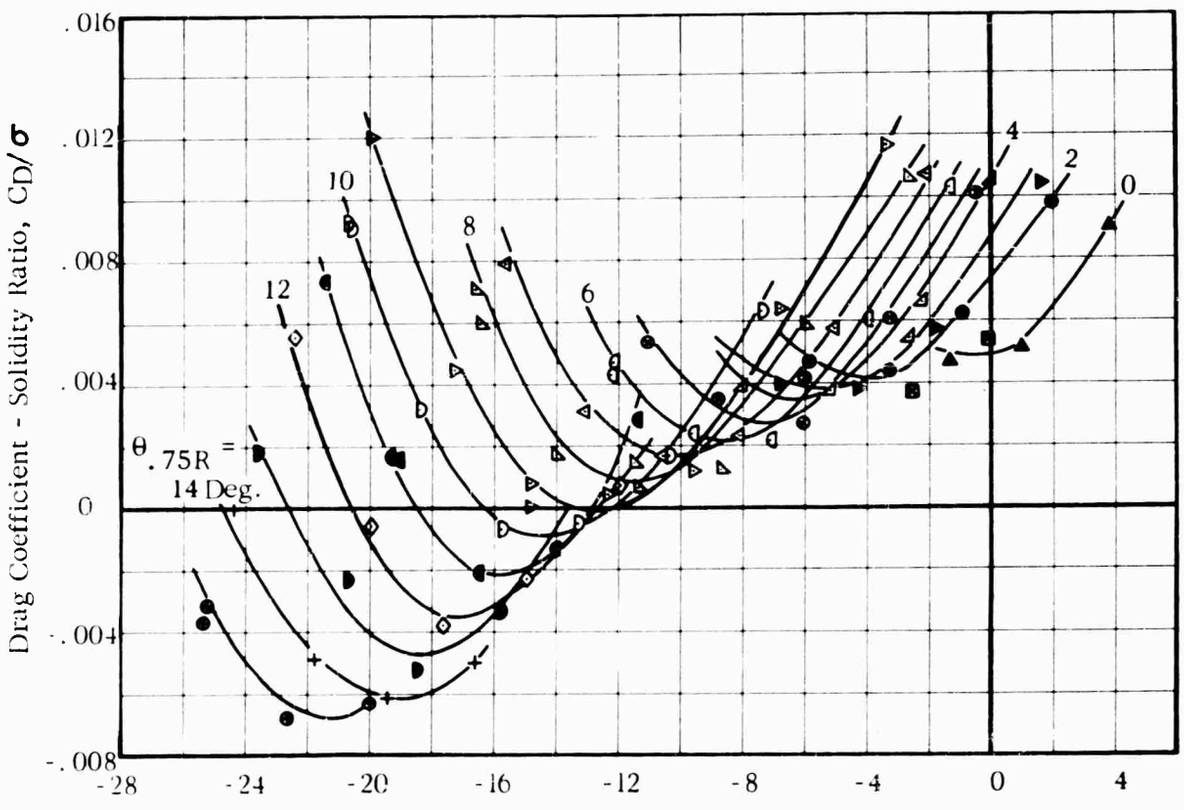

(b) C_D/σ vs α

Figure 38. -Continued

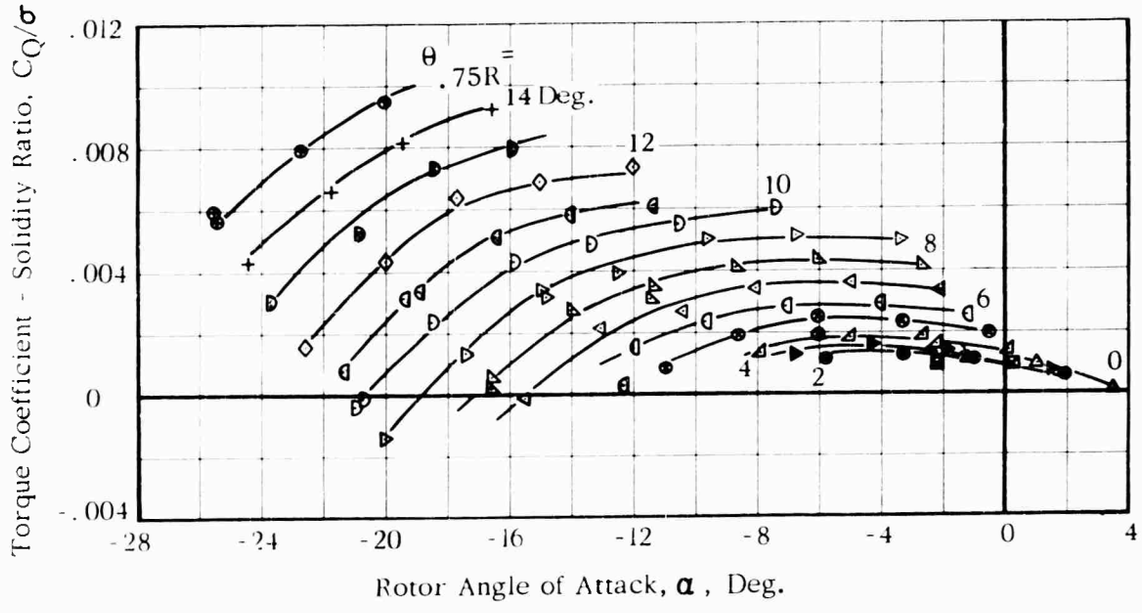

(c) C_Q/σ vs α

Figure 38. -Continued

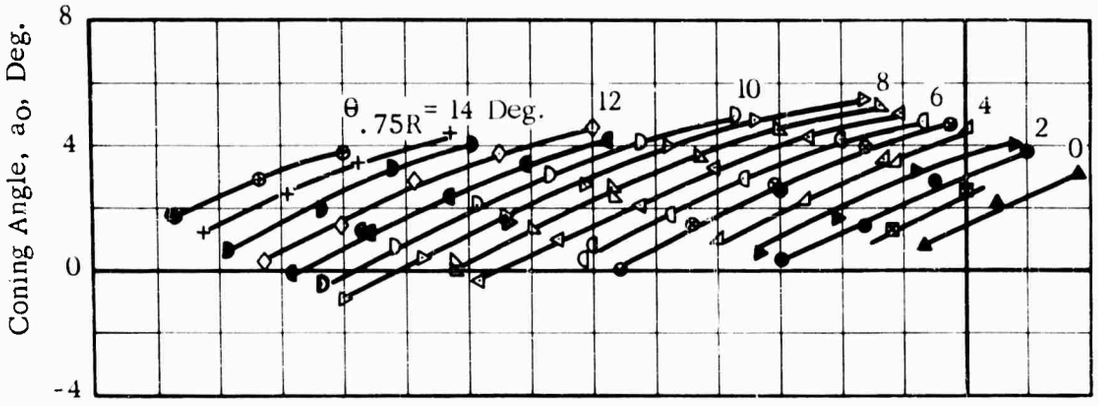

(d) a_o vs α

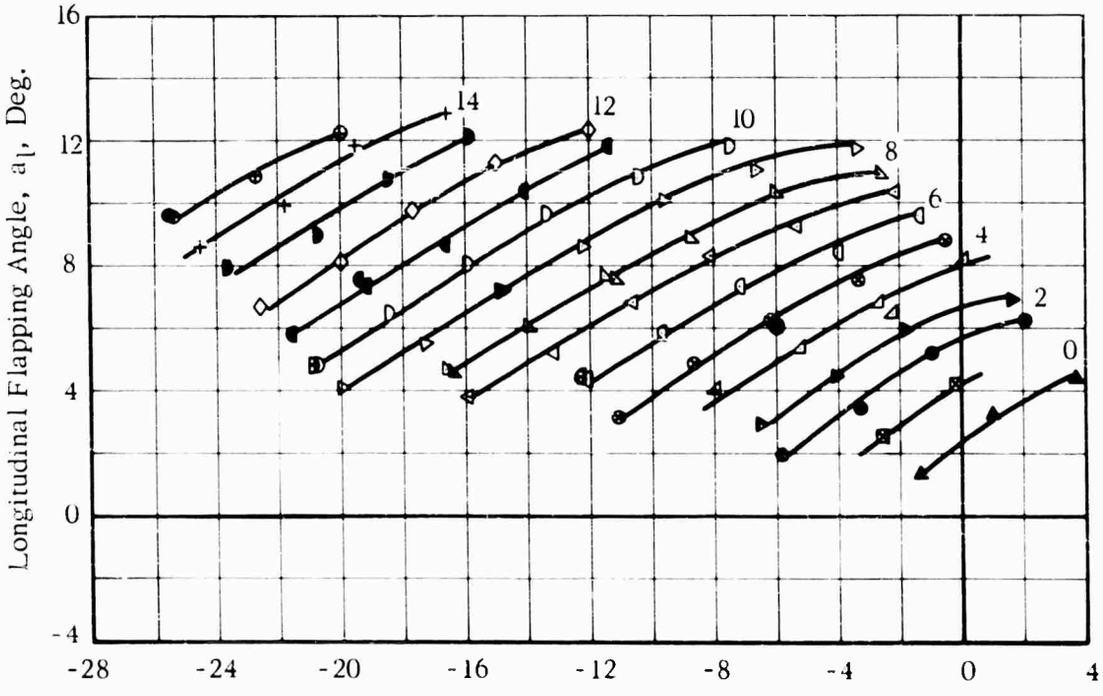

(e) a_1 vs α

Figure 38. Continued

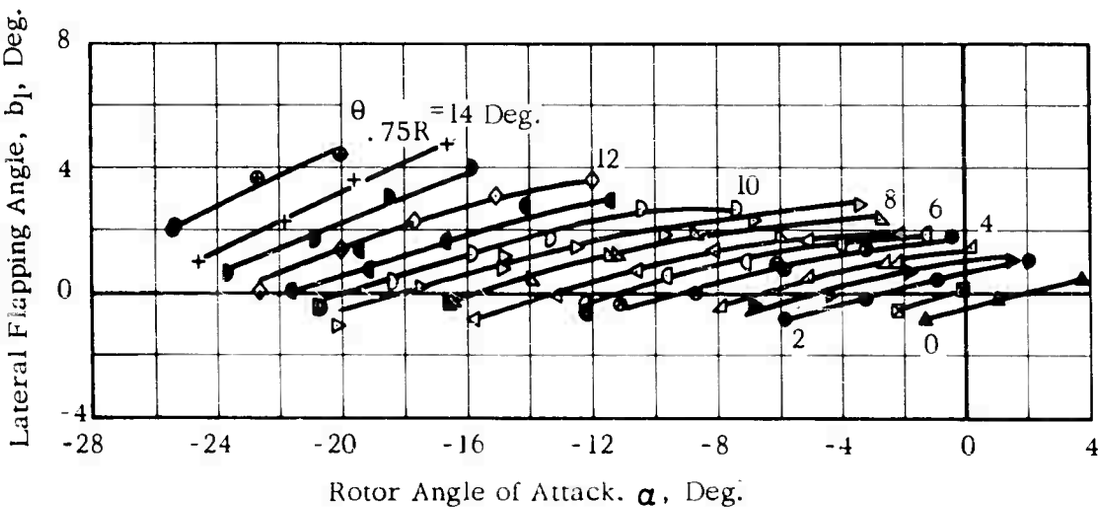

(f) b_1 vs α

Figure 38. -Concluded

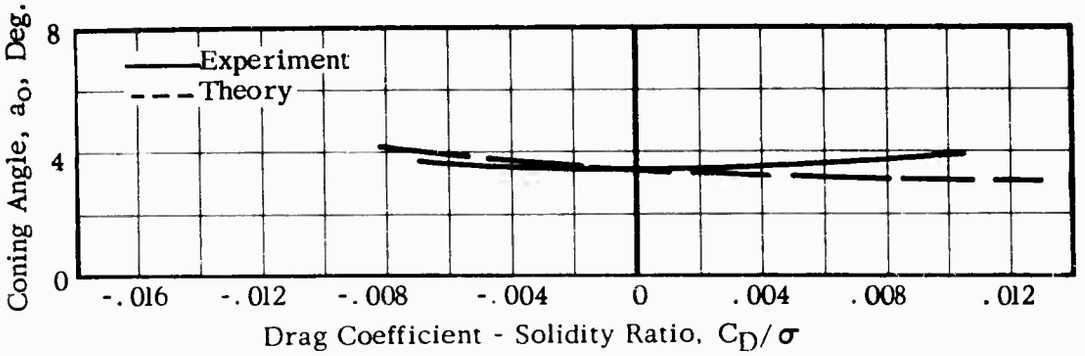

(a) Coning Angle, a_o, Deg.

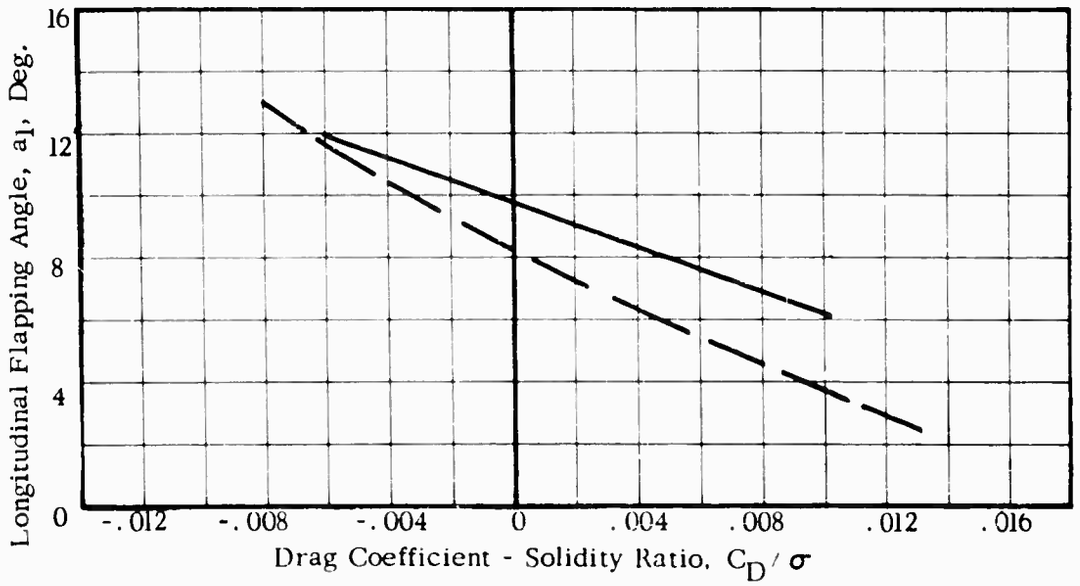

(b) Longitudinal Flapping Angle, a_1, Deg.

FIG.39. COMPARISON OF THEORETICAL AND EXPERIMENTAL BLADE MOTIONS

V = 161 Kts. ΩR = 580 Ft/Sec. $L/\pi R^2$ = 4.0 LB./FT.^{2}

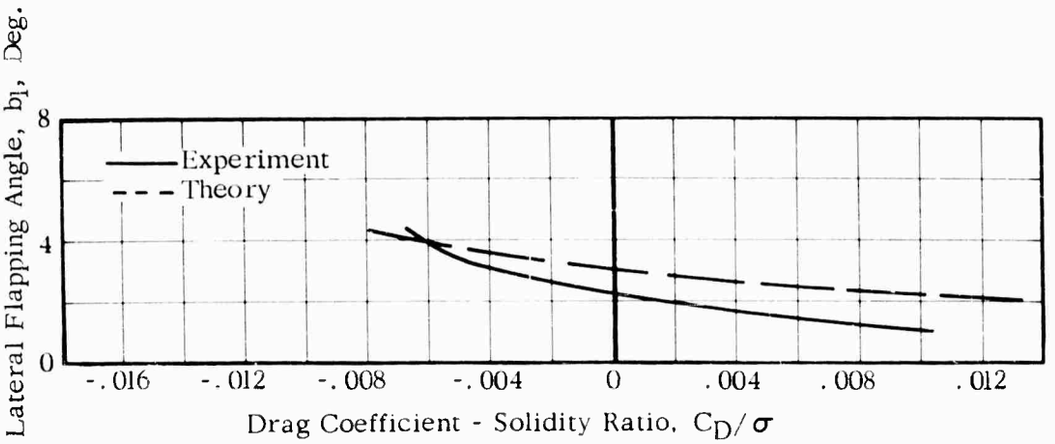

(c) Lateral Flapping Angle, b_1, Deg.

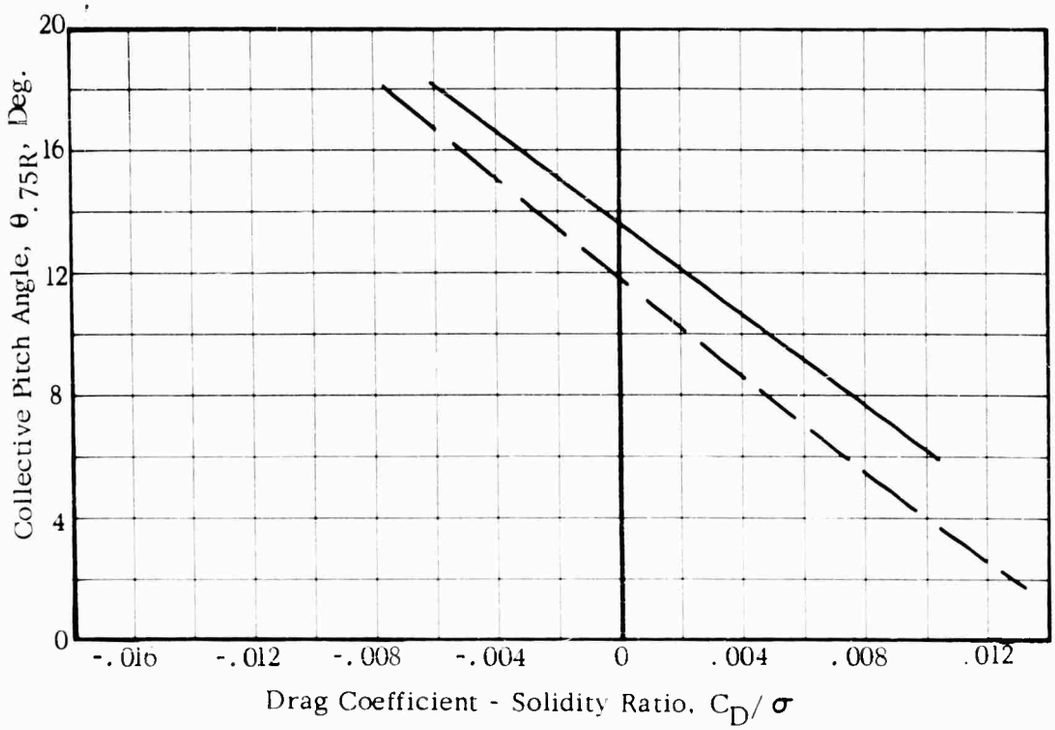

(d) Collective Pitch Angle, $\theta_{.75R}$, Deg.

Figure 39. -Concluded

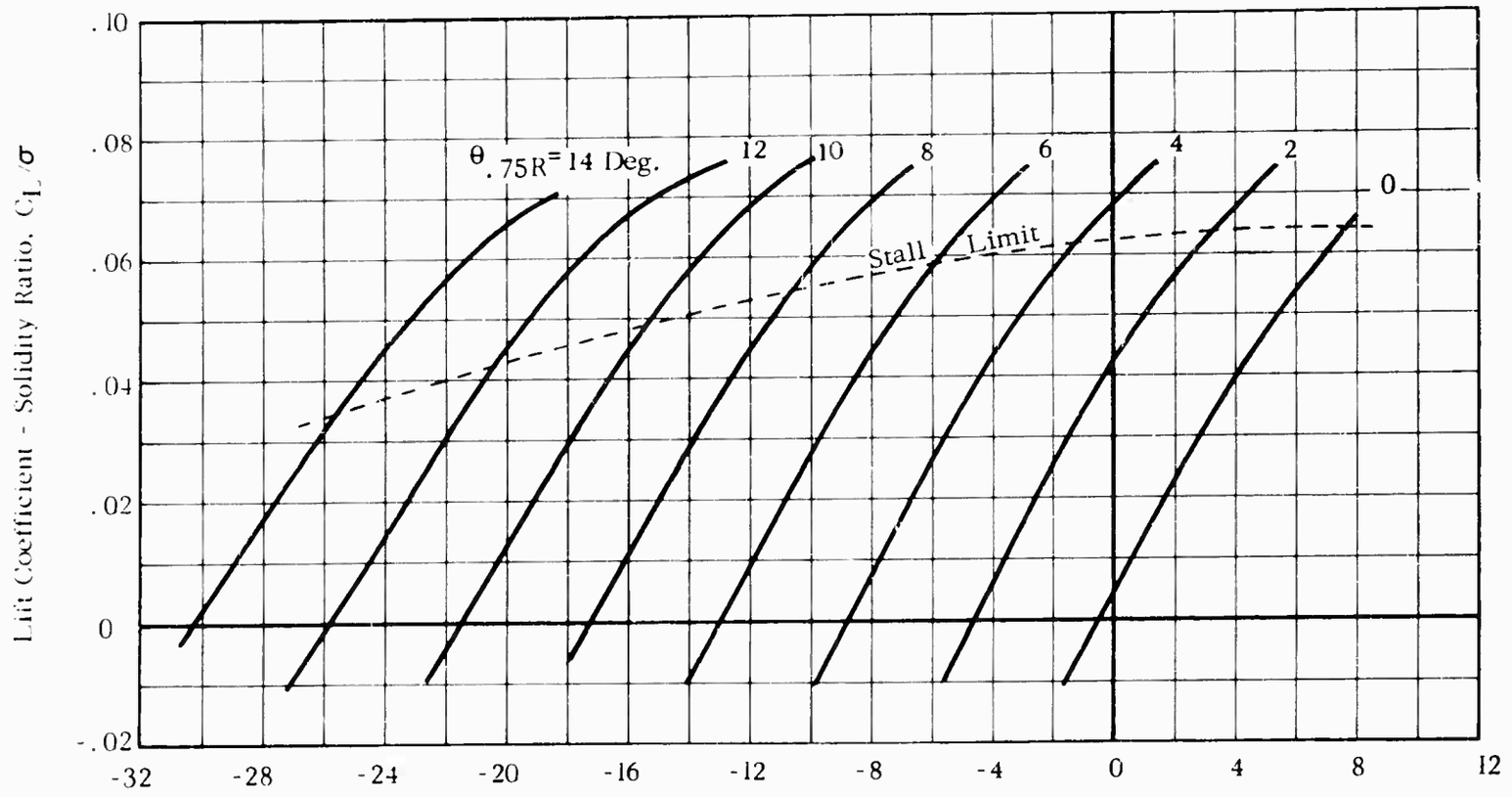

(a) C_L/σ vs α

FIG. 40. THEORETICAL ROTOR PERFORMANCE AND BLADE MOTIONS

V = 161 Kts. ΩR = 700 Ft/Sec. μ = 0.39

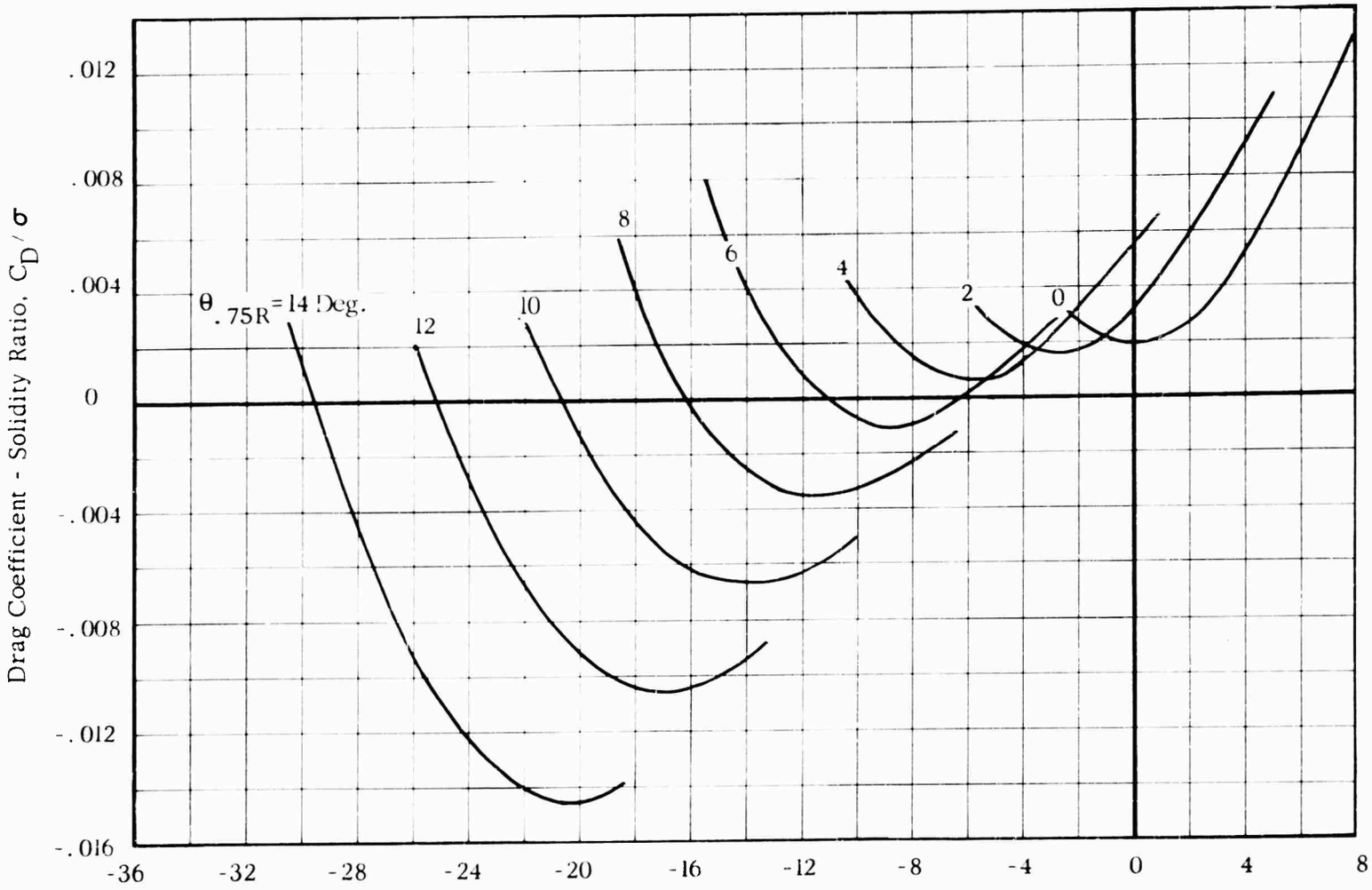

(b) C_D/σ vs α

Figure 40. - Continued

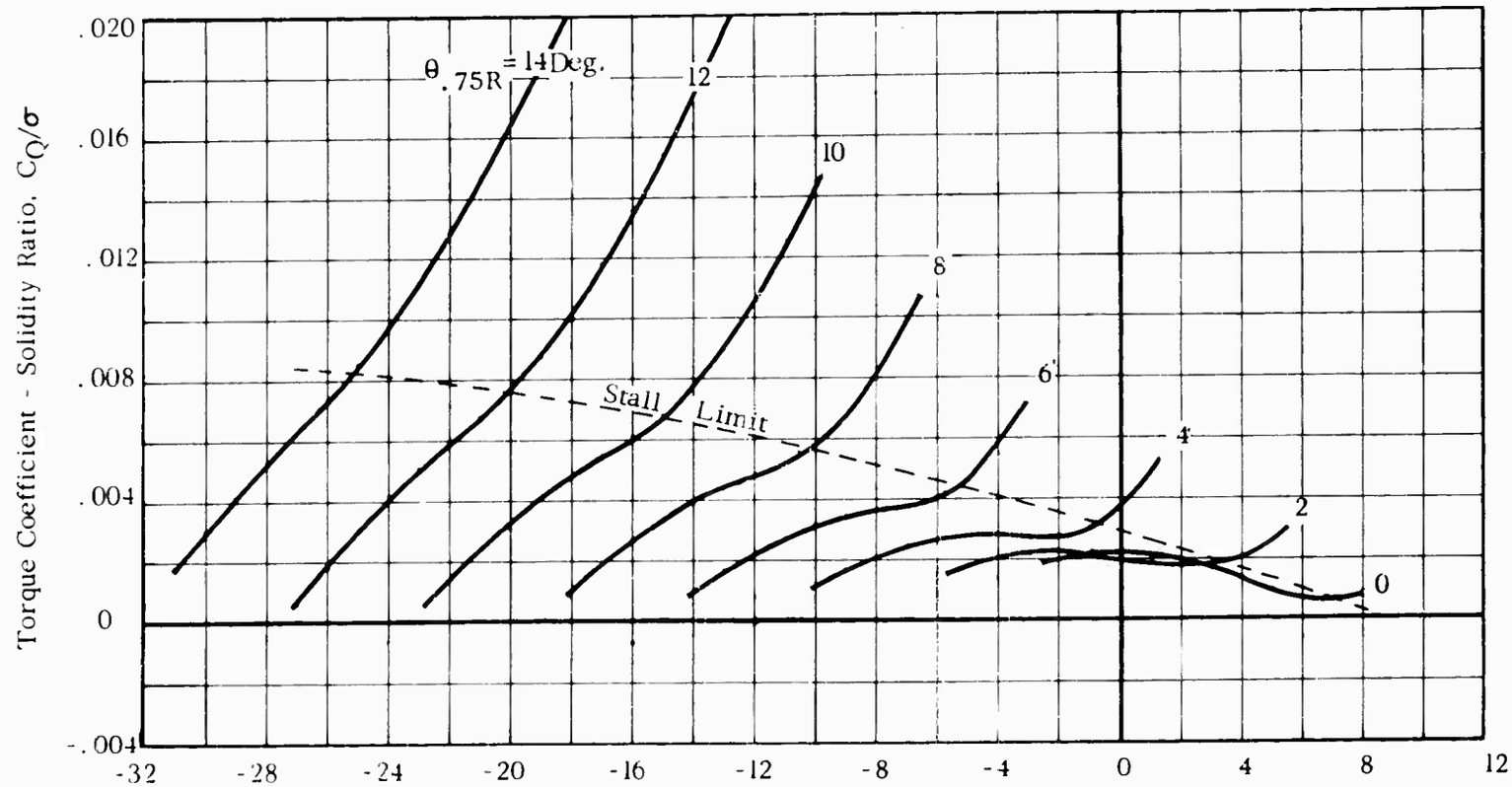

(c) C_Q/σ vs α

Figure 40. - Continued

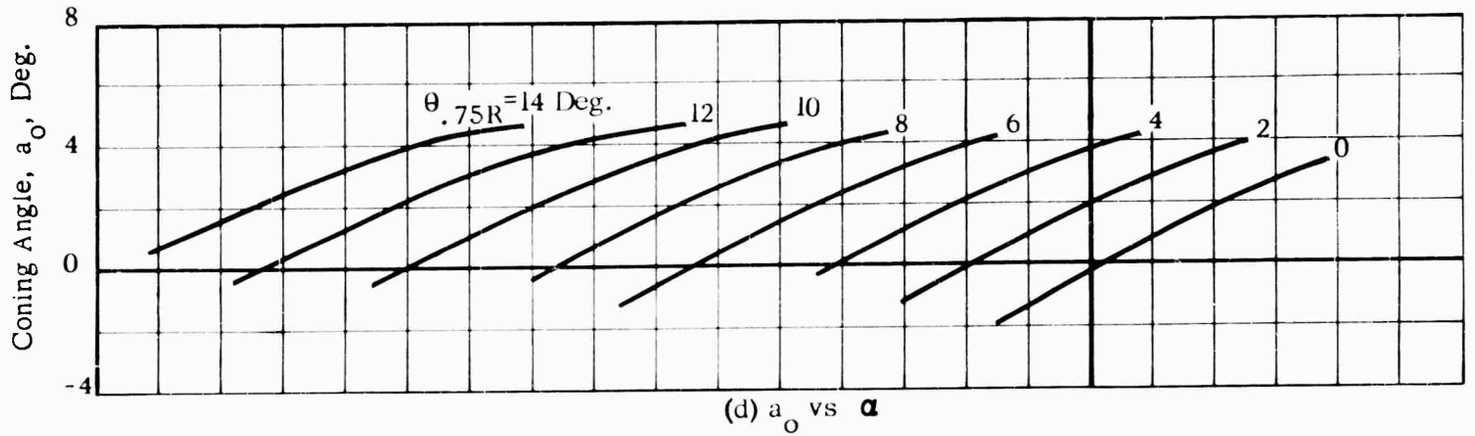

(d) a_o vs α

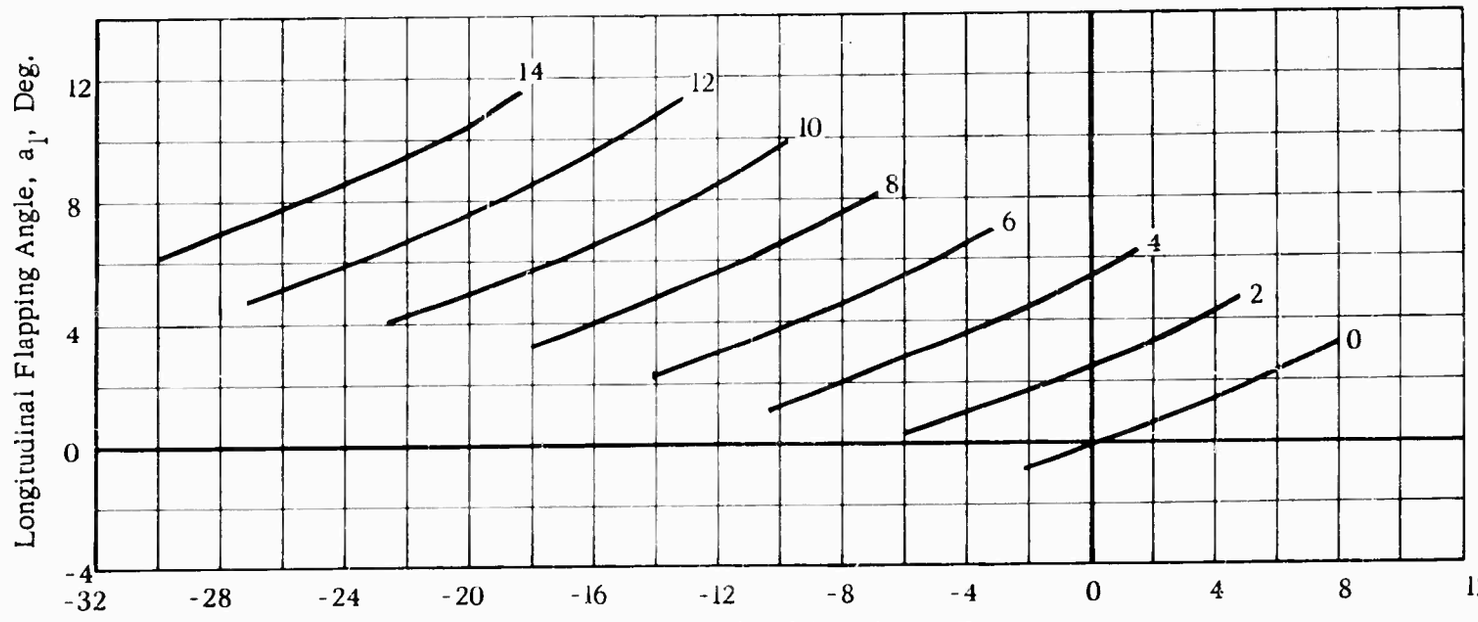

(e) a_1 vs α

Figure 40. -Continued

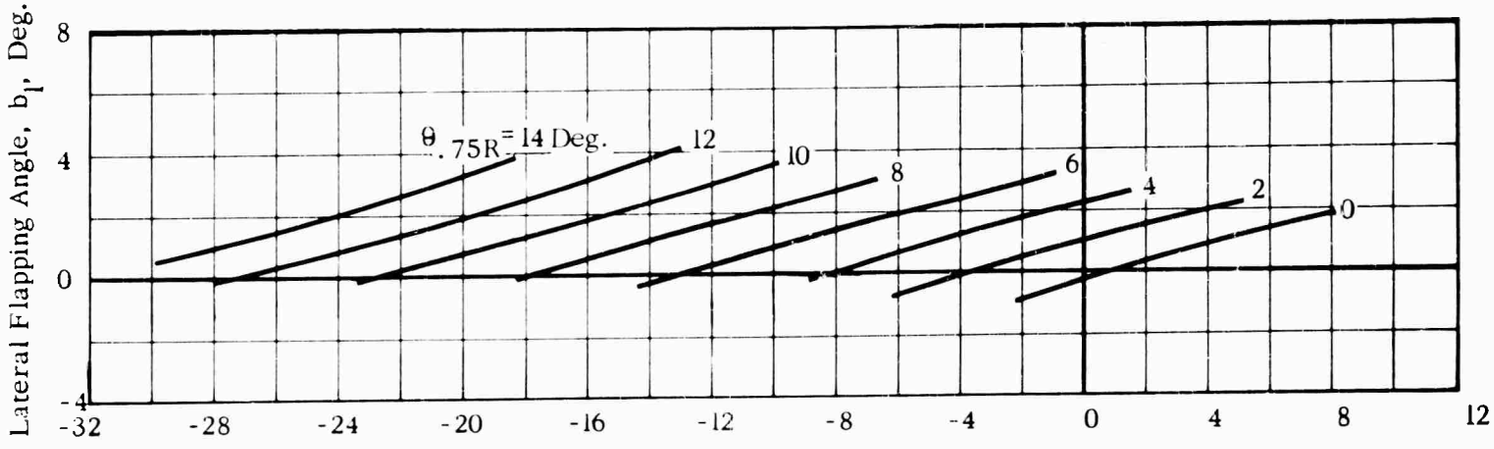

(f) b_1 vs α

Figure 40. -Concluded

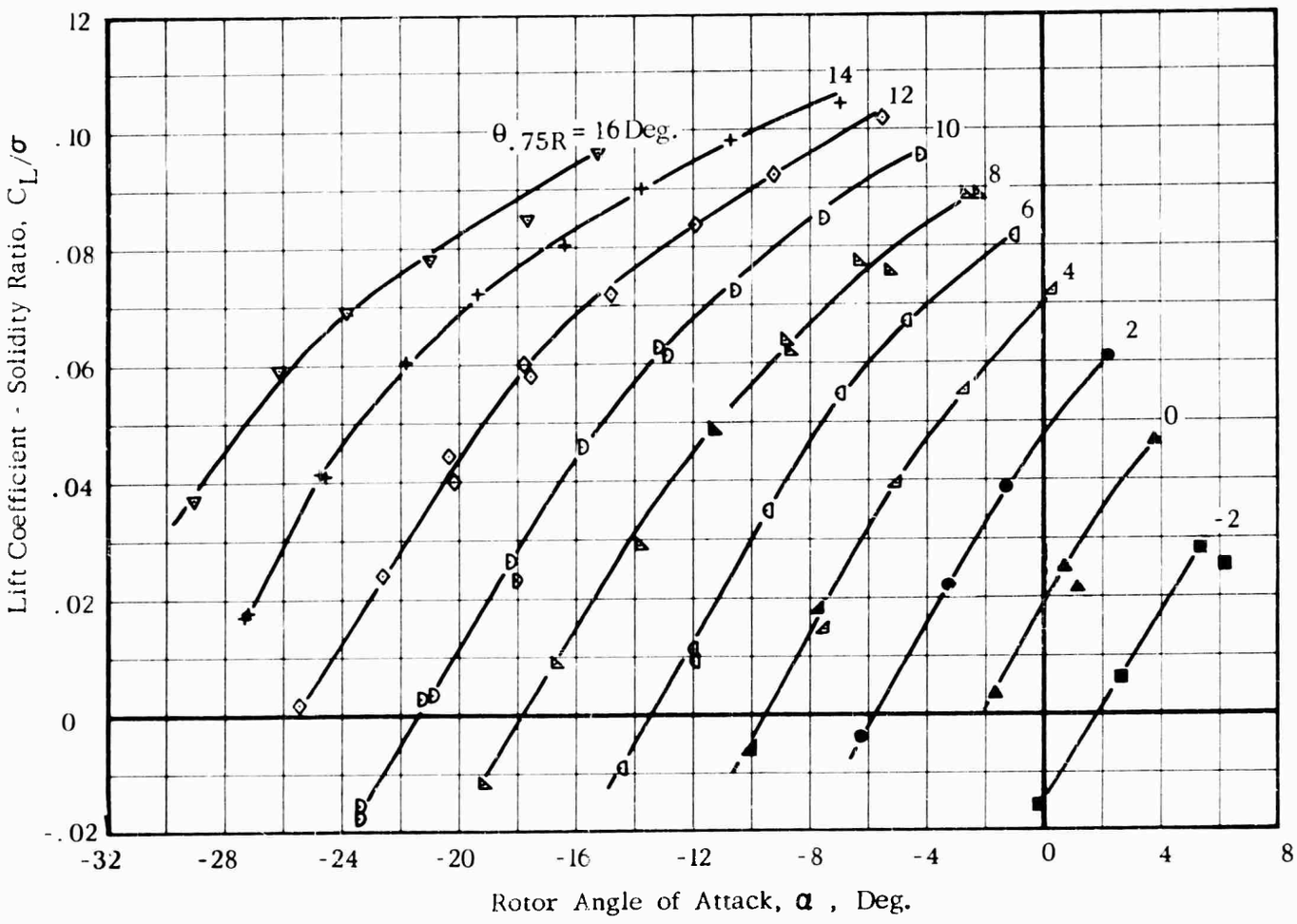

(a) C_L/σ vs α

FIG. 41. EXPERIMENTAL ROTOR PERFORMANCE AND BLADE MOTIONS

V = 161 Kts. ΩR = 700 Ft/Sec. μ = 0.39

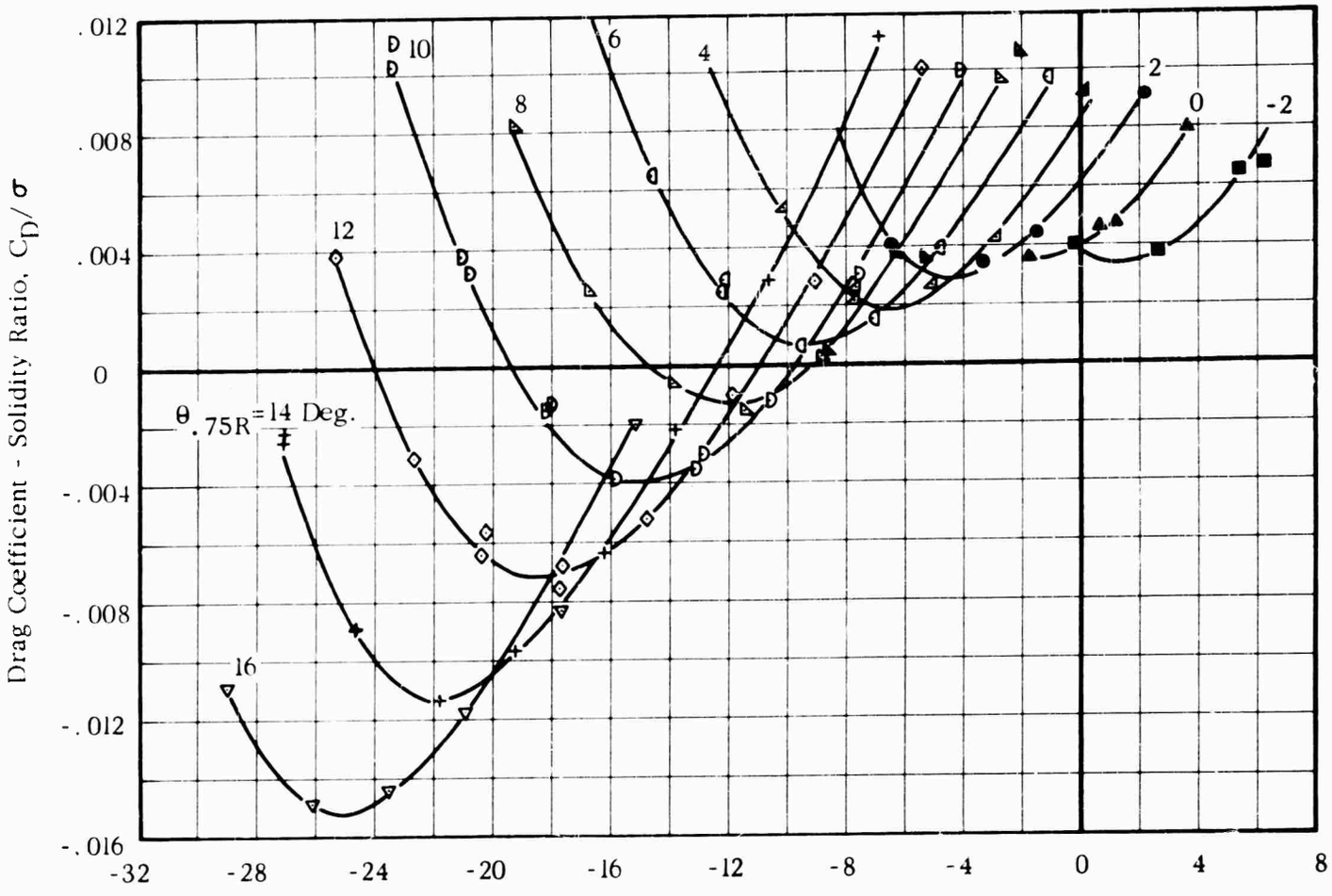

(b) C_D/σ vs α

Figure 41. -Continued

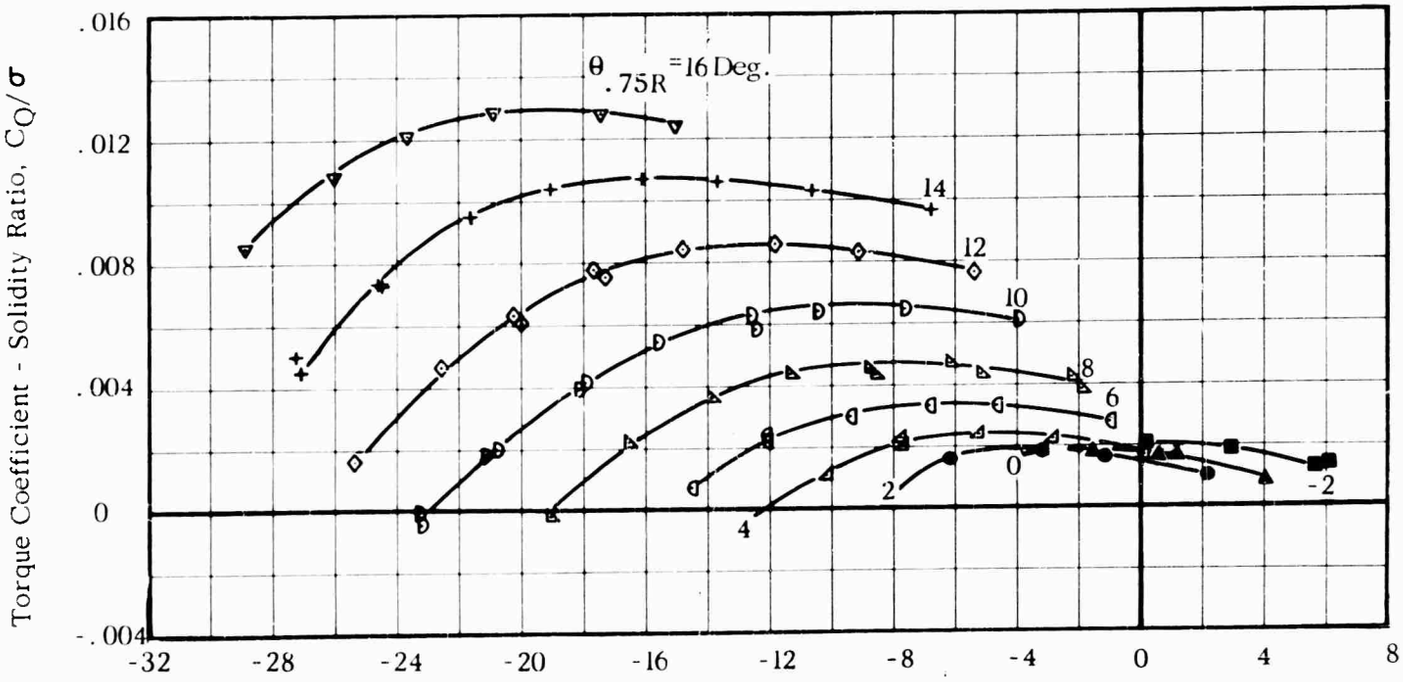

(c) C_Q/σ vs α

Figure 41. -Continued

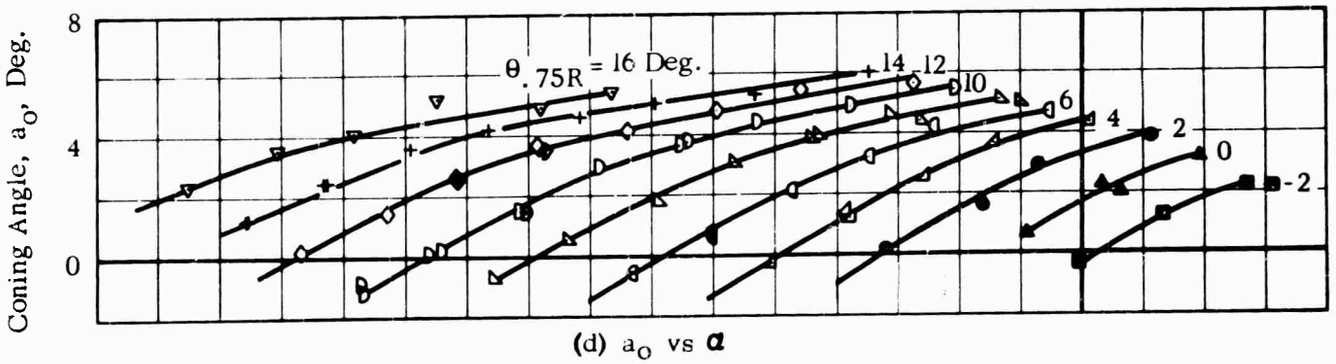

(d) a_o vs α

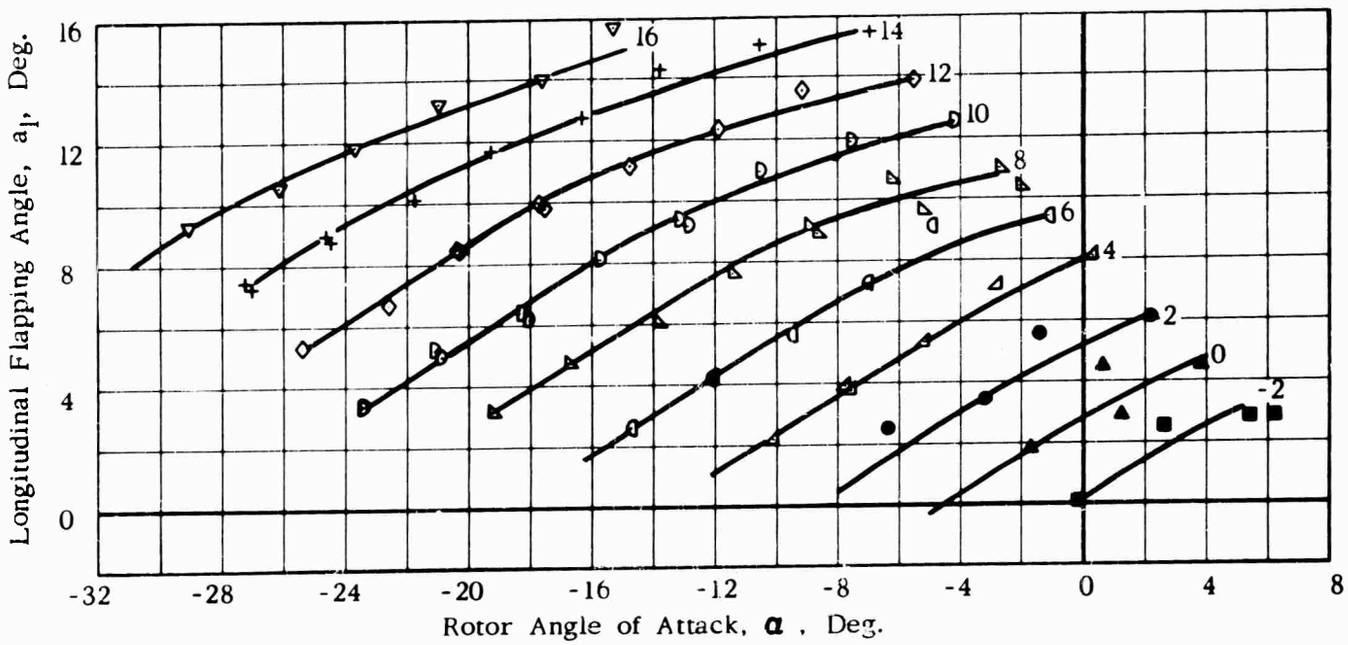

(e) a_1 vs α

Figure 41. Continued

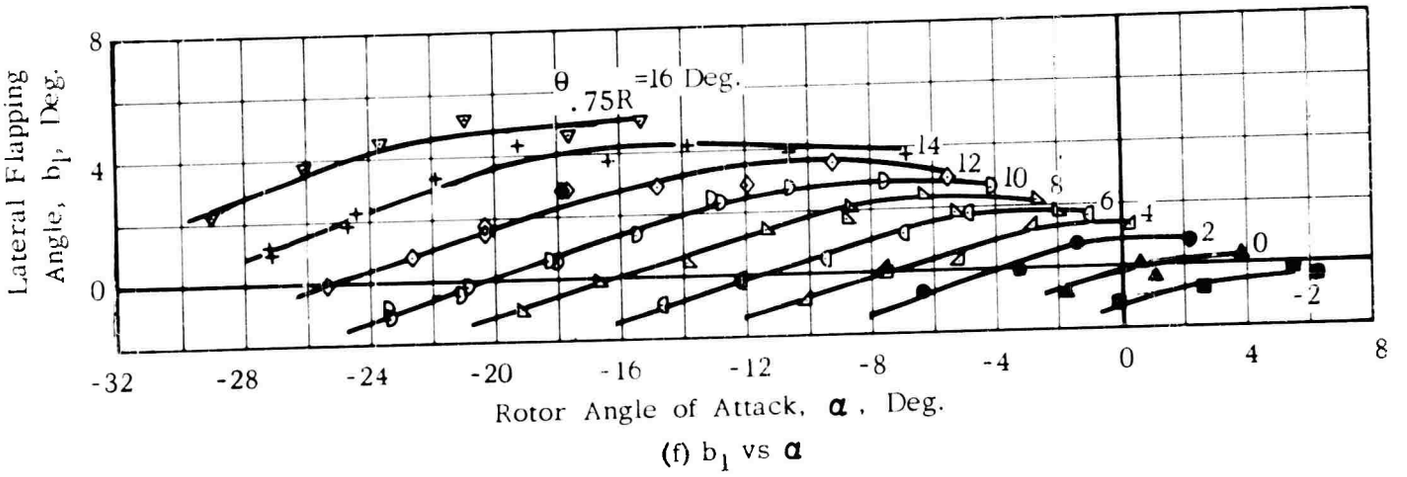

(f) b_1 vs α

Figure 41. -Concluded

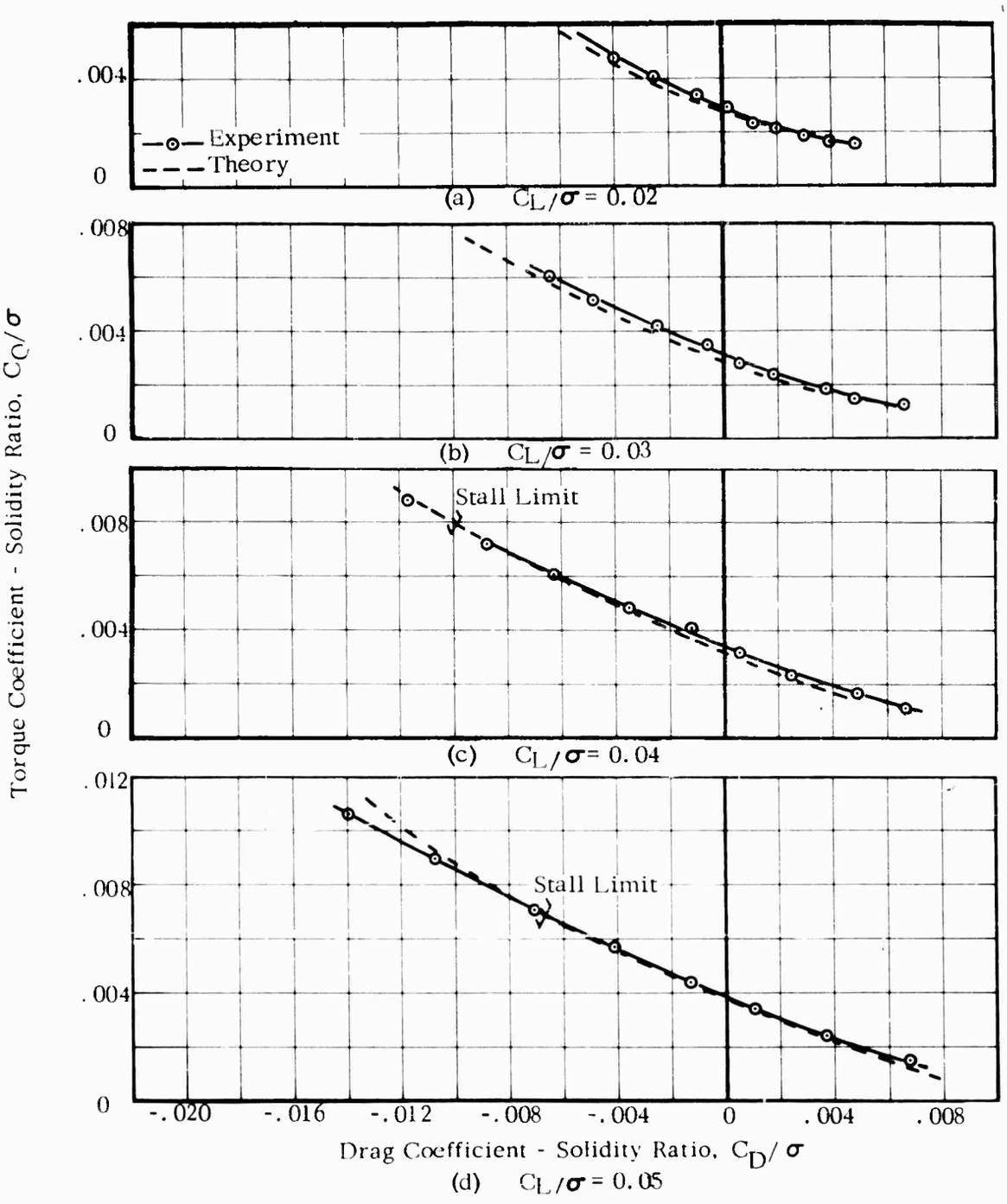

FIG. 42. COMPARISON OF THEORETICAL AND EXPERIMENTAL ROTOR POWER REQUIRED AT CONSTANT LIFT

V = 161 Kts. ΩR = 700 Ft/Sec. μ = 0.39

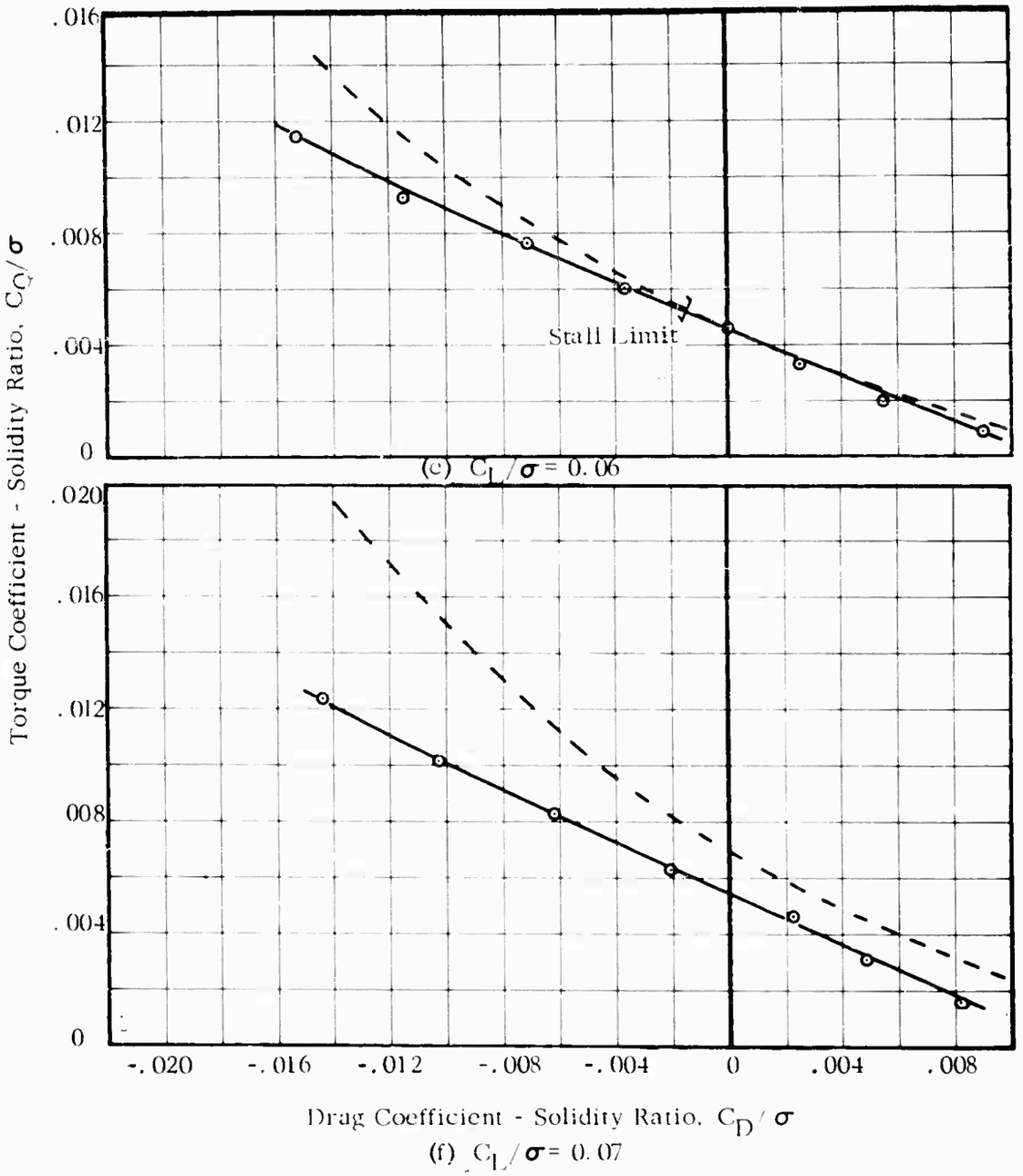

Figure 42. -Concluded

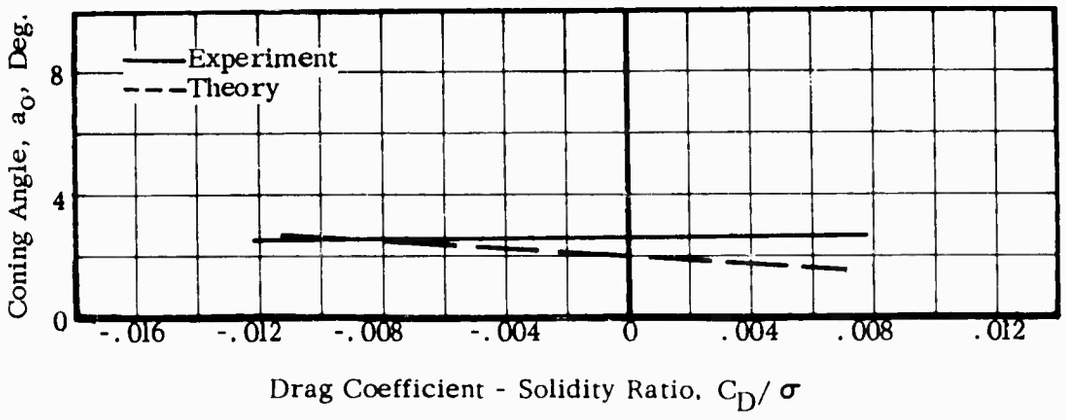

(a) Coning Angle, a_o, Deg.

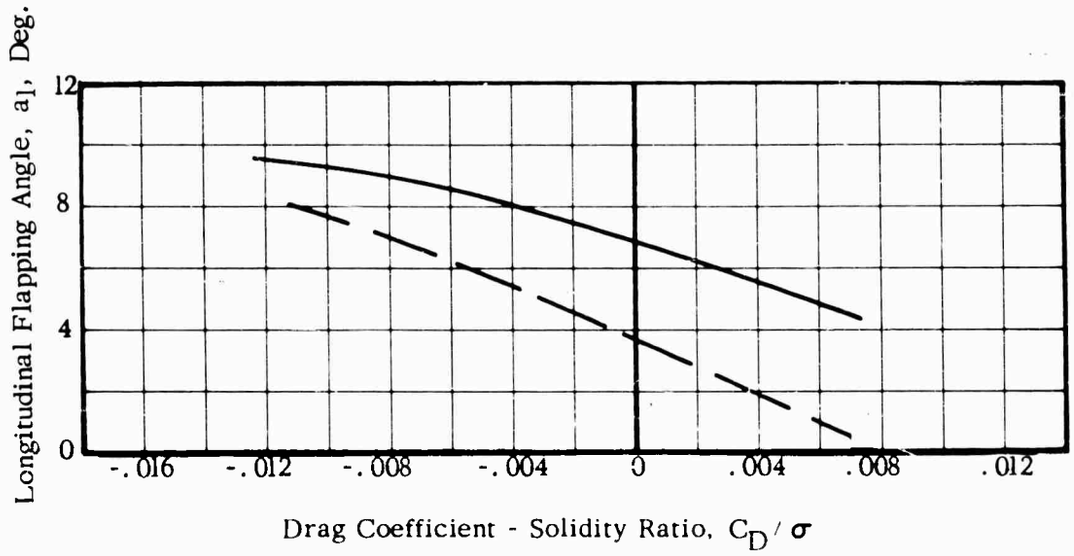

(b) Longitudinal Flapping Angle, a_1, Deg.

FIG.43. COMPARISON OF THEORETICAL AND EXPERIMENTAL BLADE MOTIONS

V = 161 Kts. ΩR = 700 Ft/Sec. $L/\pi R^2 = 4.0$

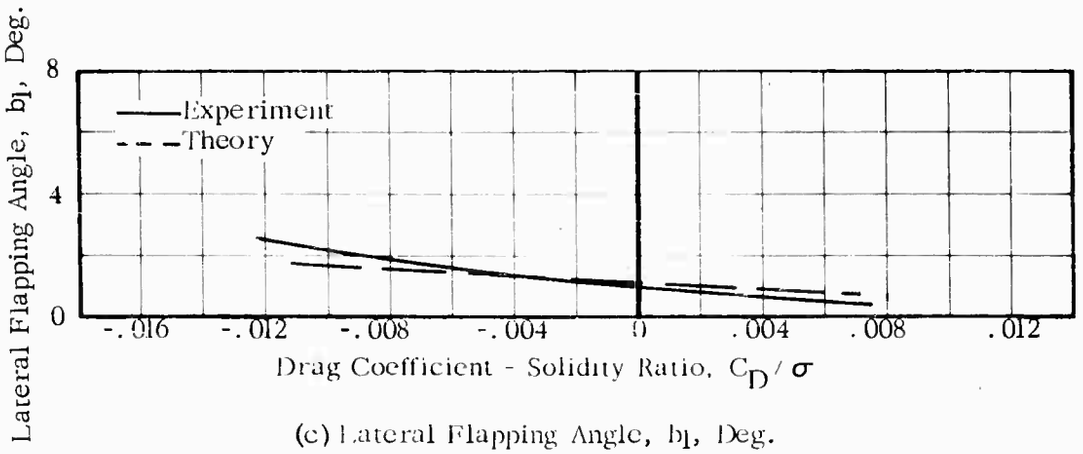

(c) Lateral Flapping Angle, b_1, Deg.

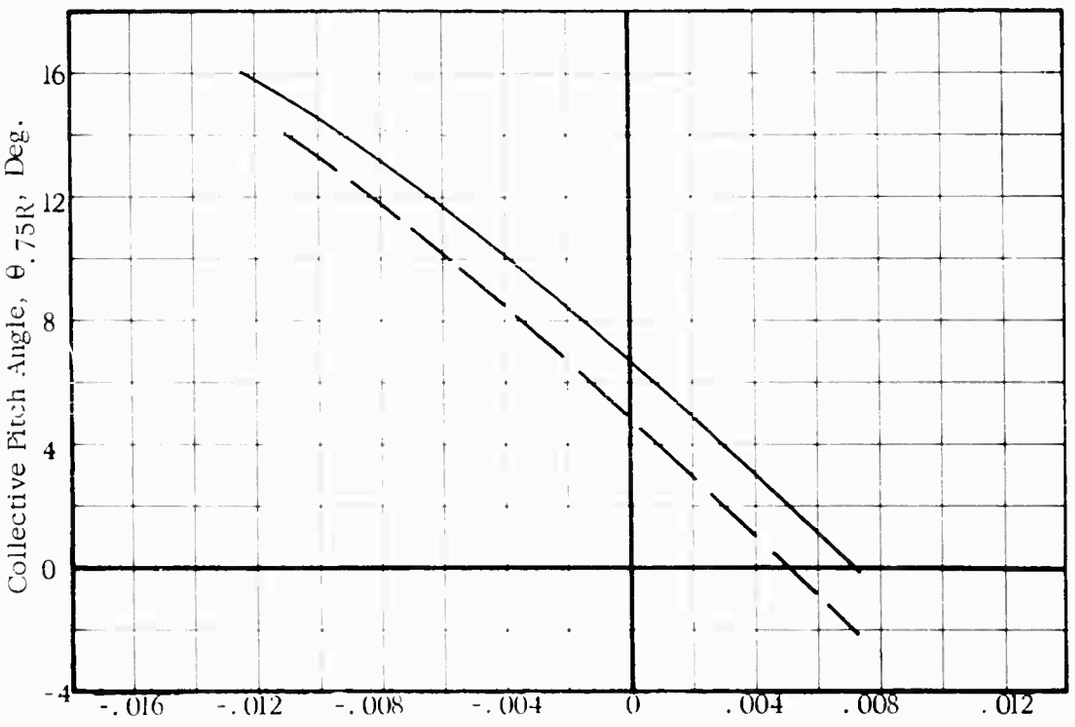

(d) Collective Pitch Angle, $\theta_{.75R}$, Deg.

Figure 43. -Concluded

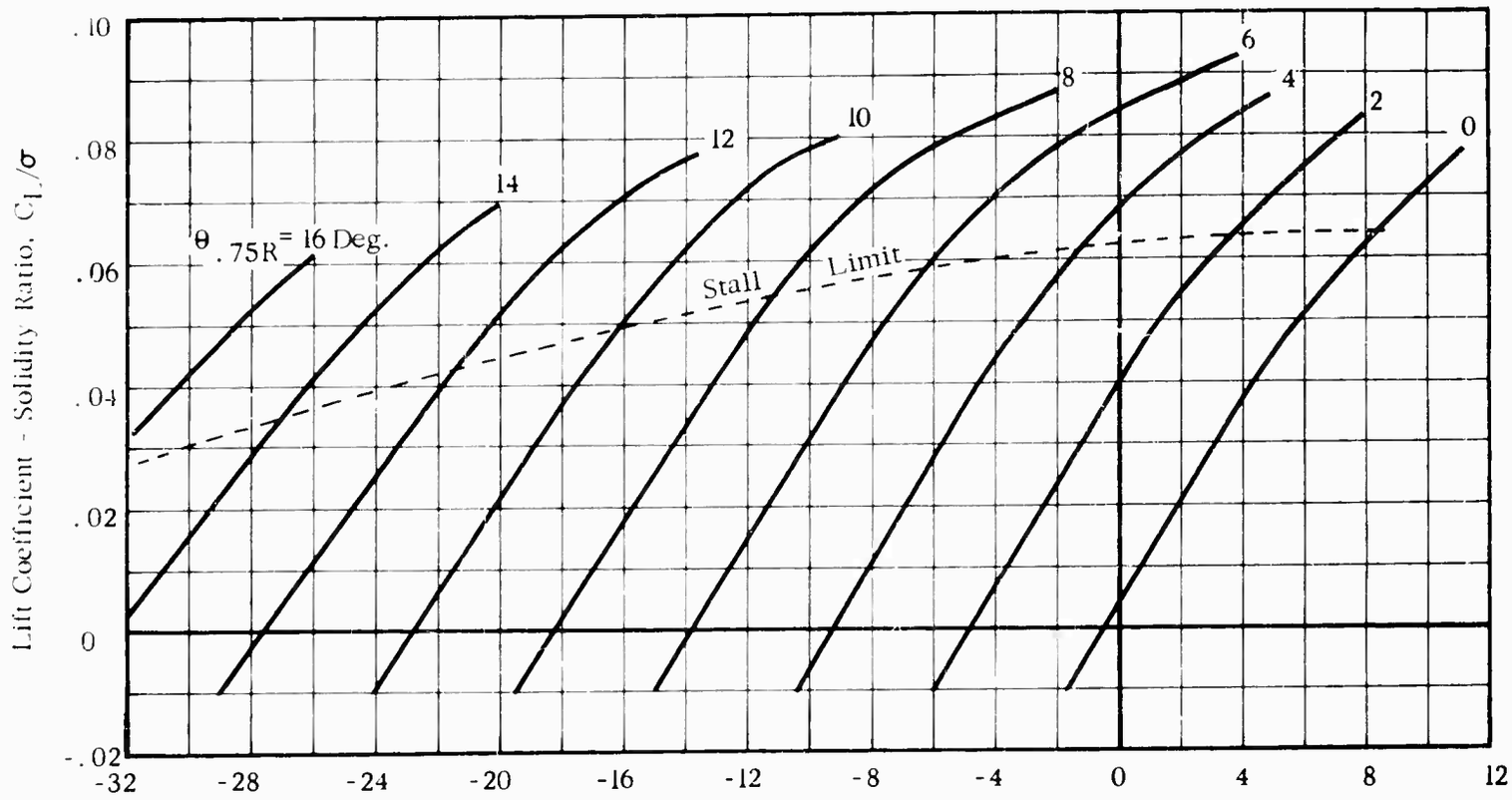

(a) C_L/σ vs α

FIG. 44. THEORETICAL ROTOR PERFORMANCE AND BLADE MOTIONS

V = 161 Kts. ΩR = 750 Ft/Sec. μ = 0.36

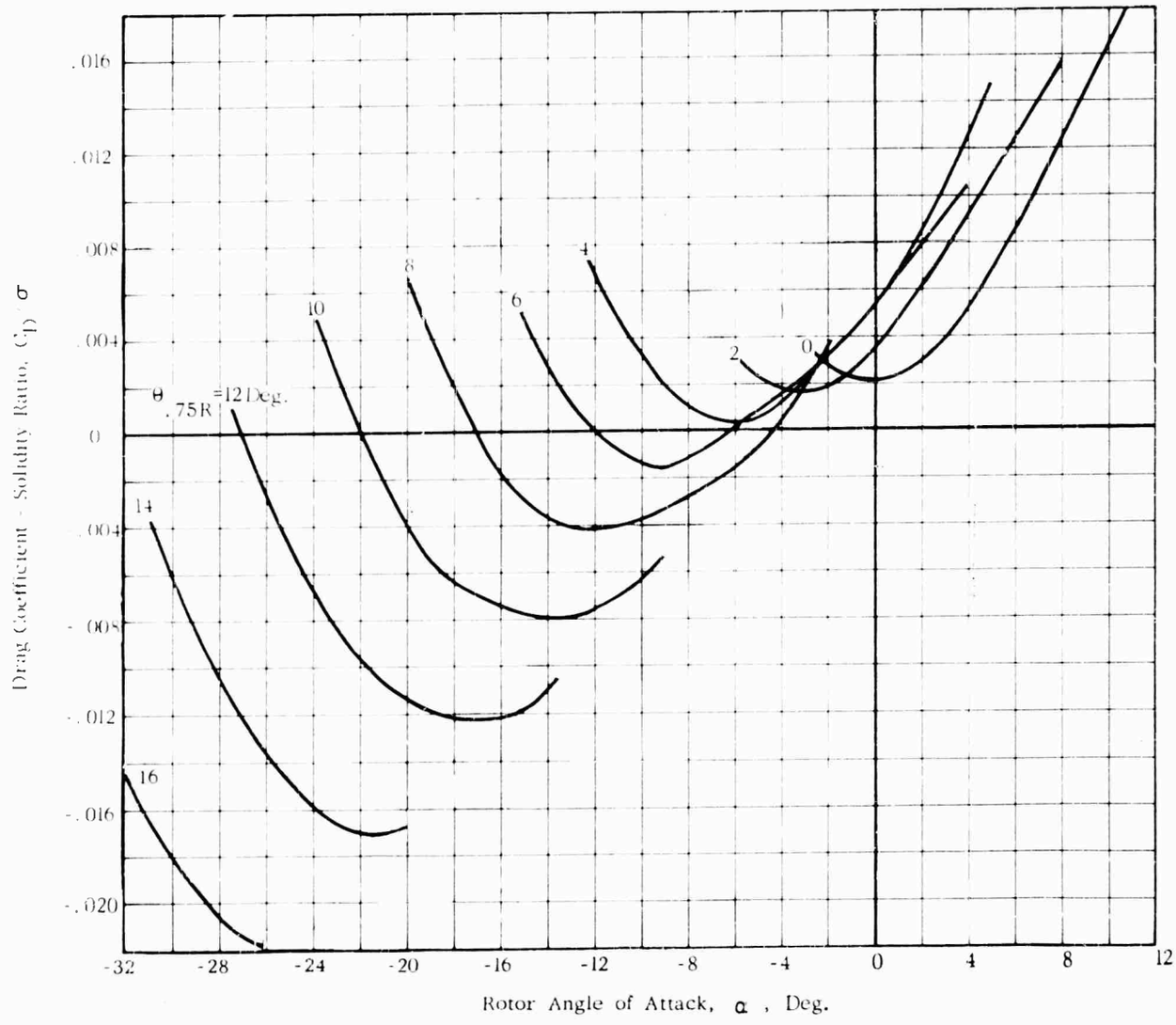

(b) C_D/σ vs α

Figure 44. -Continued

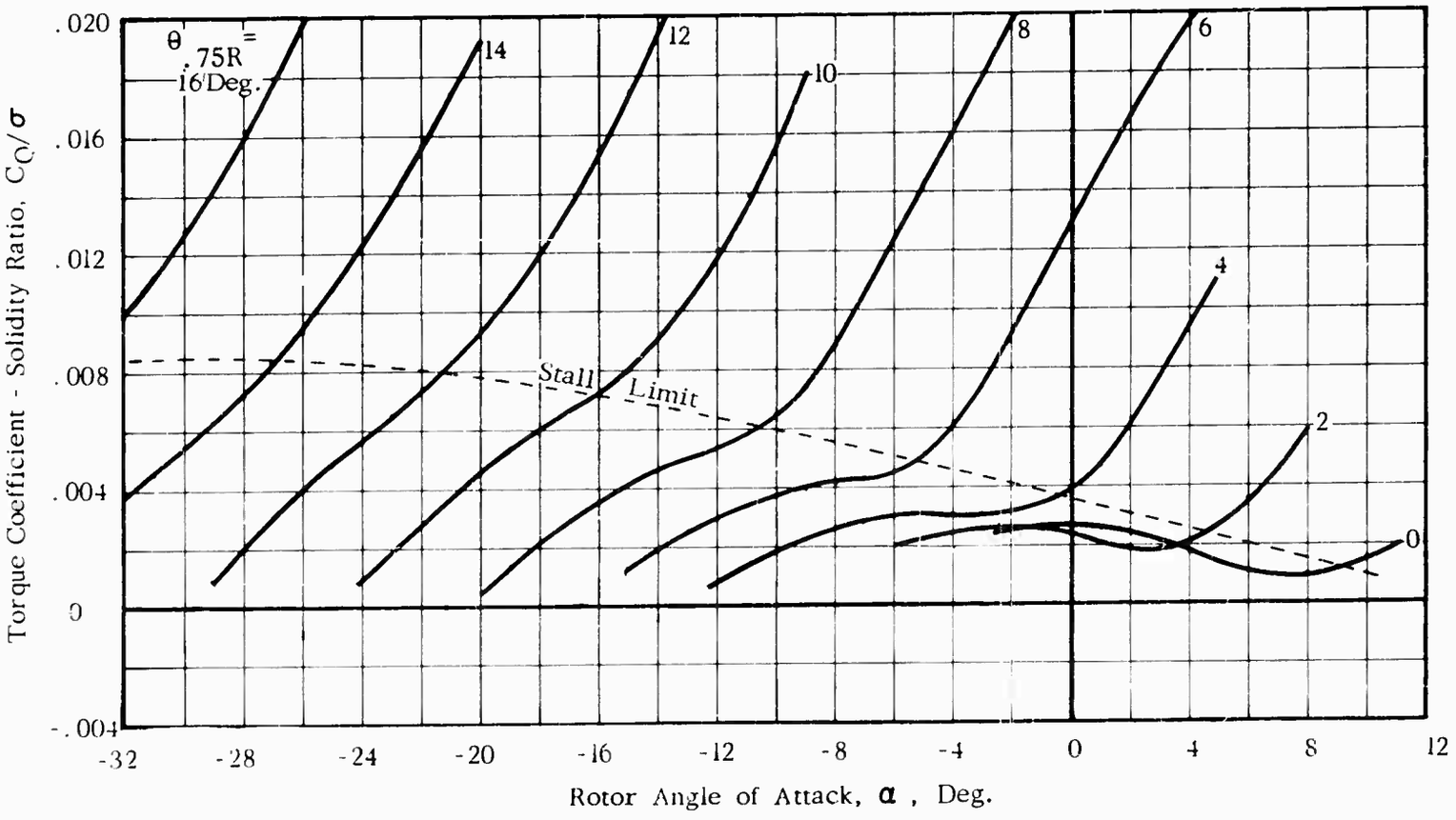

(c) C_Q/σ vs α

Figure 44. -Continued

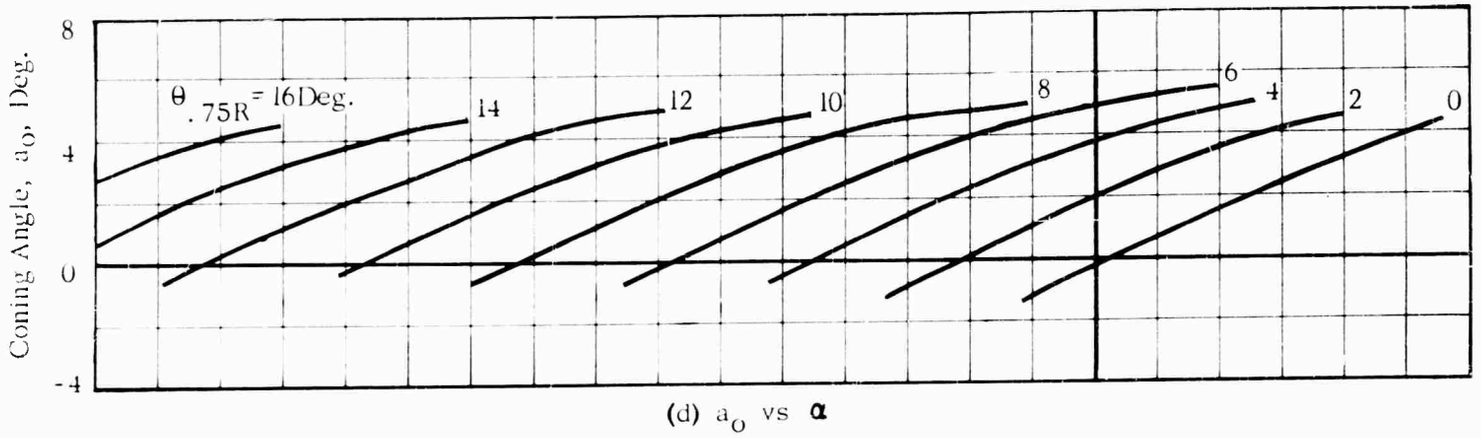

(d) a_o vs α

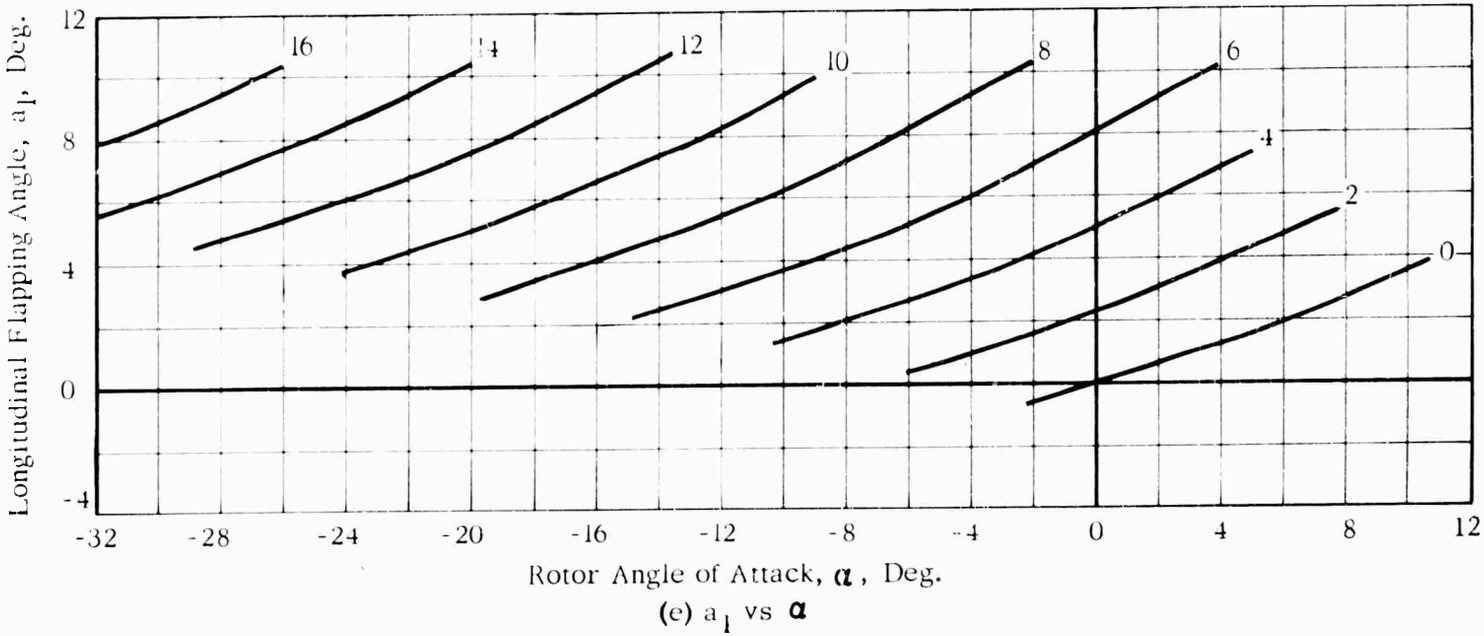

(e) a_1 vs α

Figure 44. Continued

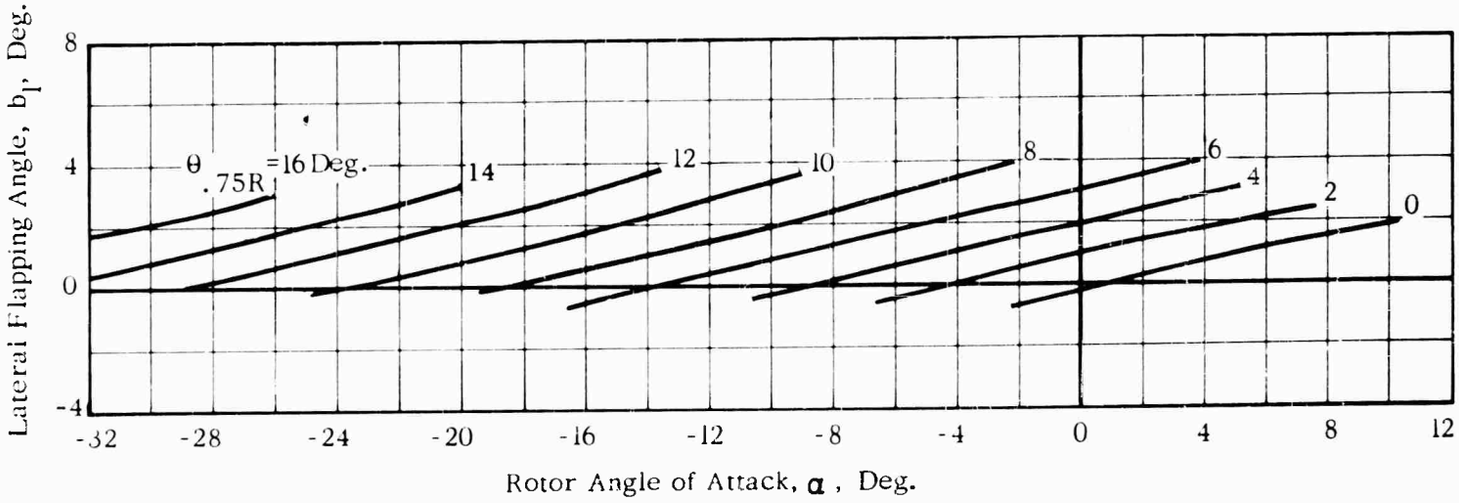

(f) b_1 vs α

Figure 44. -Concluded

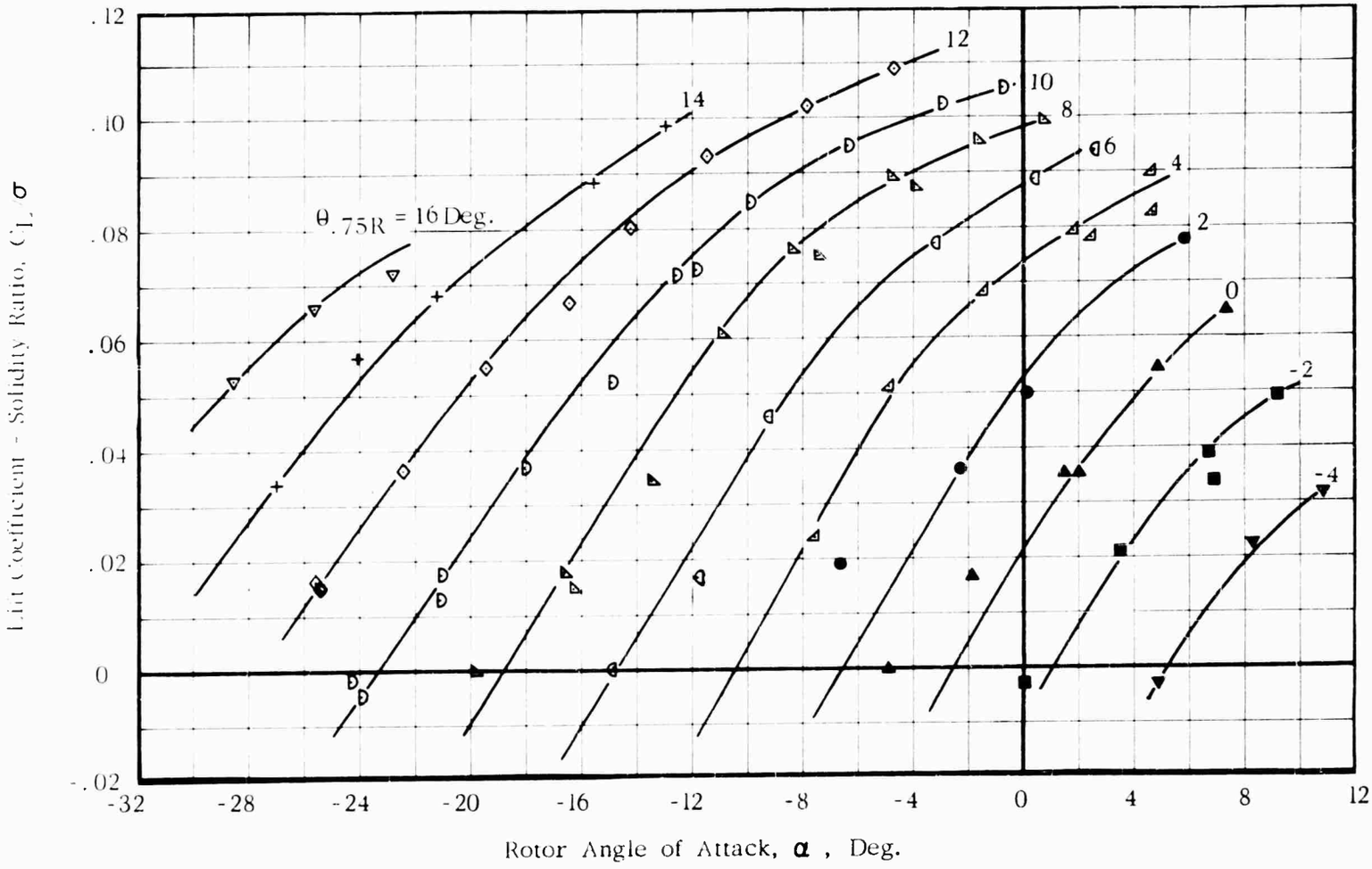

(a) C_L/σ vs α

FIG. 45. EXPERIMENTAL ROTOR PERFORMANCE AND BLADE MOTIONS

V = 161 Kts. ΩR = 750 Ft/Sec. μ = 0.36

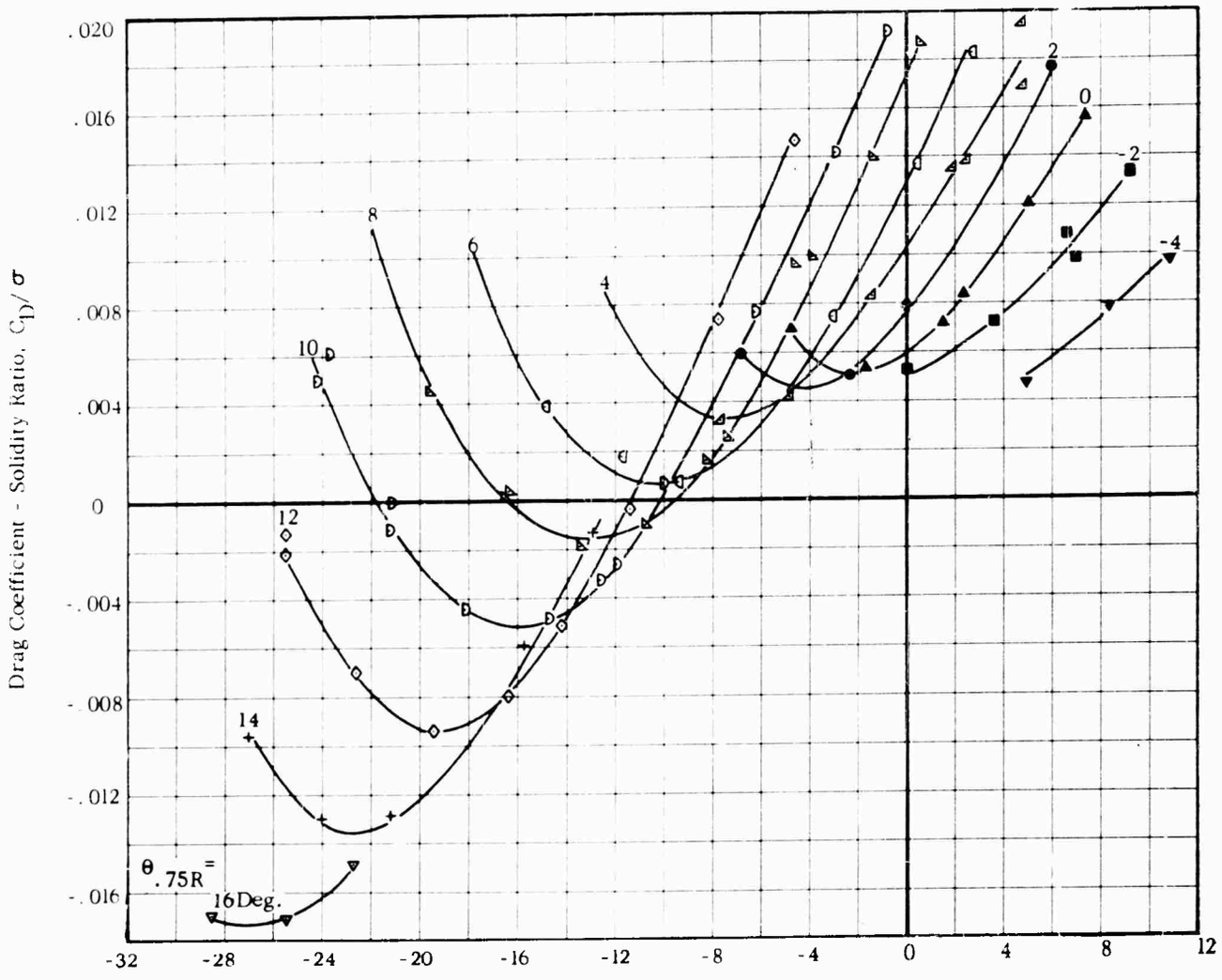

(b) C_D/σ vs α

Figure 45. -Continued

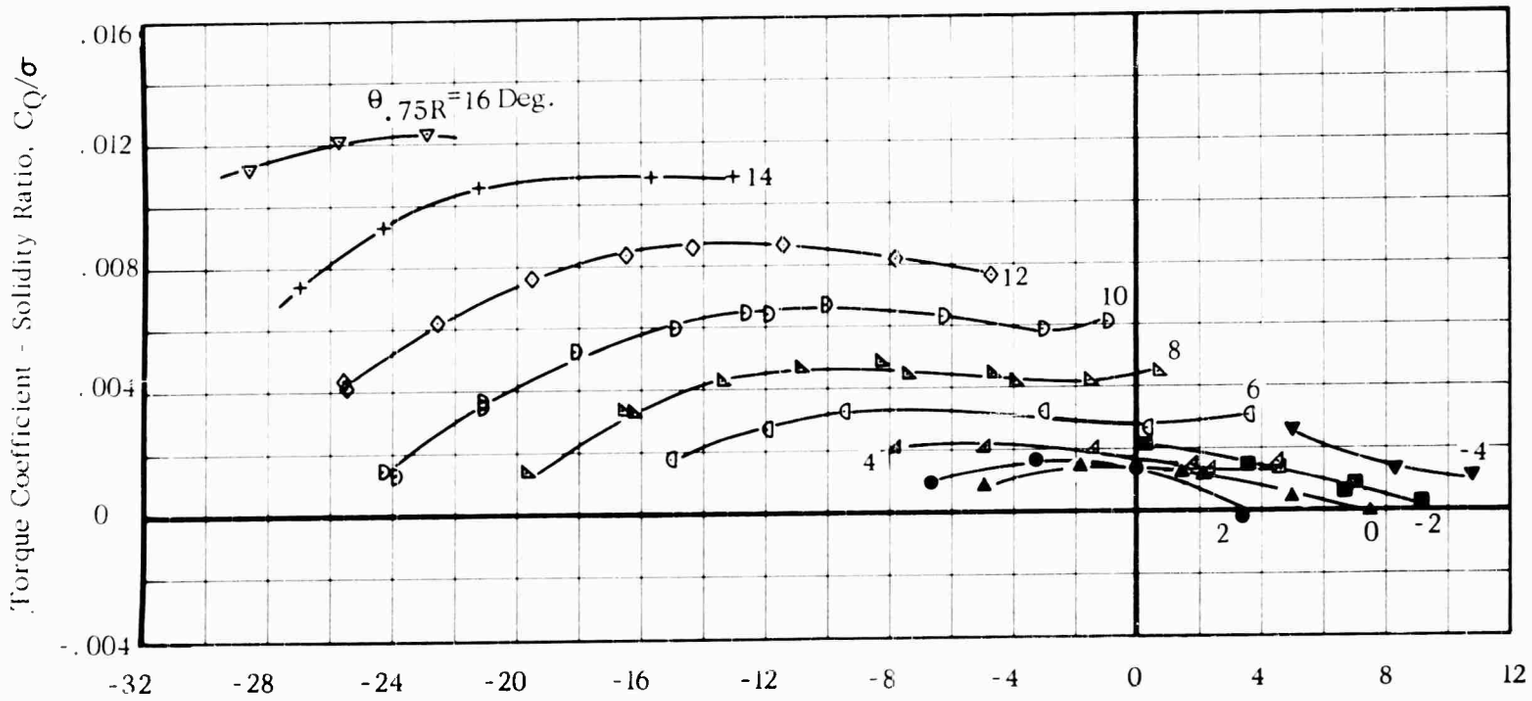

(c) C_Q/σ vs α

Figure 45. -Continued

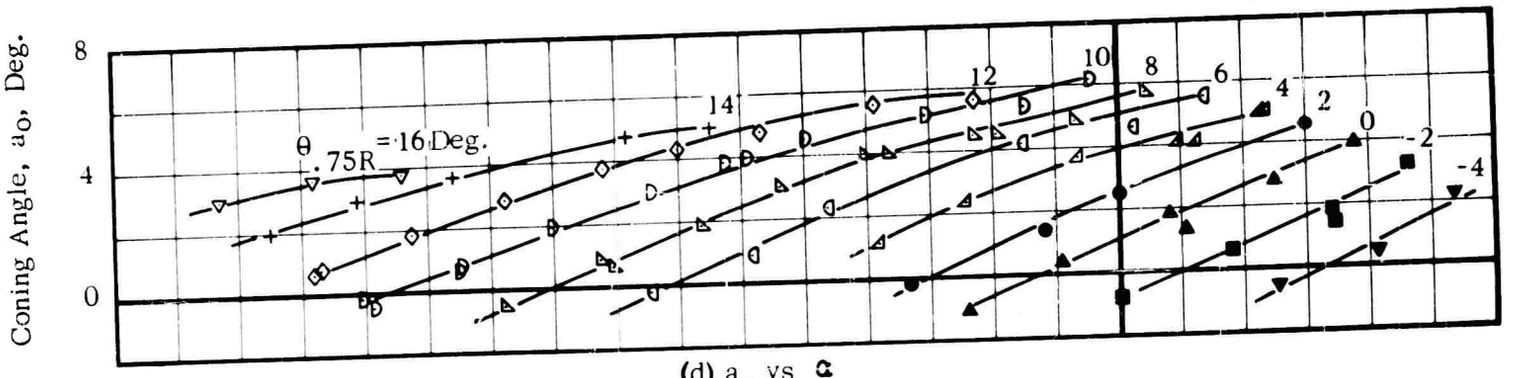

(d) a_o vs α

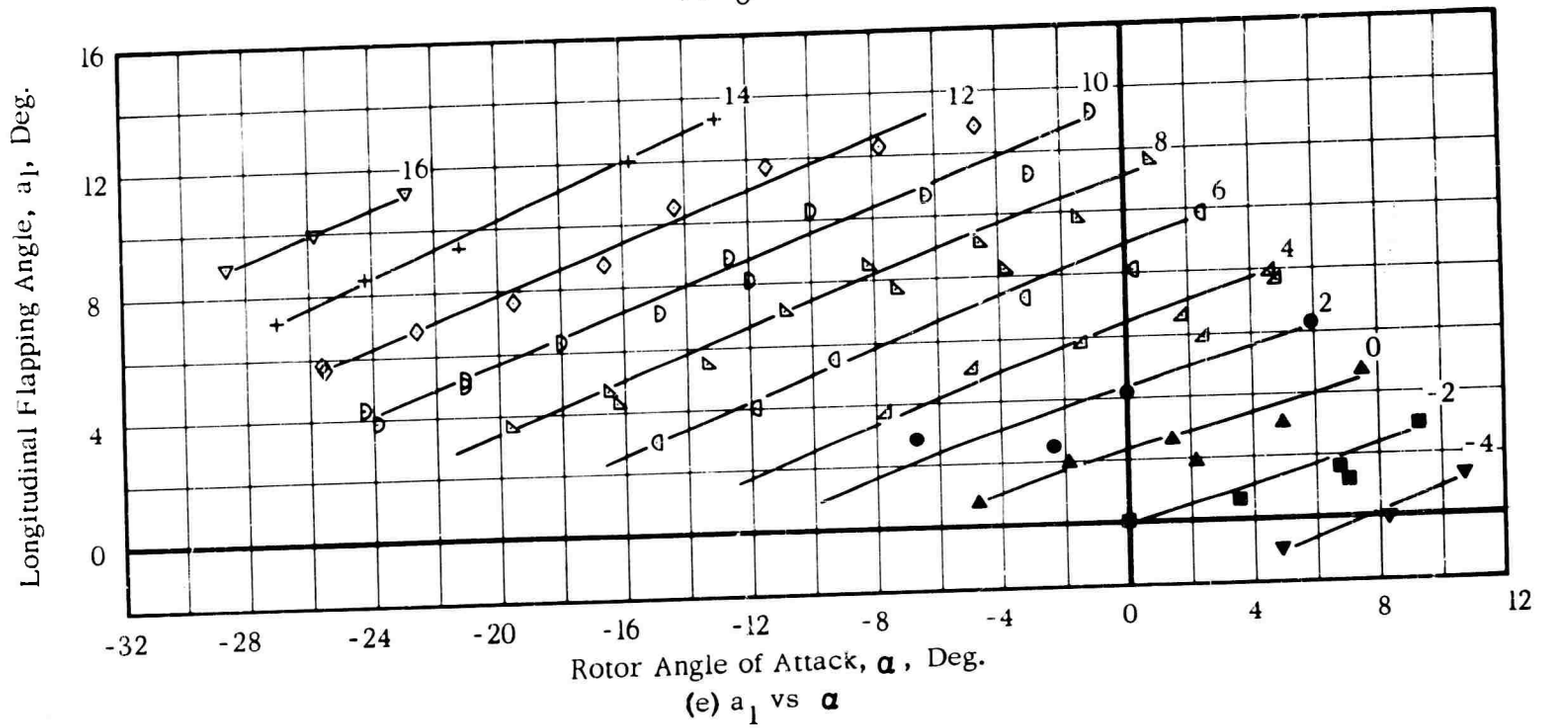

(e) a_1 vs α

Figure 45. Continued

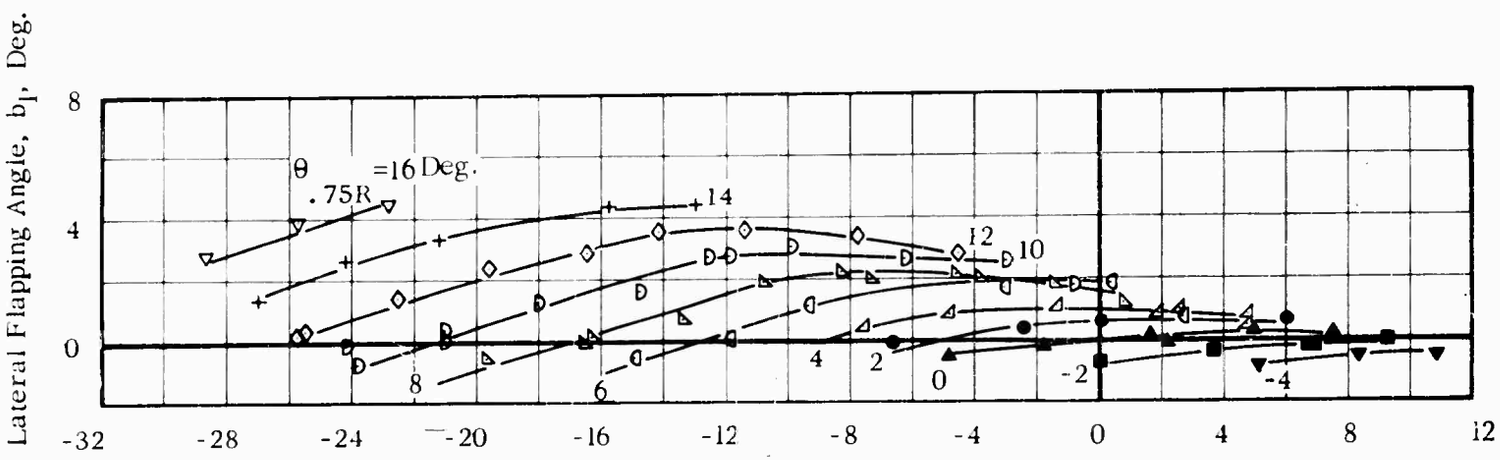

(f) b_1 vs α

Figure 45. -Concluded

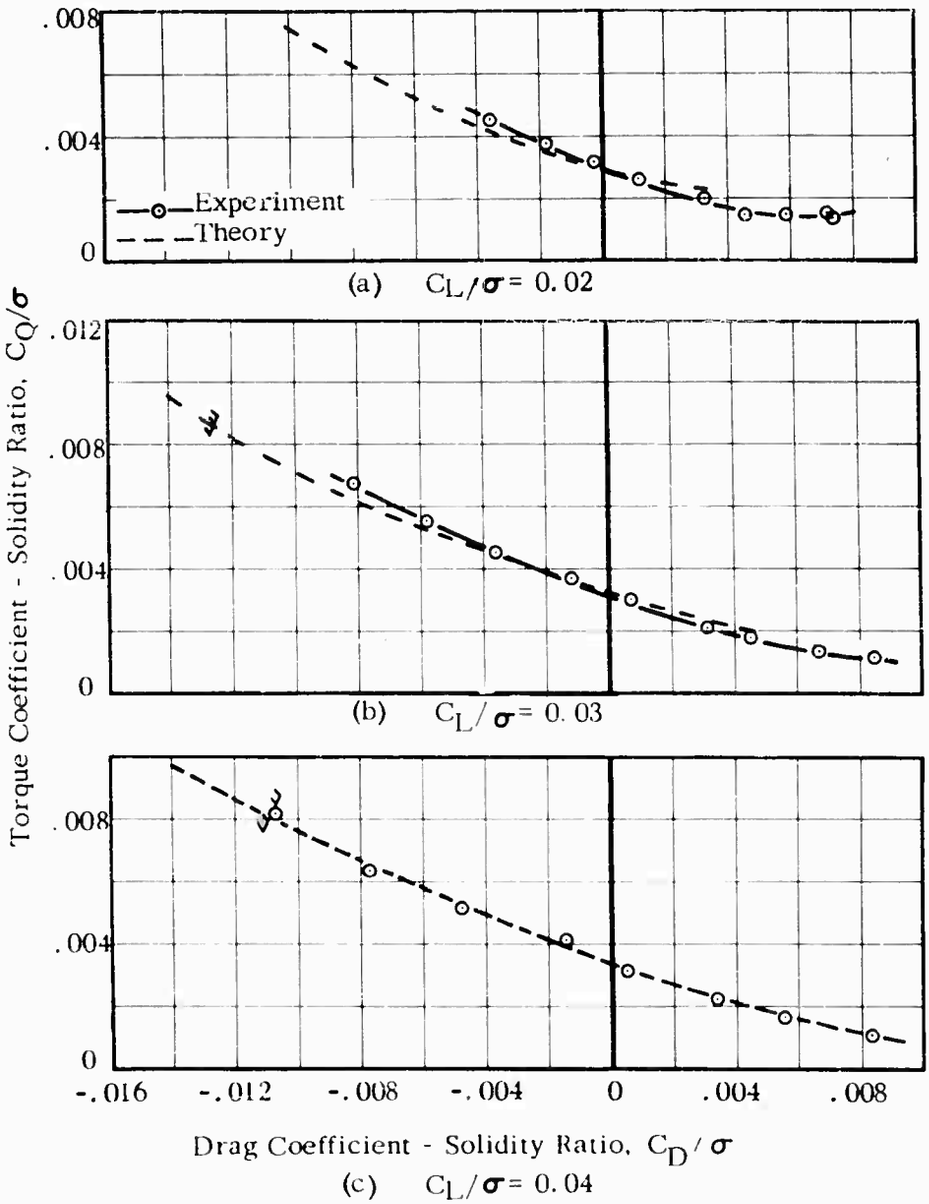

FIG. 46. COMPARISON OF THEORETICAL AND EXPERIMENTAL ROTOR POWER REQUIRED AT CONSTANT LIFT

V = 161 Kts. ΩR = 750 Ft/Sec. μ = 0.36

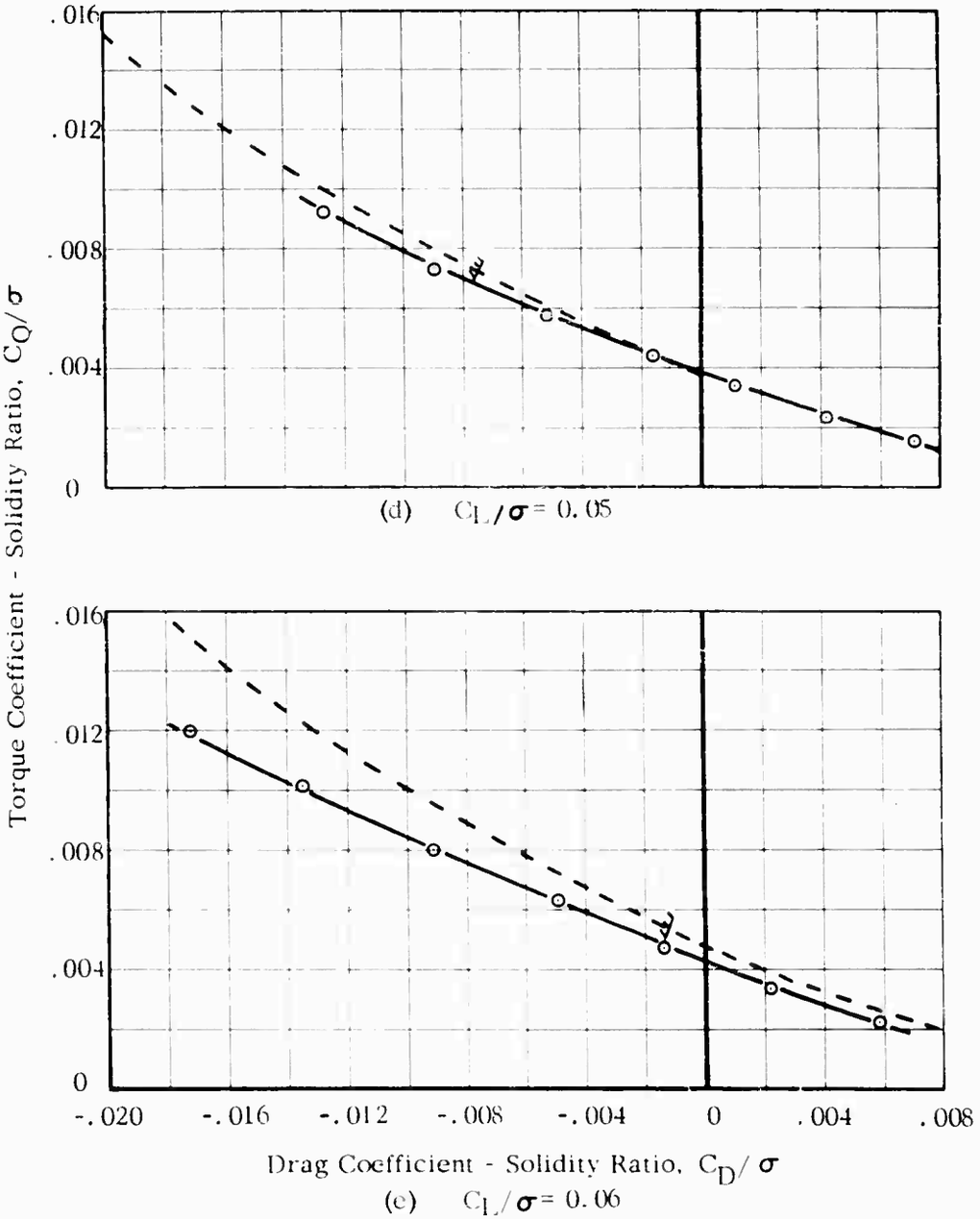

Figure 46. -Continued

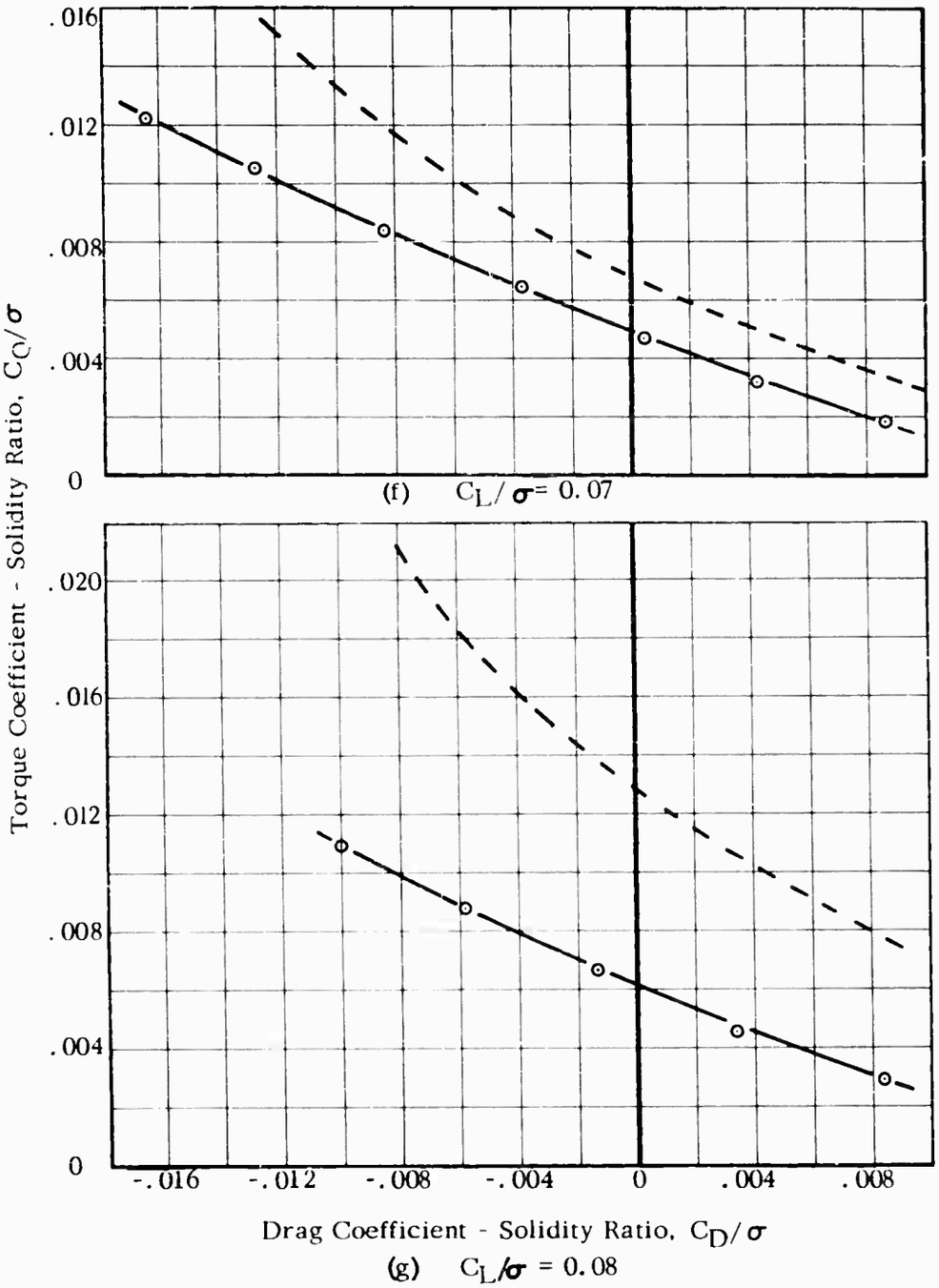

Figure 46. -Concluded

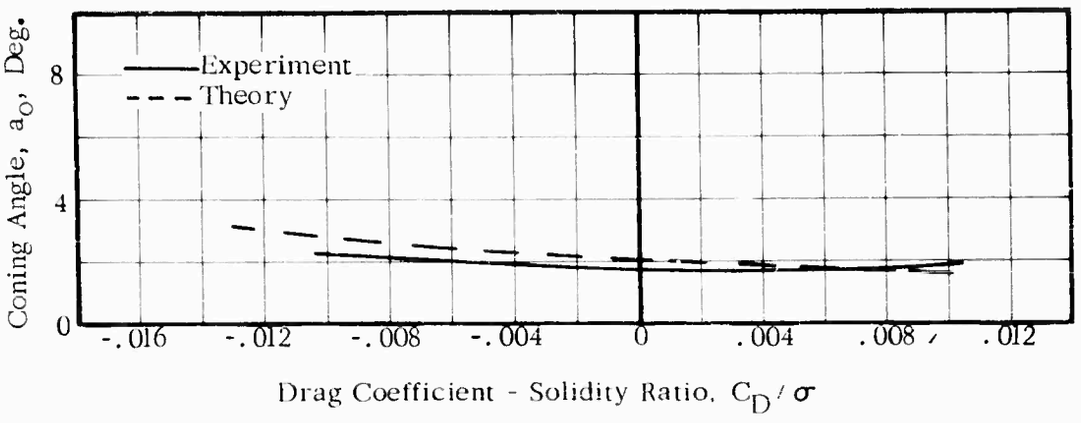

(a) Coning Angle, a_o, Deg.

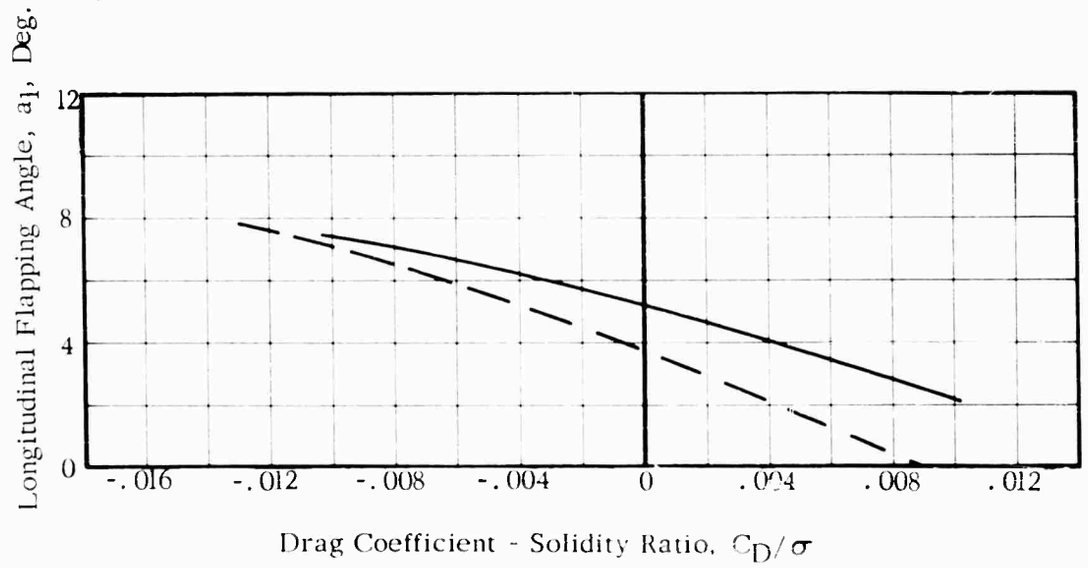

(b) Longitudinal Flapping Angle, a_1, Deg.

FIG.47.COMPARISON OF THEORETICAL AND EXPERIMENTAL BLADE MOTIONS

V = 161 Kts. ΩR = 750 Ft/Sec. $L/\pi R^2$ = 4.0 LB./FT.^{2}

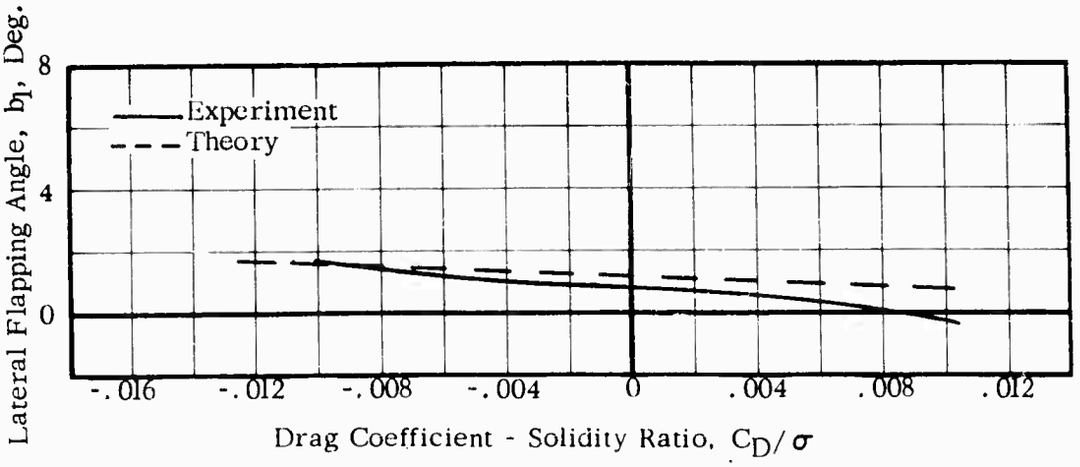

(c) Lateral Flapping Angle, b_1, Deg.

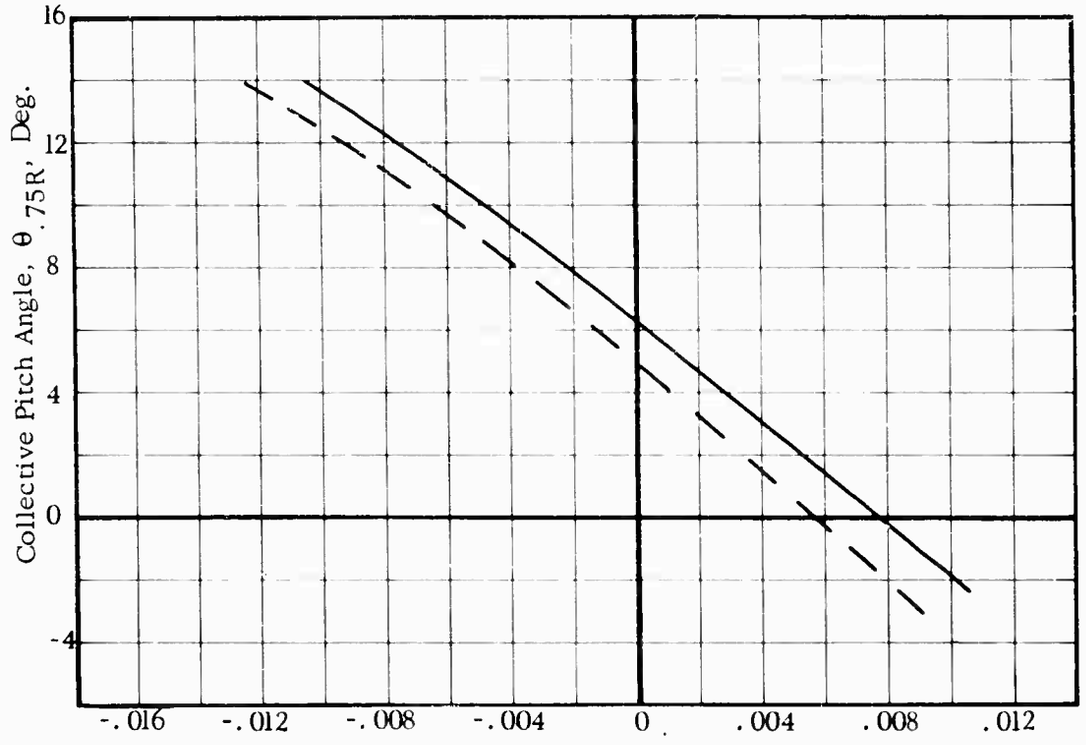

(d) Collective Pitch Angle, $\theta_{.75R}$, Deg.

Figure 47. -Concluded

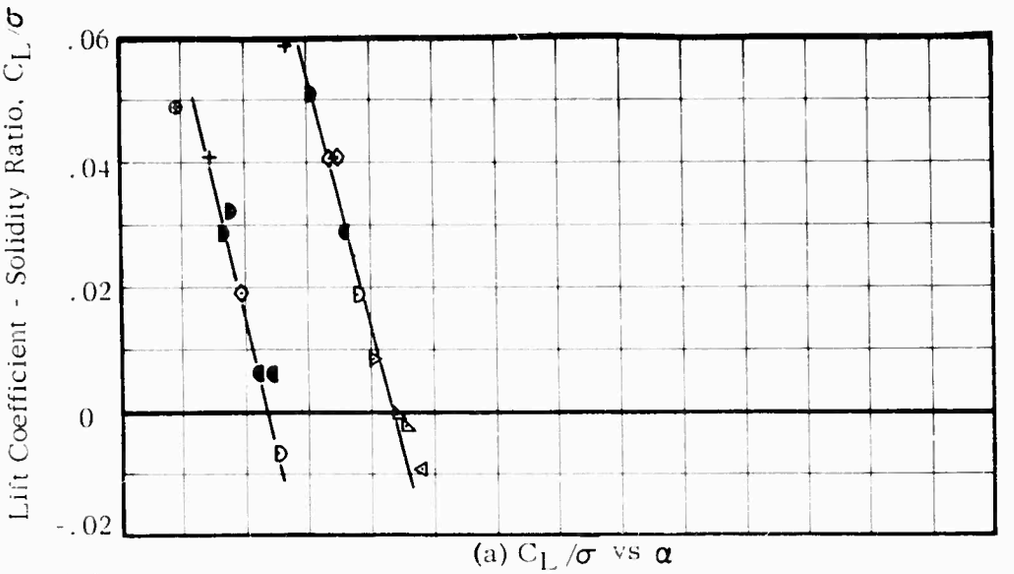

(a) C_L/σ vs α

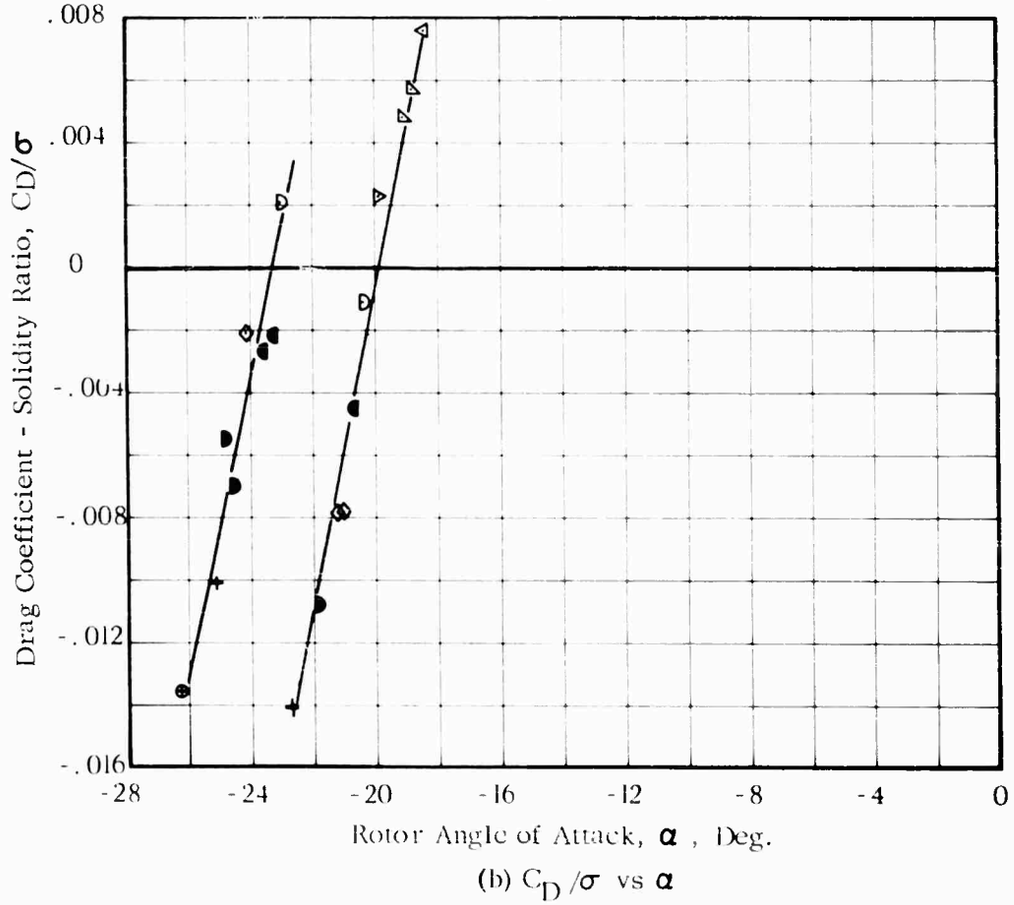

(b) C_D/σ vs α

FIG. 48. EXPERIMENTAL ROTOR PERFORMANCE AND BLADE MOTIONS
V = 161 Kts. ΩR = 800 Ft/Sec.

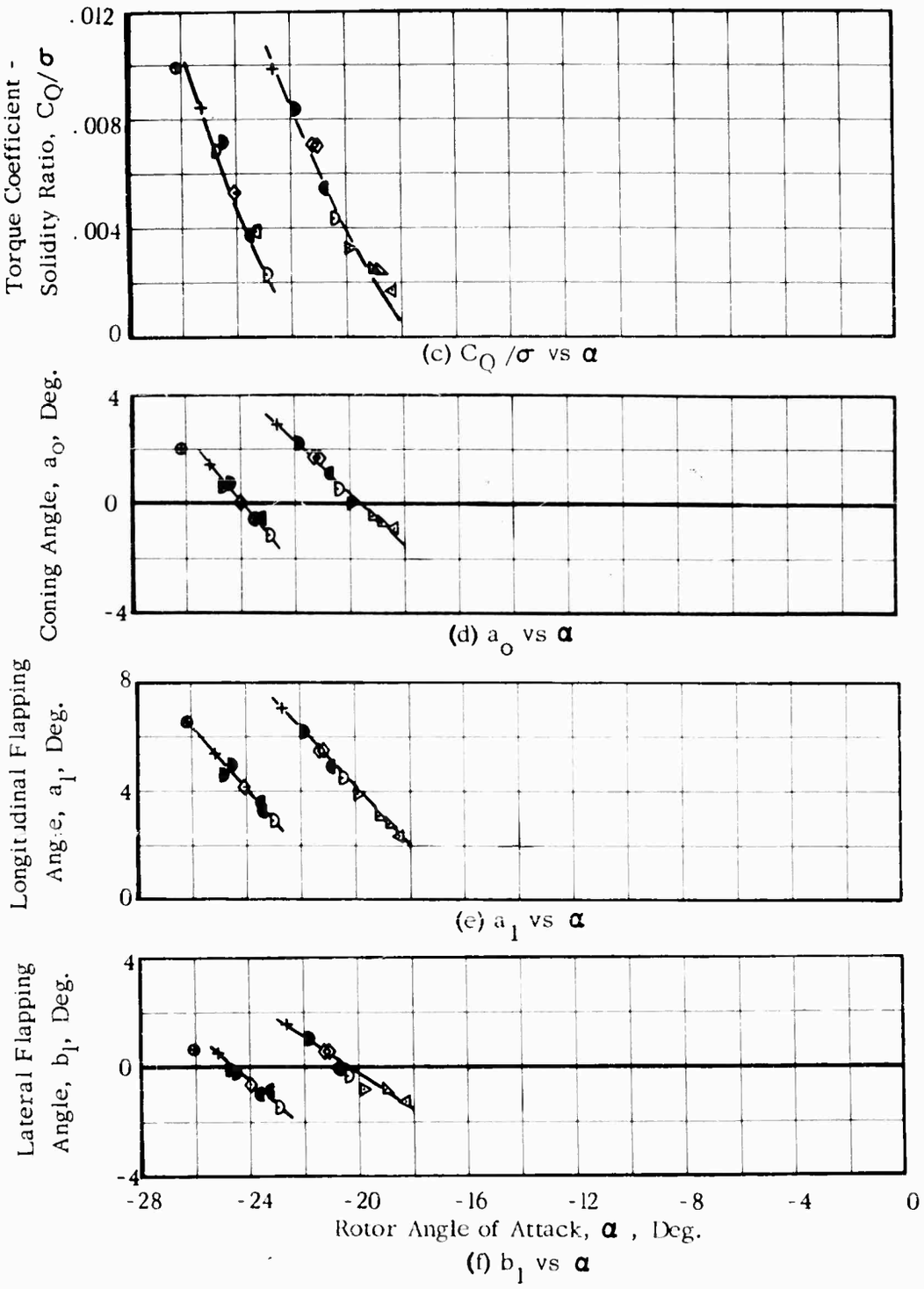

Figure 48. -Concluded

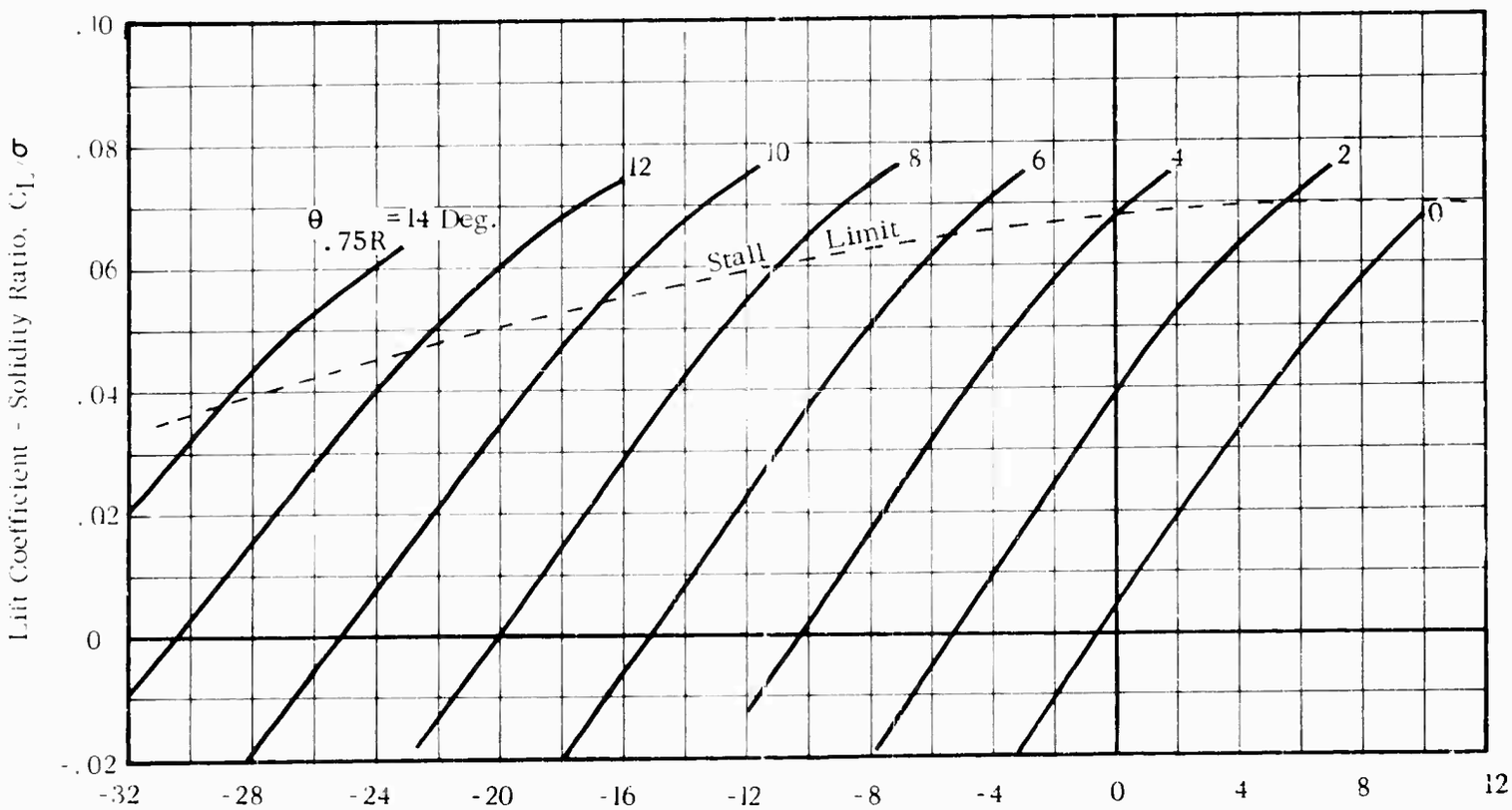

(a) C_L/σ vs α

FIG. 49. THEORETICAL ROTOR PERFORMANCE AND BLADE MOTIONS

V = 161 Kts. ΩR = 850 Ft/Sec. μ = 0.32

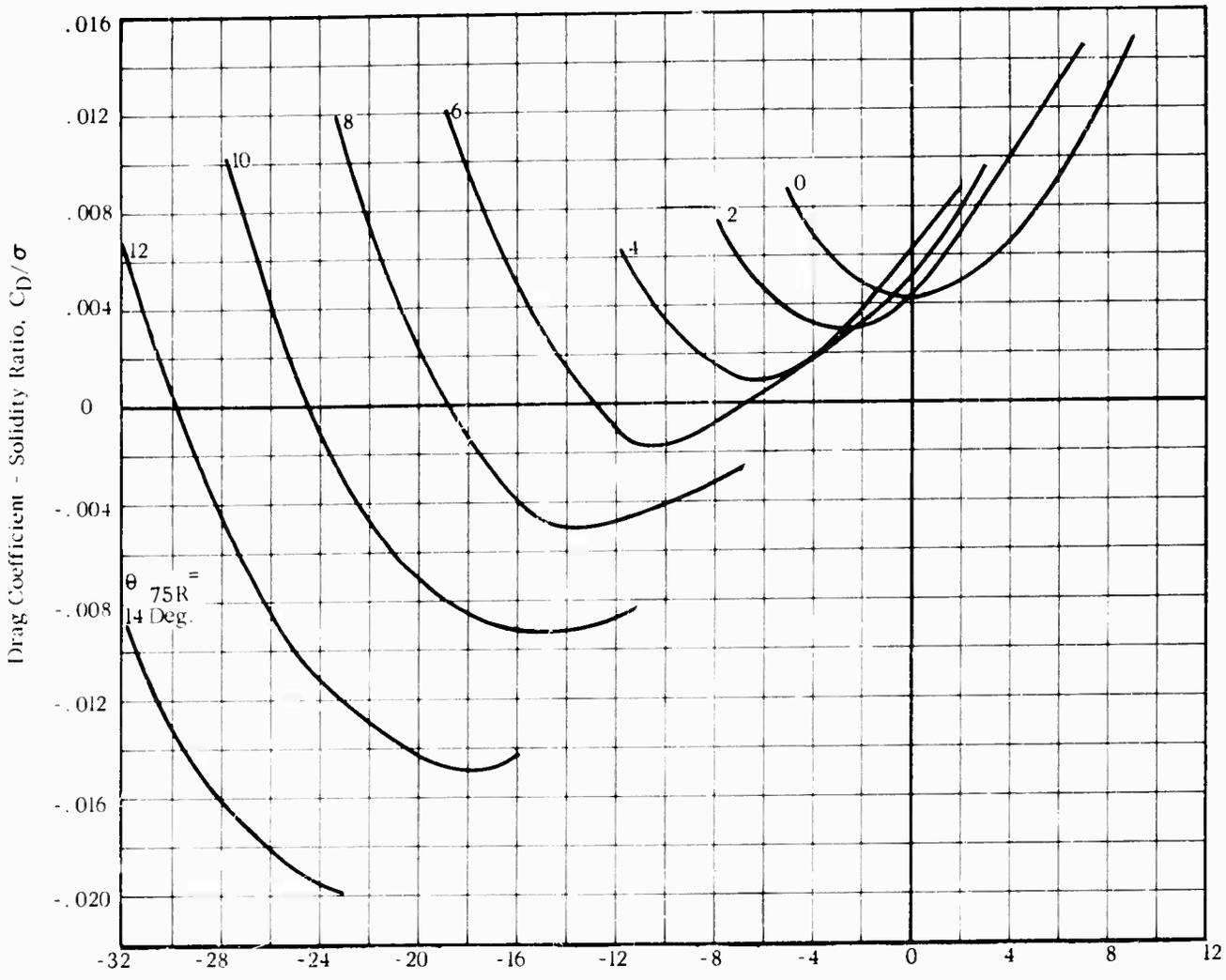

(b) C_D/σ vs α

Figure 49. -Continued

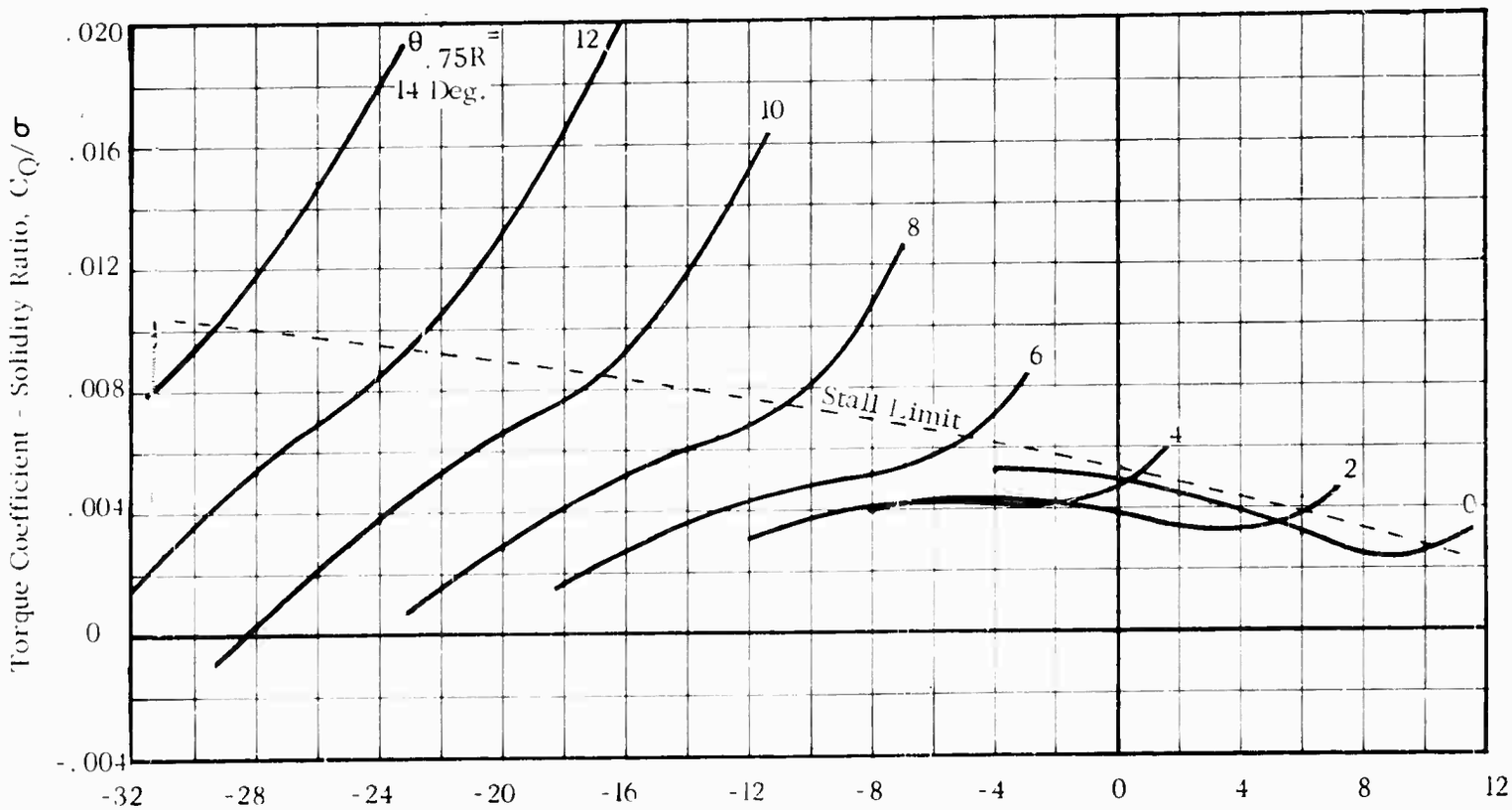

(c) C_Q/σ vs α

Figure 49. -Continued

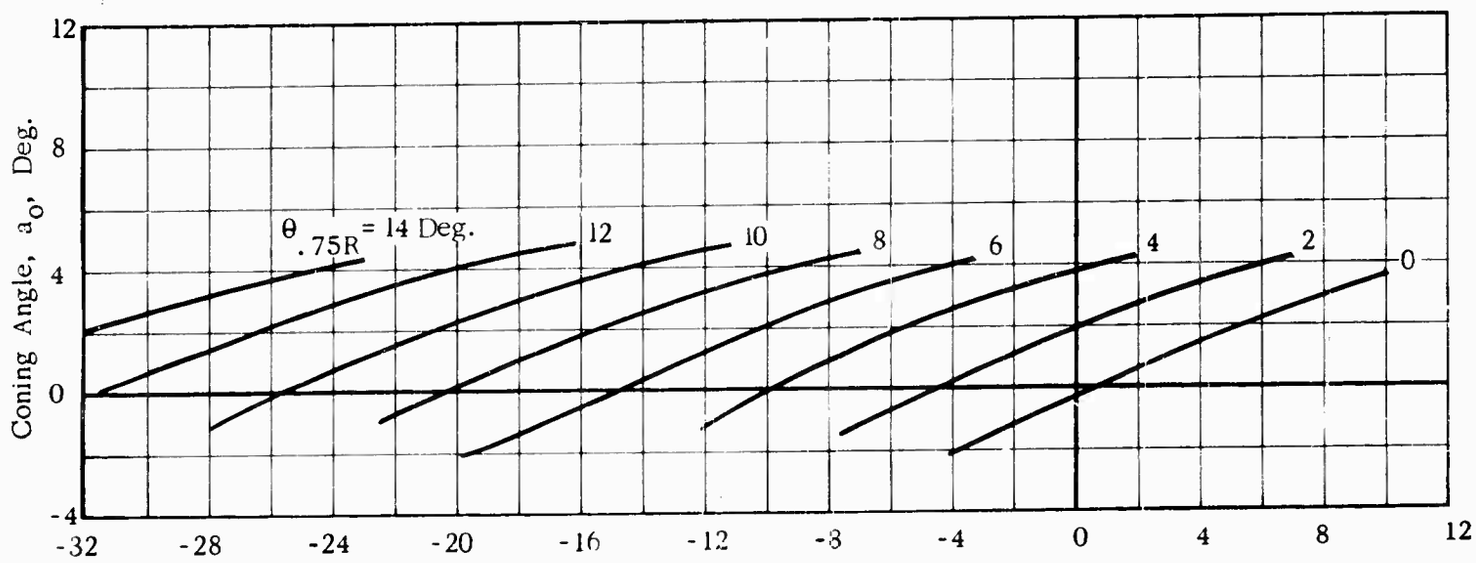

(d) a_o vs α

Figure 49. -Continued

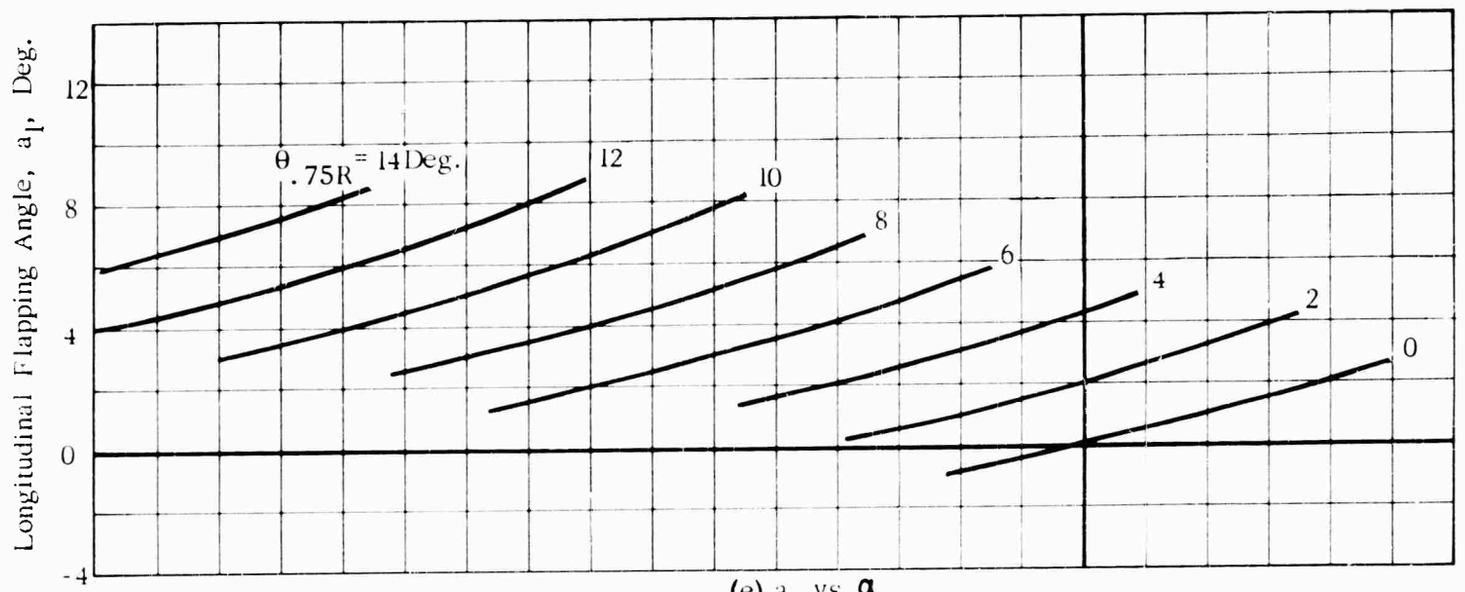

(e) a_1 vs α

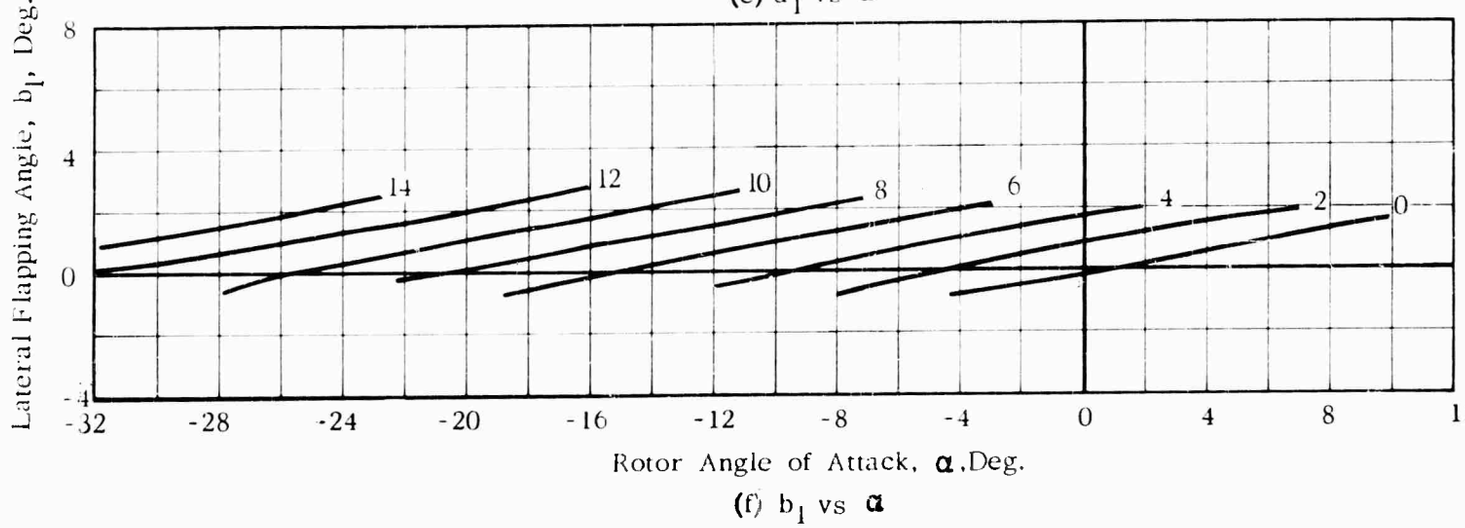

(f) b_1 vs α

Figure 49. -Concluded

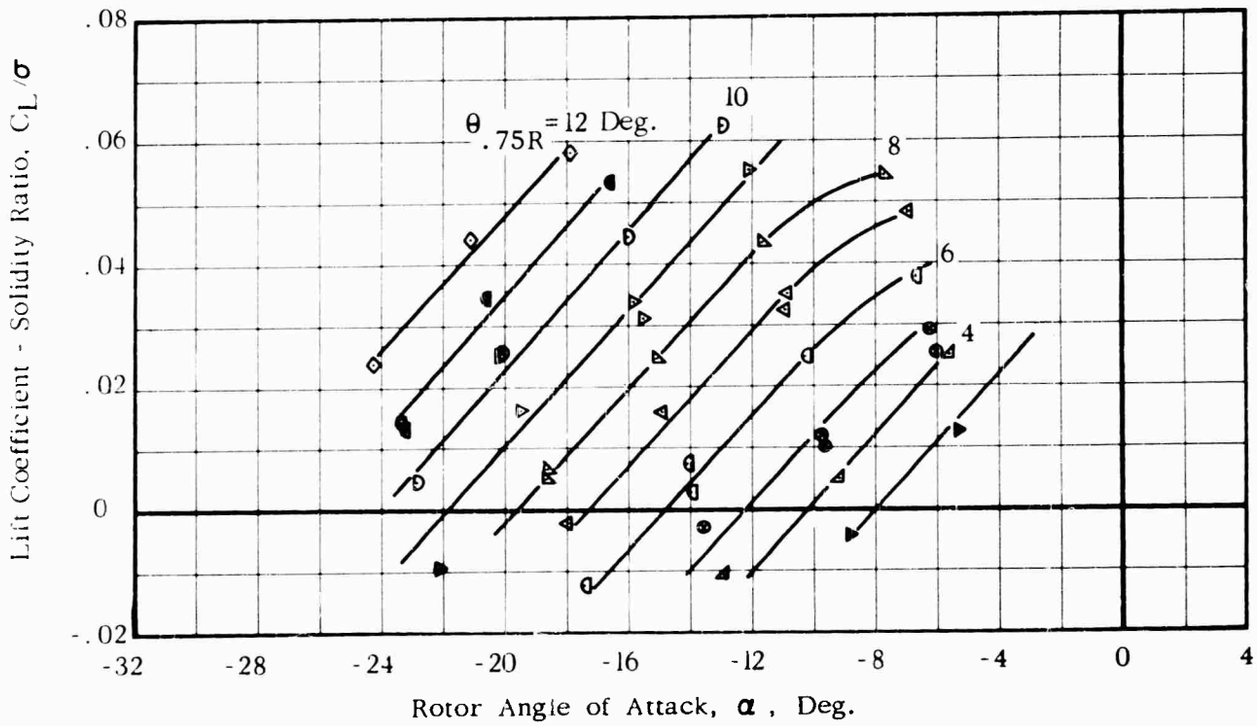

(a) C_L/σ vs α

FIG. 50. EXPERIMENTAL ROTOR PERFORMANCE AND BLADE MOTIONS

V = 161 Kts. ΩR = 850 Ft/Sec. μ = 0.32

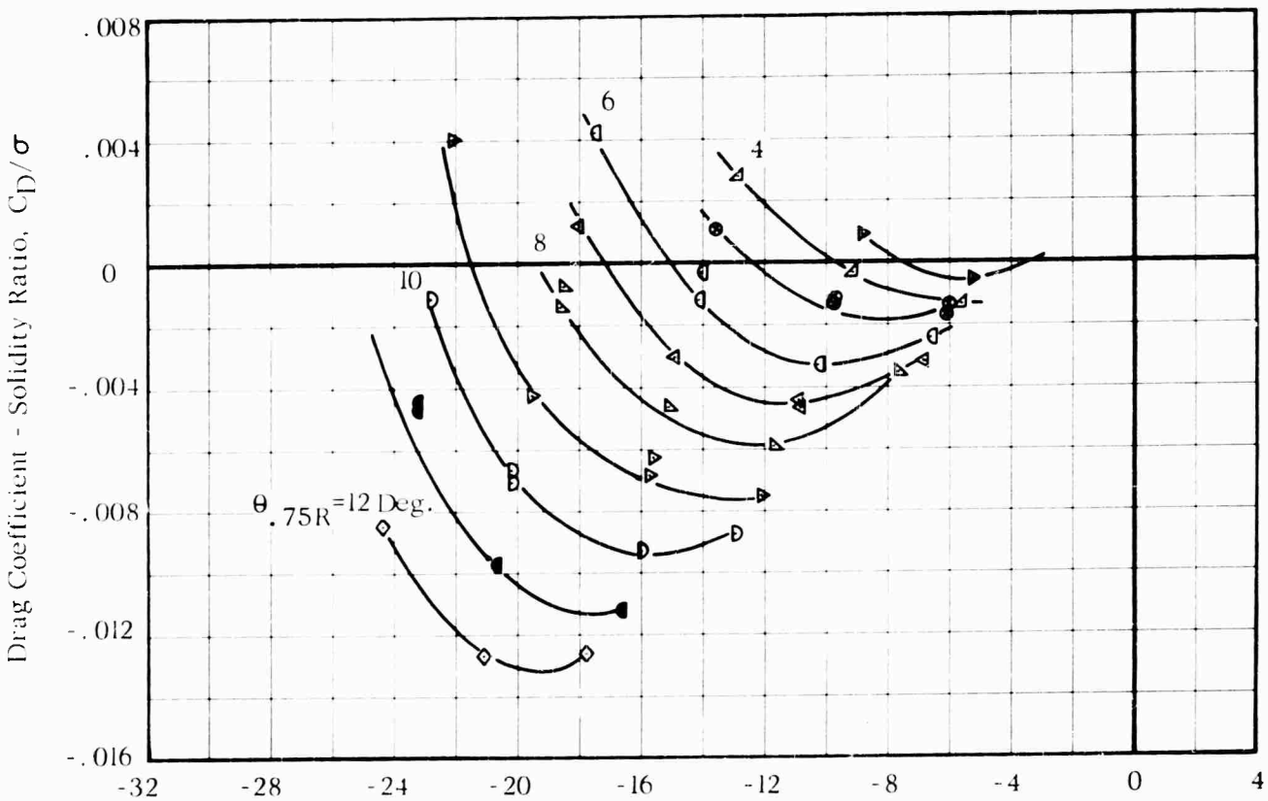

(b) C_D/σ vs α

Figure 50. -Continued

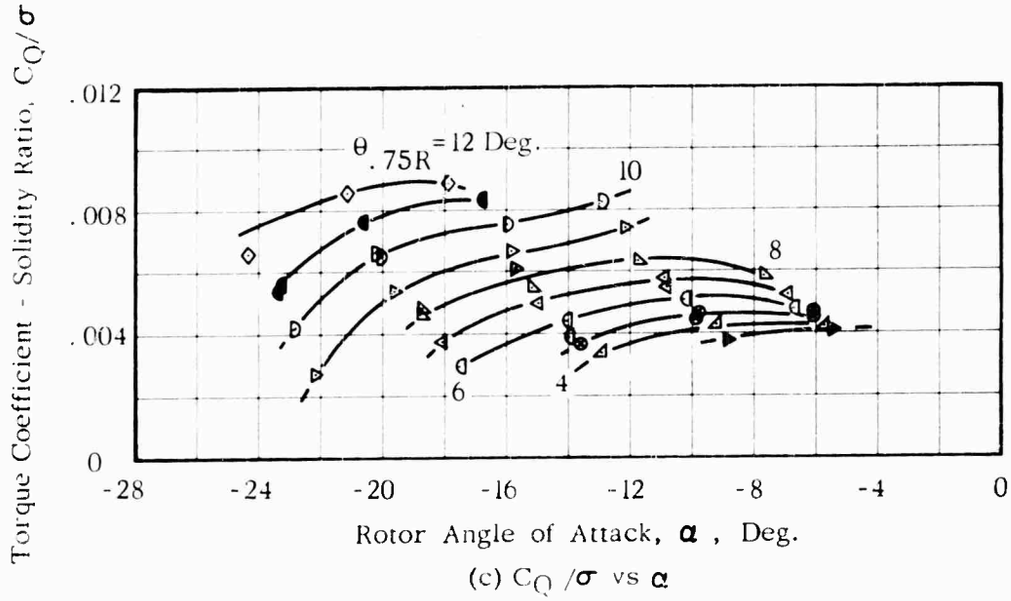

(c) C_Q/σ vs α

Figure 50. -Continued

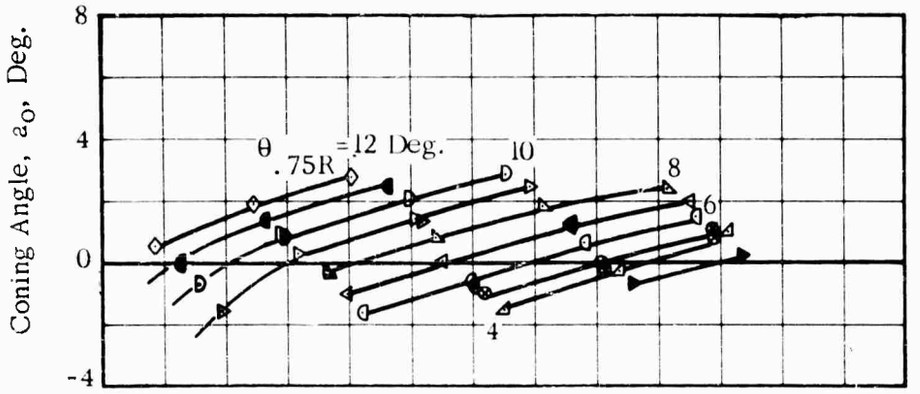

(d) a_o vs α

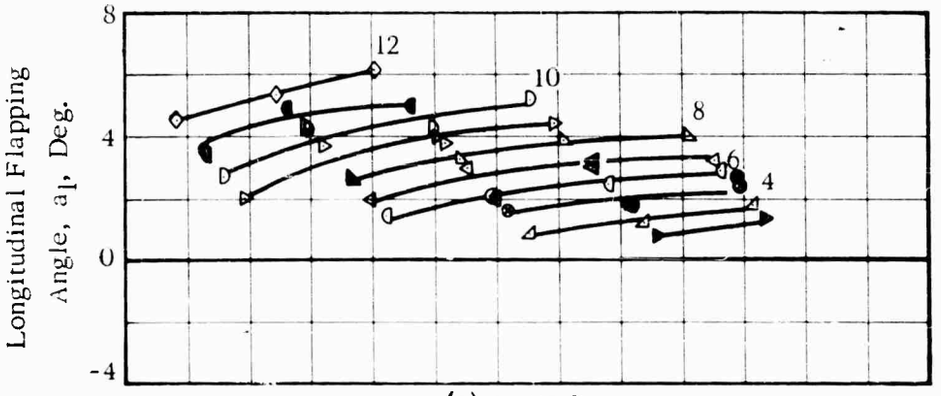

(e) a_1 vs α

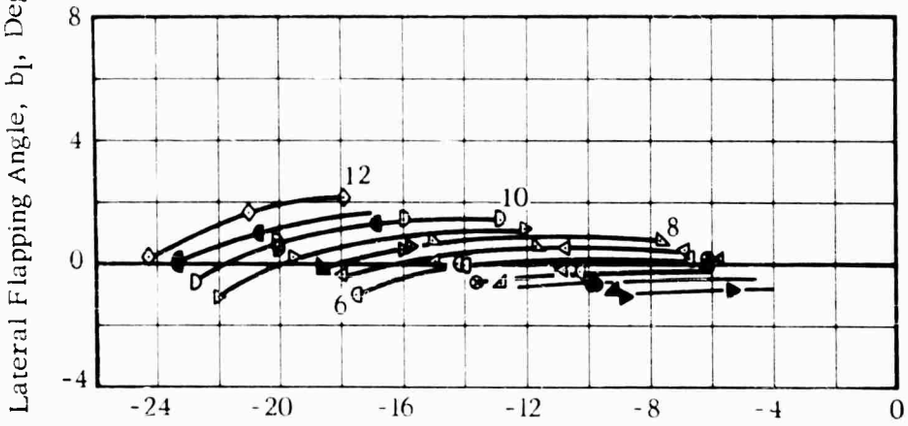

(f) b_1 vs α

Figure 50. -Concluded

APPENDIX II

Rotor blade vibratory stress amplitudes (equal to one-half the peak-to-peak stress) are presented in figures 51, 52, and 53, for the following conditions:

Forward Speed, V, Knots	Tip Speed, ΩR, feet per second
161	580
161	700
161	750

The section modulus for chordwise stresses is based on the distance from the neutral axis to the blade leading edge. To obtain chordwise stresses corresponding to the trailing edge of the spar, the plotted stresses should be multiplied by 0.7.

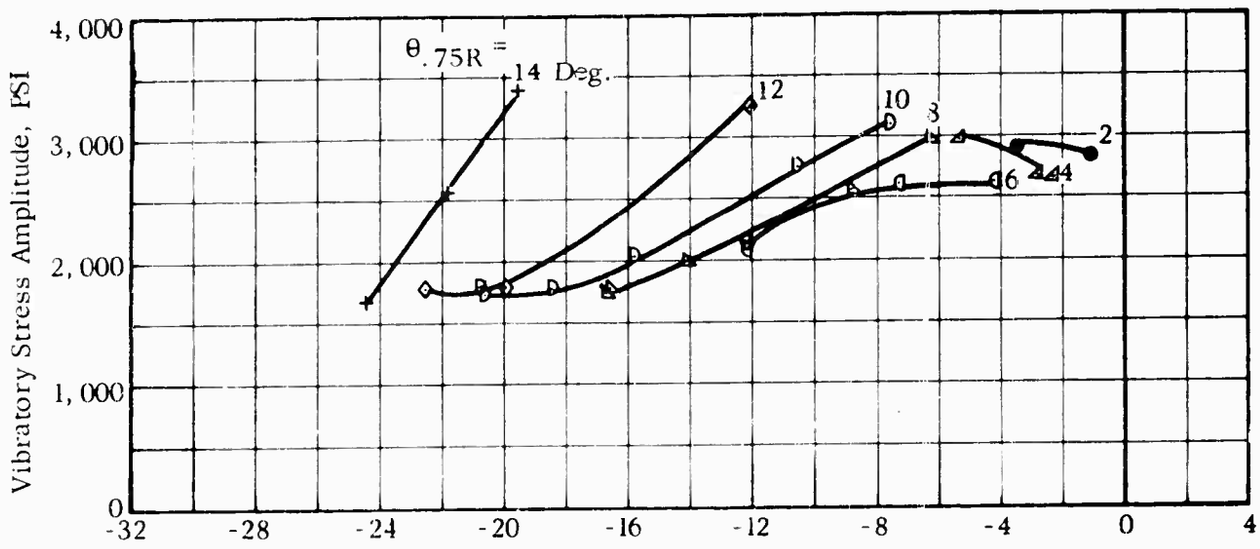

(a) Flatwise Stress at 21.0% Radius

FIG. 51. EXPERIMENTAL VIBRATORY STRESS AMPLITUDE

V = 161 Kts. ΩR = 580 Ft/Sec. μ = 0.47

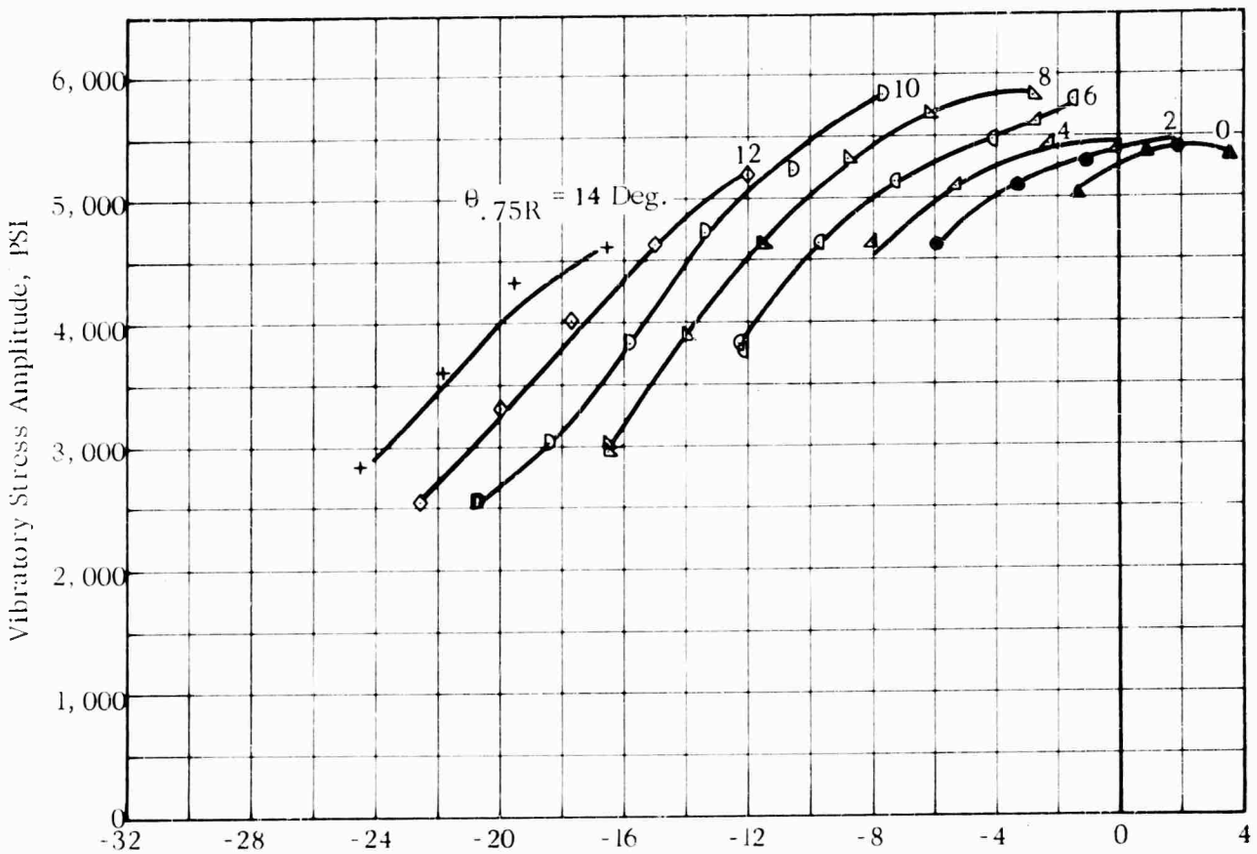

(b) Flatwise Stress at 33.3% Radius

Figure 51. -Continued

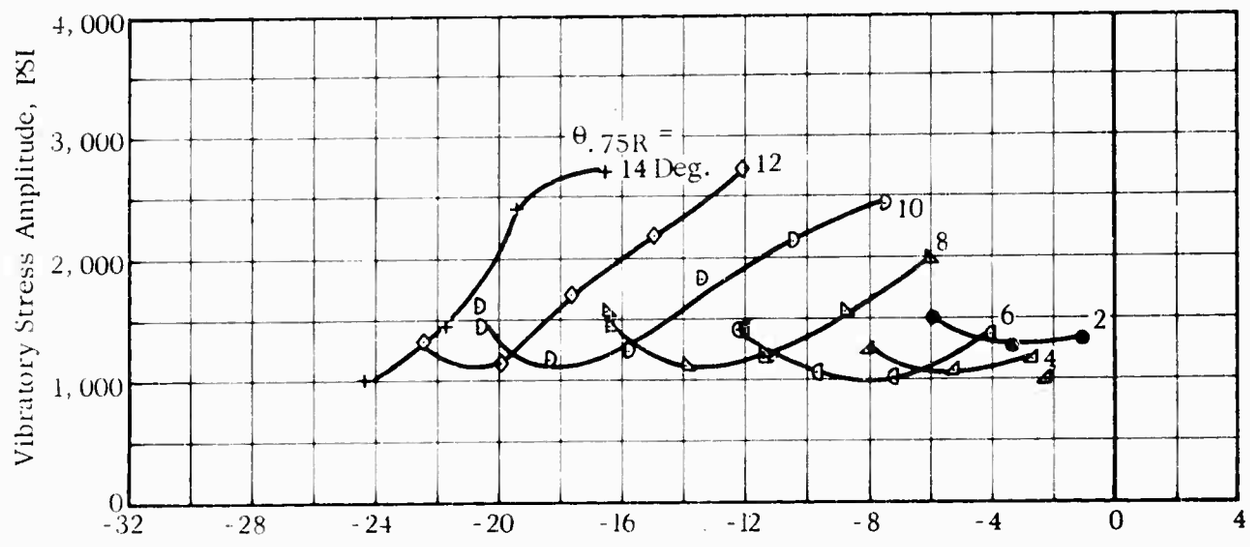

(c) Chordwise Stress at 21.0% Radius

Figure 51. -Continued

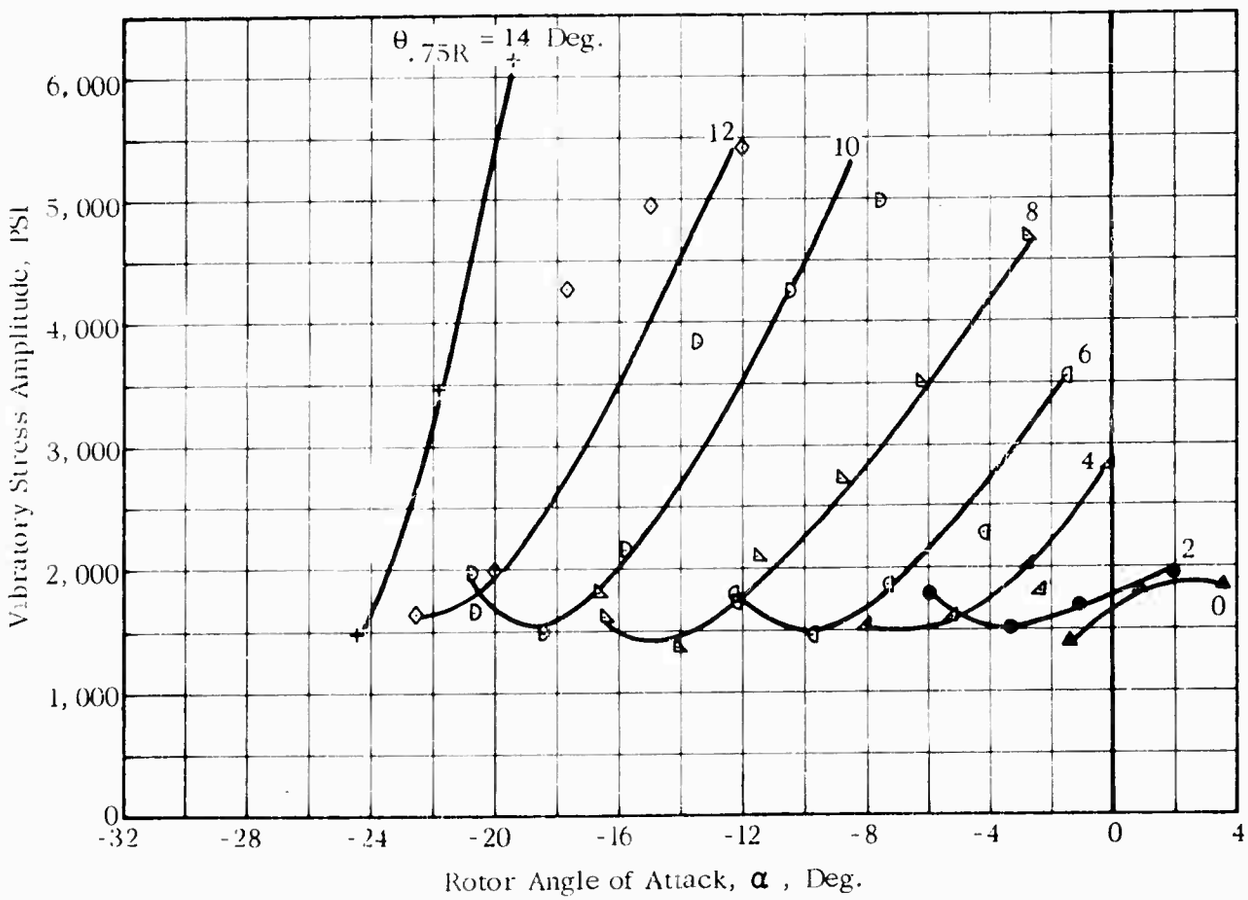

(d) Chordwise Stress at 33.3% Radius

Figure 51. -Continued

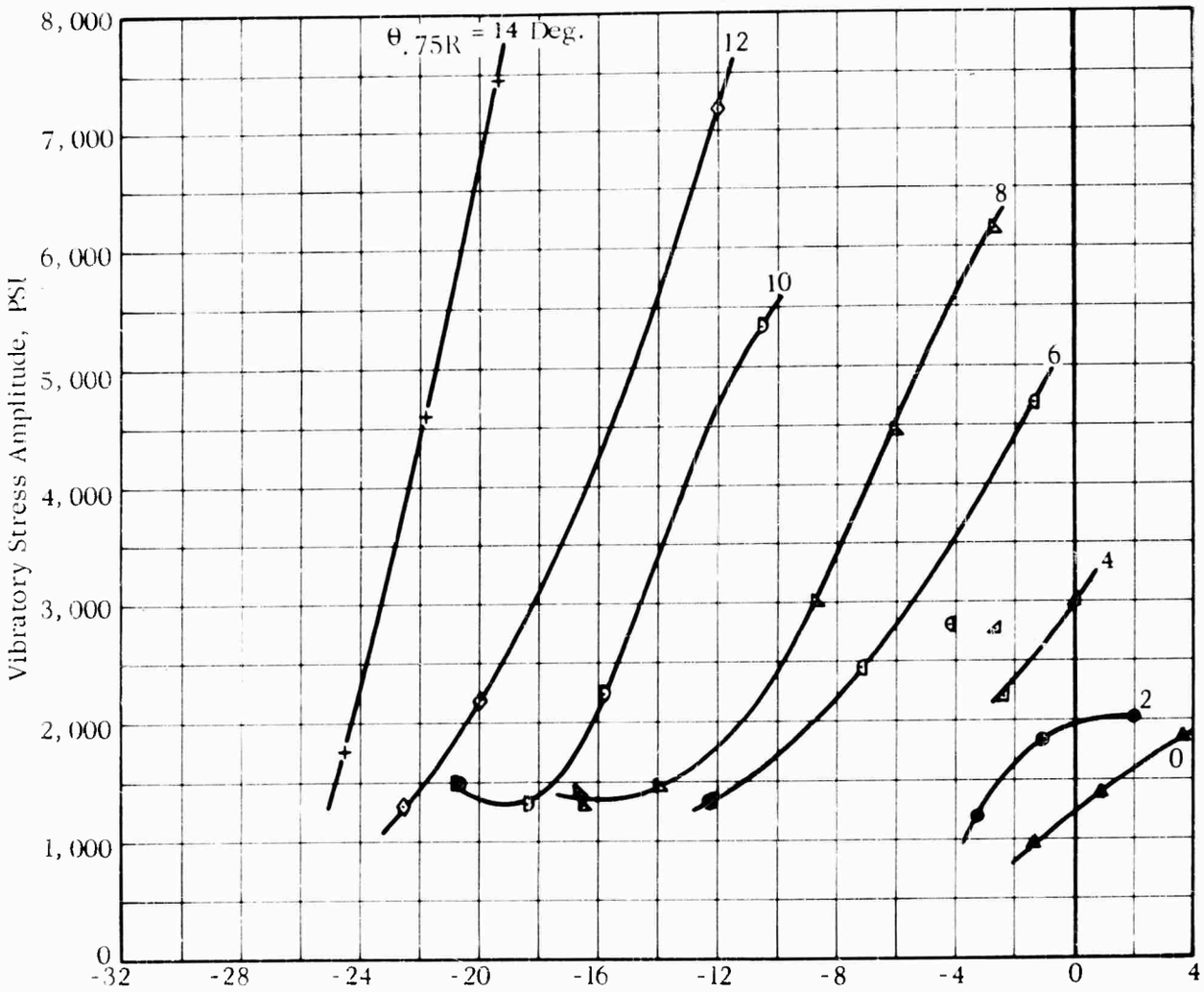

(e) Chordwise Stress at 47.2% Radius

Figure 51. -Continued

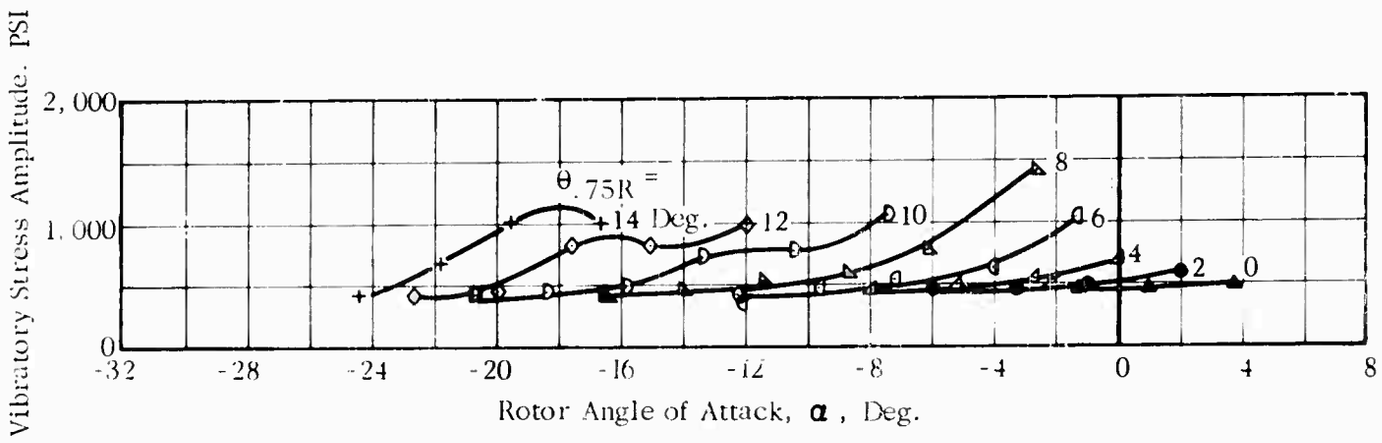

(f) Torsion Stress at 36.3% Radius

Figure 51. -Concluded

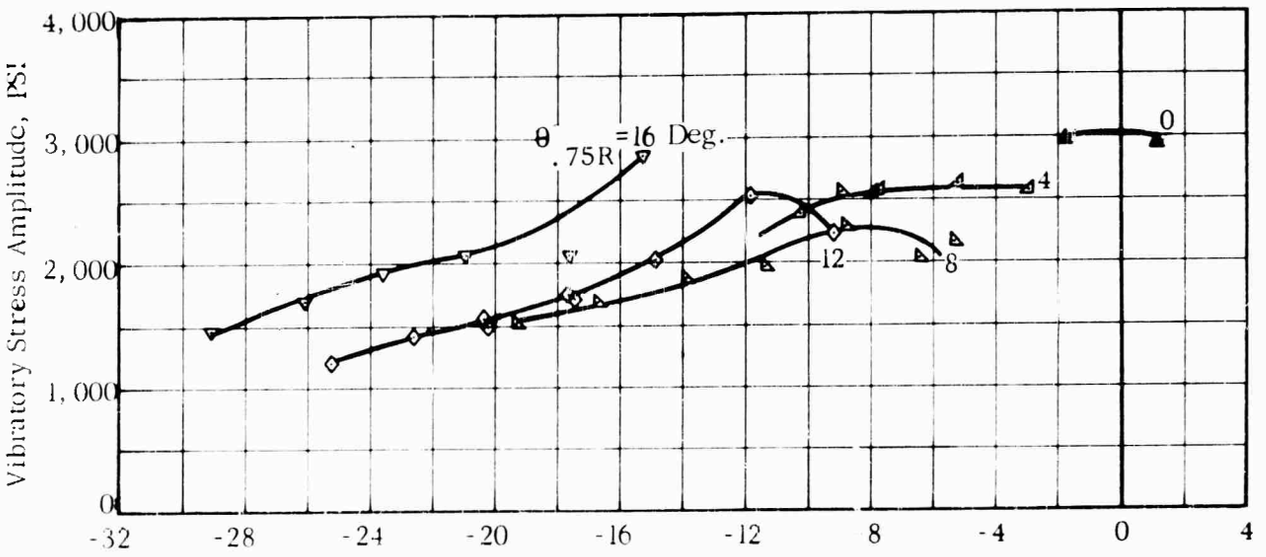

(a) Flatwise Stress at 21.0% Radius

FIG. 52. EXPERIMENTAL VIBRATORY STRESS AMPLITUDE

V = 161 Kts. ΩR = 700 Ft/Sec μ = 0.39

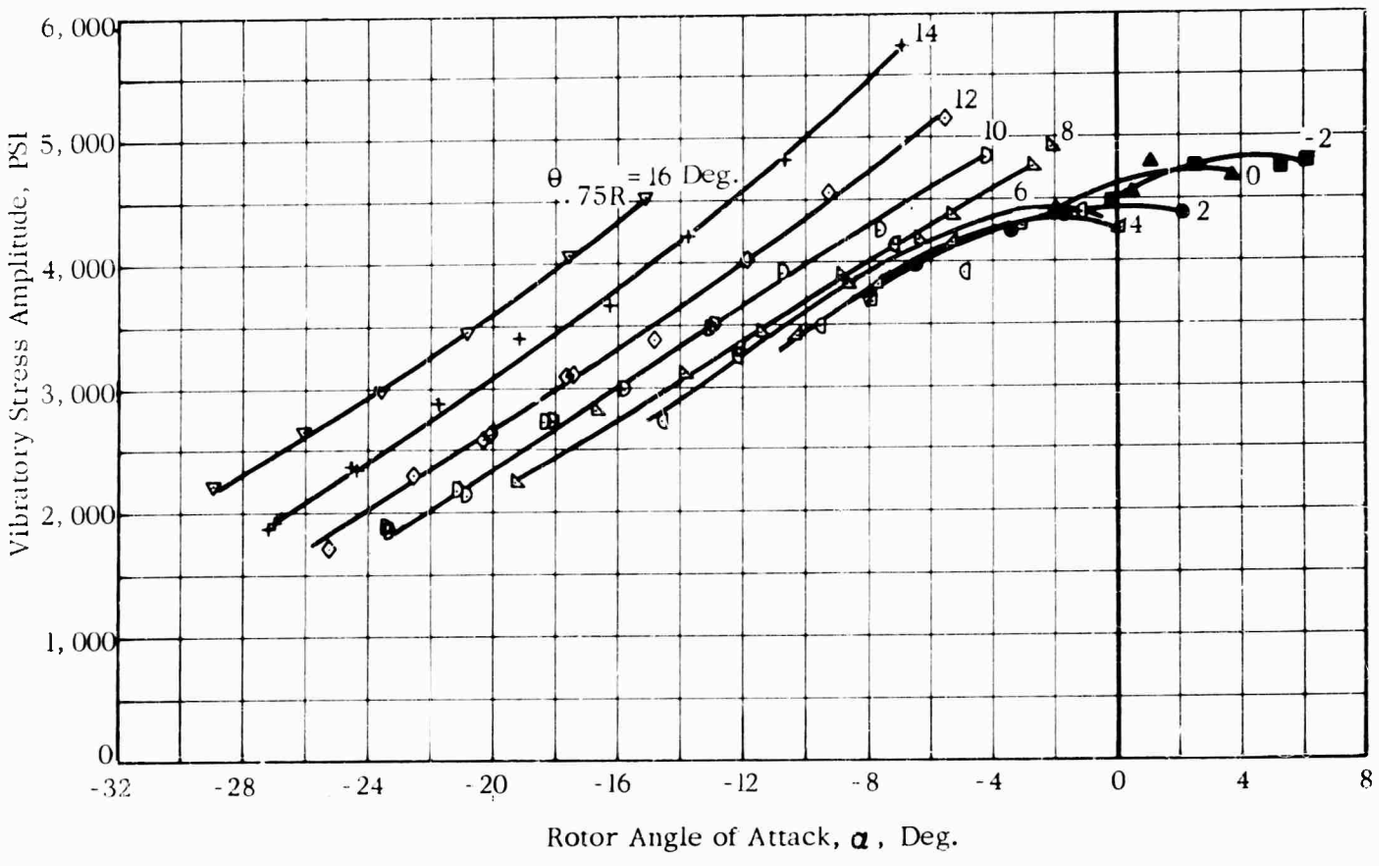

(b) Flatwise Stress at 33.3% Radius

Figure 52. -Continued

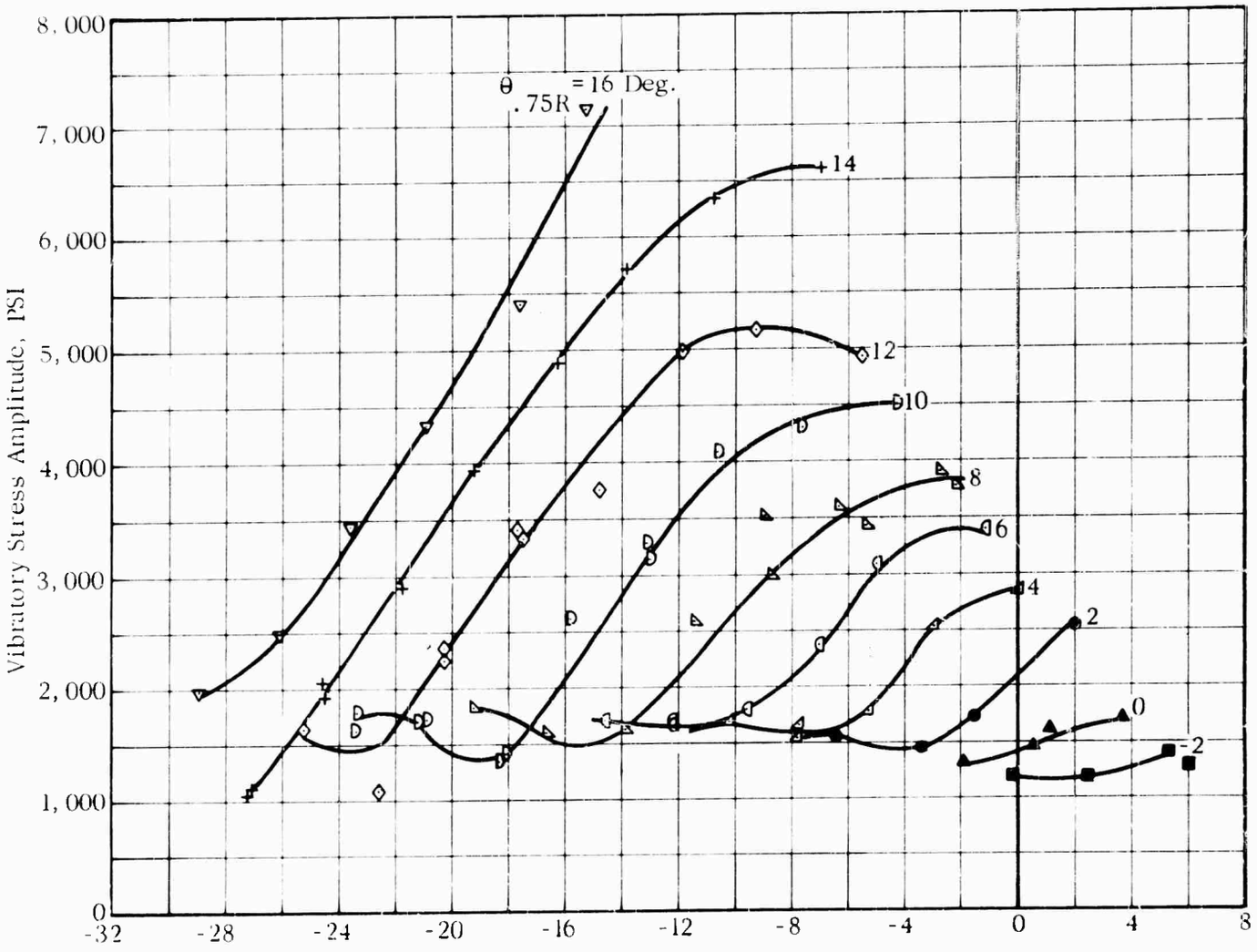

(c) Chordwise Stress at 33.3% Radius

Figure 52. -Continued

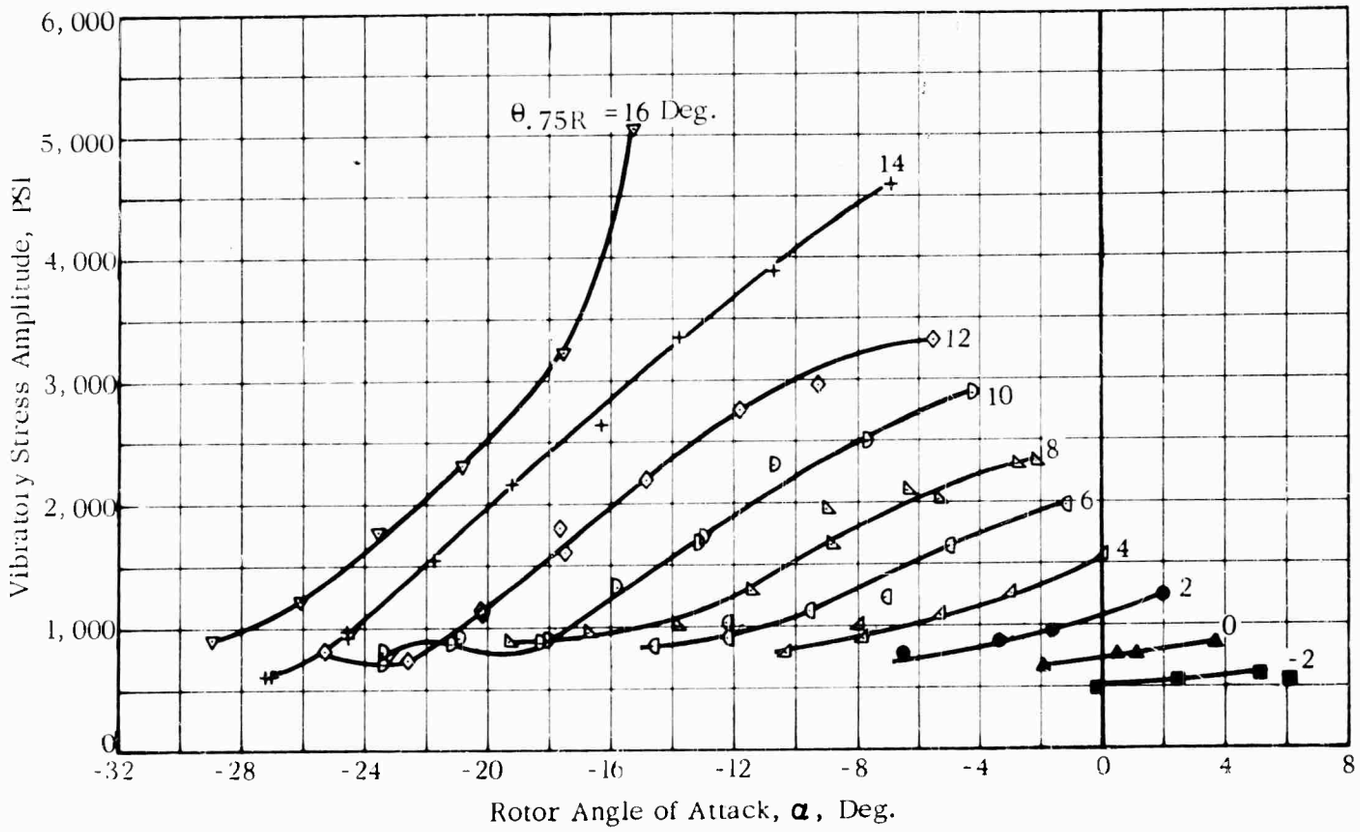

(d) Chordwise Stress at 47.2% Radius

Figure 52. -Continued

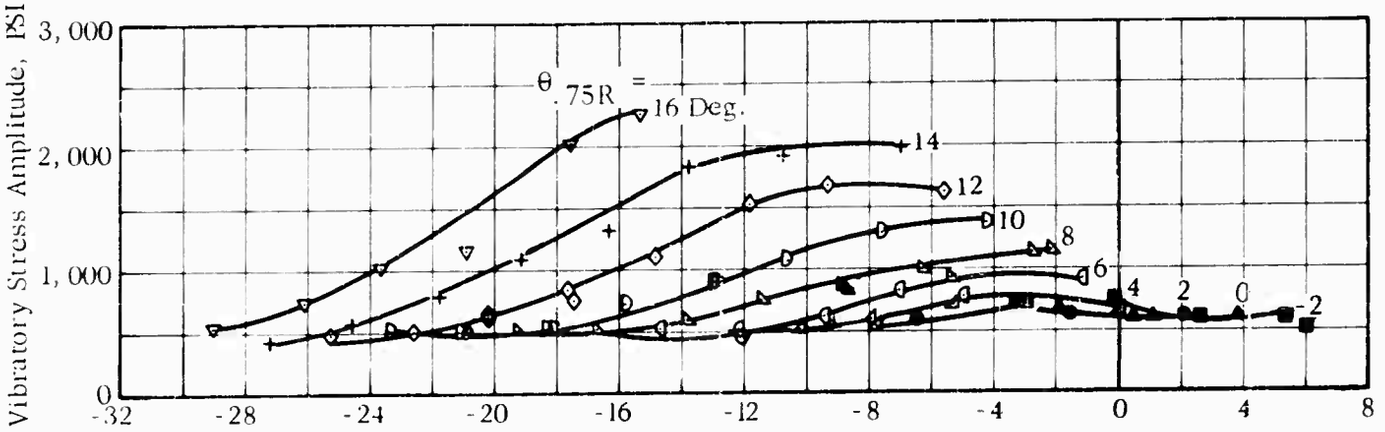

(e) Torsion Stress at 36.3% Radius

Figure 52. -Concluded

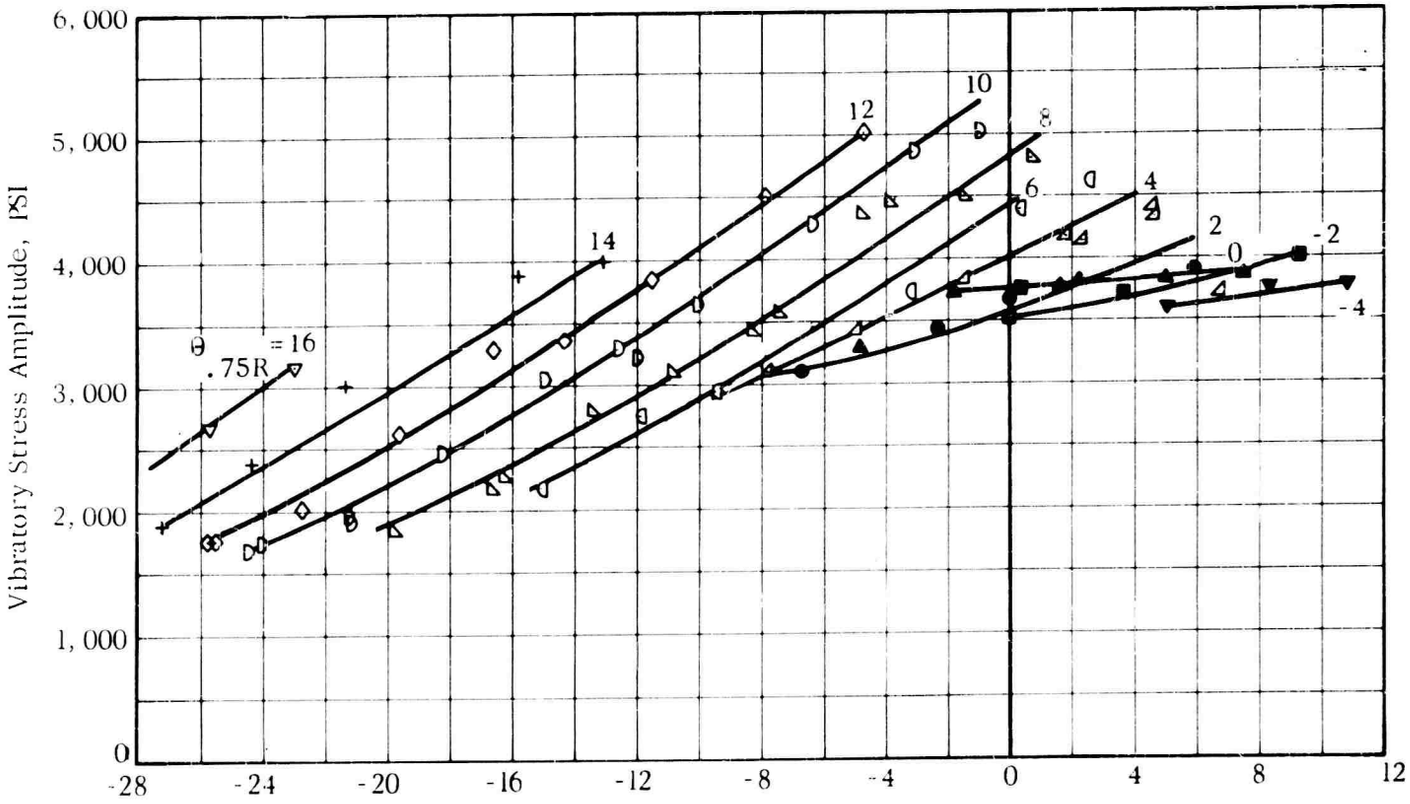

(a) Flatwise Stress at 33.3% Radius

FIG. 53. EXPERIMENTAL VIBRATORY STRESS AMPLITUDE

V = 161 Kts. ΩR = 750 Ft/Sec. μ = .36

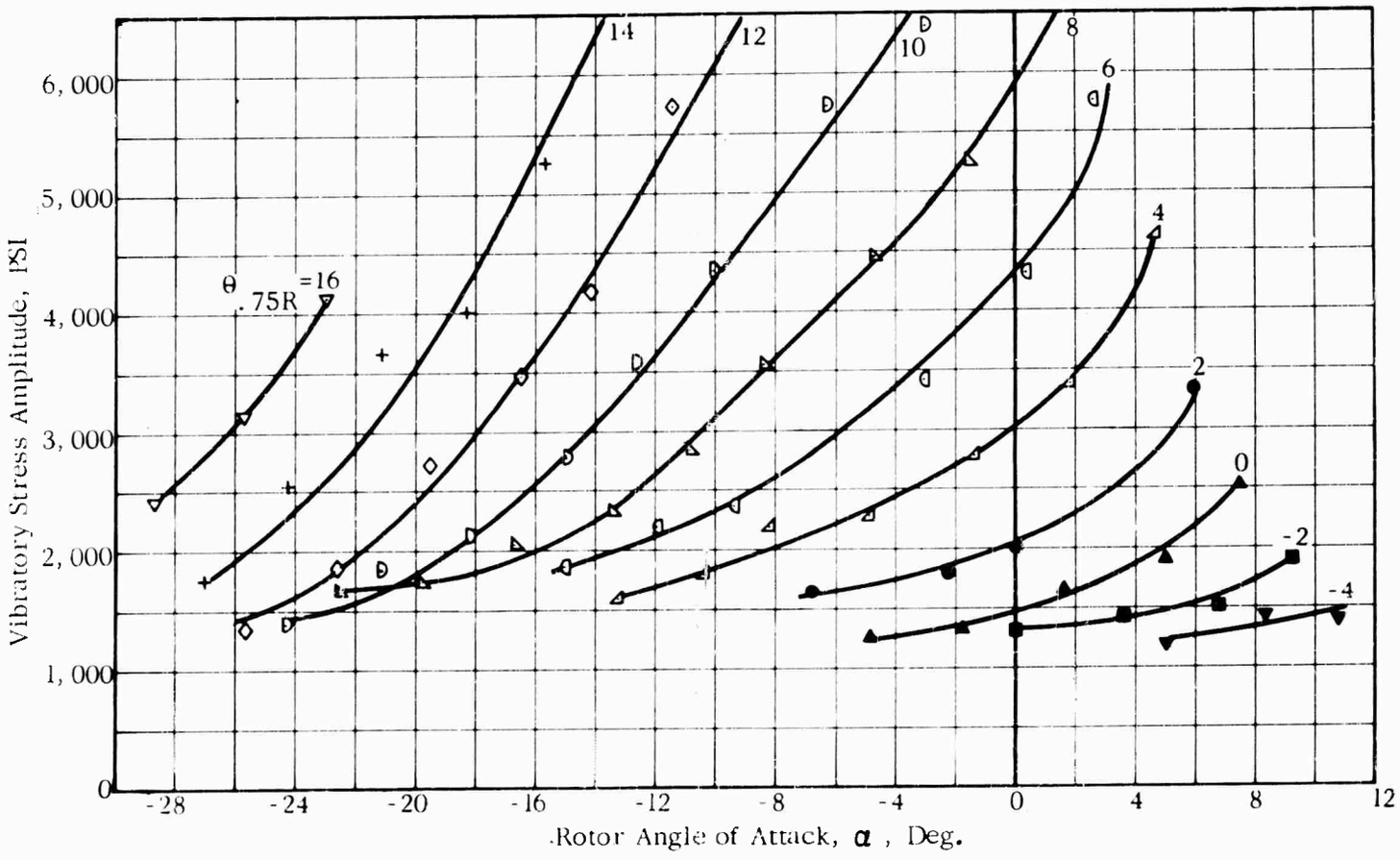

(b) Chordwise Stress at 47.2% Radius

Figure 53. -Concluded

DISTRIBUTION LIST

President
United States Army Aviation Board
Attn: ATBG-DG (1)
Fort Rucker, Alabama

Headquarters
U. S. Army Aviation Test Office
Attn: FTZAT (1)
Edwards Air Force Base, California

Chief of Research & Development
Attn: Air Mobility Division (1)
Department of the Army
Washington 25, D. C.

Commander
Naval Air Test Center
Attn: U. S. Army Liaison Officer (1)
Patuxent River, Maryland

Chief of Transportation
Attn: TCDRD (1)
Attn: TCAFO-R (1)
Department of the Army
Washington 25, D. C.

Commanding Officer
U. S. Army Transportation Research Command
Attn: Research Reference Center (4)
Attn: Aviation Directorate (5)
Attn: Military Liaison & Advisory Office (4)
Attn: Deputy Commander for Plans and Programs (1)
Attn: Deputy Commander for Aviation (1)
Attn: Long Range Technical Forecast Office (1)
Fort Eustis, Virginia

Commanding Officer
U. S. Army Transportation Research Command
Liaison Office
Attn: MCLATS (1)
Wright Patterson Air Force Base, Ohio

Commanding General
U. S. Army Transportation Materiel Command
Attn: Deputy for Surface Engineering (1)
P. O. Box 209, Main Office
St. Louis 66, Missouri

Chief
U. S. Army Research & Development Liaison
Group (9851 DU)
Attn: USATRECOM Liaison Officer (1)
APO 757, New York, New York

Chief of Naval Research
Code 461, Maj L. C. Robertson (1)
Washington 25, D. C.

Chief, Bureau of Naval Weapons
Department of the Navy
Attn: RA-4
Washington 25, D. C.

Commanding Officer and Director
David Taylor Model Basin
Aerodynamics Laboratory Library (1)
Washington 7, D. C.

National Aeronautics and Space Administration
Attn: Bertram M. Mulcahy
Assistant Director of Technical Information (1)
1520 H. Street, N. W.
Washington 25, D. C.

Librarian
Langley Research Center
National Aeronautics and Space Administration (1)
Langley Field, Virginia

Ames Research Center
National Aeronautics and Space Administration
Attn: Library (1)
Moffett Field, California

U. S. Army Standardization Group, U. K.
Box 65, U. S. Navy 100
FPO New York, New York (1)

Office of the Senior Standardization Representative
U. S. Army Standardization Group, Canada
c/o Director of Equipment Policy
Canadian Army Headquarters
Ottawa, Canada (1)

Canadian Army Liaison Officer
Liaison Group, Room 208
U. S. Army Transportation School
Fort Eustis, Virginia (3)

British Joint Services Mission (Army Staff)
Attn: Lt. Col. R. J. Wade, RE (3)
DAQMG (Mov & Tn)
3100 Massachusetts Avenue, N. W.
Washington 8, D. C.

Commander
Armed Services Technical Information Agency
Attn: TIPCR (10)
Arlington Hall Station
Arlington 12, Virginia

Bell Helicopter Company
Division of Bell Aerospace Corporation
Attn: Robert Lynn (1)
P. O. Box 482
Fort Worth 1, Texas

Doman Helicopters, Incorporated
Danbury Municipal Airport
P. O. Box 603
Danbury, Connecticut (1)

Hiller Aircraft Corporation
Attn: Library (1)
Palo Alto, California

Hughes Tool Company
Aircraft Division
Attn: Mr. Ken Amer (1)
Culver City, California

Kaman Aircraft Corporation
Attn: Library (1)
Bloomfield, Connecticut

Kellett Aircraft Corporation
Attn: Library (1)
P. O. Box 35
Willow Grove, Pennsylvania

Lockheed Aircraft Corporation
Attn: Library (1)
Burbank, California

McDonnell Aircraft Corporation
Attn: Library (1)
St. Louis, Missouri

Piasecki Aircraft Corporation
Island Road, International Airport
Philadelphia, Pennsylvania (1)

Republic Aviation Corporation
Helicopter Division
Farmingdale, Long Island, New York (1)

Vertol Division
The Boeing Company
Attn: Mr. Joe Mallen (1)
Morton, Pennsylvania

AD ______________ Accession No. ______________

Sikorsky Aircraft Division, United Aircraft Corporation, Stratford, Connecticut. COMPARISON OF THEORETICAL AND EXPERIMENTAL MODEL HELICOPTER ROTOR PERFORMANCE IN FORWARD FLIGHT - John P. Rabbott, Jr.

Report No. TREC 61-103, July, 1961, 181 pp. (Contract DA 44-177-TC-548) USATRECOM Proj 9R58-13-014-02. Unclassified Report

A program was conducted to determine the degree of correlation between theoretical and experimental dynamically scaled model rotor performance over a range of forward speeds to 161 knots, tip speeds to 850 feet per second, and tip Mach Numbers to 1.0. Theory and experiment correlate well below the theoretically predicted stall boundary, but above stall the theory is unduly conservative in predicting rotor power required. The effects of compressibility can be accurately predicted and a rotor with an NACA 0012 airfoil section incurs substantial profile power losses when the advancing tip Mach Number exceeds 0.85 to 0.90.

Significant amounts of model rotor blade dynamic twisting-up to 5 degrees-occur both in hovering and forward flight. The inclusion of dynamic twist in forward flight significantly improves the correlation of theory and experiment at a given collective pitch.

UNCLASSIFIED

1. Helicopters - Performance
2. Helicopters - Aerodynamic Characteristics
3. Helicopters - Model Test Results

I. Rabbott, J. P. Jr.
II. Contract DA 44-177-TC-548

AD ______________ Accession No. ______________

Sikorsky Aircraft Division, United Aircraft Corporation, Stratford, Connecticut. COMPARISON OF THEORETICAL AND EXPERIMENTAL MODEL HELICOPTER ROTOR PERFORMANCE IN FORWARD FLIGHT - John P. Rabbott, Jr.

Report No. TREC 61-103, July, 1961, 181 pp. (Contract DA 44-177-TC-548) USATRECOM Proj 9R58-13-014-02. Unclassified Report

A program was conducted to determine the degree of correlation between theoretical and experimental dynamically scaled model rotor performance over a range of forward speeds to 161 knots, tip speeds to 850 feet per second, and tip Mach Numbers to 1.0. Theory and experiment correlate well below the theoretically predicted stall boundary, but above stall the theory is unduly conservative in predicting rotor power required. The effects of compressibility can be accurately predicted and a rotor with an NACA 0012 airfoil section incurs substantial profile power losses when the advancing tip Mach Number exceeds 0.85 to 0.90.

Significant amounts of model rotor blade dynamic twisting-up to 5 degrees-occur both in hovering and forward flight. The inclusion of dynamic twist in forward flight significantly improves the correlation of theory and experiment at a given collective pitch.

UNCLASSIFIED

1. Helicopters - Performance
2. Helicopters - Aerodynamic Characteristics
3. Helicopters - Model Test Results

I. Rabbott, J. P. Jr.
II. Contract DA 44-177-TC-548

AD ______________ Accession No. ______________

Sikorsky Aircraft Division, United Aircraft Corporation, Stratford, Connecticut. COMPARISON OF THEORETICAL AND EXPERIMENTAL MODEL HELICOPTER ROTOR PERFORMANCE IN FORWARD FLIGHT - John P. Rabbott, Jr.

Report No. TREC 61-103, July, 1961, 181 pp. (Contract DA 44-177-TC-548) USATRECOM Proj 9R58-13-014-02. Unclassified Report

A program was conducted to determine the degree of correlation between theoretical and experimental dynamically scaled model rotor performance over a range of forward speeds to 161 knots, tip speeds to 850 feet per second, and tip Mach Numbers to 1.0. Theory and experiment correlate well below the theoretically predicted stall boundary, but above stall the theory is unduly conservative in predicting rotor power required. The effects of compressibility can be accurately predicted and a rotor with an NACA 0012 airfoil section incurs substantial profile power losses when the advancing tip Mach Number exceeds 0.85 to 0.90.

Significant amounts of model rotor blade dynamic twisting-up to 5 degrees-occur both in hovering and forward flight. The inclusion of dynamic twist in forward flight significantly improves the correlation of theory and experiment at a given collective pitch.

UNCLASSIFIED

1. Helicopters - Performance
2. Helicopters - Aerodynamic Characteristics
3. Helicopters - Model Test Results

I. Rabbott, J. P. Jr.
II. Contract DA 44-177-TC-548

AD ______________ Accession No. ______________

Sikorsky Aircraft Division, United Aircraft Corporation, Stratford, Connecticut. COMPARISON OF THEORETICAL AND EXPERIMENTAL MODEL HELICOPTER ROTOR PERFORMANCE IN FORWARD FLIGHT - John P. Rabbott, Jr.

Report No. TREC 61-103, July, 1961, 181 pp. (Contract DA 44-177-TC-548) USATRECOM Proj 9R58-13-014-02. Unclassified Report

A program was conducted to determine the degree of correlation between theoretical and experimental dynamically scaled model rotor performance over a range of forward speeds to 161 knots, tip speeds to 850 feet per second, and tip Mach Numbers to 1.0. Theory and experiment correlate well below the theoretically predicted stall boundary, but above stall the theory is unduly conservative in predicting rotor power required. The effects of compressibility can be accurately predicted and a rotor with an NACA 0012 airfoil section incurs substantial profile power losses when the advancing tip Mach Number exceeds 0.85 to 0.90.

Significant amounts of model rotor blade dynamic twisting-up to 5 degrees-occur both in hovering and forward flight. The inclusion of dynamic twist in forward flight significantly improves the correlation of theory and experiment at a given collective pitch.

UNCLASSIFIED

1. Helicopters - Performance
2. Helicopters - Aerodynamic Characteristics
3. Helicopters - Model Test Results

I. Rabbott, J. P. Jr.
II. Contract DA 44-177-TC-548

AD _____ Accession No _____

Sikorsky Aircraft Division, United Aircraft Corporation, Stratford, Connecticut. COMPARISON OF THEORETICAL AND EXPERIMENTAL MODEL HELICOPTER ROTOR PERFORMANCE IN FORWARD FLIGHT - John P. Rabbott, Jr.

Report No. TREC 61-103, July 1961, 181 pp.
(Contract DA 44-177-TC-548) USATRECOM Proj 9R38-13-014-02
Unclassified Report

A program was conducted to determine the degree of correlation between theoretical and experimental dynamically scaled model rotor performance over a range of forward speeds to 161 knots, tip speeds to 850 feet per second, and tip Mach Numbers to 1.0. Theory and experiment correlate well below the theoretically predicted stall boundary, but above stall the theory is unduly conservative in predicting rotor power required. The effects of compressibility can be accurately predicted and a rotor with an NACA 0012 airfoil section incurs substantial profile power losses when the advancing tip Mach Number exceeds 0.85 to 0.90.

Significant amounts of model rotor blade dynamic twisting-up to 5 degrees occur both in hovering and forward flight. The inclusion of dynamic twist in forward flight significantly improves the correlation of theory and experiment at a given collective pitch.

UNCLASSIFIED

1. Helicopters - Performance
2. Helicopters - Aerodynamic Characteristics
3. Helicopters - Model Test Results

I. Rabbott, J. P. Jr.

II. Contract DA 44-177-TC-548

AD _____ Accession No. _____

Sikorsky Aircraft Division, United Aircraft Corporation, Stratford, Connecticut. COMPARISON OF THEORETICAL AND EXPERIMENTAL MODEL HELICOPTER ROTOR PERFORMANCE IN FORWARD FLIGHT - John P. Rabbott, Jr.

Report No. TREC 61-103, July 1961, 181 pp.
(Contract DA 44-177-TC-548) USATRECOM Proj 9R38-13-014-02,
Unclassified Report

A program was conducted to determine the degree of correlation between theoretical and experimental dynamically scaled model rotor performance over a range of forward speeds to 161 knots, tip speeds to 850 feet per second, and tip Mach Numbers to 1.0. Theory and experiment correlate well below the theoretically predicted stall boundary, but above stall the theory is unduly conservative in predicting rotor power required. The effects of compressibility can be accurately predicted and a rotor with an NACA 0012 airfoil section incurs substantial profile power losses when the advancing tip Mach Number exceeds 0.85 to 0.90.

Significant amounts of model rotor blade dynamic twisting-up to 5 degrees occur both in hovering and forward flight. The inclusion of dynamic twist in forward flight significantly improves the correlation of theory and experiment at a given collective pitch.

UNCLASSIFIED

1. Helicopters - Performance
2. Helicopters - Aerodynamic Characteristics
3. Helicopters - Model Test Results

I. Rabbott, J. P. Jr.

II. Contract DA 44-177-TC-548

AD _____ Accession No _____

Sikorsky Aircraft Division, United Aircraft Corporation, Stratford Connecticut. COMPARISON OF THEORETICAL AND EXPERIMENTAL MODEL HELICOPTER ROTOR PERFORMANCE IN FORWARD FLIGHT - John P. Rabbott, Jr.

Report No. TREC 61-103, July, 1961, 181 pp.
(Contract DA 44-177-TC-548) USATRECOM Proj 9R38-13-014-02.
Unclassified Report

A program was conducted to determine the degree of correlation between theoretical and experimental dynamically scaled model rotor performance over a range of forward speeds to 161 knots, tip speeds to 850 feet per second, and tip Mach Numbers to 1.0. Theory and experiment correlate well below the theoretically predicted stall boundary, but above stall the theory is unduly conservative in predicting rotor power required. The effects of compressibility can be accurately predicted and a rotor with an NACA 0012 airfoil section incurs substantial profile power losses when the advancing tip Mach Number exceeds 0.85 to 0.90.

Significant amounts of model rotor blade dynamic twisting-up to 5 degrees occur both in hovering and forward flight. The inclusion of dynamic twist in forward flight significantly improves the correlation of theory and experiment at a given collective pitch.

UNCLASSIFIED

1. Helicopters - Performance
2. Helicopters - Aerodynamic Characteristics
3. Helicopters - Model Test Results

I. Rabbott, J. P. Jr.

II. Contract DA 44-177-TC-548

AD _____ Accession No. _____

Sikorsky Aircraft Division, United Aircraft Corporation, Stratford, Connecticut. COMPARISON OF THEORETICAL AND EXPERIMENTAL MODEL HELICOPTER ROTOR PERFORMANCE IN FORWARD FLIGHT - John P. Rabbott, Jr.

Report No. TREC 61-103, July, 1961, 181 pp.
(Contract DA 44-177-TC-548) USATRECOM Proj 9R38-13-014-02,
Unclassified Report

A program was conducted to determine the degree of correlation between theoretical and experimental dynamically scaled model rotor performance over a range of forward speeds to 161 knots, tip speeds to 850 feet per second, and tip Mach Numbers to 1.0. Theory and experiment correlate well below the theoretically predicted stall boundary, but above stall the theory is unduly conservative in predicting rotor power required. The effects of compressibility can be accurately predicted and a rotor with an NACA 0012 airfoil section incurs substantial profile power losses when the advancing tip Mach Number exceeds 0.85 to 0.90.

Significant amounts of model rotor blade dynamic twisting-up to 5 degrees occur both in hovering and forward flight. The inclusion of dynamic twist in forward flight significantly improves the correlation of theory and experiment at a given collective pitch.

UNCLASSIFIED

1. Helicopters - Performance
2. Helicopters - Aerodynamic Characteristics
3. Helicopters - Model Test Results

I. Rabbott, J. P. Jr.

II. Contract DA 44-177-TC-548

AD _____ Accession No _____

Sikorsky Aircraft Division, United Aircraft Corporation, Stratford, Connecticut. COMPARISON OF THEORETICAL AND EXPERIMENTAL MODEL HELICOPTER ROTOR PERFORMANCE IN FORWARD FLIGHT - John P. Rabbott, Jr.

Report No. FREC 61-103, July, 1961, 181 pp
(Contract DA 44-177-TC-548) USATRECOM Proj 9R58-13-014-02
Unclassified Report

A program was conducted to determine the degree of correlation between theoretical and experimental dynamically scaled model rotor performance over a range of forward speeds to 161 knots, tip speeds to 850 feet per second, and tip Mach Numbers to 1.0. Theory and experiment correlate well below the theoretically predicted stall boundary, but above stall the theory is unduly conservative in predicting rotor power required. The effects of compressibility can be accurately predicted and a rotor with an NACA 0012 airfoil section incurs substantial profile power losses when the advancing tip Mach Number exceeds 0.85 to 0.90

Significant amounts of model rotor blade dynamic twisting-up to 5 degrees-occur both in hovering and forward flight. The inclusion of dynamic twist in forward flight significantly improves the correlation of theory and experiment at a given collective pitch

UNCLASSIFIED

1. Helicopters - Performance
2. Helicopters - Aerodynamic Characteristics
3. Helicopters - Model Test Results

I Rabbott, J. P. Jr.

II Contract DA 44-177-TC-548

AD _____ Accession No. _____

Sikorsky Aircraft Division, United Aircraft Corporation, Stratford, Connecticut. COMPARISON OF THEORETICAL AND EXPERIMENTAL MODEL HELICOPTER ROTOR PERFORMANCE IN FORWARD FLIGHT - John P. Rabbott, Jr.

Report No. FREC 61-103, July, 1961, 181 pp
(Contract DA 44-177-TC-548) USATRECOM Proj 9R58-13-014-02.
Unclassified Report

A program was conducted to determine the degree of correlation between theoretical and experimental dynamically scaled model rotor performance over a range of forward speeds to 161 knots, tip speeds to 850 feet per second, and tip Mach Numbers to 1.0. Theory and experiment correlate well below the theoretically predicted stall boundary, but above stall the theory is unduly conservative in predicting rotor power required. The effects of compressibility can be accurately predicted and a rotor with an NACA 0012 airfoil section incurs substantial profile power losses when the advancing tip Mach Number exceeds 0.85 to 0.90

Significant amounts of model rotor blade dynamic twisting-up to 5 degrees-occur both in hovering and forward flight. The inclusion of dynamic twist in forward flight significantly improves the correlation of theory and experiment at a given collective pitch

UNCLASSIFIED

1. Helicopters - Performance
2. Helicopters - Aerodynamic Characteristics
3. Helicopters - Model Test Results

I Rabbott, J. P. Jr.

II Contract DA 44-177-TC-548

AD _____ Accession No _____

Sikorsky Aircraft Division, United Aircraft Corporation, Stratford, Connecticut. COMPARISON OF THEORETICAL AND EXPERIMENTAL MODEL HELICOPTER ROTOR PERFORMANCE IN FORWARD FLIGHT - John P. Rabbott, Jr.

Report No. FREC 61-103, July, 1961, 181 pp
(Contract DA 44-177-TC-548) USATRECOM Proj 9R58-13-014-02
Unclassified Report

A program was conducted to determine the degree of correlation between theoretical and experimental dynamically scaled model rotor performance over a range of forward speeds to 161 knots, tip speeds to 850 feet per second, and tip Mach Numbers to 1.0. Theory and experiment correlate well below the theoretically predicted stall boundary, but above stall the theory is unduly conservative in predicting rotor power required. The effects of compressibility can be accurately predicted and a rotor with an NACA 0012 airfoil section incurs substantial profile power losses when the advancing tip Mach Number exceeds 0.85 to 0.90

Significant amounts of model rotor blade dynamic twisting-up to 5 degrees-occur both in hovering and forward flight. The inclusion of dynamic twist in forward flight significantly improves the correlation of theory and experiment at a given collective pitch

UNCLASSIFIED

1. Helicopters - Performance
2. Helicopters - Aerodynamic Characteristics
3. Helicopters - Model Test Results

I Rabbott, J. P. Jr.

II Contract DA 44-177-TC-548

AD _____ Accession No. _____

Sikorsky Aircraft Division, United Aircraft Corporation, Stratford, Connecticut. COMPARISON OF THEORETICAL AND EXPERIMENTAL MODEL HELICOPTER ROTOR PERFORMANCE IN FORWARD FLIGHT - John P. Rabbott, Jr.

Report No. FREC 61-103, July, 1961, 181 pp.
(Contract DA 44-177-TC-548) USATRECOM Proj 9R58-13-014-02.
Unclassified Report

A program was conducted to determine the degree of correlation between theoretical and experimental dynamically scaled model rotor performance over a range of forward speeds to 161 knots, tip speeds to 850 feet per second, and tip Mach Numbers to 1.0. Theory and experiment correlate well below the theoretically predicted stall boundary, but above stall the theory is unduly conservative in predicting rotor power required. The effects of compressibility can be accurately predicted and a rotor with an NACA 0012 airfoil section incurs substantial profile power losses when the advancing tip Mach Number exceeds 0.85 to 0.90

Significant amounts of model rotor blade dynamic twisting-up to 5 degrees-occur both in hovering and forward flight. The inclusion of dynamic twist in forward flight significantly improves the correlation of theory and experiment at a given collective pitch

UNCLASSIFIED

1. Helicopters - Performance
2. Helicopters - Aerodynamic Characteristics
3. Helicopters - Model Test Results

I Rabbott, J. P. Jr.

II Contract DA 44-177-TC-548